THE ECOLOGY OF SCATTERING LAYER BIOTA AROUND INDIAN OCEAN SEAMOUNTS AND ISLANDS

Philipp Hanno Boersch-Supan

A Thesis Submitted for the Degree of PhD
at the
University of St Andrews

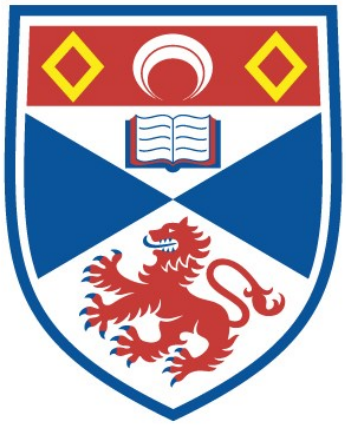

2014

The ecology of scattering layer biota around Indian Ocean seamounts and islands

Philipp Hanno Boersch-Supan

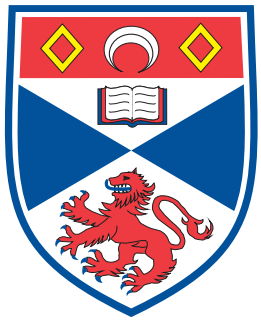

A thesis submitted in partial fulfilment for the degree of
Doctor of Philosophy

School of Biology
University of St Andrews

April 2014

Declarations

I, Philipp Hanno Boersch-Supan, hereby certify that this thesis, which is c. 40 000 words in length, has been written by me, that it is the record of work carried out by me, and that it has not been submitted in any previous application for a higher degree. I was admitted as a research student in October 2009 and as a candidate for the degree of PhD in September 2010; the higher study for which this is a record was carried out at the University of St Andrews and the University of Oxford between 2009 and 2013.

date _____ *signature of the candidate* _____

I hereby certify that the candidate has fulfilled the conditions of the Resolution and Regulations appropriate for the degree of PhD at the University of St Andrews and that the candidate is qualified to submit this thesis in application for that degree.

date _____ *signature of the supervisor* _____

In submitting this thesis to the University of St Andrews I understand that I am giving permission for it to be made available for use in accordance with the regulations of the University Library for the time being in force, subject to any copyright vested in the work not being affected thereby. I also understand that the title and the abstract will be published, and that a copy of the work may be made and supplied to any *bona fide* library or research worker, that my thesis will be electronically accessible for personal or research use unless exempt by award of an embargo as requested below, and that the library has the right to migrate my thesis into new electronic forms as required to ensure continued access to the thesis. I have obtained any third-party copyright permissions that may be required in order to allow such access and migration, and have requested the appropriate embargo below.

The following is an agreed request by candidate and supervisor regarding the electronic publication of this thesis:

Access to all or part of printed copy but embargo of the electronic copy for a period of one year on the following ground: publication would preclude future publication.

We request this embargo to allow us time to publish the research carried out in the analysis chapters of this thesis.

date _____ *signature of the candidate* _____

date _____ *signature of the supervisor* _____

Abstract

The waters of the open ocean constitute the largest living space on Earth but despite its obvious significance to the biosphere, the open ocean remains an unexplored frontier. With a regional focus on the Indian Ocean, this thesis investigates (i) the distribution of pelagic biota on basin scales, (ii) the effect of abrupt topography on pelagic biota and their predator-prey relationships, and (iii) the use of genetic techniques to elucidate population connectivity and dispersal of pelagic taxa.

(i) Pelagic scattering layers (SLs) were surveyed with scientific echosounders across the southwest (SWIO) and central Indian Ocean to investigate their vertical and geographical distribution. Structurally distinct SL regimes were found across the Subantarctic Front, and may explain recently observed foraging behaviours of southern elephant seals. Regression models indicated a close relationship between sea surface temperature and mean volume backscatter, with significantly elevated backscatter in the subtropical convergence zone. The heterogeneous distribution of scattering layer biota may have implications for predator foraging and carbon cycling in the Indian Ocean.

(ii) Acoustic surveys revealed diverse interactions between SLs, aggregations and topography around islands as well as shallow (<200m) and intermediate (200-800m) seamounts at spatial scales from 1 to 100 km. Epi- and mesopelagic backscatter was increased around reefs and banks of the Chagos archipelago, indicating connectivity between oceanic and neritic systems. SWIO seamounts harboured summit-associated aggregations, but the distributions of surrounding SLs did not follow a general pattern. Downstream SL depletion was observed in one location and combined with stomach content analyses, provides an insight into the mechanics of prey flux between open-ocean and seamount ecosystems.

(iii) A mitochondrial marker was used to assess the population structure and demography of the hatchetfish *Argyropelecus aculeatus* in the SWIO. The results are suggestive of a single, well-connected population and indicate a recent population expansion around 0.14 million years ago. This highlights that even highly abundant mesopelagic populations are vulnerable to global climatic changes.

Dispersal and recruitment are key ecological processes structuring seamount communities and are directly relevant for the management of exploited populations. Genetic barcoding was evaluated as a means to identify cryptic larval specimens of eels (leptocephali) and spiny lobsters (phyllosomata). Identification success was limited, but indicated the presence of 3-4 phyllosoma clades and 5-6 leptocephalus clades along the SWIR.

Acknowledgements

I wish to thank my supervisors, Andrew Brierley and Alex Rogers for their support, sage advice and encouragement, and for giving me the freedom to develop my own research ideas during this endeavour. I have learnt a lot from them.

The Cusanuswerk provided a maintenance grant, my continuation fees and a generous contribution to the Chagos expedition and I am thankful for the great sense of community and intellectual stimulation provided by my fellow 'Cusaners'. The Lesley & Charles Hilton-Brown Scholarship provided my university fees. Additional funds came from the German National Academic Foundation, the Rehbock Fund, the Fisheries Society of the British Isles, and the Marine Alliance for Science and Technology for Scotland (MASTS) pooling initiative (Grants DSSG1 and SG98).

Data collection in the Southwest Indian Ocean was undertaken as part of the Southwest Indian Ocean Seamounts Project (www.iucn.org/marine/seamounts) supported by the EAF Nansen Project, the Food and Agriculture Organization of the United Nations, the Global Environment Facility, the International Union for the Conservation of Nature, the Natural Environment Research Council (Grant NE/F005504/1), the Leverhulme Trust (Grant F00390C) and the Total Foundation. Shiptime in the Chagos was funded by the UK Foreign and Commonwealth Office.

Thanks to the officers, crew, and scientific parties of *RV Dr. Fridtjof Nansen* (Cruise 2009-410), *RRS James Cook* (Cruise JCO66/67) and *FPV Pacific Marlin* (Chagos Pelagic Expedition). Tom Letessier and Jessica Meeuwig are thanked for inviting me on the Chagos expedition. The South African Institute for Aquatic Biodiversity and the Scripps Institution of Oceanography Archives also provided excellent facilities during research visits.

Martin Cox introduced me to the Echoview acoustic processing software, helped me get my head around COM automation and provided helpful advice. Celia Bell got the work on the pelagic larvae started. Jennifer Freer has been a most tremendous helper with both the hatchetfish genetics and the stomach contents. Lauren Sumner-Rooney, Clara Kloecker and Chris Taylor were summer interns in the Oxford lab and assisted with stomach content sorting and some molecular work. I am grateful to Jane Read, Vladimir Laptikhovski, Tom

Letessier, Kirsty Kemp and Lewis Fasolo for sharing unpublished manuscripts and data. Anni Djurhuus and Michelle Taylor are thanked for commenting on various drafts of the manuscript.

I would like to thank my examiners Arnaud Bertrand and Patrick Miller for their constructive comments and suggestions in my viva.

A large part of my research, from survey planning to data processing, statistical analyses, data visualisation, figure preparation and lastly the typesetting of this document was achieved with free and open-source software. I am indebted to the developers and communities behind software projects like R, GRASS, GMT and LaTeX.

The members, past and present, of the Pelagic Ecology Research Group at St Andrews and the Ocean Research and Conservation Group at Oxford are thanked for their friendship through the past 4 years, and for helping me to survive the mobilisation and demobilisation of three expeditions, long hours at sea, and various lab and office moves.

The Djurhuus family provided a home from home through part of the write-up – túsund takk fyri! – and I would not be where I am today, were it not for the love and support from my family. My parents have inspired me to pursue a challenging path and have been supportive throughout this journey; my sisters have provided welcome reminders that there is indeed a whole world outside the oceans. Finally, I am eternally grateful to my soon-to-be wife Anni for her love, patience and support, for late-night chicken soup and apple crumbles.

Contents

List of acronyms

AC	Agulhas Current
ACC	Antarctic Circumpolar Current
AIC	Akaike Information Criterion
AL	Agulhas Leakage
AMOVA	Analysis of Molecular Variance
AR(n)	n^{th} order autoregressive model
ARC	Agulhas Return Current
ATL	Atlantis bank
AU	arbitrary units
BC	Benguela Current
BLAST	Basic Local Alignment Search Tool
BOLD	Barcode of Life database
bp	Base pairs
CI	Confidence Interval
COI	Cytochrome c Oxidase Subunit I
CTD	Conductivity, temperature, depth probe
DFN	*Research Vessel Dr. Fridtjof Nansen*
DNA	Deoxyribonucleic acid
DSL	Deep scattering layer
DVM	Diel vertical migration
EAF	Ecosystems approach to fisheries
EoT	Equation of time
EMC	East MadagascarCurrent
FishBOL	The Fish Barcode of Life Initiative
FL	Fragment length
GAM	Generalized additive model
GAMM	Generalized additive mixed model
GEBCO	General Bathymetric Chart of the Oceans
GMT	Generic Mapping Tools
GRASS	Geographic Resources Analysis Support System
IMOS	Australia's Integrated Marine Observing System
JCO	Royal Research Ship James Cook
MEGA	Molecular Evolutionary Genetics Analysis
MEL	Melville bank

MOTU	Molecular Operational Taxonomic Unit
MOW	Middle of What seamount
MR	Madagascar Ridge
mt	mitochondrial
MUSCLE	Multiple Sequence Comparison by Log-Expectation
MVBS	mean volume backscatter
mya	Million Years Ago
nmi	nautical mile
OLS	Ordinary Least Squares
ORN	Off-ridge North
OSTIA	Operational sea surface temperature and sea ice analysis
PAM	Partitioning around medoids
PB	post breeding
PF	Polar front
PCR	Polymerase chain reaction
PM	post-moult
rRNA	ribosomal ribonucleic acid
SA	sub-adult
SACC	Southern ACC front
SAF	Subantarctic front
SAP	Sapmer bank
SCUBA	self contained underwater breathing apparatus
SCZ	Subtropical convergence zone
SEC	South Equatorial Current
SECC	South Equatorial Countercurrent
SIG	Southern Indian Subtropical Gyre
SL	Scattering layer
SST	Sea-surface temperature
STF	Subtropical Front
SWIO	Southwest Indian Ocean
SWIOR	Southwest Indian Ocean Ridge
SWIR	Southwest Indian Ridge
TL	total length
TS	Target strength
UTC	Coordinated Universal Time
UV	Ultra violet
WAL	A seamount near Walter's shoal

List of symbols

Commonly used symbols

n	Sample size
$\mathrm{s_a}$	area backscattering coefficient
$\mathrm{s_A}$	nautical area backscattering coefficient
$\mathrm{s_v}$	volume backscattering coefficient
$\mathrm{S_v}$	volume backscattering strength
$\Delta\mathrm{S_v}$	$\mathrm{S_v}$ difference
σ_{bs}	backscattering cross-section
z	depth

Chapter 1

a_{es}	equivalent spherical radius
D	depth
e	roundness
f	incident frequency
f_o	spherical resonance freqeuncy
f_p	prolate resonance frequency
γ	specific heat ratio
μ_1	shear modulus
ρ	tissue density
P	pressure
Q	resonance quality factor
V_0	sampled volume

Chapter 2

r	Pearson's product-moment correlation coefficient
t_{local}	local time
t_{UTC}	UTC time
T_0	axial surface temperature of a front
k	number of clusters
lo_i	longitude
$\bar{s}(k)$	mean silhouette width
φ	AR(1) correlation coefficient

Chapter 4

D	test statistic of Kolmogorov-Smirnov test
F_{max}	fluorescence maximum

λ rate constant
r distance to topographic feature
Z_{14} depth of 14°C isotherm

Chapter 5

d distance between transects
D digestive state index
F fullness index
F_o frequency of occurrence
L_T transect length
λ wavelength
m_c stomach content mass
n_T number of transects
φ_U angle relativ to current
φ_N angle relative to compass North
$\vec{U}$ mean current vector
Δz vertical displacement

Chapter 6

β slope coefficient
F_ST Pairwise differentiation
h haplotype diversity
k Expected number of alleles
μ Mutation rate
M size of a haploid population
N_h Number of haplotypes
π nucleotide diversity
ΔT Temperature difference
u Mutation rate
θ Molecular diversity indices
θ_k Molecular diversity using the number of alleles
θ_π Molecular diversity using the number of pairwise distances
τ Time of expansion estimate

Chapter 1

General Introduction

> There is not an intermediate fauna between [200 fathoms] and the bottom [...]
>
> Agassiz (1892)

> There is no such things as mountains and valleys on the deep-sea bottom.
>
> Moseley (1880)

1.1 Introduction

This Ph.D. project is part of an international research project on seamount ecosystems which aims to deliver baseline data for an ecosystems approach to high-seas fisheries management. Submarine mountains are common features of the ocean floor(Yesson et al., 2011), but they are among the least-understood habitats of our planet. Seamounts have been hypothesized to be sites of increased biological production and diversity, and their abrupt topography can drastically influence oceanographic patterns (Rogers, 1994; Clark et al., 2010). However, the effects of seamounts on pelagic ecology remain largely unknown.

Specifically, my research project aims to describe the pelagic environment along the Southwest Indian Ridge (SWIR) on two different scales and using two complementary methodological approaches. On a local scale, fisheries acoustics and nets will be used to obtain information about the distribution, abundance and biodiversity of zooplankton and nekton around single seamounts. This will be aimed at providing information on the interactions between pelagic and demersal/benthic ecosystems, and will contribute to efforts to determine principal drivers of seamount ecosystem processes. Genetic analyses will then be used to look at the structure and connectivity of pelagic populations between seamounts and the dispersal ranges of planktonic larvae on a scale spanning the entire ridge. Phylogenetic work, in the form of barcoding, is also used to complement my ecological studies. The study area has been very poorly sampled to date, and there is no comprehensive picture of the diversity and systematics of the pelagic communities in this part of the world ocean.

While benthic communities form an important part of the overarching project, they themselves are only of secondary interest for this Ph.D. project and will not be discussed in detail here. Comprehensive reviews can be found in Rogers (1994),Pitcher et al. (2007) and (Clark et al., 2010).

1.2 The ecological role of mesopelagic micronekton

Mesopelagic micronekton, particularly mesopelagic fishes, have been largely neglected in models of pelagic food-web dynamics for productive marine ecosystems. They form diverse and abundant assemblages, a large proportion of these animals undertakes vertical migrations, generally moving from the mesopelagic zone (200-1000 m) into more produc-

tive surface waters at night, and returning to depth at dawn. This behaviour is thought to balance foraging requirements with predation pressure, as well as as confer energetic benefits to migrators (Angel, 1985; Pearre, 2003), but the understanding of both proximate and ultimate causes is far from complete. The dominant mode of vertical migration occurs in a diel cycle, although migration patterns can include complex seasonal (Barham, 1957; Urmy et al., 2012) and/or ontogenetical patterns (Staby et al., 2011) both on the level of a population and the individual (Kaartvedt et al., 2011). Many vertical migrators feed on epipelagic phyto- and zooplankton in surface waters and thereby contribute to the transport of carbon and nitrogen (Steinberg et al., 2008; Buesseler and Boyd, 2009) and influence oxygen dynamics (Bianchi et al., 2013a).

Mesopelagic fishes are often not considered in ecosystems and biogeochemical models, presumably because their abundance and ecological impact are not considered significant relative to other the epipelagic schooling grazers and planktivores. For example, a recent Atlantis model for the northern California Current was parameterized such that the biomass of deep vertical migrators was about 10% that of the small epipelagic planktivorous fishes, based on trawl-derived abundance estimates from the 1960s (Horne et al., 2010). More recent research, however, suggests that mesopelagic fish biomass in this particular ecosystem is on par with, if not greater than the biomass of epipelagic forage fish such as anchovy and sardine (Koslow et al., 2013).

Similarly, biomass estimates for midwater fishes have been revised upward by about an order of magnitude in recent years, based on combined use of acoustics, trawl sampling and modelling (Koslow et al., 1997; Kloser et al., 2009). There is evidence that midwater fishes efficiently avoid trawls (Kaartvedt et al., 2012) and escape through the meshes of large trawls. Clearly, the trophic impact of mesopelagic fishes cannot be disregarded in considering the interactions between the zooplankton and their predators in marine ecosystems. Likewise, the biomass, trophic interactions and role in biogeochemical cycling of gelatinous and other zooplankton groups at mesopelagic and bathypelagic depths is also poorly understood (e.g. Robison, 2004; Steinberg et al., 2008; Bianchi et al., 2013b).

Mesopelagic fishes are highly diverse. In the well-sampled California Current Ecosystem they make up over a third of identified ichthyoplankton taxa (Moser and Watson, 2006). Remarkably, much of this diverse assemblage appears to respond coherently to environmental forcing (Koslow et al., 2011), in particular changes to deepwater oxygen concentration (Koslow et al., 2013; Bianchi et al., 2013a). Yet little is known about the responses of the marine ecosystem to large decadal-scale change in the biomass of mesopelagic zoo-

planktivores. Potentially, such perturbations of the marine food web enable us to probe fundamental issues related to the structure and dynamics of marine ecosystems.

1.3 Acoustic Investigations of the Pelagic Realm

Sound waves can travel over very long distances through water, while visible light usually only penetrates a few metres below the sea surface. Sound pulses or "pings" transmitted by echosounders can therefore be used to detect marine life or other submerged objects at long ranges. An insonified target will scatter the transmitted sound, resulting in echoes which can be detected by the receiving part of the instrument.

Interpreting the echoes to extract information (size, species etc.) about the target is known as the inverse scattering problem. Ideally, one wants to determine the species and sizes of animals in the water column, as well as determine the number or biomass of the targets.

Abundance measures

In plankton and micronekton acoustics the targets are usually very small and numerous. Consequently, their echoes combine to form a signal which is more or less continuous with varying amplitude. While it is usually not possible to resolve individual targets in this situation, the echo intensity is still a measure of the biomass present in the water column. The basic acoustic measurement in this case is the volume backscattering coefficient $\mathrm{s_v}$ (MacLennan et al., 2002), which is obtained by echo-integration:

$$\mathrm{s_v} = \frac{\sum \sigma_{bs}}{V_0} \tag{1.1}$$

where σ_{bs} is the backscattering cross-section of an individual target and V_0 is the sampled volume. Its units are $\mathrm{m^{-1}}$. Commonly, this is reported as a logarithmic measure, the volume backscattering strength $\mathrm{S_v}$; its units are dB re 1 $\mathrm{m^{-1}}$ (MacLennan et al., 2002):

$$\mathrm{S_v} = 10 \log (\mathrm{s_v}). \tag{1.2}$$

When $\mathrm{s_v}$ is averaged over volumes much larger than V_0, for example several pings, the resulting logarithmic quantity is called the mean volume backscattering strength or MVBS.

In principle, a direct conversion of MVBS into biomass is possible, but requires rather detailed knowledge about species and size composition of the insonified population (Simmonds and MacLennan, 2005).

The area backscattering coefficient $\mathrm{s_a}$ (MacLennan et al., 2002) is a measure of the energy returned from a layer between two depths z_1 and z_2 in the water column. It is defined as

$$\mathrm{s_a} = \int_{z_1}^{z_2} s_v \, \mathrm{d}z. \tag{1.3}$$

Since $\mathrm{s_a}$ is a product of s_v and a distance, it is dimensionless. As defined above, the units are ($\mathrm{m^2/m^2}$), more commonly, however, it is reported as nautical area scattering coefficient (NASC) for which the symbol $\mathrm{s_A}$ is used. This is defined as ($\mathrm{m^2/nmi^2}$). The conversion formula is

$$\mathrm{s_A} = 4\pi(1852)^2 \, \mathrm{s_a}. \tag{1.4}$$

Acoustic observability and identification of pelagic animals

The echo returned from a target depends on the target's size, shape, orientation and material properties as well as the incident frequency. This enables the use of multi-frequency echosounders for species identification, a technique that has become fairly widespread in fisheries and fisheries research. The great diversity of shapes, sizes and body structure of planktic organisms makes species identification from acoustic data difficult if not impossible. However, some acoustical classification can be achieved. achieved. Stanton et al. (1996) proposed three broad groups of organisms which differ substantially in their anatomical make-up and thus in the relative frequency response of their echoes (Fig. 1.1).

Fluid-like scatterers have roughly cylindrical body composed of weakly-scattering soft tissue. The whole body contributes to the echo. Examples are most animals without gas-filled or hard structures, such as fish without swimbladders, crustacean zooplankton or many gelatinous animals. Elastic shelled scatterers have soft tissue surrounded by a hard shell that has an opercular opening. The echo comes primarly from the shell. Examples are pteropod gastropods. Gas bearing scatterers have a soft body which contains a gas-bubble that provides a strong echo. Examples are fish with a swimbladder (Fig. 1.2) or gas-bearing siphonophores (Fig. 1.3). If the gas/tissue volume is small, relative to body size, the contribution of the fluid-like body to the overall backscatter can be significant.

While the shape of the relative frequency response tends to be similar within a scattering class, the echo strength can vary widely. For example, Stanton et al. (1996) demonstrated

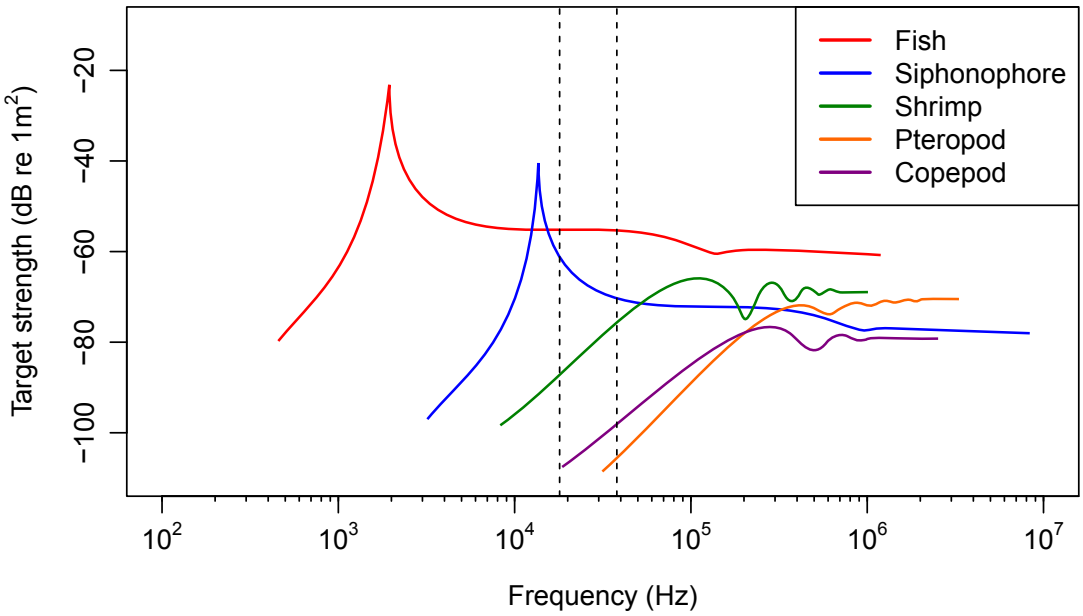

Figure 1.1: Target strength of various marine organisms over a range of incident frequencies. Dashed vertical lines mark the sampling frequencies used in this thesis (18 and 38 kHz). Adapted from Stanton (2009).

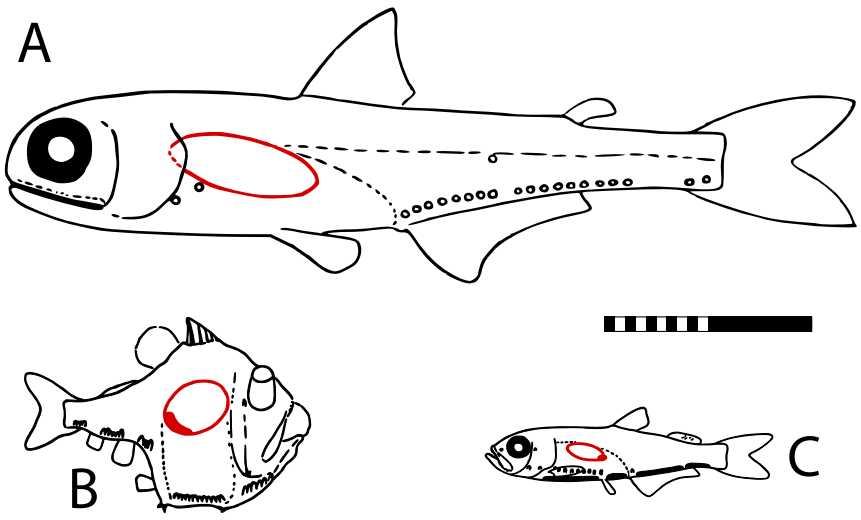

Figure 1.2: Some numerically dominant fishes in the SWIO and their swimbladders (red). Scale bar 20 mm. A: Myctophid, B: *Argyropelecus aculeatus*, C: *Maurolicus muelleri*. Adapted from Marshall (1960).

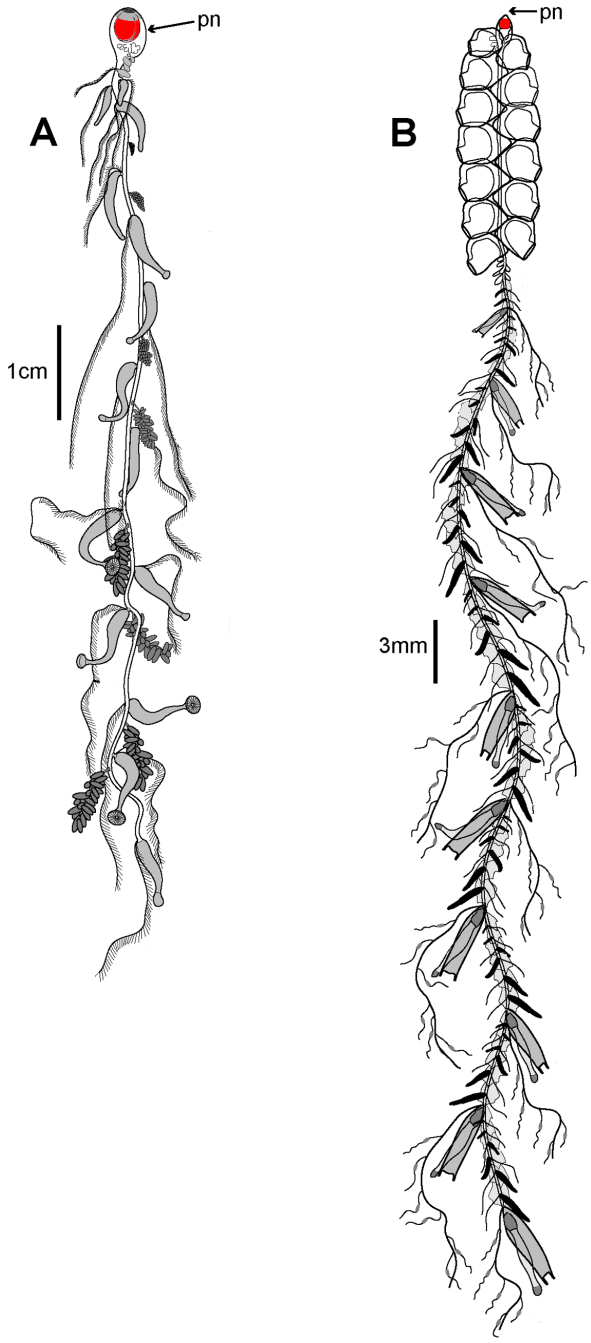

Figure 1.3: Examples of gas-bearing siphonophores. A: Long-stemmed cystonect *Rhizophysa eysenhardti*. B: Long-stemmed physonect *Nanomia bijuga*. Pneumatophores (floats; pn) are highlighted in red. Adapted from Mapstone (2014).

that the relative echo energy per unit biomass at 200 kHz is about 260 times higher (on a linear scale) for a decapod shrimp when compared with a salp.

Acoustic classification can be achieved to some degree by comparing S_v at different frequencies directly (Mitson et al., 1996), or by comparing $\delta S_{v(f1-f2)}$, differences in volume backscattering strength between two frequencies f_1 and f_2 (Madureira et al., 1993). Classification can deliver relatively good results for zooplankton when working with single-target echoes. For plankton aggregations, however, the situation is more complex, as individual animals are not homogeneously oriented and of the same size. The resulting echo structure is usually less clear and may not be evident at all. Acoustic classification in these cases requires sophisticated inverse modelling to quantify the contributions of different scattering classes (e.g. Fernandes et al., 2006; Cox et al., 2013) and is often restricted to assemblages with a limited number of dominant species (e.g. Brierley et al., 1998b).

Acoustic classification success depends on the availability of data from multiple frequncies, and in particular high frequencies (>100 kHz) to elucidate backscatter contributions from soft tissues. High frequencies, however, are not suited for shipborne deep-water observations from hull-mounted echosounders, as high-frequency sound is rapidly absorbed by seawater, thereby limiting its use to the 10-100 m of the water column (Fig. 1.4; Francois and Garrison, 1982). The work in this thesis therefore relied on two relatively low frequencies, namely 18 kHz and 38 kHz, which are able to penetrate the top 1000 m of the watercolumn without substantial loss of signal.

Because most mesopelagic and many demersal fish species have gas-filled swim-bladders (Marshall, 1960), they are good acoustic targets at these low frequencies and backscatter at 38 kHz originating from deep scattering layers has been widely interpreted as originating from mesopelagic fishes (e.g. Kloser et al., 2009; Davison, 2011a; O'Driscoll et al., 2009; Escobar-Flores et al., 2013; Irigoien et al., 2014). Some mesopelagic and demersal fishes, however lack swimmbladders, or a gas-filled swimmbladder is only present in larval and juvenile stages and regresses with age, or is filled with lipids and/or wax esters to provide buoyancy (Neighbors and Nafpaktitis, 1982; Davison, 2011b). As a result these fish will have comparably low target strengths (Yasuma et al., 2010), even at large body sizes. For example the seamount-associated orange roughy (*Hoplostethus atlanticus*) has a wax ester filled swimbladder as thus at c. 35 cm length has a similar TS as a c. 6 cm long myctophid with a gas-filled swimbladder (Kloser et al., 2002, 2013).

Physonect and cystonect siphonophores are the strongest invertebrate scatterers at low frequencies, as they carry a gas-filled float, the pneumatophore (Fig. 1.3; Barham, 1966;

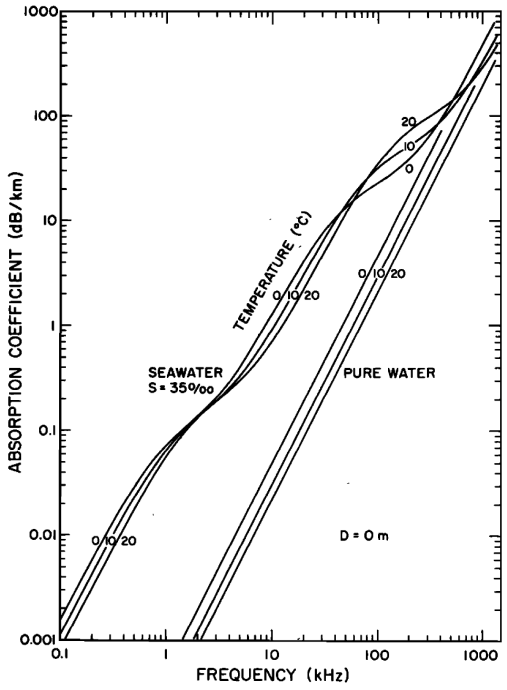

Figure 1.4: Seawater and pure water absorption at different temperatures for sound frequencies from 100 Hz to 1 MHz. Reproduced from Francois and Garrison (1982).

Benfield et al., 2003). Most other invertebrate mesopelagic micronekton fall into the fluid-like or elastic-shelled categories and are weak targets at low frequencies.

Gas bladder resonance

At low frequencies resonant scattering from gas bladders can substantially contribute to the target strength (TS) of pelagic animals. The relationship of normal incident TS of gas-filled swimbladders with depth and frequency is illustrated here using a simple resonance model following the notation and parameterization of Kloser et al. (2002) and Holliday (1972):

$$TS = 10 \log_{10}(\sigma_{bs}) \tag{1.5}$$

$$\sigma_{bs} = a_{es}^2 \left(\left(\left(\frac{f_p}{f} \right)^2 - 1 \right)^2 + \frac{1}{Q^2} \right)^{-1} \tag{1.6}$$

$$f_p = f_o\sqrt{2}e^{-\frac{1}{3}}(1-e^2)^{\frac{1}{4}}\left(\ln\left(\frac{1+\sqrt{1-e^2}}{1-\sqrt{1-e^2}}\right)\right)^{-\frac{1}{2}} \tag{1.7}$$

$$f_o = \frac{1}{2\pi a_{es}}\sqrt{\frac{3\gamma P + 4\mu_1}{\rho}} \tag{1.8}$$

$$P = (1 + 0.103D) \times 10^5 \tag{1.9}$$

Where, σ_{bs} is the acoustic backscattering cross section at the incident acoustic frequency (f) of the equivalent spherical swimbladder volume of radius a_{es} with a prolate resonant frequency (f_p), and resonance quality factor of Q. The prolate resonant frequency is a function of the prolate spheroid roundness (e) and the spherical resonant frequency (f_o) at a hydrostatic pressure (P) for a given depth (D) and fish tissue density (ρ), with a ratio of specific heats for the swimbladder gas (γ) and the real part of the complex shear modulus of the fish tissue defined by μ_1. e is defined by the ratio of the minor semi-axis to the major semi-axis and is assumed to be 0.2. Furthermore, the following values were assumed: $\mu_1 = 10^5$ Pa, $\gamma = 1.4$, $\rho = 1,075\,\mathrm{kg{\cdot}m^{-3}}$, and Q = 5. The gas bladder radius a_{es} was set to 1.4 mm for a small fish, e.g. a myctophid, and 5.1 mm for a larger fish, e.g. a macrourid.

Model predictions show that gas bladder resonance is an important factor to consider when using an incident frequency of 18 kHz to observe mesopelagic organisms such as myctophid fish and physonect siphonophores. For a myctophid with a swimmbladder radius of 1.4 mm the model predicted resonance at 18 kHz at approx. 500 m depth (Fig. 1.5), which is in the range at which DSLs are commonly observed acoustically. The effect is much smaller for larger fish.

At 38 kHz resonance effects are less noticable for the modelled swimbladder sizes and depth range, although the minute gas bladders in larval myctophids and siphonophore larvae which have bubble diameters <0.4 mm exhibit resonance at frequencies of up to 200 kHz (Benfield et al., 2003; Simmonds and MacLennan, 2005).

1.3.1 History of deep-scattering layer research

Despite strong initial scepticism about the existence of life in the deep ocean (Forbes, 1844) and especially in the deep pelagos (Agassiz, 1892), mesopelagic communities and their diel vertical migration were discovered in the early days of deep-sea biology (Fuchs, 1882;

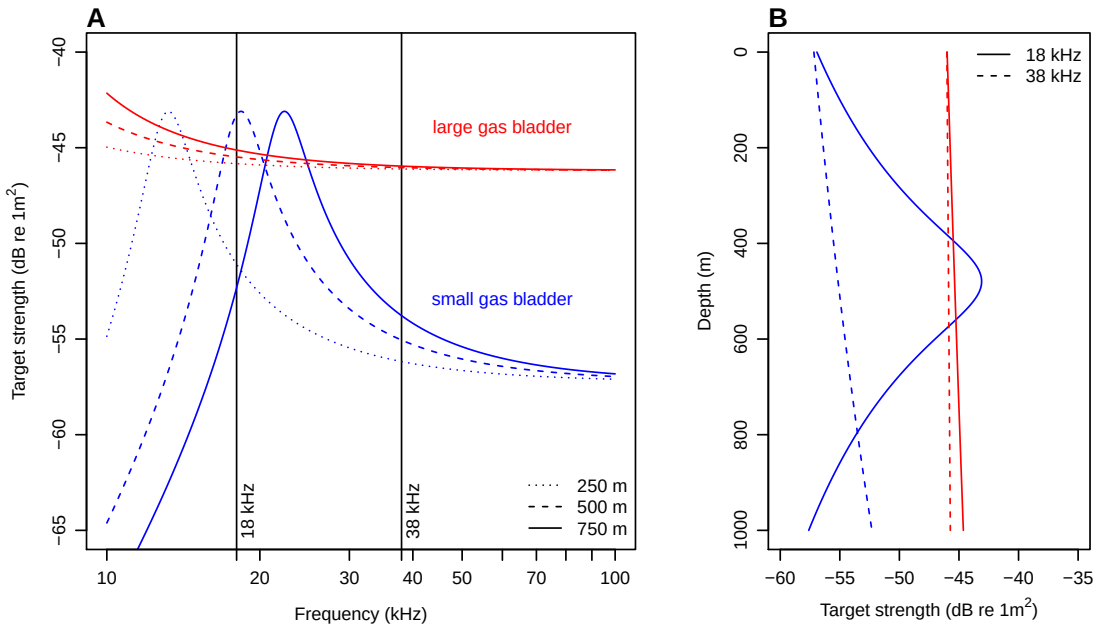

Figure 1.5: Simple resonance target strength model of a spheroidal gas bladder for small (blue; radius 1.4 mm; e.g. myctophids) and large (red; radius 5.1 mm; e.g. macrourids) fishes at 18 and 38 kHz. A: Target strength as a function of incident acoustic frequency at different depths. B: Target strength as a function of depth. Models assume constant swimbladder volume. Model based on Kloser et al. (2002) (Eqs. 1.5–1.9)

Chun, 1887, 1899).

The development of echosounders during World War II led to the rediscovery of these communities as ”deep scattering layers” (Eyring et al., 1942). Initially mistaken for phantom bottom echoes (Lyman, 1947) the biological origin of the sound scattering was soon discovered (Tucker, 1951; Marshall, 1951; Christensen et al., 1946) and - when records were unclassified - sparked a period of intensive scattering layer research around the globe (Farquhar, 1970).

Today it is accepted that oceanic scattering layers are composed of zooplankton and micronekton, and several key processes driving their formation and vertical movements are thought to be understood, e.g. predator avoidance and foraging requirements (Angel, 1985; Pearre, 2003). Nevertheless, many aspects of the biology of scattering layers remain to be explained. For example the exact species composition of scattering layers is still unknown, even for layers in the well-explored waters of the North Sea which were investigated by Mair et al. (2005) using a combination of acoustics, towed plankton samplers and nets.

While acoustic techniques were essential in the discovery of scattering layers, and have

provided most of what we know about their occurrence, spatial extent and vertical movements, much of what we know about their composition comes from netting techniques. Acoustic backscatter has been shown to be a highly significant predictor of pelagic biomass (Simmonds and MacLennan, 2005) and this has been verified for components of micronekton layers by measuring target strength-biomass relationships of individual animals in experimental settings (Benoit-Bird and Au, 2002). The conversion, however is not straightforward and requires good knowledge of the species composition, and the sound-reflecting properties of a given organism (the "target strength", which in turn is dependent on the size of the animal and the aspect of ensonification). Traditional fisheries acoustics methodology therefore requires ground-truthing with nets to supply additional information about target strengths, species composition and size distributions (Simmonds and MacLennan, 2005). Netting techniques, however, are limited in several respects, too. Net avoidance is a major problem (Kaartvedt et al., 2012) leading to biased estimates of size distribution and species composition and as nets integrate over large volumes of water, their spatial resolution of trawl data is often not capable of observing sub-kilometer scale features apparent in echograms such as small scale patchiness (Benoit-Bird, 2009). Additionally, target strengths have yet to be determined for most micronektic species. Modern multi-frequency techniques (Korneliussen and Ona, 2003; Madureira et al., 1993) and/or the application of theoretical models (Simmonds and MacLennan, 2005) can sidestep some of these problems. The full suite of frequencies of scientific vessel-mounted echosounders, however, is limited to the epipelagic realm (0–200 m), as high-frequency soundwaves are rapidly attenuated in the water column, and lowered transducers are required to gather multi-frequency acoustic data from deep water scatterers (e.g. Kloser et al., 2002, 2009).

1.3.2 Scattering layers around islands, seamounts and ridges

The scattering layers of the mesopelagic boundary community of the Hawaiian Islands have been studied with nets (Reid et al., 1991) and acoustics (**?**Benoit-Bird and Au, 2004) and are possibly the best understood in terms of acoustic properties. Target strengths and backscatter-biomass relationships have been determined for the dominant non-gelatinous scatterers (Benoit-Bird and Au, 2001, 2002) and the dependency of the frequency response on species composition, animal size and animal density has been studied using an optical and acoustical profiling device and a vessel mounted multi-frequency echosounder (Benoit-Bird, 2009).

Since the seminal paper of Isaacs and Schwartzlose (1965) which presented acoustic observations of interception of scattering layers by seamount associated rockfish, scattering layers around shallow seamounts have been the subject of a number of studies with different objectives. Generalised conclusions about scattering layer distributions and vertical movements have been drawn from biological backscatter recorded with acoustic Doppler current profilers (ADCPs), both vessel-mounted (Haury et al., 2000) and moored devices (Valle-Levinson et al., 2004). ADCP-derived backscatter, however, usually cannot provide biomass estimates or even insights into species composition (Brierley et al., 1998a).

Wilson and Boehlert (2004) used a 38 kHz vessel-mounted echosounder and a starburst-shaped survey pattern to investigate the interactions of currents and micronekton aggregations over Hancock seamount and to map the relative acoustic abundance of the scatterers. Biomass estimates were not obtained from the acoustic data.

Single-frequency echo-sounders and repeated transects in flow direction were used by Genin et al. (1988) and Genin et al. (1994) on different Californian seamounts to demonstrate the formation of gaps in scattering layers downstream of seamounts as a result of predation by rockfish.

With the exception of Valle-Levinson et al. (2004), all acoustic studies on seamounts cited so far stem from data collected in the late 1980s to mid-1990s. Little research seems to have been done since, although both Martin and Christiansen (2009) and De Forest and Drazen (2009) mention "unpublished results" from ADCP and/or echosounder observations.

Opdal et al. (2008) describe scattering layers down to 2000 m and possible topographical, hydrographical and biological processes shaping them along the mid-Atlantic Ridge between 40°N and 60°N. (Priede et al., 2013) present backscatter data from the Reykjanes ridge that indicates enrichment of deep scattering layers along the ridge crest. Biovolume estimates have been derived using multi-frequency inversions for epipelagic scatterers above the mid-Atlantic ridge near the Charlie-Gibbs Fracture Zone (Cox et al., 2013). No ridge effect could be observed in this study.

In summary, the influence of abrupt topography on scattering layer density and ecology is still incompletely understood. This research aims to examine interactions between scatterers and topography in a previously unsurveyed region, thereby adding to a more complete global picture of the influence of topography on pelagic ecology.

1.4 Seamount Biology

Seamounts are submerged marine mountains that rise steeply from the deep-ocean floor into the water column, sometimes well into the euphotic zone. Despite being an extremely common landform on earth (Yesson et al., 2011), they are among the least understood habitats of our planet.

Although seamounts were originally defined as isolated underwater volcanoes rising more than 1 km above the seabed (Menard, 1964), the current usage of the term usually includes any geographically isolated topographic feature on the seafloor with an elevation greater than 100 m (Staudigel et al., 2010). This is both a result of advances in marine surveying technology, enabling the detection of smaller features, as well as the development of a diverse and multidisciplinary research community studying geological, oceanographical and biological aspects of these topographic features.

Seamounts are a common feature of the seafloor landscape. Although less than 10% of the world's seafloor have been surveyed directly by (echo)sounding (Kim and Wessel, 2011), satellite sensed bathymetry can be used to estimate seamount locations. Current estimates differ due to different underlying data and methodologies, but suggest the existence of 8,500 (Kim and Wessel, 2011) to 33,000 (Yesson et al., 2011) large seamounts (>1 km) and between 16,500 and 138,000 smaller features (1 km > $h \geq$ 0.1 km). Seamount density is particularly high in the Pacific Ocean and along the approximately 60,000-km-long mid-oceanic ridge system (see Fig. 1.6).

Seamounts have been hypothesized to be sites of increased biological production and diversity (McClain, 2007). The abrupt topography of seamounts can drastically influence local and regional oceanographic patterns for example by upwelling and with it the mid-water community. However, the effects of seamounts on pelagic ecology remain largely unknown. While numerous hypotheses have been brought forward, proposing several fundamental processes that shape seamount ecosystems (Pitcher and Bulman, 2007), actual evidence is sparse (McClain, 2007).

Hubbs (1959) laid the foundations of seamount biology by posing a number of fundamental questions about seamount ecosystems:

- What species inhabit seamounts and how regular and abundant are they?
- What factors influence the abundance of life around seamounts and are seamount-associated species abundant enough to sustain profitable fisheries?

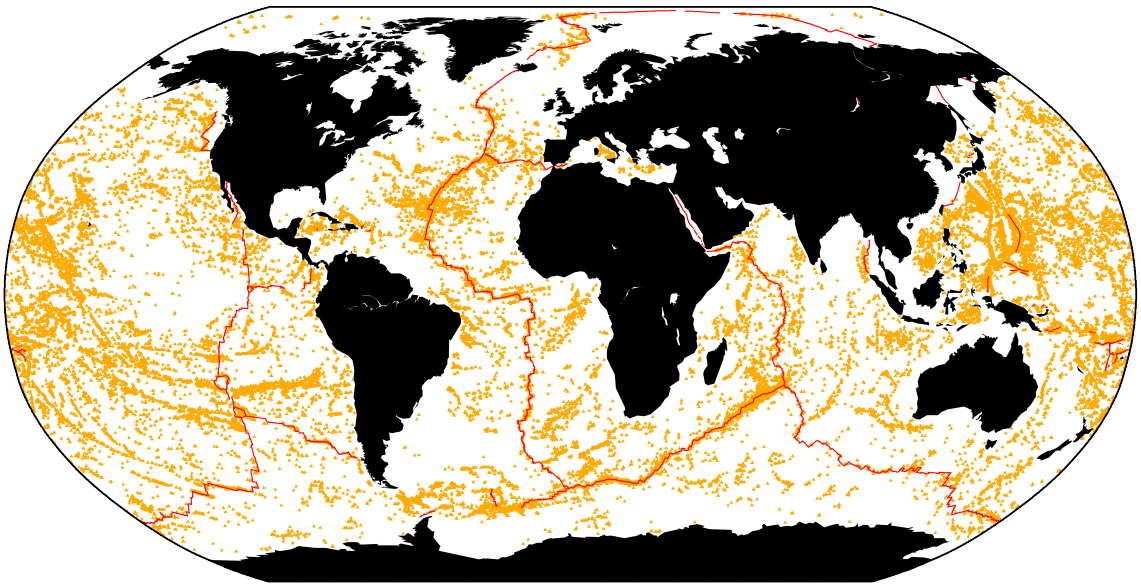

Figure 1.6: Global distribution of about 33,000 seamounts of 1 km height or more that have been identified using bathymetry data derived from satellite altimetry. Seamount locations from Yesson et al. (2011), plate boundaries from Coffin et al. (1998)

- How does species dispersal influence the establishment of seamount communities?
- Are seamounts stepping stones for cosmopolitan species?

More than 60 years later our understanding of seamount ecosystems is still far from comprehensive, and these question remain to be fully answered. The broad variation in seamount morphology, depth and location leads to a similarly diverse set of ecological settings for individual seamounts (Rogers, 1994; McClain, 2007). Nonetheless a few general patterns apply and these are discussed below.

1.4.1 Biophysical coupling

Seamounts and ridges have complex effects on ocean circulation and both the diversity in seamount morphology and the complexity of the currents impinging on them lead to a wide array of current-topography interactions. Seamount effects on currents have been observed on a range of scales from the immediate surroundings of a peak to ocean basin wide effects (Rogers, 1994). At scales of hundreds to thousands of kilometres seamount chains can perturb or even deflect major currents like the Gulf Stream (Vastano and Warren, 1976) or the Kuroshio extension (Roden, 1987). On local scales current-topography

interactions include trapped waves, the reflection or perturbation of internal waves and complex tidal flow patterns (Rogers, 1994; White et al., 2007). Internal tides on seamounts and ridges play an important role in deep-ocean mixing (Garrett, 2003; Nikurashin and Ferrari, 2010).

Seamount effects can also result in the production of jets and eddies. Trapped eddies forming a closed circulation pattern are known as Taylor columns or Taylor cones, and are thought to occur when a steady current impinging on a seamount causes upwelling. As a result of upwelling isopycnals are compressed and anticyclonic vorticity is induced generating the closed eddy, a retentive hydrographic structure (White et al., 2007).

Even though their significance for biological processes has been disputed (see below), Taylor column-like flows continue to be the subject of oceanographic research and have sparked several modeling studies in recent years, some of them trying to explain flow patterns around actual topographic features (Mohn et al., 2009; Mohn and Beckmann, 2002b,a; Beckmann and Mohn, 2002), while others bear little, if any resemblance to physiographic structures and oceanographic conditions encountered in the real ocean (Zavala Sanson and Provenzale, 2009). A more or less permanent Taylor column-like feature has been observed on the North Georgia Rise (NGR; South Atlantic) and is responsible for enhanced primary production above this bathymetric feature (Meredith et al., 2003).

1.4.2 Pelagic aggregations

Zooplankton and nekton aggregations are frequently observed over abrupt topographies like seamounts, canyons and shelf breaks (Genin, 2004) and attract higher predators such as sharks, marine mammals and fishermen. The processes sustaining these aggregations are probably driven by current-topography interactions and four possible mechanisms are presented below.

Upwelling

Early hypotheses about the biological drivers of seamount ecosystems have relied heavily on the upwelling connected with Taylor column-like flows (Rogers, 1994). The basic rationale of these hypotheses is that the upwelling of nutrients enhances primary productivity over the seamount, while the Taylor column retains the phytoplankton biomass. This in turn enables higher trophic levels to subsist on the seamount. Even without enhanced primary productivity, detrivorous communities could profit from Taylor columns as detritus,

excreta and other particulate organic matter is retained above the seamount (Pitcher and Bulman, 2007). However actual evidence for Taylor columns is sparse. Most observations suggest, they are ephemeral features on time scales of days to weeks (Genin et al., 1989; Richardson, 1980). Enhanced primary – and in some cases even secondary – production has been observed in a few cases (Genin, 1987), but these too have proven to be short lived events and it is thought to be unlikely that they are able to sustain large pelagic or bentho-pelagic communities (but see Meredith et al. (2003) for a notable exception).

Topographic blockage

A substantial proportion of zooplankton and mikronekton biomass migrates daily between the surface and deeper layers. Shallow topography can block the descent of these animals, exposing them to predators and/or concentrating them on the summits and flanks of submarine banks and seamounts. This mechanism is described as "topographic blockage" in the literature (Genin, 2004). As a result biomass of demersal fish, cephalopods and cetaceans may be elevated in the vicinity of seamounts compared to adjacent deep waters. This in turn has led to the development of high-seas fisheries that are largely unregulated and, as a result, some of the biological communities associated with seamounts (e.g. orange roughy, *Hoplostethus atlanticus*, and deep-sea corals) are threatened (Pitcher and Bulman, 2007).

Topographic blockage was first observed with sonar technology by Isaacs and Schwartzlose (1965) over a shallow ridge off Baja California (100 m summit depth). Similar dynamics were reported by Genin et al. (1988), who used a combination of acoustics (12, 200 and 520 kHz), stratified net sampling and stomach content analysis of predatory fish over a bank of similar depth in the southern California bight. Gut content analyses confirmed that resident rockfish (*Sebastes* spp.) mainly fed on the dominant migrating euphausiid. Rockfish predation furthermore led to a depletion of the scattering layer and thus an increased plankton patchiness downstream of the seamount (Haury et al., 2000). This "gap-formation" in the scattering layer was also observed from Sixty Mile Bank (110 km southwest of San Diego, California) using high-frequency acoustics (120 kHz) and plankton nets, sampling along transects oriented with the prevailing current across the feature(Genin et al., 1994). Predation of seamount fish on migrating scatterers has also been reported from seamounts in the central Pacific and subtropical northeast Atlantic (Genin, 2004). All mentioned reports are from shallow seamounts (<300 m).

Isaacs and Schwartzlose (1965) estimated that the topographic blockage leads to a 40-fold higher influx of carbon than by primary production alone, thus enabling the existance of large populations of planktivorous fish. Most vertically migrating zooplankters are confined to the top-most few hundred meters (Angel, 1985). Observations of topographic blockage to date, therefore, have not explained aggregations of orange roughy and oreosomatids over deep seamounts (700-1500 m).

Enhanced horizontal flux

Current-topography interactions over slopes and peaks often result in greatly amplified near-bottom flows (Mohn and Beckmann, 2002a,b). Enhanced fluxes of suspended food particles and lateral advection of zooplankton may help in sustaining high densities of benthic organisms and – directly and indirectly – resident demersal fish (Genin, 2004; Hirch and Christiansen, 2010).

Fluxes of particulate organic matter and plankton are essential for the establishment of benthic suspension feeders. Photographic surveys combined with current-meter moorings revealed that seamounts harbour rich benthic communities like deep-sea coral reefs at exposed sites which experience high currents and therefore high particle fluxes (Genin et al., 1986; Genin, 1987). These in turn may sustain resident populations of benthivorous fish.

Planktivorous fish can profit directly from strong near-bottom flows, as proposed by the "feed-rest" hypothesis of Genin (2004): site-attached planktivorous fish can rest in quiescent shelters on the seamount surface between feeding intervals while the strong currents replenish the food source. Pelagic fish, in contrast, have to actively swim to renew their exposure to food-replete waters.

Several observations from seamount ecosystems support this feed-rest-benefit (Wilson, 1992) and matching behavioural patterns have been reported from *Sebastes alutus* (Brodeur, 2001) and orange roughy (Lorance et al., 2002). The feed-rest benefit should not be restricted to horizontal fluxes, but might also apply to fish populations supplied by the topographic blockage mechanism discussed above.

Behavioural aspects

In some species of fish intra-specific behaviour (e.g. mating, spawning) causes the formation of dense aggregations over seamounts. This applies to a number of comercially

targeted species like orange roughy (*Hoplostethus atlanticus*), pelagic armorhead (*Pseudopentaceros wheeleri*) and oreosomatids (Zeiformes; Rogers, 1994; Koslow et al., 2000).

Wilson and Boehlert (2004) used a 38 kHz echosounder and an ADCP to demonstrate that behavioural patterns can help to maintain micronekton aggregations on seamounts in the absence of closed circulation patterns. They investigated populations of the sternoptychid fish *Maurolicus muelleri* and the mysid crustacean *Gnatophausia longispina* over an isolated seamount on the northern Hawaiian Ridge. Both species appeared to be able to outswim prevailing currents and thereby resist advective losses.

1.4.3 Pelagic communities

The majority of seamount studies indicate qualitative and quantitative differences between pelagic assemblages in the open ocean and over seamounts (Rogers, 1994). Planktic biomass can be both increased, probably as a result of upwelling (e.g. Genin, 1987) or decreased, probably as a result of predation and the displacement of migrating scatterers during the day (e.g. Genin et al., 1988; Martin and Christiansen, 2009).

Species composition can also be quite different on seamounts and in the surrounding open ocean. Wilson (1992) and Boehlert and Seki (1984) reported that the dominant species of seamount-associated scattering layers (*M. muelleri*, *G. longispina* and the squid *Iridoteuthis iris*) on Hancock seamount were rare or absent in net samples from scattering layers of the surrounding open ocean. Similarly Parin and Prut'ko (1985) report a myctophid, *Diaphus suborbitalis*, that is dominant over Emperor Seamount but rare in the surrounding waters. In a recent study on seamounts in the northeast Atlantic Martin and Christiansen (2009) report the near absence of zooplankton size classes >0.5 cm in net samples from above the summits of two seamounts, while these size classes are found over the slopes and on far-field control stations. Their report, however, is ataxonomic and no conclusions can be drawn from it about differences in species composition. A detailed assessment of the mesopelagic micronekton communities on and close to Cross Seamount was published by De Forest and Drazen (2009) based on an extensive trawl survey. They report a summit assemblage that is dominated by juvenile epipelagic fish and crustacean larvae, whereas the open-ocean assemblage is dominated by myctophids. Furthermore one species of fish (the myctophid *Benthosema fibulatum*) and one cephalopod (the chranchiid squid *Liocranchia reinhardti*) are common over the summit and rare in surrounding waters and are considered as seamount-associated species by the authors.

Both Genin et al. (1988) and De Forest and Drazen (2009) report the absence of vertically migrating taxa in net samples from above shallow seamounts. While Genin et al. (1988) suggested that this might be a result of displacement around the seamount, De Forest and Drazen (2009) speculate on active avoidance.

Reid et al. (1991) coin the term ”mesopelagic boundary fauna” for a micronektonic assemblage occurring around the slopes of the Hawaiian islands but not in the surrounding open ocean.

1.4.4 Benthic communities

A considerable amount of the available literature deals with the benthic communities found on seamounts. Seamounts exhibit broad depth ranges, a variety of substratum types, steep slopes and are often impinged by fast currents. This makes them unique habitats for a wide variety of benthic organisms (Rogers, 1994). Of special interest among the benthic communities are deep-sea corals. Comprehensive reviews can be found in Rogers (1994) and Pitcher et al. (2007).

1.4.5 Seamount diversity and endemism

Seamounts have been hypothesized to be sites of increased diversity and endemism (e.g. de Forges et al., 2000) and have been likened to islands *sensu* MacArthur and Wilson (1967) (Rogers, 1994; McClain, 2007). These claims apply largely to the benthic fauna and the high reported rates of endemism (de Forges et al. (2000) report up to 34% endemic species on southwest Pacific seamounts) have to be treated with care. It is difficult to distinguish between true local endemicity and sampling artefacts, given the overall poor knowledge of the populations inhabiting seamounts and continental slopes worldwide.

Samadi et al. (2006) observed genetic population differentiation in *Nassaria problematica*, a non-planktotrophic gastropod with limited larvae dispersal, between individual seamounts on the Norfolk chain (southwest Pacific). However, no evidence for genetic structuring was found for several crustacean and gastropod species with plantotrophic dispersal stages. McClain et al. (2009) demonstrated that a large percentage of the species found on a Californian seamount are cosmopolitan with ranges extending over much of the Pacific Ocean. While species composition was similar to that of comparable non-seamount habitats, species rank order was reversed on the seamount. This may indicate a fundamental

difference in the structure of benthic seamount communities compared to the continental slope.

While genetic structure has been observed for pelagic open-ocean species and benthic seamount species, the few studies on seamount-associated pelagic species focus on commercial fish stocks (Clark et al., 2010). These studies have generally shown patterns of genetic homogeneity at oceanic or at regional geographic scales among populations sampled on seamounts, as well as the slopes of oceanic islands and continental margins. However, at the regional scale, genetic differentiation has been identified between populations of fish. For example, Patagonian toothfish, *Dissostichus eleginoides*, in the Southern Ocean show genetic differentiation between seamount and non-seamount populations (Rogers et al., 2006). Given that micronekton populations can be retained on seamounts through oceanographical and/or behavioural mechanisms (see Chapter 1.4.2), it would be interesting to investigate their population genetics.

1.4.6 Connectivity of seamount communities

To understand patterns of species richness, and population dynamics of seamount communities it is crucial to obtain knowledge about the connectivity between seamounts in space and time. Factors influencing dispersal and connectivity between populations include intrinsic biological characteristics of species (e.g. life-history traits) and their interaction with the extrinsic features of the marine environment (e.g. currents, bio-physical coupling over seamounts). Together they are responsible for large variations in dispersal distances between species and subsequently seamount community (Clark et al., 2010).

Seamount connectivity has been considered in the context of island-biogeography (see above, McClain (2007)). However, assumptions about connectivity cannot be made from the presence of a given species on several seamounts but direct genetic testing is required (Rogers et al., 2006), and genetic studies are scarce. Furthermore, despite long standing research efforts, connectivity is poorly understood even in littoral communities, let alone in offshore seamounts. Making generalizations about connectivity between seamounts is therefore difficult. The need for additional research is apparent especially as a good understanding of seamount connectivity is critical for conservation and management efforts (Clark et al., 2010).

1.5 The South West Indian Ocean

Unlike the Atlantic and Pacific, the Indian Ocean was only scarcely explored in the early days of deep-sea exploration. It was not until the International Indian Ocean Expedition of 1960-1965 (Zeitschel, 1973) that a substantial part of this ocean, including deep-sea areas, was extensively and systematically sampled. Since then, no similar effort has been undertaken for most of the area, and deep-sea research has largely focused on the Arabian Sea. In general the deep-sea ecosystems of the rest of the region remain poorly explored (Banse, 1994; Ingole and Koslow, 2005).

1.5.1 Physiography

A map of the major physiographic features is given in Figure 1.7, some details concerning the South West Indian Ocean Ridge (SWIOR) and the Madagascar Ridge are given below.

The SWIOR marks the divergent boundary between the Antarctic and the African Plates and dominates the sea-floor of the southwestern Indian Ocean. The ridge has an ultra-slow spreading rate of 12-16 mm/year (Dick et al., 2003). The ridge extends 7700 km from the Bouvet triple junction at 55°S, 0°E to the Rodrigues triple junction at 25°S, 70°E. It is characterised by a very deep (>5000m in places) and rough median valley and is cut by a series of deep, north - south running transform faults (Fisher and Goodwillie, 1997; Sclater et al., 2005). The Ridge features a multitude of submarine mountains and banks, many of which reach into mesopelagic depths (200 m–1000 m), some even into the euphotic zone (<200 m) (Romanov, 2003). However, the bathymetry of the ridge is poorly mapped by direct methods and current knowledge is largely restricted to depth estimates derived from satellite altimetry.

The Madagascar Ridge is an aseismic plateau of intermediate crustal thickness and is directly linked to the microcontinent of Madagascar (Fisher and Goodwillie, 1997). While the broad ridge crest is 1000-2500 m deep, the plateau rises to less than 20 m on the summit of Walter's Shoals which is located roughly 720 km south of Madagascar at 33°12'S, 43°50'E. A total area of 400 km^2 is estimated to be shallower than 500 m and the slopes of the Shoals are reported to be steep (Groeneveld et al., 2006). Other seamounts along the Madagascar Ridge are reported to have summit depths between 84 m to 1100 m (Romanov, 2003). However, soundings from a recent cruise (P. Boersch-Supan, personal observation) indicate that the satellite-derived bathymetry grossly overestimates seamount heights along the

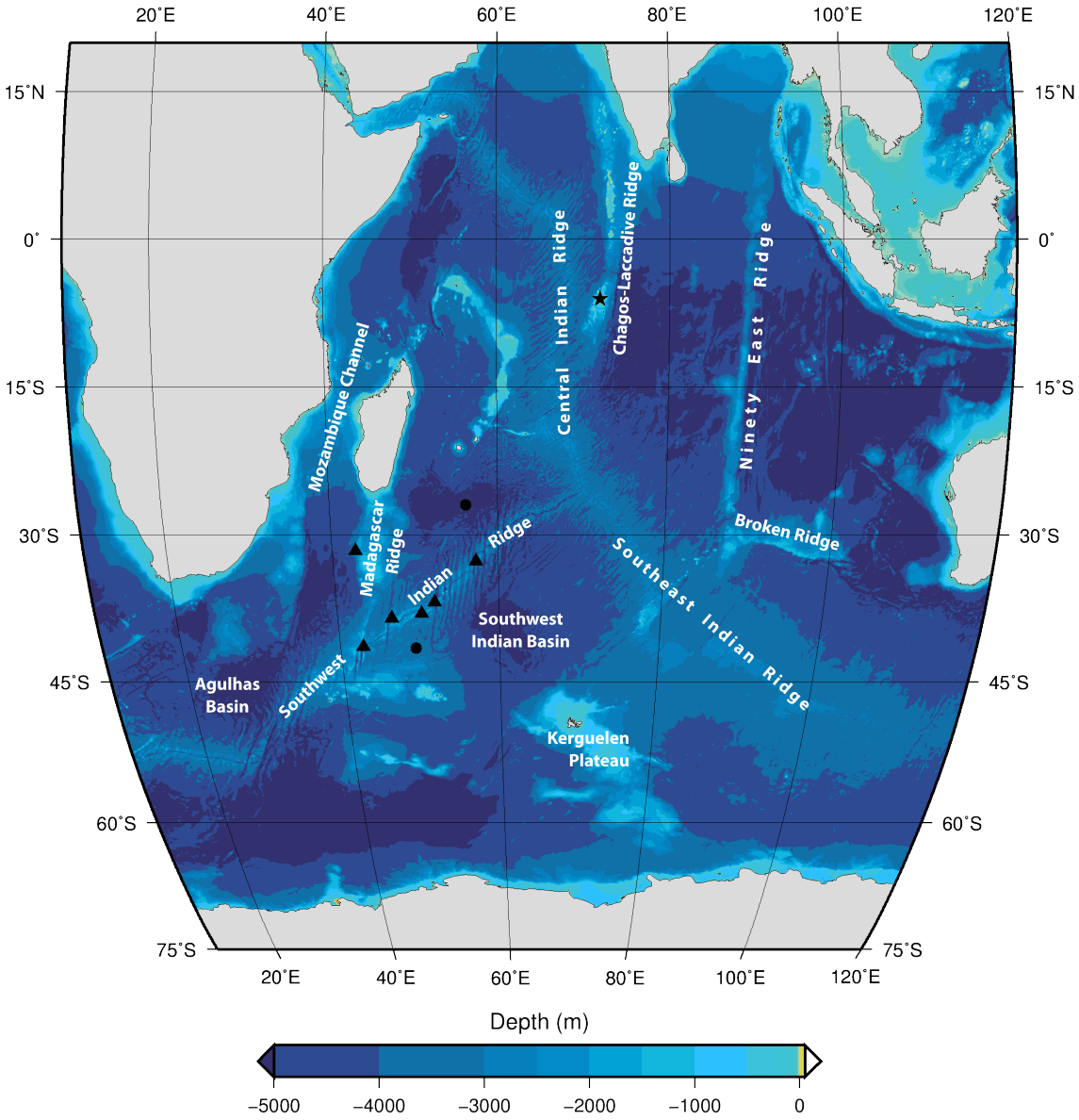

Figure 1.7: Major physiographic features of the Indian Ocean. The main survey locations of this PhD project were 5 seamounts on the Southwest Indian Ridge (SWIR) and 1 seamount on the Madagascar Ridge (triangles), two stations over deep water north and south of the SWIR indicated (circles) and a number of banks and atolls in the Chagos Archipelago (star). Bathymetry data from GEBCO (2010). Feature names from Tomczak and Godfrey (1994)

western slope of the bank.

1.5.2 Regional oceanography

The SWIR is set within an area where the Aghulas Return Current, the Sub-Tropical Front and the Sub-Antarctic Front, further to the south, create one of the most energetic and important hydrographic regions of the world (Read et al., 2000). The seamounts of the ridge lie within an area of complex biogeochemistry, phytoplankton composition and productivity associated with the transition from sub-tropical conditions to Sub-Antarctic. Based largely on patterns of primary production, the Sub-Tropical/Sub-Antarctic Front is also thought to represent a major biogeographic boundary in the Southern Indian Ocean dividing two distinct faunal provinces (Longhurst, 1998; Vierros et al., 2009). In deeper water, the South West Indian Ocean Ridge acts as a major physical barrier to the flow of deep water masses and separates areas of deep-sea floor on the Enderby Abyssal Plain, the Aghulas Basin and the Crozet Basin.

1.5.3 Biology

The fauna inhabiting seamounts in the Indian Ocean are particularly poorly known and there is an urgent requirement to explore these ecosystems to gain a broader understanding of the biodiversity and productivity associated with the Indian Ocean (Ingole and Koslow, 2005). Until now the main sources of information on the biology of these seamounts have been scientific / fisheries reports of past Soviet expeditions related to exploratory fishing which are focused on large-bodied fish populating the ridges of the Indian Ocean (Romanov, 2003; Vereshchaka, 1995). Additional records for some pelagic taxa, mostly mesozooplankton, are available from the International Indian Ocean Expedition (Zeitschel, 1973). However, geographical coverage of the SWIOR is sparse and the records are usually limited to the epipelagic realm and based on relatively small, fine-meshed nets.

Vereshchaka (1995) summarises several investigations on the macrozooplankton occurring on slopes and seamounts in the Indian Ocean, based on net-samples of the benthic boundary layer. Two distinct communities are described, species that were mainly pelagic and decrease in numbers towards the seabed, and seabed-associated ones. The latter group fall into several categories including: animals that are found near the seabed at night but disappear by day, presumably because they migrate to benthic habitats during

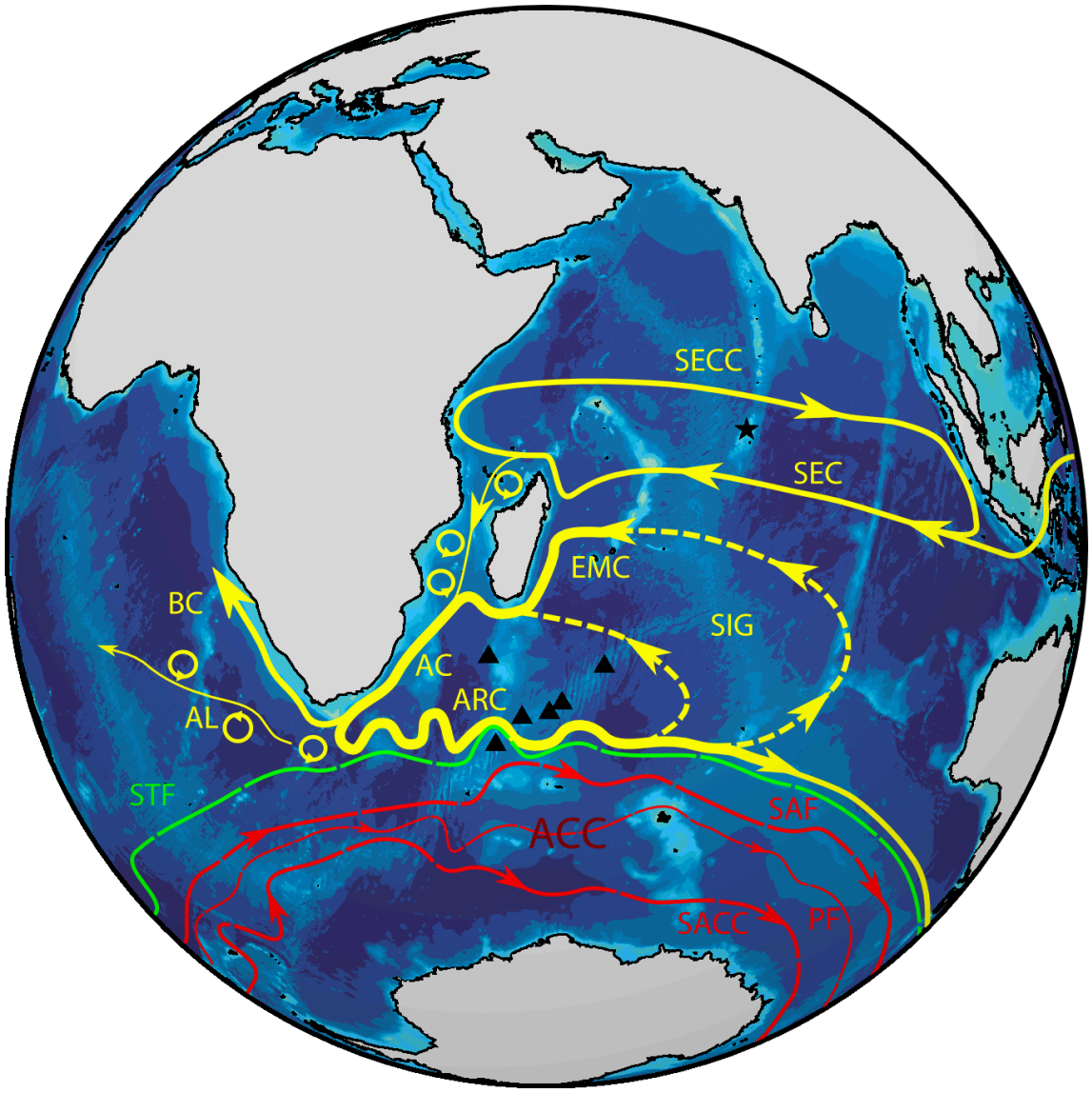

Figure 1.8: Important surface currents and fronts of the Southwest and Central Indian Ocean. Triangles mark the locations of seamounts investigated during 2009 and 2011. The star marks the location of the Chagos archipelago, visited in 2012. Dashed lines mark the subsurface return flow of the Southern Indian Subtropical Gyre. AC, Agulhas Current; ARC, Agulhas Return Current; AL, Agulhas Leakage; SEC, South Equatorial Current; SECC, South Equatorial Countercurrent; EMC, East Madagascar Current; SIG, Southern Indian Subtropical Gyre; BC, Benguela Current; STF, Subtropical Front; SAF, Subantarctic Front; PF, Polar Front; ACC, Antarctic Circumpolar Current; SACC, Southern ACC Front. Figure compiled from Schott et al. (2009); Bard and Rickaby (2009); Tomczak and Godfrey (1994); Talley et al. (2011) and Read and Pollard (2013a). Bathymetry data from ETOPO5 (Sloss, 2005).

daylight hours; animals found well above the seabed by night and descend to the seabed by day; larval animals which are found mainly over areas of seabed inhabited by adults.

Investigations of high seas areas over the Madagascar and Southwest Indian Ocean Ridges for fish resources were undertaken by Soviet research vessels and exploratory fishing vessels from the 1960s to 1998 using heavy trawl gear. Whilst detailed information is not available in English, an extensive list of species present along the SWIOR from 1969-1998 has been published in Romanov (2003). It was noted that species presence was highly variable among seamounts.

As with zooplankton and nekton, the distribution of higher predators, including cetaceans and birds in the region are largely unknown (Shotton, 2006).

1.6 Aims

The micronekton and zooplankton forming oceanic sound scattering layers are a crucial component of open ocean food webs and global biogeochemical cycles. Seamounts, ridges and oceanic islands impact on many aspects of the ecology of these animals. Better knowledge of the processes governing distribution, dispersal and predator-prey dynamics of pelagic biota will determine the spatial and temporal scales at which ecological interactions occur, and have applications in ecosystem modelling, ultimately aiding ecosystems management.

To characterise the influence of abrupt topography on ecological processes in the open ocean this PhD project considered the following aspects:

- The basin scale (10^3 km) distribution of pelagic scattering layers in the southwest Indian Ocean (Chapter 2).
- The potential effects of scattering layer structure on marine mammal foraging (Chapter 3).
- The local scale (10^1 km) distribution of pelagic scattering layers around banks and atolls in the central Indian Ocean (Chapter 4).
- The local scale (10^1 km) distribution and dynamics of scattering layers around SWIR seamounts and the trophic consequences for seamount-associated fish (Chapter 5).

- The population connectivity of a common micronekton species, the hatchetfish *Argyropelecus aculeatus* (Chapter 6).
- The application of molecular identification methods to identify dispersal stages of seamount animals (Chapter 7).

Chapter 2

The distribution of pelagic sound scattering layers across the southwest Indian Ocean

> In developing [the volume reverberation] equation, not only were scatterers assumed to be present in the body of the ocean, but they were considered to be uniformly distributed. From the point of view of scattering, such an ocean would be so simple as to be uninteresting.
>
> Eyring et al. (1942)

Abstract Shallow and deep scattering layers (SLs) were surveyed with split-beam echosounders across the southwest Indian Ocean (SWIO) to investigate their vertical and geographical distribution. Cluster analysis was employed to objectively classify vertical backscatter profiles. Correlations between backscatter and environmental covariates were modelled using generalized additive mixed models (GAMMs) with spatial error structures. Structurally distinct SL regimes were found across the Subantarctic Front. GAMMs indicated a close relationship between sea surface temperature and mean volume backscatter, with significantly elevated backscatter in the subtropical convergence zone. The heterogeneous distribution of scattering layer biota may have implications for predator foraging and carbon cycling in the Indian Ocean.

2.1 Introduction

Pelagic biota in the open ocean are structured at a broad range of spatial and temporal scales (Haury et al., 1978; Steele, 1978). Abundance and assemblage composition vary on scales from millimetres, to miles, to entire ocean basins. Temporal variation encompasses minutes to decades, incorporating daily patterns such as diel vertical migration (Angel, 1985), seasonal cycles (Urmy et al., 2012; Cisewski et al., 2010) and inter-annual trends (O'Driscoll et al., 2009). Drivers of the patchiness are numerous physical and biological factors such as temperature, mixing, current patterns, predator density and food availability.

A substantial proportion of biomass below the photic zone is concentrated in so called sound scattering layers (SLs) which have been observed since the invention of echosounders in the mid 20th century (Christensen et al., 1946; Lyman, 1947). Scattering layer assemblages encompass species from diverse taxa such as myctophid and stomiiform fishes, squids, decapod shrimps and various groups of gelatinous zooplankton (Farquhar, 1977; Bradbury et al., 1970; Pakhomov and Froneman, 2000). They often exhibit high species diversity and as a result acoustic species discrimination and consequently direct biomass estimation are usually not possible. Nonetheless backscatter data, particularly when using multiple acoustic frequencies, can provide rich ecological information. Already in the early decades of scattering layer research, attempts were made to link acoustic information with species abundance and diversity data. For example, investigations were undertaken to determine whether pelagic biogeographical provinces were reflected in the acoustic backscatter signature (Backus and Craddock, 1977; Tont, 1976) or to determine the effects of hydrographic features such as fronts and eddies on scattering layer structure and composition (Cole et al., 1970; Conte et al., 1986). More recently, distinct differences in the vertical structure and/or migration dynamics of pelagic SLs combined with species turnover have been observed across mesoscale oceanographic fronts (Lara-Lopez et al., 2012; Ohman et al., 2013; Cox et al., 2013) and eddies (Godø et al., 2012), confirming that biogeographic patterns are not only reflected in backscatter spectra but also the vertical organisation of scattering layers.

A large proportion of scattering layer biomass undertakes diel vertical migrations (DVM), generally moving from the mesopelagic zone (200-1000 m) into more productive near-surface waters at night, and returning to depth at dawn. This behaviour is thought to balance predation pressure with the need for foraging (Pearre, 2003). Vertical migrators play an important role in marine food-webs as they link surface primary production with

higher trophic levels, but also in marine biogeochemical cycles, as they actively contribute to the downward flux of nutrients and particulate matter (Hidaka et al., 2001; Al-Mutairi and Landry, 2001; Steinberg et al., 2008). Both aspects have only recently been incorporated into in global models of the Earth system (Lehodey et al., 2010; Bianchi et al., 2013b) and there is a need to provide robust estimates of biomass distributions and migration dynamics as inputs into these ecosystem models. This need is particularly pressing, as there is great uncertainty about the global standing stock of scattering layer biota. Recent acoustic studies suggest that the global biomass of mesopelagic fish may have been underestimated by an order of magnitude or more (Kloser et al., 2009; Kaartvedt et al., 2012).

The predators of SL organisms are a diverse set of oceanic nekton, including species of commercial interest such as tunas and billfish (Potier et al., 2007, 2005), marine mammals (Naito et al., 2013; Arranz et al., 2011) and species of conservation concern such as oceanic sharks (Howey-Jordan et al., 2013). Trophic interactions between scatterers and their predators are constrained in space and time by the vertical SL structure and SL migration dynamics on one hand, and the diving capabilities of the predators on the other. Along the continental slope and near oceanic islands and seamounts abrupt topography can mediate predator-prey relationships, as SL organisms can become trapped on these physical features by being blocked on their vertical descent (Isaacs and Schwartzlose, 1965) and/or as a result of diverse flow-topography interactions (Genin, 2004). The import of oceanic biomass through biophysical coupling has been suggested as an explanation for the occurrence of rich benthic communities (Genin et al., 1986; Rowden et al., 2010b) as well as substantial aggregations of high trophic level biota around seamounts (Tseytlin, 1985; Koslow, 1997; Morato et al., 2008, 2009), of which the latter are targeted globally by commercial high-seas fisheries (Pitcher et al., 2010).

Despite the vast expanse of the mid-ocean ridge system, and the ubiquity of seamounts in the global ocean (Yesson et al., 2011; Kim and Wessel, 2011), little is known about the influence of these topographic features on pelagic scattering layers and, ultimately, oceanic food-webs and biogeochemical cycles at a global scale. While locally enriched biomass has been observed, Priede et al. (2013) suggested that, on a basin scale, ridges have a neutral effect on biomass, as the increased benthic biomass on topographic features is balanced by the displacement of pelagic biomass by the topography itself. Opdal et al. (2008) describe scattering layers along the northern Mid-Atlantic Ridge and possible topographical, hydrographical and biological processes shaping them. They report increased pelagic backscatter above a fracture zone that coincides with the northern Subpolar Front. Cox et al. (2013)

used multi-frequency acoustics to estimate epipelagic (<200 m) zooplankton biovolumes and scattering classes across the same front. Their acoustic observations are indicative of faunal turnover across the Subpolar Front, but do not detect a ridge effect.

Apart from a largely descriptive study of scattering layer structure and elephant seal foraging (Boersch-Supan et al., 2012, Chapter 3 of this thesis), no research has been conducted on the large scale distribution of scattering layers in the Southern Indian Ocean or along the Southwest Indian Ridge (SWIR) and this study intends to fill this gap. An understanding of the influence on scattering layers of the regional oceanography and the ridge as a whole is not just important in understanding ecological and biogeochemical processes at the basin scale, but also as a background to understanding the local-scale interactions (c. 10 km) between pelagic biota and individual seamounts, discussed in subsequent chapters of this thesis.

Fisheries acoustic data possess a number of properties which make their statistical analysis challenging. These features include patchiness, scale dependency and spatio-temporal correlation. Modelling acoustic data in a statistically appropriate matter is therefore not trivial, and there is currently a lack of appropriate analytical tools (Ciannelli et al., 2008). Spatio-temporal correlation is particularly pertinent for observations of oceanic SLs, with their continuous extent over large geographic distances, and their often complex vertical migration cycles. Individual sampling units along a vessel's trajectory are highly correlated in space and time. Furthermore space and time are usually confounded in opportunistically collected data, where the movement of the vessel is largely determined by other objectives such as fishing or other surveying tasks and often no replicates are collected at any one location. Positive spatial auto-correlation violates the usual assumption of independence between data points and leads to the underestimation of standard errors, and elevated type I errors, if not accounted for (Legendre, 1993).

Fisheries acoustics are widely employed in routine stock assessments (Fernandes et al., 2002) and a variety of statistical approaches both in survey planning and data analysis are employed to estimate and minimize the effects of non-random sampling in space (e.g. Rivoirard et al., 2000; Petitgas, 2001). Most scattering layer studies, however, have not addressed the issue of spatio-temporal correlation in a systematic fashion. A substantial proportion of the literature is mostly descriptive (e.g. Opdal et al., 2008; Klevjer et al., 2012), while the more quantitative studies tend to address autocorrelation by averaging over space and/or time (e.g. Godø et al., 2012) or reducing spatially explicit observations to derived indices (e.g. Burgos and Horne, 2008; Urmy et al., 2012), resulting in the loss of information,

and complicating the transfer of results into the parameterisation of ecosystems models. Yet other studies do not address the issue of spatial autocorrelation at all (e.g. Hazen and Johnston, 2010).

More recently, generalized additive models (GAMs; Wood 2006) have gained popularity for modelling non-linear relationships between acoustic backscatter and environmental variables (e.g. Zwolinski et al., 2009; Hazen and Johnston, 2010; Murase et al., 2013). GAMs are non-parametric extensions of generalized linear models with a linear predictor involving a sum of smooth functions of covariates. The advantage of a GAM over the explicit specification of non-linearities e.g. in a non-linear least squares framework, is that no *a priori* functional relationship between response and dependent variable has to be assumed. GAMs are data-driven and the data determine the nature and smoothness of the relationship between response and predictors. Cross-validation or likelihood-based methods are employed to prevent over-fitting (Wood, 2006). These methods, however, rely on independent observations, and will not adequately perform when confronted with non-independent observations. In this case there is a risk that an overly-complex smooth term is fitted, leading to false estimates of the functional relationship between a predictor and the dependent variable (Ciannelli et al., 2008).

In this study correlations between environemtal variables and backscattering strength are explored using a modelling framework based on linear mixed models (Pinheiro and Bates, 2000) that incorporates spatial correlation structures, while retaining the flexibilities of GAMs.

2.2 Material and Methods

2.2.1 Data collection

Basin-scale observations of acoustic backscatter were made from two research vessels (*RV Dr. Fridtjof Nansen*, DFN; *RSS James Cook*, JCO) and three fishing vessels in the period between November 2009 and April 2012. Data from the research vessels were collected for the purpose of this thesis, while the data from fishing vessels were collected as part of the Australian Integrated Marine Observing System's Bio-Acoustic Ship Of Opportunity Programme (IMOS; Ryan, 2011). IMOS data were obtained through the IMOS Ocean Portal (http://imos.aodn.org.au/imos/) as mean echointegrated volume backscattering coefficient (s_v (m^{-1}); MacLennan et al., 2002) for cells of 1000 m distance and 10 m depth.

Data from fishing vessels were collected using Simrad ES60 echosounders (Kongsberg Maritime AS, Horten, Norway) operating at 38 kHz, while the research vessels employed Simrad EK60 echosounders operating at 38 kHz and 18 kHz. All echosounders were calibrated following the recommendations of Foote et al. (1987), and accounting for the systematic triangle wave error that is embedded in the ES60 data (Ryan and Kloser, 2004). Calibration parameters for DFN and JCO can be found in Table B.1. All sampling programmes involved the collection of data while the vessels were in transit between sampling stations or fishing locations, usually at speeds around 5 ms^{-1}. Survey tracks are illustrated in Figure 2.1.

2.2.2 Acoustic data processing

Echoview software (Version 4.90, Myriax Pty Ltd, Hobart, Tasmania, Australia) was used to visualise acoustic data in the form of calibrated echograms. Transducer parameters were adjusted during this step using calibration data and environmental parameters were calculated from CTD data using algorithms of Fofonoff and Millard (1983). Processing of the DFN and JCO data followed the IMOS processing framework (Ryan, 2011), which involved filters to remove intermittent noise spikes (Anderson et al., 2005), attenuated pings, persistent intermittent noise and finally background noise (De Robertis and Higginbottom, 2007). The workflow is detailed in Appendix B.2.

Integrated mean volume backscatter (S_v (dB re m^2); MacLennan et al., 2002) was exported as georeferenced cells of 1000 m distance and 10 m depth, to a maximum depth of 1000 m. IMOS data were converted into the log-domain using the relationship

$$S_v = 10 \log_{10}(s_v). \tag{2.1}$$

Apparent solar time for every cell was calculated from midpoint longitude lo_i and UTC timestamp $t_{UTC,i}$ as

$$t_{local,i} = t_{UTC,i} + (lo_i/15) \times 3600 + EoT(t_{UTC,i}) \tag{2.2}$$

where EoT is the equation of time (Meeus, 1998) as implemented in the insol package for R (Corripio, 2013). Sunrise and sunset times were calculated using routines provided by the maptools package (Lewin-Koh and Bivand, 2010). Cells were classified into day, night or twilight, where twilight was defined as 1.5 hours before and after sunset and sunrise (Kloser et al., 2009), and into Austral Summer or Austral Winter.

Table 2.1: Breakdown of along-track sampling units of 1 km length retained for analysis by data source, frequency, time of day and season. Numbers in brackets give the numbers of individual calender days for which data were collected.

		38 kHz				18 kHz		
		IMOS	JCO	DFN	Σ	JCO	DFN	Σ
Time of day	Day	10335	93	2641	13069	150	2641	2791
	Night	9980	70	1811	11861	91	1811	1902
	Twilight	6922	45	1509	8476	93	1509	1602
	Σ	27237	208	5961	**33406**	334	5961	**6295**
Season	Austral Summer	14795	208	5961	20964	334	5961	6295
		(38)	(16)	(26)	(80)	(16)	(26)	(42)
	Austral Winter	12442	0	0	12442	0	0	0
		(31)	(0)	(0)	(31)	(0)	(0)	(0)
	Σ	27237	208	5961	**33406**	334	5961	**6295**
		(69)	(16)	(26)	**(111)**	(16)	(26)	**(42)**

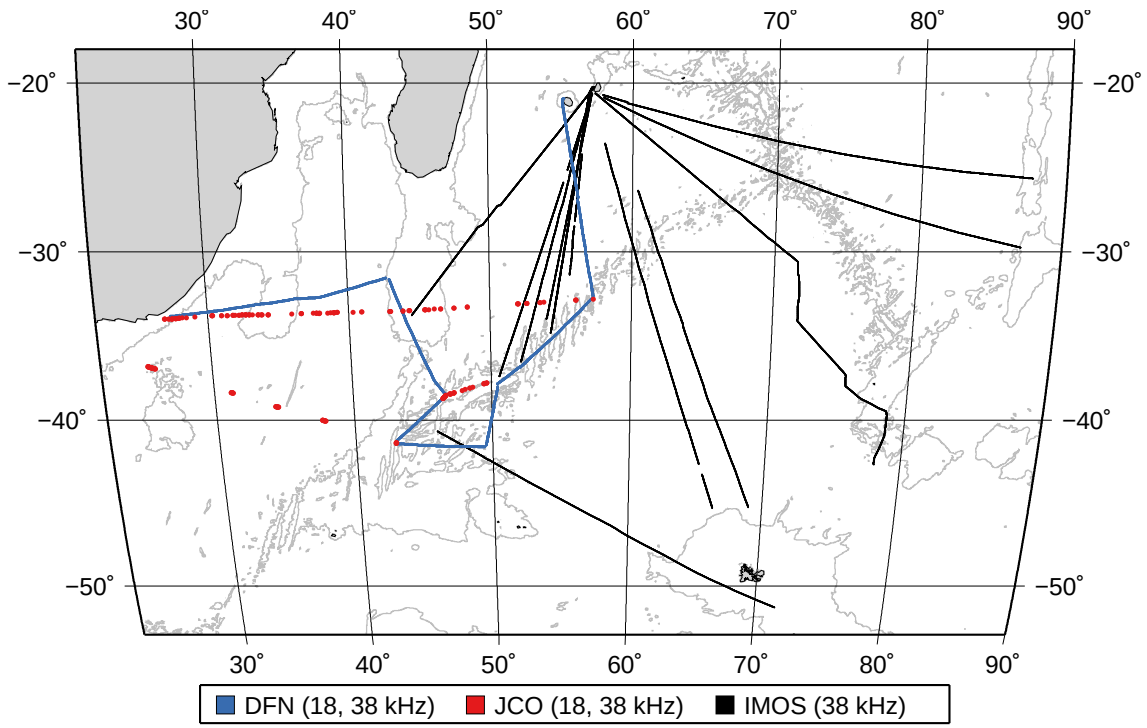

Figure 2.1: Sampling locations, frequencies and sources of acoustic data used in this study. Colours encode the project responsible for sampling. 3000m isobath traced from GEBCO (2010). DFN: *RV Dr. Fridtjof Nansen* Cruise 2009-410; JCO: *RRS James Cook* Cruise 66/67; IMOS: Australian Integrated Marine Observing System, Ships of Opportunity Bio-Acoustic sub-facility.

2.2.3 Environmental covariates

As no *in situ* observations for environmental parameters were available for the IMOS data, environmental parameters were sampled for each acoustic sampling unit from gridded data products based on remote-sensing observations of the sea surface. As the environment at the sea surface is not experienced directly by the vast majority of SL organisms, these predictors can only serve as habitat-proxies.

Sea surface temperature (SST) was sampled from the Operational Sea Surface Temperature and Sea Ice Analysis (OSTIA; Donlon et al., 2012) at a spatial resolution of 1/20°. Surface chlorophyll concentrations were sampled from GlobColour grids at a spatial resolution of 1/24° (Anon., 2010) using monthly model-averaged observations for case 1 water (CHL_1 parameter of GlobColour). Water depth was sampled from the GEBCO bathymetric grid at a resolution of 30 arc seconds (GEBCO, 2010). Sampling from gridded datasets was achieved using a combination of the netCDF operators (NCO Version 4.3.0; Zender, 2008) and the raster package for R (Hijmans and van Etten, 2012).

Distance to the ridge and distance to the nearest coastline were calculated using GRASS (Version 7.0.svn; Neteler et al., 2011) and the geosphere package for R (Hijmans et al., 2012). Spreading ridge axes were taken from Coffin et al. (1998), the axis of the Ninety East Ridge as well as all shorelines were extracted from GEBCO bathymetry.

Remotely sensed SST and chlorophyll concentration were validated against *in situ* surface measurements of temperature and fluorescence made using an SBE 21 SeaCat thermosalinograph (Sea-Bird Electronics, Bellevue, WA, USA) during the two scientific expeditions. OSTIA SST showed a consistent positive offset of about 1°C across the measured SST range, but was otherwise in very close agreement (Pearson's $r = 0.994$, Fig. 2.2A). GlobColour monthly averaged chlorophyll concentrations correlated reasonably well with *in situ* fluorescence measurements (Pearson's $r = 0.536$, Fig. 2.2B). The weaker correlation between the two chlorophyll measures is likely the result of a strong diel fluctuation of the *in situ* fluorescence signal, which is an artefact of physiological and photochemical effects rather than an indication of biomass fluctuations (Falkowski and Kolber, 1995). Direct measurements of *in situ* chlorophyll concentrations were not available at the time of writing.

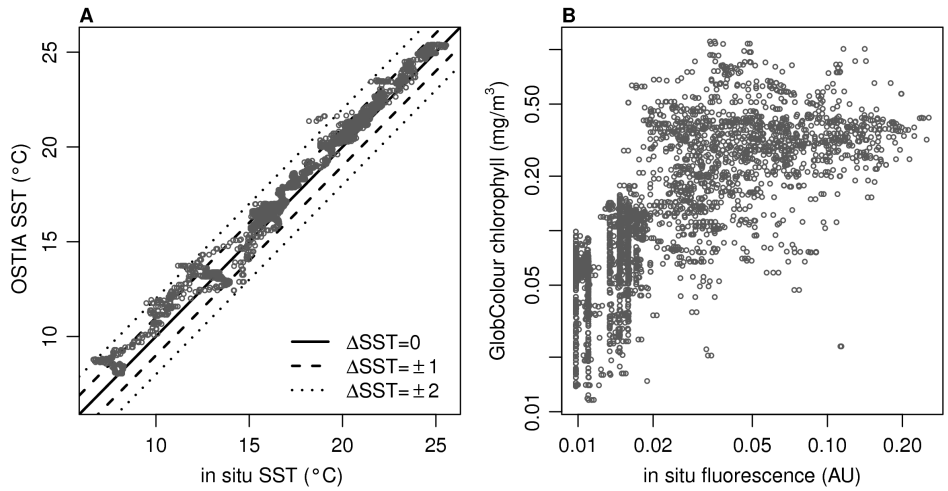

Figure 2.2: Correlations between *in situ* surface measurements and gridded products. **A**: *In situ* sea surface temperature (SST) versus OSTIA SST (Donlon et al., 2012); Pearson's r=0.99. **B**: Log-log plot of *in situ* fluorescence and GlobColour chlorophyll concentration (Anon., 2010); Pearson's r=0.53

.

2.2.4 Statistical analyses

Analyses were performed using the R environment for statistical computing (Version 2.14; R Development Core Team, 2010).

Cluster analysis

Vertical S_v profiles were subjected to cluster analysis in an attempt to objectively classify scattering layer regimes with differing vertical structures. Unconstrained clustering was achieved using *k*-medoids clustering as implemented in the partitioning around medioids algorithm (PAM; Kaufman and Rousseeuw, 1990) as implemented in the cluster package for R (Maechler et al., 2012). PAM was run on distance matrices based on euclidean distances as well as a similarity coefficient described by Gower (1971). The latter measures the similarity between two sites i and j as a weighted average of similarities for all depth strata that are available for both sites

$$S_{ij} = \sum_{k=1}^{n} s_{ijk}\delta_{ijk} / \sum_{k=1}^{n} \delta_{ijk} \tag{2.3}$$

where n is the number of depth strata, s_{ijk} is the similarity between i and j calculated on the kth depth stratum and δ_{ijk} is equal to 0 if the value of the kth depth stratum is missing for one of the sites and 1 it is present at both sites. For each stratum k comprising n sites with $\mathrm{S_v}$ values $x_1, x_2, \ldots, x_n$ the inter-site difference is calculated as

$$s_{ijk} = 1 - \frac{|x_i - x_j|}{R_k} \tag{2.4}$$

where R_k is the range of $\mathrm{S_v}$ values in the stratum.

Goodness of clustering solutions for different prespecified numbers of clusters k was assessed using the overall average silhouette width ($\bar{s}(k)$; Rousseeuw, 1987). This defined as follows: Assume n observations have been clustered into k clusters. For each observation n_i, let $a(i)$ be the average dissimilarity between n_i and all other points of the cluster A to which n_i belongs[1]. $a(i)$ can be interpreted as a measure of how well i is assigned to its cluster (the smaller the value, the better the assignment). For all other clusters C, let $d(i, C)$ be the average dissimilarity of n_i to all observations in C. The smallest of these $d(i, C)$ is

$$b(i) := \min_{C \neq A} d(i, C),$$

which can be seen as the dissimilarity between n_i and the nearest cluster to which it does not belong. Finally,

$$s(i) = \frac{b(i) - a(i)}{\max\{a(i), b(i)\}} \tag{2.5}$$

Observations with a large $s(i)$ (almost 1) are very well clustered, a small $s(i)$ (around 0) means that the observation lies between two clusters, and observations with a negative $s(i)$ are probably placed in the wrong cluster. Thus

$$\bar{s}(k) = \frac{\sum_{1}^{n} s(i)}{n} \tag{2.6}$$

is a measure of how appropriately the data has been clustered.

[1] if n_i is the only observation in its cluster, $s(i) := 0$ without further calculations.

Statistical modelling

Generalised additive mixed models (GAMMs; Wood, 2006) were used to investigate the relationship between environmental variables and backscattering strength in different depth strata and at different frequencies. This family of models allows the inclusion of correlation structures to model the inherent autocorrelation of acoustic survey data.

Models were fitted using different combinations of explanatory variables and optimal models for each response were selected by Akaike's information criterion (AIC; Akaike, 1973). Where multiple models had similarly low AIC scores and did not show significant differences in a likelihood ratio test, the more parsimonious model was selected. Time of day was modelled using a cyclic regression spline. Autocorrelation of residuals was modelled using a first-order autoregressive error structure (AR(1); Pinheiro and Bates, 2000). The AR(1) model was nested within individual survey legs. Models were fitted to integrated backscatter between the surface and 200 m (shallow scattering layer; SSL) and between 200 m and 1000 m (deep scattering layer; DSL) using an identity link function and Gaussian errors.

2.3 Results

A total of 33 406 km of survey track were analysed in this study, largely based on 38 kHz data. 6 295 km of survey track also included observations at 18 kHz. A detailed overview of the data sources and their distribution with respect to echosounder frequency, season and time of day is provided in Table 2.1.

Survey coverage from JCO is sparse, as interference with geophysical and oceanographic echosounders prohibited continuous data collection. Furthermore severe bubble entrainment under the JCO's hull severely degraded data quality and resulted in the rejection of over 80% of the collected pings during initial processing.

2.3.1 Vertical structure

Variations in the vertical backscatter structure were examined using cluster analysis. Average silhouette widths indicated weak structure ($\bar{s}(k) \approx 0.25$; Nagpaul, 1999) and favoured a two cluster solution in all cases. Partitions based on Gower's similarity coefficient had consistently higher $\bar{s}(k)$ values than those based on euclidean distances, indicating tighter clustering (Fig. 2.3).

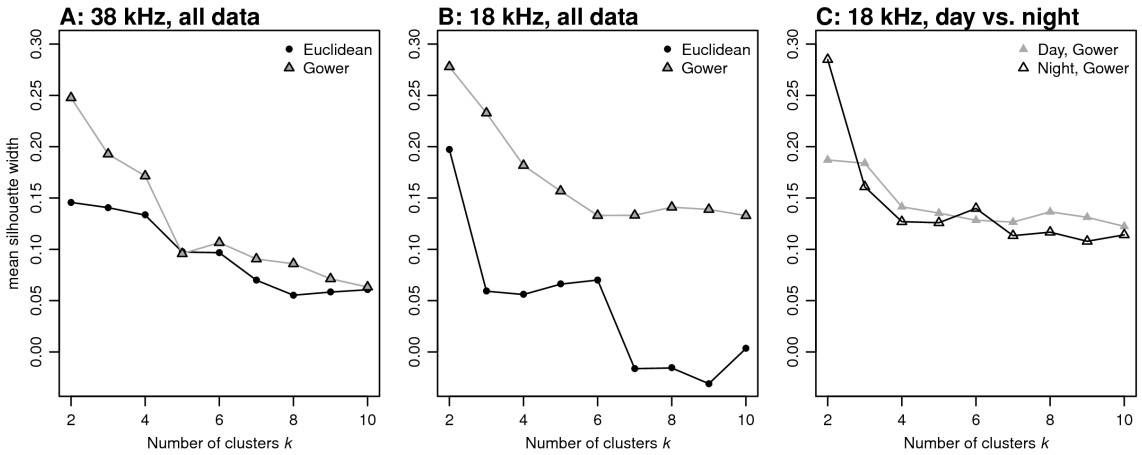

Figure 2.3: Goodness of clustering for different numbers of clusters k and different distance metrics. A: Clustering of all 38 kHz S_v profiles using different distance metrics. B: Clustering of all 18 kHz S_v profiles using different distance metrics. C: Separate analyses for daytime and nighttime 18 kHz S_v profiles based on Gower's metric.

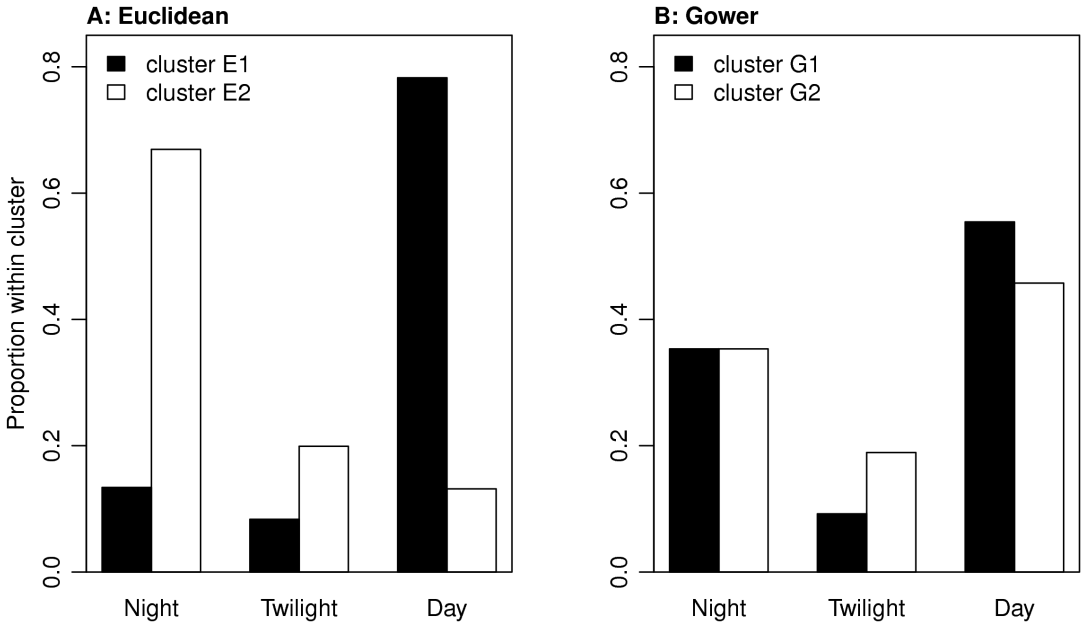

Figure 2.4: Compositions of 38 kHz clusters by diel phase for $k = 2$ based on two different dissimilarity measures.

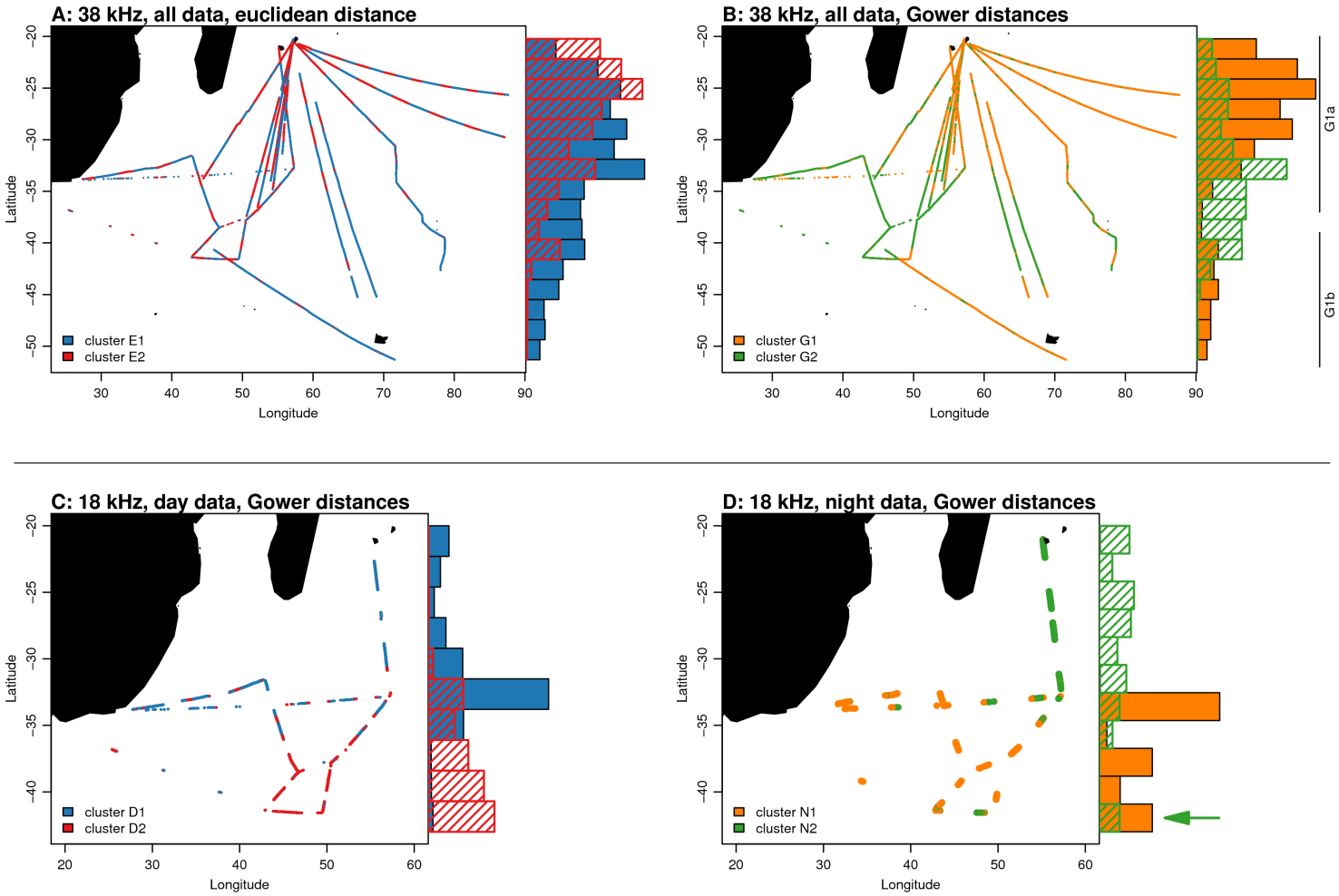

Figure 2.5: Maps of cluster allocations for the 38 kHz and 18 kHz datasets. Marginal histograms visualize the latitudinal composition of each cluster. In all cases $k = 2$ was the optimal partition. A: Euclidean distances partition the 38 kHz S_v profiles into a daytime and a nighttime cluster (cf. Fig. 2.4). B: Gower's distance metric partitions the data into two clusters, of which G1 is geographically discontinuous and can be separated into two sub-clusters G1a and G1b. C: The partitioning of daytime 18 kHz S_v profiles based on Gower's metric splits the dataset into a northern and southern cluster. D: The partition of nighttime S_v profiles largely corresponds to that of the daytime data. The green arrow highlights a transect section near 42°S 48°E classified as belonging to the northern cluster N2.

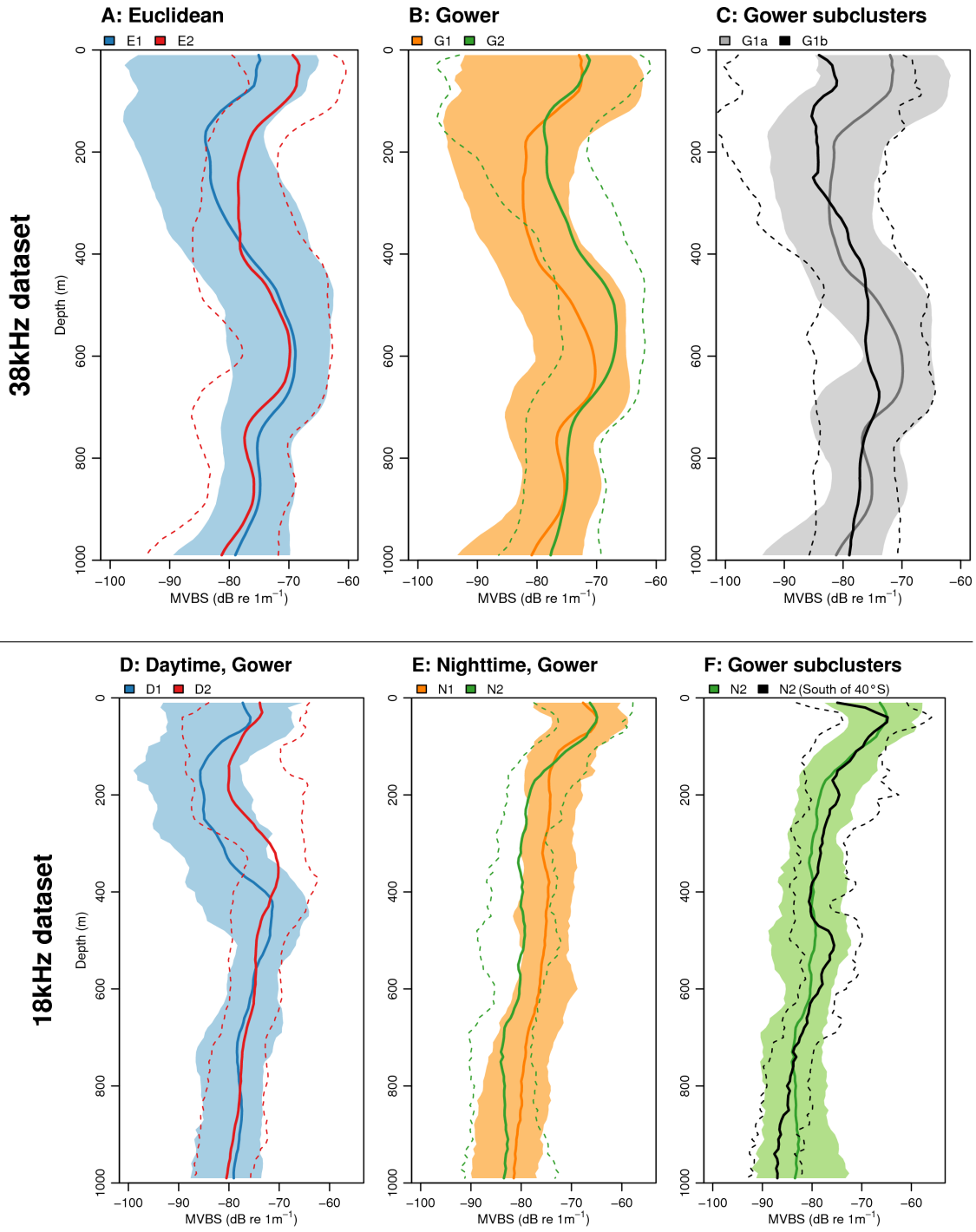

Figure 2.6: Vertical S_v profiles (2.5th, 50th and 97.5th percentile) for the clusters mapped in Figure 2.5. A: Day/night split achieved by euclidean distances. B: Geographic split achieved by the Gower distance metric. C: Geographic subclusters derived from G1. D: Geographic split achieved within the 18 kHz daytime data. E: Geographic split achieved within the 18 kHz nighttime data. D: Subcluster derived from N2.

38 kHz data

For the 38 kHz dataset the composition of the optimal partitions differed markedly between the two underlying dissimilarity metrics. The two clusters based on euclidean distances (E1, E2; Fig. 2.5A) cover the entire geographical range of the data, but their composition with respect to time-of-day is distinct. Cluster E1 contains mostly daytime samples and cluster E2 mostly nighttime samples (Fig. 2.4A). The vertical backscatter profiles differ the most in the top 400 m of the water column (Fig. 2.6A), with the night time cluster E2 exhibiting increased backscatter in this depth interval. The two 38 kHz clusters based on Gower's distances (G1, G2; Fig. 2.4B) are largely indistinguishable with respect to time-of-day, but are well separated in geographic space (Fig. 2.5B). Cluster G2 occupies the latitudinal centre of the survey area (32°S-42°S), while cluster G1 is geographically discontinuous and occupies the northern (<32°S) and southern (>42°S) edges of the survey area. The largest difference in the backscatter profiles is found between 200 m and 700 m depth (Fig. 2.6B), with mid-latitude cluster G2 exhibiting elevated backscatter in this depth interval, as well as a slight upward shift of the shallow S_v maximum in G2 to approx. 50 m. Based on the bimodal latitudinal distribution, G1 can be separated into two subclusters (G1a, G1b; Fig. 2.6C), both of which show less backscatter than the central cluster. The depth profile of the northern cluster G1a shows a distinct shallow and deep scattering layer, which is similar to the layer structure in G2, whereas the layer structure in the south (G1b) is quite distinct indicating several, less pronounced sub-layers.

18 kHz data

For the 18 kHz data the k=2 partitions for both dissimilarity measures resulted in a day-night split. In an attempt to extract a possible geographic structure the dataset was subdivided into daytime and nighttime S_v profiles and subjected to separate PAM analyses based on Gower dissimilarities (Fig. 2.3C), as clusters based on this distance measure had higher $\bar{s}(k)$ values compared to euclidean distances. Spatially separated clusters were obtained for both time periods, with a North-South divide near 35°S in both cases (Fig. 2.5C,D). Daytime S_v profiles differed between the two clusters in the depth of the subsurface S_v maximum (Fig. 2.6D). In the northern cluster D1 deep backscatter peaks around 400 m, whereas D2 exhibits a peak some 50 m shallower as well as elevated backscatter in the surface layer. Nighttime S_v profiles differed in backscattering strength below 100 m, with consistently lower levels in the Northern cluster N2. A short segment of a transect near

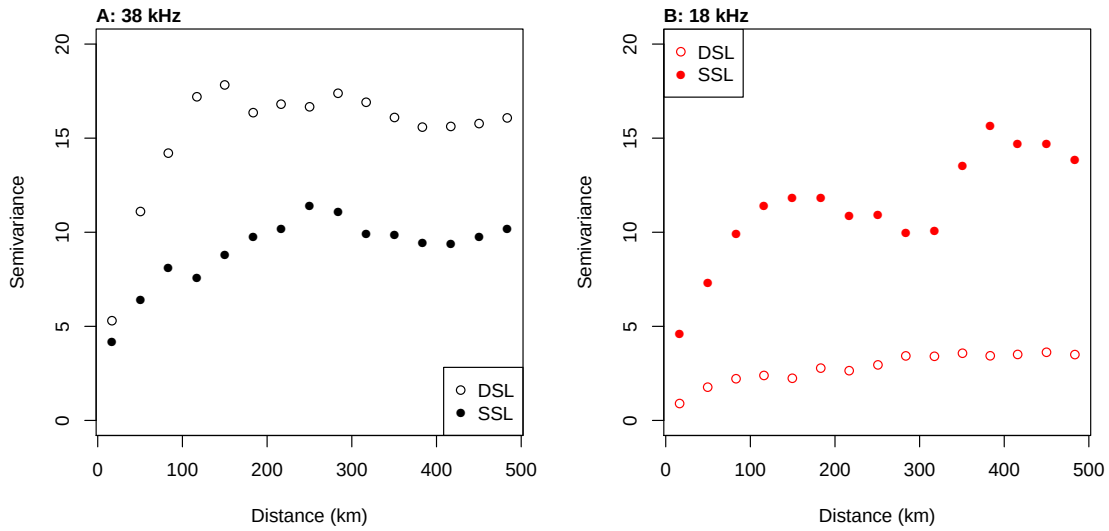

Figure 2.7: Sample variograms of SSL and DSL data. Semivariance increases up to a range of approx. 100 km.

42°S 48°E was classified as belonging to the northern cluster N2 (Fig. 2.5D). S_v profiles in this segment differed from the remainder of cluster N2 by the presence of two deep S_v maxima near 100 m and 500 m depth, respectively (Fig. 2.6F).

2.3.2 Environmental drivers of backscattering strength

Temperature and time of day consistently emerged as important predictors in all models, while chlorophyll concentration was the only predictor that was not included in any of the final models. The correlation coefficient φ of the AR(1) error structure was close to 1 in all cases, indicating strong positive autocorrelation among the residuals. Sample variograms showed increasing semivariance up to a range of approx. 100 km (Fig. 2.7).

38 kHz data

The optimal model for S_v $^{\mathbf{DSL38}}$, the backscatter from the DSL at 38 kHz included smooths of SST (stratified by season), time of day and distance to the nearest shoreline (r^2_{adj}=0.35, AIC=38 418, φ=0.985; Table 2.2, Fig. 2.8). Model output showed that variations in SST across the survey area had the largest effect on S_v $^{\mathbf{DSL38}}$. During Austral Summer the deep scattering layer exhibits a pronounced maximum at approximately 18°C and then drops off substantially towards colder temperatures (Fig. 2.8A). Model predictions for the Winter

Table 2.2: Explanatory variables and corresponding parameters for the GAMMs used to model mean volume backscatter S_V in the deep and shallow scattering layers.

	Dependent variable			
	38 kHz		18 kHz	
	S_v **DSL38**	S_v **SSL38**	S_v **DSL18**	S_v **SSL18**
Parametric terms[a]				
(Intercept)	-76.918^{***}	-73.031^{***}	-75.587^{***}	-73.407^{***}
	(0.154)	(0.306)	(0.0565)	(0.2691)
Depth		$2.64 \times 10^{-4**}$		
		(7.33×10^{-5})		
Smooth terms[b]				
s(SST):Summer	7.999^{***}	8.195^{***}	8.565^{***}	6.422^{**}
	(85.59)	(52.38)	(48.70)	(3.665)
s(SST):Winter[d]	6.940^{***}	8.329^{***}		
	(24.28)	(95.48)		
s(Time of day)	5.905^{***}	7.873^{***}		
	(17.75)	(240.41)		
s(Time of day):OnSWIR			7.168^{***}	7.610^{***}
			(19.66)	(75.20)
s(Time of day):OffSWIR			6.699^{***}	7.320^{***}
			(24.77)	(28.70)
s(Depth)			6.743^{***}	2.825^{***}
			(17.07)	(9.717)
s(DistRidge)		1.929^{***}	8.023^{***}	
		(24.61)	(22.00)	
s(DistCoast)	8.735^{***}		7.589^{***}	
	(22.20)		(12.87)	
Terms excluded from all models during model selection				
Chlorophyll				
AR(1) correlation coefficient[c]				
φ	0.985	0.936	0.815	0.943
	(0.983,0.987)	(0.931,0.940)	(0.792,0.836)	(0.933,0.952)
Other measures				
AIC	38 418	100 150	15 380	20 389
r^2_{adj}	0.356	0.663	0.732	0.545
Num. obs.	32 456	32 456	6 166	6 166

$^{***}\ p < 0.0001$, $^{**}\ p < 0.001$, $^{*}\ p < 0.01$

[a] parameter estimate (std. error)

[b] effective degrees of freedom (F)

[c] parameter estimate (95% CI)

[d] 18 kHz data were only collected during Austral Summer

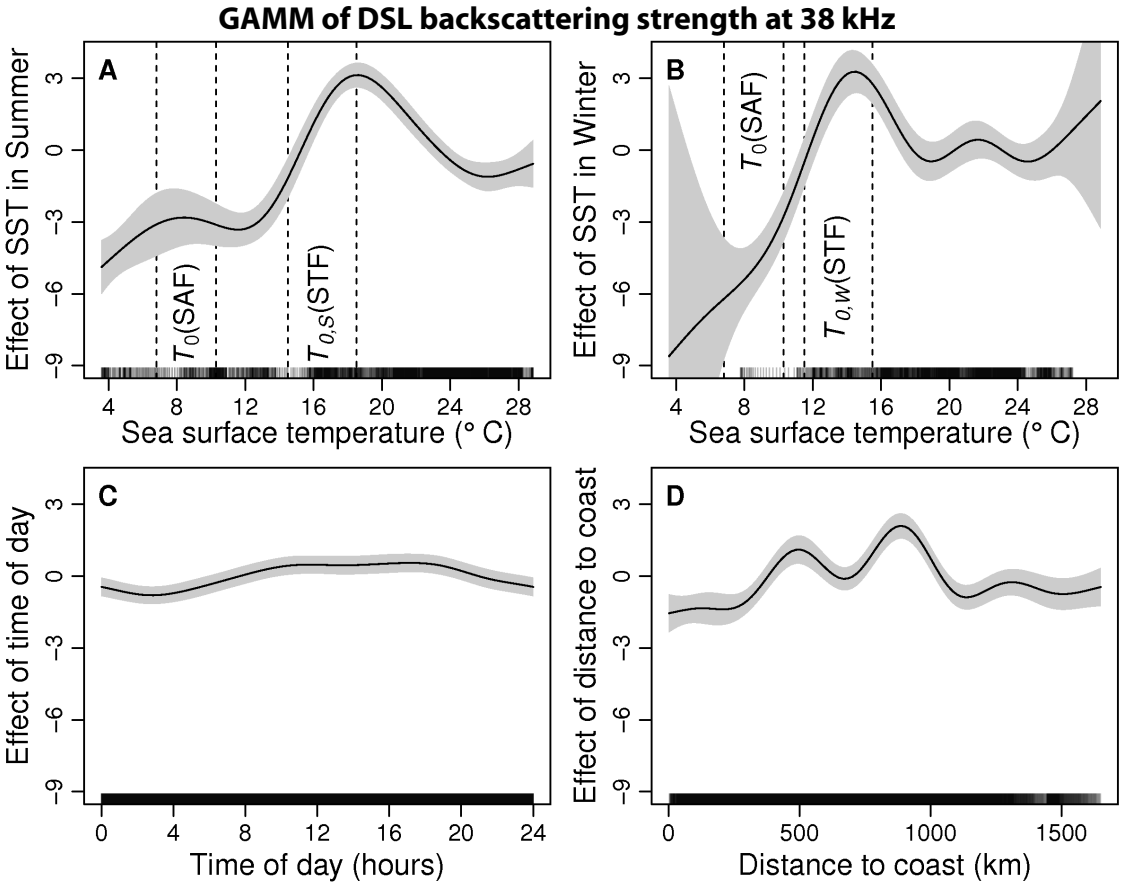

Figure 2.8: Smooths of generalized additive model terms showing the effect of various continuous variables on DSL backscattering strength at 38 kHz. The solid lines are the estimates of the smooths, the shaded areas are standard errors of the estimated smooths, taking into account the error in the model intercept. Dashed vertical lines in panel A and B indicate the axial temperature ranges T_0 of the subantarctic (SAF) and subtropical fronts (STF), respectively (Belkin and Gordon, 1996). Subscripts *S* and *W*, denote STF Summer and Winter T_0 ranges, respectively.

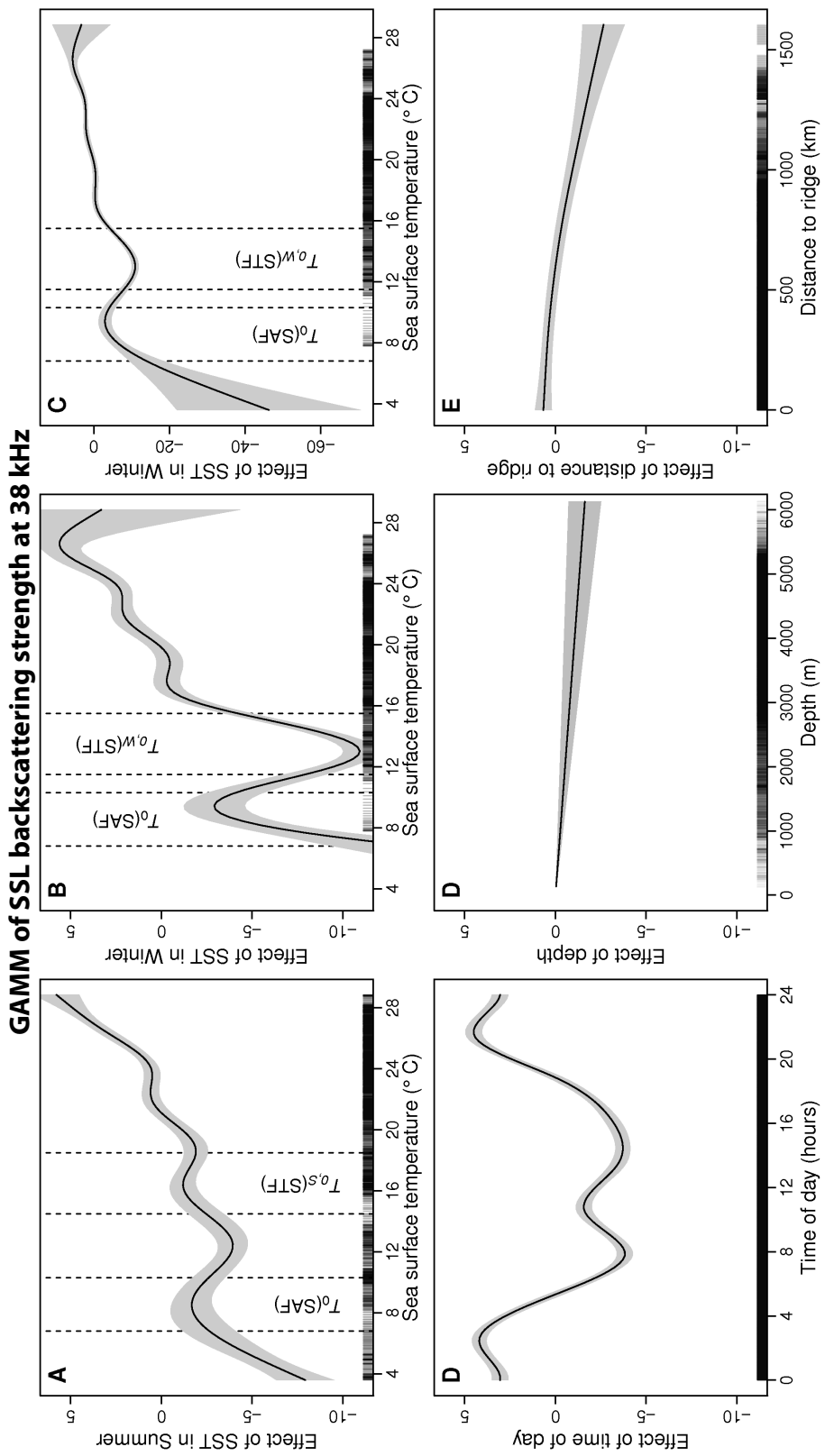

Figure 2.9: Smooths of generalized additive model terms showing the effect of various continuous variables on SSL backscattering strength at 38 kHz. The solid lines are the estimates of the smooths, the shaded areas are standard errors of the estimated smooths, taking into account the error in the model intercept. Panels B and C show the same smooth term, but with different y-axis scales. Dashed vertical lines in panel A and B indicate the axial temperature ranges T_0 of the subantarctic (SAF) and subtropical fronts (STF), respectively (Belkin and Gordon, 1996). Subscripts S and W, denote STF Summer and Winter T_0 ranges, respectively.

have much larger standard errors at the extremes of the sampled temperature range, but the model exhibits a local $S_v^{\mathbf{DSL38}}$ maximum at 14°C (Fig. 2.8B). Time of day shows a weaker effect on $S_v^{\mathbf{DSL38}}$, with a minimum around 03:00 hrs local time and peaks during local daytime (Fig. 2.8C). Distance to shore proved to be a highly significant predictor during model selection and show moderate effect sizes and a complex relationship with $S_v^{\mathbf{DSL38}}$ (Fig. 2.8D).

The optimal model for backscatter from the SSL at 38 kHz ($S_v^{\mathbf{SSL38}}$) included a linear depth term and smooths of SST (stratified by season), time of day, and distance to the nearest ridge (r^2_{adj}=0.66, AIC=100 150, φ=0.936; Table 2.2, Fig. 2.9). Again, SST showed the largest effect on backscatter, although for the SSL there is a general trend of decreasing $S_v^{\mathbf{SSL38}}$ with temperature (Fig. 2.9A-C). Two local maxima appear during summer near 17°C and 8°C, while during winter there is a pronounced local minimum at 13°C and a local maximum at 9°C. Time of day shows a pronounced effect with elevated backscatter at night time, peaking just before and just after midnight and a local maximum during noon (Fig. 2.9D). The influence of water depth is weak, with $S_v^{\mathbf{SSL38}}$ increasing linearly towards shallower depths (Fig. 2.9E), and the distance to ridge term shows fairly stable levels of backscatter within 500 km of a ridge followed by a slight decrease (Fig. 2.9F).

18 kHz data

The optimal model for $S_v^{\mathbf{DSL18}}$, the backscatter from the DSL at 18 kHz, included smooths of SST, time of day (stratified by location on or off SWIR) and depth, and both distance measures (r^2_{adj}=0.73, AIC=15 380, φ=0.815; Table 2.2, Fig. 2.10). Model output showed that distance to the Ridge had the largest individual effect on $S_v^{\mathbf{DSL38}}$, with a sharp increase at distances beyond 1200 km (Fig. 2.10E). Temperature also had a large effect with a local $S_v^{\mathbf{DSL18}}$ maximum at approximately 17°C followed by relatively high values towards colder temperatures and another rise in backscatter at temperatures below 10°C (Fig. 2.10A). Time of day showed a weaker effect on $S_v^{\mathbf{DSL38}}$, that differed significantly at locations on the SWIR relative to elsewhere. In both cases, daytime backscatter was elevated relative to night time backscatter, with afternoon backscatter on the ridge being elevated relative to off the ridge (Fig. 2.10B,C). The influence of water depth is moderate at depths, with $S_v^{\mathbf{SSL38}}$ increasing linearly from 1500 m towards shallower depths (Fig. 2.10D). No depth effect was seen at depths beyond 1500 m. Distance to shore proved to be a highly significant predictor during model selection and show decreasing $S_v^{\mathbf{DSL18}}$ towards both extremes of the predictor range (Fig. 2.10F).

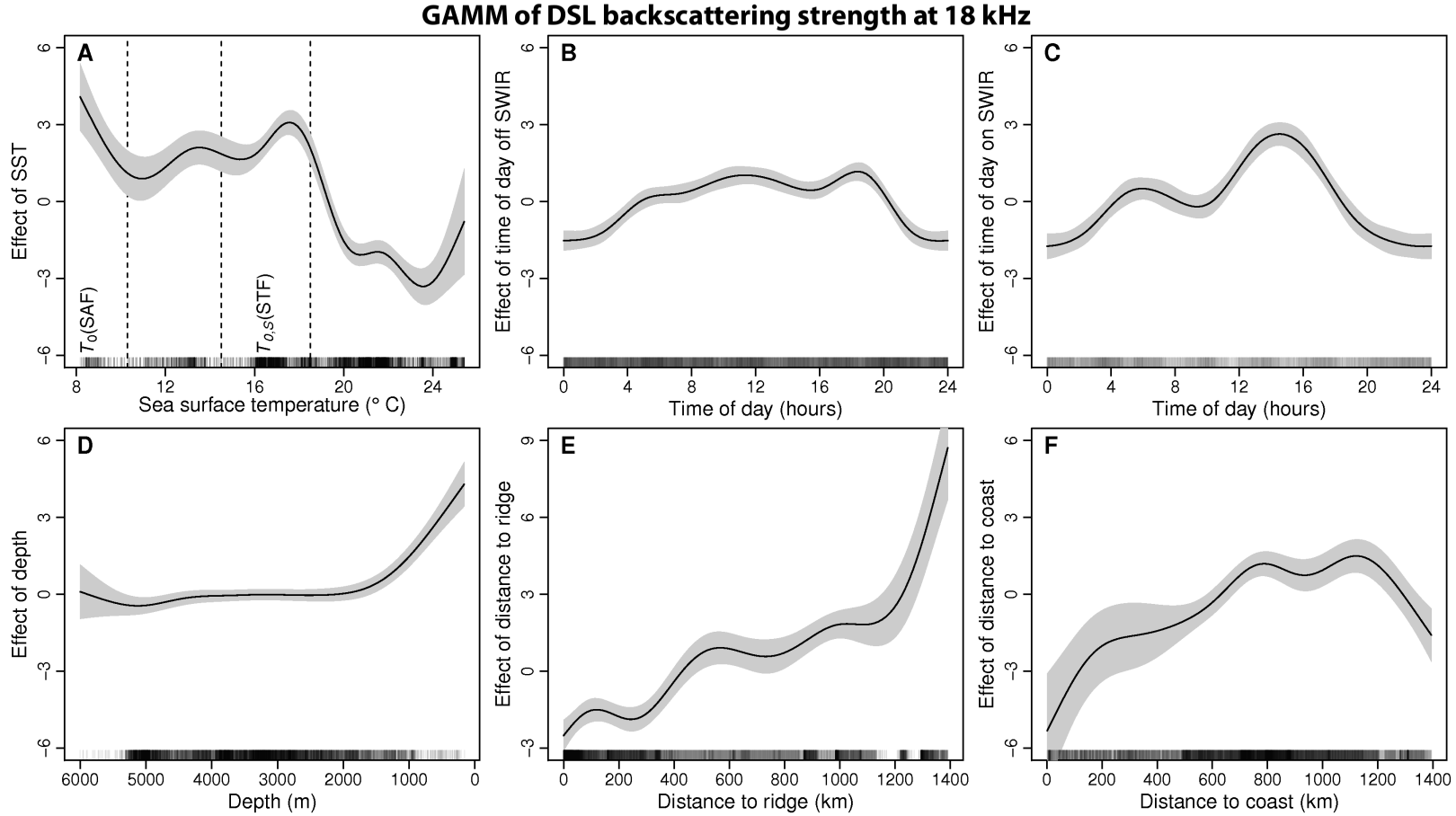

Figure 2.10: Smooths of generalized additive model terms showing the effect of various continuous variables on DSL backscattering strength at 18 kHz. The solid lines are the estimates of the smooths, the shaded areas are standard errors of the estimated smooths, taking into account the error in the model intercept. The y-axis of panel D is shifted relative to the remaining panels to accommodate the range of the effect, but the scale is not altered. Dashed vertical lines in panel A and B indicate the axial temperature ranges T_0 of the subantarctic (SAF) and subtropical fronts (STF), respectively (Belkin and Gordon, 1996).

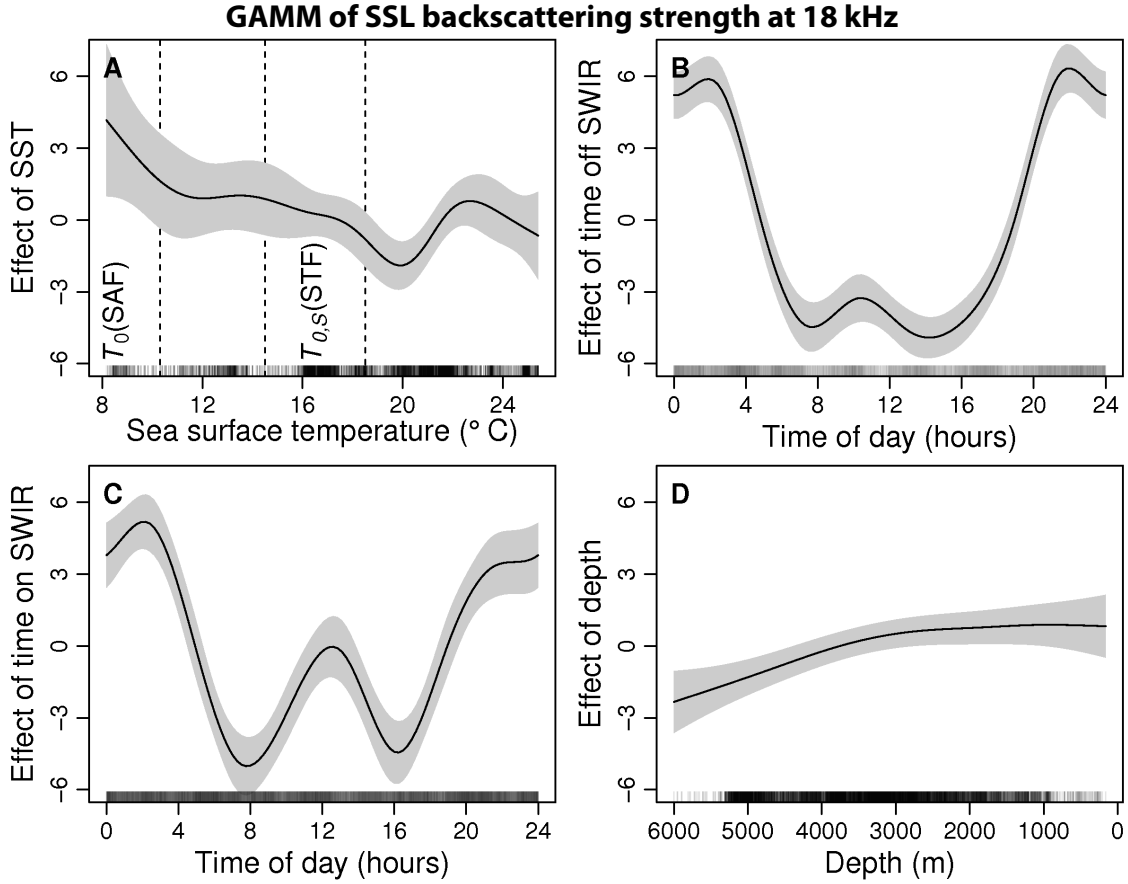

Figure 2.11: Smooths of generalized additive model terms showing the effect of various continuous variables on SSL backscattering strength at 18 kHz. The solid lines are the estimates of the smooths, the shaded areas are standard errors of the estimated smooths, taking into account the error in the model intercept. Dashed vertical lines in panel A and B indicate the axial temperature ranges T_0 of the subantarctic (SAF) and subtropical fronts (STF), respectively (Belkin and Gordon, 1996).

The optimal model for backscatter from the SSL at 18 kHz (S_v $^{\mathbf{SSL18}}$) included smooths of SST, time of day (stratified by location on or off SWIR), and distance to the nearest ridge (r^2_{adj}=0.55, AIC=20 389, φ=0.943; Table 2.2, Fig. 2.11). Time of day showed the largest effect on backscatter. In both strata S_v $^{\mathbf{SSL18}}$ was elevated during the night, but while off the ridge backscatter remains low during the day (Fig. 2.11B), there is a secondary backscatter peak around noon on the ridge (Fig. 2.11C). There is a general trend of increasing S_v $^{\mathbf{SSL18}}$ with decreasing temperatures, with a local minimum at 20°C (Fig. 2.11A). The influence of water depth is comparably weak, with S_v $^{\mathbf{SSL18}}$ decreasing linearly from 3000 m towards deeper depths (Fig. 2.11D).

2.4 Discussion

2.4.1 Vertical structure

Clustering based on Gower's dissimilarities provided weak evidence of three structurally distinct scattering layer regimes for both frequencies. The approximate boundaries of these regions are along 32°S and 42°S, which roughly corresponds to the boundaries of the Subtropical convergence zone (SCZ). The northern and central regimes are structurally similar, both exhibiting a pronounced shallow and deep scattering layer, although the vertical positions of these layers are shifted upwards by 50–100 m in the SCZ. The scattering layer structure in the area south of 42°S was quite different, with backscatter being distributed more uniformly through the water column. These results confirm an earlier, descriptive analysis of scattering layer structure across the Subantarctic Front (Boersch-Supan et al., 2012, Chapter 3 of this thesis), and are in line with step changes in scattering layer structure observed across oceanographic fronts elsewhere (Cole et al., 1970; Lara-Lopez et al., 2012; Ohman et al., 2013). In particular, the shallowing of the daytime 18 kHz DSL south of the convergence is consistent with a faunal turnover from species with larger swimbladders in the North to species with smaller swimmbladders in the South, which would shift the resonance depth upwards in the watercolumn (cf. Fig. 1.5. This matches observations from trawl samples, which feature the myctophid *Ceratoscopelus warmingii* and the hatchetfish *Argyropelecus aculeatus* as numerically dominant species in the North, whereas the smaller sternoptid *Maurolicus muelleri* is dominant in the South (K. Kemp, pers. comm.; see Fig. 1.2 for a size comparison).

The Subtropical (STF) and Subantarctic Fronts (SAF) are thought to represent major

biogeographic boundaries, dividing distinct faunal provinces in the southern Indian Ocean (Longhurst, 1998; Vierros et al., 2009). Previous research, as well as the biological sampling programme run concurrently to the acoustic surveys analysed in this study, confirms the role of the SAF as a faunal boundary across multiple trophic levels from microbes (Djurhuus and Rogers, 2013) and macrozooplankton/micronekton (Pakhomov et al., 1994; Letessier et al., 2014) to cephalopods (Laptikovsky et al., 2014) and fishes (K. Kemp, personal communication). As both acoustic properties and vertical position in the water column are species specific properties, the drastic change in the vertical structure of the SLs is not surprising.

2.4.2 Backscatter and sea surface temperature

GAMM results indicate a strong effect of SST on the backscattering strength. There is a pronounced local maximum in backscatter from the DSL at both observation frequencies in temperature range indicative of the STF (Figs. 2.8A,B and 2.10A), and this S_v maximum appears to follow the seasonal shift of the STF axial temperature (Figs. 2.8A,B). Increased backscatter, as well as increased net-sampled macrozooplankton/micronekton biomass have also been observed in the SCZ south of Cape Agulhas (c. 20°E; Barange et al., 1998; Pakhomov et al., 1994), while no net increase in acoustic backscatter was reported across the STF east of New Zealand, where the frontal temperature gradient is much shallower (McClatchie et al., 2004). Another local maximum in DSL backscatter appears in the axial temperature range of the SAF. This more pronounced in the 18 kHz data (Fig. 2.10A) than in the 38 kHz data (Fig. 2.8B), and not evident for the Winter subset of the 38 kHz, where sparse observations lead to very large model errors (Fig. 2.8B). Increased 18 kHz backscatter across a subpolar front was also observed by Opdal et al. (2008) in the North Atlantic.

The pattern is not quite as clear for backscatter from the SSL. The 38 kHz backscatter generally decreases with temperature. The vertical S_v profiles for these data suggest that this might be an artefact caused by the shallowing of the SSL across the SCZ (Fig. 2.6B), resulting in the movement of scatterers into the so called surface deadzone, i.e. the part of the water column, that is shallower than the downward-looking, hull-mounted echosounder transducer can sample (O'Driscoll et al., 2009). However, the S_v profile for 38 kHz backscatter south of the SAF (Cluster G1b, Fig. 2.6C) further suggests an actual decrease in surface backscatter in the southern part of the survey area. This might be reflected in the

steeper decrease in $S_v^{\mathbf{SSL}38}$ south of the SAF (Fig. 2.9A), although it is difficult to estimate the relative contributions of both effects. 18 kHz backscatter from the SSL steadily increases across both frontal zones, which for the SAF matches the observations of Opdal et al. (2008) in the North Atlantic.

The results of this study have potential implications for energy flux to the deep sea. The southern hemisphere SCZ has been estimated to provide approximately 5% of the global net primary production in the oceans (Longhurst et al., 1995, see also Fig. 2.12). If the results of Barange et al. (1998), Pakhomov et al. (1994) and this study are indeed indicative of elevated deep micronekton biomass across the SCZ in the southern Atlantic and Indian Ocean, a larger proportion of this production than previously thought may be actively exported to the deep ocean.

2.4.3 Ridge effect on backscattering strength

No compelling evidence could be found for an effect of the ridge on backscatter. An on ridge/off ridge factor variable was discarded during model selection, as it did not improve model fit, although stratifying the time-of-day smooth by this variable did improve both 18 kHz models. However, most 18 kHz samples within the SCZ were collected on the ridge, confounding potential effects of the frontal zone with those caused by the ridge. In fact, the cluster analysis does not provide evidence for distinct vertical structures between the ridge and elsewhere within the frontal zone (Figs. 2.5C,D). Depth and distance to the ridge were retained as a predictor in the 38 kHz SSL model (Fig. 2.9E). Distance to ridge exhibited a negative effect at large distances from the ridge (>750 km), which applies to data sampled near the African continental shelf and in the wider vicinity of Kerguelen Plateau, suggesting no role of the ridges themselves in this result. Depth was the weakest predictor in this particular model and indicates slightly increased backscatter with decreasing depth More convincing evidence for a ridge effect comes from the 18 kHz DSL model. Large effect sizes (>10 dB, equivalent to >10 fold on the linear scale) are predicted (Fig. 2.10E), although again, the biggest effect is predicted at ranges >1200 km from the ridge indicating effects of the African and/or Kerguelen shelf break, rather than from the SWIR. The model, does however predict a stepwise reduction of backscatter by approximately 3 dB, equivalent to a two-fold reduction on the linear scale, within 400 km of the ridge. Depth is also retained in the 18 kHz DSL model, with a strong positive effect (3 dB) at depths shallower than 1500 m. Generally, these results have to be treated with care, as both distance measures are rather

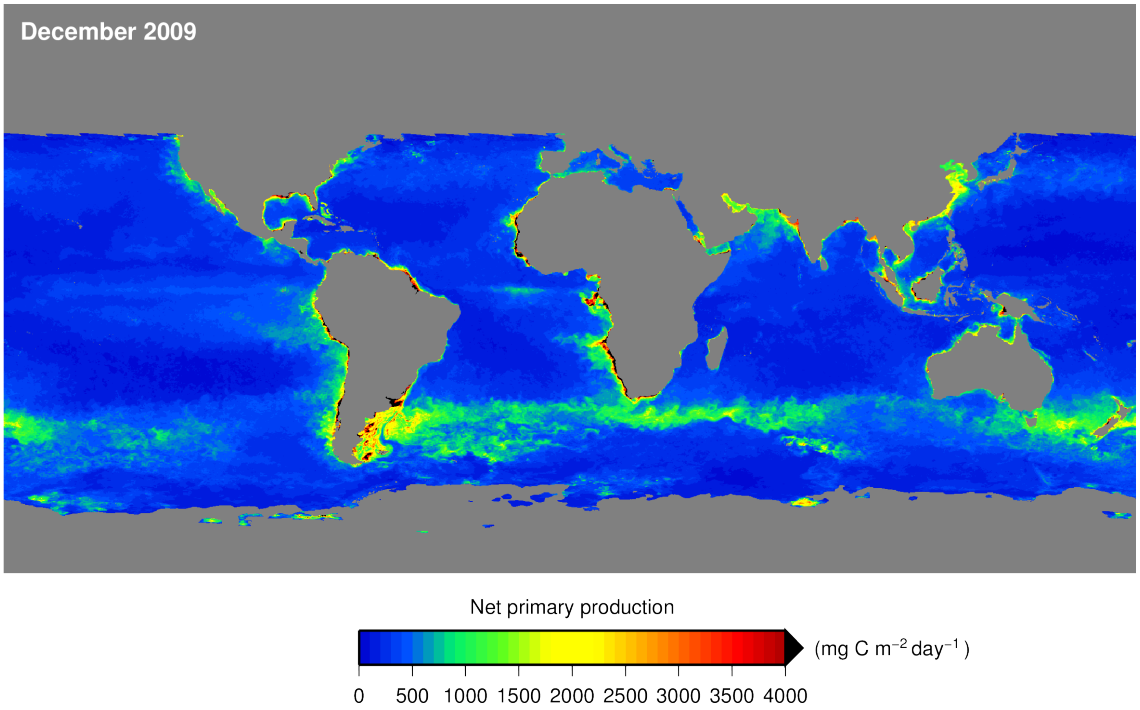

Figure 2.12: Estimate of net primary production for December 2009. The subtropical convergence zone is clearly visible as a band of elevated productivity in the southern Atlantic, southern Indian Ocean and the southwestern Pacific. Data are based on the vgpm algorithm (Behrenfeld and Falkowski, 1997) and were obtained from http://science.oregonstate.edu/ocean.productivity/.

crude metrics on a basin scale, potentially just capturing unexplained variation caused by unidentified factors.

Similar to Opdal et al. (2008) and Cox et al. (2013), this study could not detect an effect of the ridge on backscattering strength. This may be because the ridge does not exert an effect on scattering layers, at the vertical and geographical scale investigated. It contrasts observations of Priede et al. (2013), who present a notable increase of deep scattering layer biomass around the Reykjanes ridge at spatial scales of hundreds of km. However, Priede et al. (2013) ascribe this to behavioural associations with topography and not locally increased pelagic productivity, maintaining that the effect of mid-ocean ridges on basin-scale total biomass is neutral. They do not present any data to support this, and no aggregating effect is apparent for the continental slopes in their dataset, casting some doubt on the aggregation versus enhanced productivity conjecture.

2.4.4 Diel variations in backscatter

Apart from temperature, time of day consistently exhibited pronounced effects on backscatter in all models. Generally model fits indicated high levels of backscatter during the day and lower levels during the night for the DSL, and the opposite pattern for the SSL. This pattern conforms to a DVM cycle with scatterers moving out of the mesopelagic zone and into the euphotic zone at night and returning to deeper water during day (Angel, 1985; O'Driscoll et al., 2009). However, the diel backscatter cycle was more complex, with the SSL exhibiting a secondary peak around local noon as well as a secondary trough at local midnight (Figs. 2.9D and 2.9B,C). The causes for this are less clear, although a possible explanation could again be scatterers migrating into and out of the surface deadzone during the extremes of the diel cycle. Some evidence supporting this is provided by the fact that the noon peak of the DVM cycle in the 18 kHz SSL is more pronounced in the "on SWIR" smooth, compared to the "off SWIR" smooth (Fig. 2.11B,C), which corresponds to a shallower and more intense SSL in the southern cluster D2, compared to the northern cluster D1 (Fig. 2.6D).

Vertical migrations within and between sampled volumes, however, may not be the only factors causing diel backscatter variations. The acoustic target strength, i.e. the propensity of a given target to reflect acoustic energy, can be strongly dependent on the aspect at which a target is insonified. Target strength of mesopelagic fishes can vary by several orders of magnitude between extreme tilt angles, i.e. head up vs. head down (Benoit-

Bird and Au, 2001; Yasuma et al., 2003, 2010), adding considerable uncertainty to acoustic biomass estimates (e.g. Demer, 2004). Observations of the *in situ* orientation of scattering layer organisms are scarce, but significant day-night differences in the orientation of myctophids and *Cyclothone* spp. have been reported from the Pacific (Barham, 1970). Target strength furthermore is not independent of depth, as migrations through the hydrostatic depth gradient can alter swimbladder volume. This can bias target strengths, in particular near the resonance frequency, leading to artifical increases of backscatter at particular depths (Godø et al., 2009).

2.4.5 Conclusions and outlook

Overall the analysis showed a heterogeneous distribution of pelagic backscatter across the southwest Indian Ocean. Hydrographic features explained a large amount of the variation in the data, with increased backscatter at both the STF and SAF. Cluster analysis suggests structurally distinct scattering layer regimes north and south of the SAF, which together with differing $\mathrm{S_v}$ intensity patterns between the two frequencies south of the SAF indicates that acoustic observations can indeed delineate biogeographical regions. No strong evidence of a ridge effect was found at the basin scale.

GAMMs performed adequately, although they came with a high computational cost. Individual GAMMs for the full 38 kHz dataset took between 0.3 and 2.2 hrs to fit on a high-performance workstation (MacPro 5,1 with 12 processor cores and 48 GB of memory; Apple Inc., Cupertino, CA, USA), consuming about 7 GB of working memory in the process. GAMs for the same data but without a correlation structure were usually fitted in less than a minute. With programs like the IMOS Bio-Acoustic Subfacility, the amount of scattering layer data are likely to increase considerably in the future, and there is an imperative to try to make the most out of these data. Fisheries acoustics are certainly not an unbiased sampling methodology for pelagic biota, but few, if any, sampling technologies can provide information across mid to high-trophic level biota with the same spatial and temporal coverage. Computational limitations can probably be addressed by more efficient software and better hardware, but the quest for better analytical tools remains for acoustic data. This study addresses spatial and temporal correlation along the survey track, but is limited to a set of independent models with an arbitrary depth stratum of integrated backscatter as a response variable. This reduces ecological information and leaves some uncertainty in the interpretation of model results, e.g. of the underlying causes for differ-

ent time-of-day smooths. Ultimately the aim for analyses of scattering layer data should be depth-explicit models that capture both geographical as well as vertical patterns in one unified framework. Such a model could be useful to produce spatially and temporally explicit predictions of scattering layer density and diel vertical migration dynamics, which could in turn be used to parameterize ecosystems models (e.g. Lehodey et al., 2008). As fronts appeared to be important sites for SL biota future work should explore the use of environmental gradients as predictors.

Chapter 3

Scattering layer structure and elephant seals: A comment on foraging behaviour observed in the Southern Indian Ocean

Abstract McIntyre et al. (2011, Mar Ecol Prog Ser 441:257–272) concluded that climate-change related ocean warming may lead to deeper foraging dives by Southern elephant seals as their prey moves into deeper depths. They further assert that fitness for the seals will be reduced because of greater physiological costs for deep dives and the assumption that deep foraging is less successful. Their conclusions are based on an observed correlation between a temperature index and elephant seal diving depth, and do not include any observations of prey. We recently observed pronounced differences in the vertical distribution of pelagic biota – biota that may well include elephant seal prey – across the same frontal zone considered by McIntyre et al. (2011) and believe that the observed link between temperature and diving depth is actually a link between predators and prey – a reflection of adaptive foraging behaviour in a complex and dynamic pelagic system. As such, the analysis of McIntyre et al. (2011) is uninformative about likely impacts of ocean warming.

3.1 Introduction

The southern elephant seal (*Mirounga leonina*) is an abundant apex predator in the circumpolar Southern Ocean ranging from the Subtropical Front to the Antarctic continent (Biuw et al., 2007; Ling and Bryden, 1992). It is the deepest diving pinniped with adult males able to reach depths in excess of 2300 m (Costa et al., 2010). Elephant seals are wide-ranging long-lived animals in a dynamic and heterogeneous environment and must be adapted to large variations in prey availability on large temporal and spatial scales (Costa, 1993; Biuw et al., 2007; Forcada et al., 2008). Their foraging behaviour is ultimately driven by the distribution of their prey in space and time (Hindell et al., 2011; Dragon et al., 2012), and elephant seals have been observed to be able to adapt their diving behaviour seasonally and in differing hydrographic conditions (Bailleul et al., 2007; Biuw et al., 2007, 2010).

McIntyre et al. (2011) studied the diving behaviour of southern elephant seals Mirounga leonina from Marion Island (southwest Indian Ocean) in relation to a number of hydrographic and biological variables, and observed a significant positive correlation between a temperature index and the diving depth. They concluded that diving behaviour is influenced by ocean temperature, and further, that as the Southern Ocean warms because of climate change, elephant seals will have to dive deeper. However, their analysis and the employed predictors are not suitable to detect effects of climate change for the following reasons: (1) The temperature index they use is likely to be a proxy variable for watermass and not an ocean warming indicator; (2) some statistically significant model results are not biologically meaningful; (3) data on the pelagic environment of the southwest Indian Ocean from recent transects across the subtropical convergence and Subantarctic Front demonstrate step changes in the vertical structure and community composition of pelagic biota (K. Kemp pers. comm.; Letessier et al., 2014; Laptikovsky et al., 2014), indicating distinct prey fields on either side of the frontal zone; (4) several alternative explanations such as seasonal and regional effects on diving depth were not explored in the analysis; and (5) the asserted link between time-at-depth and foraging success is tentative. Here, we address these issues and propose an alternative explanation for dive-depth variability based on prey distribution.

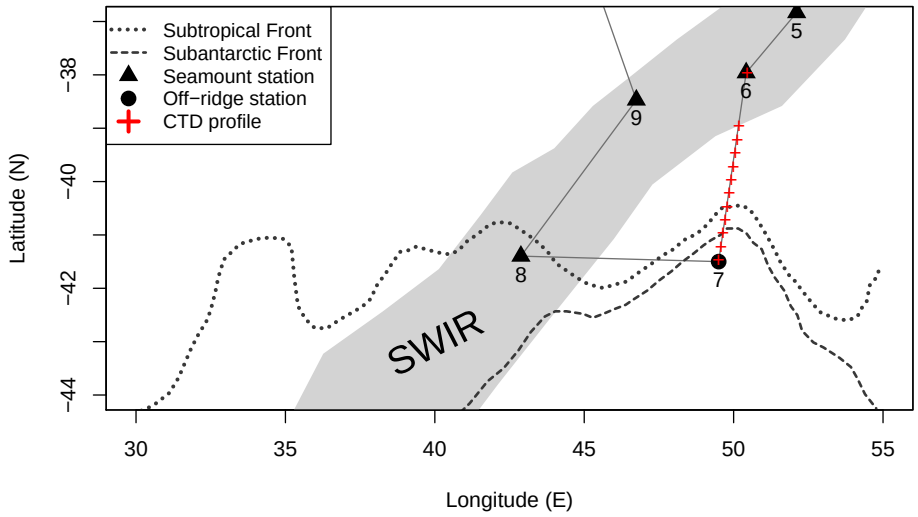

Figure 3.1: Map of the Southwest Indian Ocean and the trajectory of *Nansen* cruise 2009-410. Light shaded areas indicate submarine ridges. Dashed lines indicate approximate locations of hydrographic fronts during the survey (Read and Pollard, 2013a) Stations are: (5) Sapmer Bank, (6) Middle of What Seamount, (7) Off-ridge South, (8) Coral Seamount, (9) Melville Bank. SWIR, Southwest Indian Ridge.

3.2 Materials and Methods

This chapter is based on a small subset of the data presented in Chapter 2. Observations of acoustic backscatter and hydrography were made from *RV Dr. Fridtjof Nansen* from 27 November to 29 November 2009 during a crossing of the subtropical and subantarctic front. The study area is illustrated in Figure 3.1.

Acoustic data were collected using a Simrad EK60 echosounder operating at 38 kHz and 18 kHz. Data were processed in Echoview software (Version 4.90, Myriax Pty Ltd, Hobart, Tasmania, Australia) to remove intermittent and background noise, following the protocol of Ryan (2011), and plotted as calibrated echograms using custom R code. Sampling and data processing methods are described in detail in Chapter 2.2.2 and Appendix B.2 of this thesis.

Conductivity, temperature and pressure data were collected at 12 locations (Fig. 3.1) using a SeaBird Electronics SBE 911+ CTD and deck unit. CTD data were processed by the duty technician before being made available to scientists (T. Mork, pers. comm.). The processing path consisted of conversion from binary to ascii format, wild edit (calculating mean and standard deviation on blocks of 2 scans on the first pass and 20 scans on the second pass), correction for the cell's thermal mass , low pass filtered (conductivity, oxy-

gen and fluorescence over 0.03 and pressure over 0.15), pressure reversals or slowdowns were removed with loopedit (minimum velocity 0.25). The data were then averaged to 1 dbar and salinity and density calculated. CTD data were read into R using the oce package (Kelley, 2012) and temperature profiles were used to derive $T_{\max}100$, the maximum temperature recorded below 100 m (McIntyre et al., 2011).

Average daytime diving depths of adult and sub-adult southern elephant seals were obtained from McIntyre et al. (2011).

3.3 Results and Discussion

3.3.1 Temperature, frontal zone positions and the use of daily averages

The temperature index employed by McIntyre et al. (2011) is the daily average of the maximum temperature recorded below 100 m during a dive ($T_{\max}100$). As the thermal watercolumn structure north of the Polar Front is usually characterised by a shallow temperature-maximum and a monotonic decrease in temperature (Belkin and Gordon, 1996; Boehme et al., 2008), $T_{\max}100$ is likely to represent the temperature at, or near 100 m (Fig. 3.2), a depth that is 300 to 700 m shallower than the mean foraging depths reported by McIntyre et al. (2011, see our Fig. 3.3B). Given that they base their conclusions on the assumption that the vertical distribution of prey species will change with ocean warming it it would have been more appropriate for their models to be based on the in situ temperature at foraging depth.

Judging from temperature profiles that we collected during a crossing of the Agulhas Front, Southern Subtropical Front and Subantarctic Front in late 2009 (Rogers et al., 2009; Read and Pollard, 2013a), the $T_{\max}100$ index is closely related to the geographic location of a temperature profile relative to the individual fronts (Fig. 3.2) and therefore a proxy for watermass. In fact, the temperature at 100 m has been used for the very definition of frontal locations (Belkin and Gordon, 1996). In addition to $T_{\max}100$, McIntyre et al. (2011) employ a factor in their initial models to indicate the position of a dive relative to the fronts. This predictor is dropped in most of their final models, possibly because of collinearity with the temperature index based on the relationship between $T_{\max}100$ and watermass. Furthermore, the temperature variation encountered by foraging elephant seals in the frontal zone is likely to be influenced by smaller scale features (days, 10s of km), such as mesoscale eddies (Dragon et al., 2010, 2012; Bailleul et al., 2010; Campagna et al.,

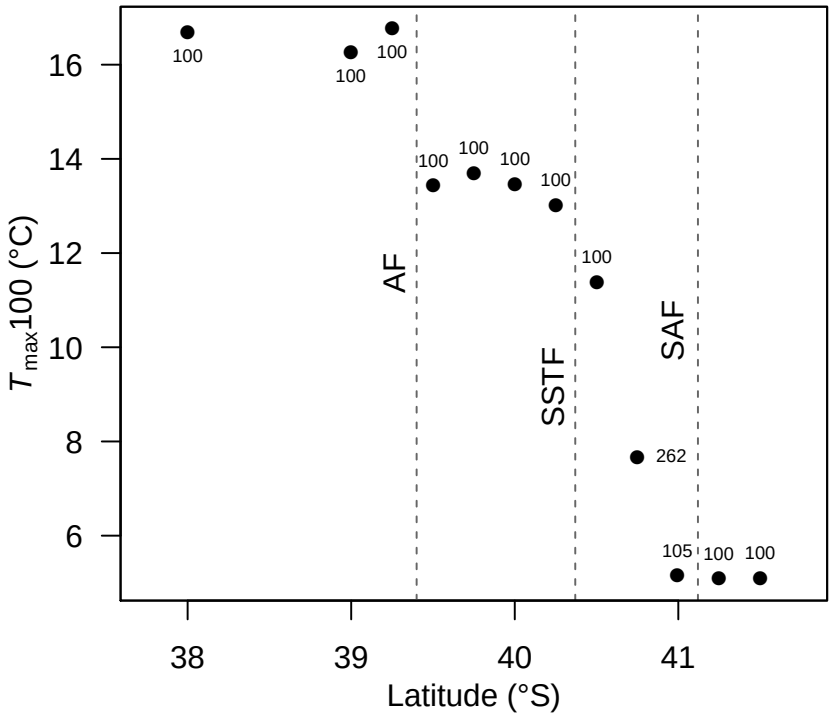

Figure 3.2: Relationship between $T_{\max}100$, $T_{\max}100$.depth and frontal locations for a CTD transect crossing the Subantarctic Frontal zone in the southwest Indian Ocean. Numerals indicate $T_{\max}100$.depth (m). Front locations were determined from full CTD casts according to criteria from Belkin and Gordon (1996) and are indicated by dashed lines. $T_{\max}100$ indices were calculated according to McIntyre et al. (2011). (AF, Agulhas Front; SSTF, Southern Subtropical Front; SAF, Subantarctic Front).

2006), while the location of a dive relative to the fronts would only explain temperature variation on large temporal and spatial scales (months, 100s of km). This scale-dependent temperature variation likely makes $T_{\max}100$ a better predictor for any variation in diving behaviour, therefore favouring it during model selection.

In addition to $T_{\max}100$ being a watermass proxy rather than an ocean warming indicator, the use of daily temperature averages is prone to confound the relationship between temperature, watermass, relative position of a dive in relation to the fronts, and seal diving behaviour, as elephant seals are capable of travelling over 100 km day^{-1} (McConnell and Fedak, 1996; Biuw et al., 2003) and forage in a highly variable environment.

3.3.2 Effect sizes and variability in predictors and model results

McIntyre et al. (2011) set out to investigate potential effects of ocean warming on elephant

seals. Their analysis, however, does not distinguish between climate effects (small, <1°C) and natural environmental variation (large, >10°C) in their study area, especially regarding the magnitude of the effect that these distinct sources of variation have on ocean temperature. Elephant seals forage in extremely diverse habitats where oceanographic and topographic features such as fronts, eddies, seamounts, and shelf breaks influence prey availability on a variety of spatial and temporal scales (Biuw et al., 2007; Charrassin et al., 2008; Simmons et al., 2010; Maxwell et al., 2012). While the biophysical coupling associated with these diverse habitats and processes is influenced by climate, the effect of present climate change is very small compared to the environmental variability within and between the habitats.

The surface waters around Marion Island have been warming at an approximate rate of 0.03 °C yr^{-1} in recent decades (Mélice et al., 2003). At intermediate depths (700 to 1000 m), warming rates have been estimated to be in the order of 0.006 °C yr^{-1} (Gille, 2002). In contrast to this, the $T_{\max}100$ index employed by McIntyre et al. (2011) has a range of approximately 10°C across the frontal zone (Fig. 1). It is difficult to see how their model could distinguish a climate signal from environmental variability when the latter is several orders of magnitude greater. In addition, any measurable climate effect on ocean temperature would be within the measurement error of at least one of the two sensor types used by McIntyre et al. (2011). Boehme et al. (2008) show that the temperature accuracy of the CTD satellite-relay data loggers (SRDLs) is between $\pm$0.005 °C and $\pm$0.03 °C after post-deployment corrections. However, this does not apply to the temperature-only Series 9000 SRDL, which incorporates an uncalibrated thermistor as a temperature probe. The manufacturer (Sea Mammal Research Unit, University of St. Andrews, UK) claims an accuracy of $\pm$0.1 °C (www.smru.st-andrews.ac.uk/protected/downloads/SRDL9000X.pdf), but does not quantify the long-term stability of accuracy.

Concerning their model results, McIntyre et al. (2011) highlight the statistical significance of the relationship between temperature and diving depths. The biological meaning of this result is, however, not explicitly discussed, and the reporting of log-transformed and untransformed coefficients side-by-side does not help the interpretation of model results. Their estimate for the temperature effect on log-transformed adult male diving depth is reported as 0.03, which approximately translates into a 1 m diving depth increase per 1°C temperature increase. Even under drastic ocean warming, a few metres of difference in diving depth are ecologically meaningless, as oscillations in scattering layer depth of 10s of m are common (cf. Fig. 3.3A, C). The effect is much more pronounced for female seals at

c. 10 m °C^{-1} (McIntyre et al., 2011), but this is also of little biological relevance in the context of minute warming rates. The female result does, however, become ecologically meaningful when considering the much greater temperature difference between watermasses. Using our temperature data and the model estimate from McIntyre et al. (2011), female southern elephant seals are expected to dive approximately 100 m deeper north of the Subantarctic Front.

3.3.3 The vertical structure of pelagic biota across fronts and eddies

We have surveyed the pelagic environment of the southwest Indian Ocean (Rogers et al., 2009) and collected data on the distribution and diversity of zooplankton and nekton in the top 1000 m of the watercolumn using a calibrated multi-frequency echosounder and a midwater trawl. Our results confirm that the Subantarctic Front is a significant biogeographic boundary (e.g. Pakhomov et al., 1994, Chapter 2 of this thesis). The environments on either side of the front are characterised by distinct micronekton assemblages (Letessier et al., 2014; Laptikovsky et al., 2014, K. Kemp, pers. comm.) as well as marked differences in the vertical structure of biomass distribution and diel vertical migration behaviour (see Chapter 2).

The environment north of the front is characterized by a thin surface-scattering layer, a very thick deep-scattering layer and moderate amounts of diffuse backscatter at depths below 700 m. The scattering layer structure south of the front is much more complex, featuring at least 4 distinct daytime layers at different depths but only weak backscatter in the deepest strata (Fig. 3.3A,C). Scattering layers on either side of the front follow different patterns of diel vertical migration. North of the front, a substantial proportion of 38 kHz backscatter is located in a non-migratory deep-scattering layer, whereas the main scattering layer at 18 kHz is migratory, rising from 300 m to the surface at night. South of the front the shallower layers show more extensive vertical migration than the deeper ones at both frequencies. The top-most layer ascends from approximately 200 m to 50 m at night while the deepest layer remains stationary.

Elephant seals are wide-ranging long-lived animals in a dynamic and heterogeneous environment and must be adapted to large variations in prey availability in time and space (Biuw et al., 2007). Their foraging behaviour is ultimately driven by prey distributions (Hindell et al., 2011; Dragon et al., 2012), and elephant seals are able to adapt their diving behaviour seasonally and in differing hydrographic conditions (Bailleul et al., 2007; Biuw

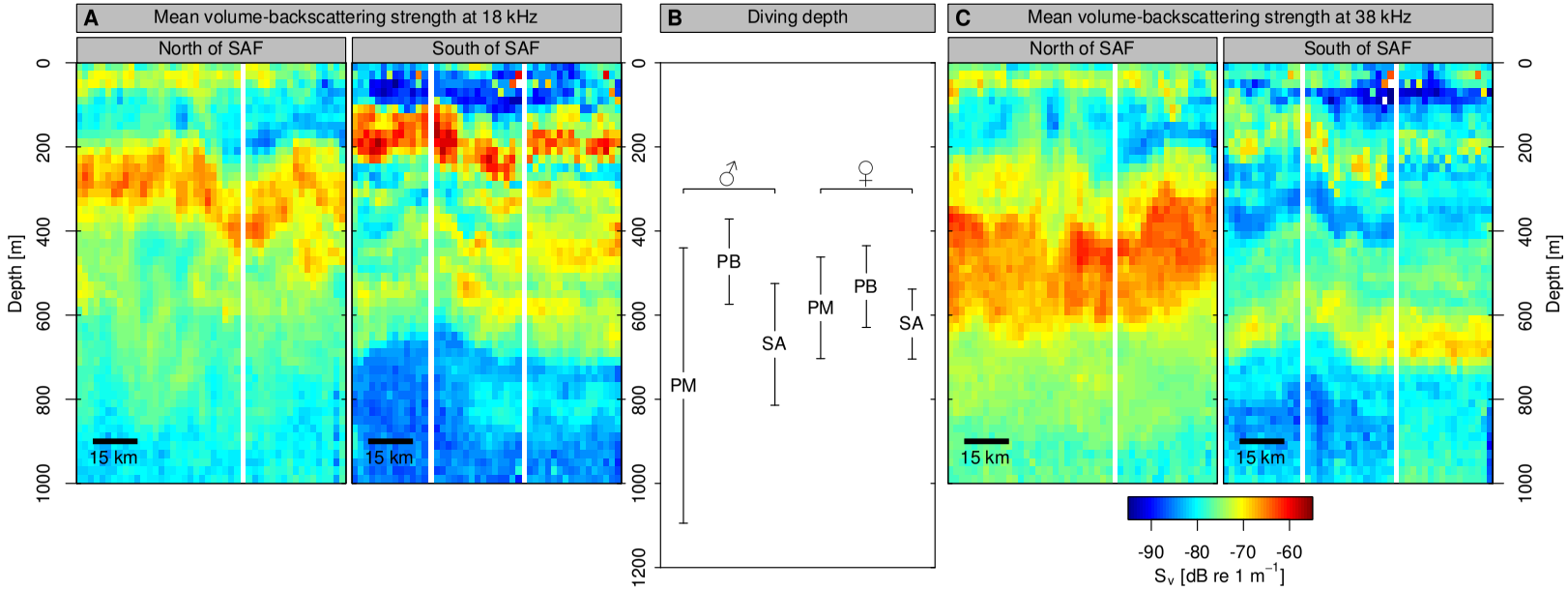

Figure 3.3: Representative echograms of the vertical structure of daytime pelagic scattering layers in the frontal zone. Data at CTD stations was excluded because of substantially elevated noise levels and echoes from the CTD rosette (white vertical lines in A and C). (A) Mean volume-backscattering strength at 18 kHz; (B) Mean ±SD daytime diving depths of different elephant seal groups (after McIntyre et al., 2011, Table 2); (C) Mean volume-backscattering strength at 38 kHz. (SAF, Subantarctic Front, PM, post-moult; PB, post-breeding; SA, sub-adult).

et al., 2007, 2010). A direct relationship between observed scattering layer depth and marine mammal foraging behaviour is not always apparent, especially when concurrent *in situ* data are unavailable. Some studies have demonstrated remarkable spatio-temporal overlap between foraging predators and backscatter features (e.g. Fiedler et al., 1998a), while in others the correlations are less pronounced (Hazen and Johnston, 2010). The mean diving depths reported by McIntyre et al. (2011, their Table 2) do not match exactly any of the echogram features observed by us, which is not surprising considering that the dive data were averaged over 4 yr and thousands of kilometres of seal tracks. The comparison does, however, show that elephant seal foraging depths overlap with pelagic scattering layers on either side of the front (Fig. 3.3), which is in line with recent research that demonstrates the importance of myctophids in the diet of elephant seals from Kerguelen, elsewhere in the southern Indian Ocean (Guinet et al., 2014). Furthermore, there are some clues that may explain the observed positive relationship between temperature and diving depth: the dominant 18 kHz scattering layer north of the front has its peak intensity at around 300 m (maximum mean volume-backscattering strength, S_v; MacLennan et al., 2002), ca. 100 m deeper than the dominant layer south of the front (maximum S_v at 200 m). In addition to this, mean volume-backscattering strength at both frequencies at depths in excess of 700 m is more than twice as intense north of the front than south of it ($\Delta S_{v;18kHz}$ =4.04 dB re 1 m^{-1}; $\Delta S_{v;38kHz}$ =3.49 dB re 1 m^{-1}).

Little is known about the vertical structure of pelagic biota in mesoscale eddies in the southwest Indian Ocean, but the foraging of southern elephant seals in eddies in this region has been documented (Dragon et al., 2010, 2012; Bailleul et al., 2010). There is also evidence from the north Atlantic that the vertical distribution of pelagic animals in eddies can be markedly different from that in surrounding waters (Conte et al., 1986), including significant increases of deep (600 to 1200 m) biomass in warm core eddies (Godø et al., 2012).

3.3.4 Alternative predictors of diving behaviour

McIntyre et al. (2011) partitioned their dive data to account for differences between the sexes and age classes of elephant seals, as well as diel differences in behaviour, but seasonal and/or regional effects were not sufficiently considered. They briefly discuss the fact that the 'track day' variable is a significant predictor in all of their models for female seals, but no attempt is made to investigate seasonality (e.g. by exploring 'day of the year' as a predictor;

see also Biuw et al., 2010), even though the data presented for the subadult male individual OO405 indicate a non-random seasonal trend for diving depth, encountered temperature and time-at-depth. The possibility of detecting seasonal effects is further hindered by the restriction to the first 150 d at sea for the females' data. Although the seasonality of the vertical distribution of mesopelagic communities is poorly understood, it has been well established that seasonal processes influence scattering layer structures (e.g. Staby et al., 2011).

As we suggest here, spatial effects can play an important role (see also Anderson et al., 2005). The relationship between foraging location and ocean temperature has been discussed in detail in 'Temperature, frontal zone positions and the use of daily averages' above, but foraging location is also important when considering differences between pelagic and benthic dives (Maxwell et al., 2012). A variable for bottom depth was a significant predictor for dive depth in some of McIntyre et al.'s (2011) models. While there is a close relationship between bottom and diving depth for benthic dives, bottom depth is — in our experience — often a poor predictor in pelagic systems where the ecology at foraging depth is largely decoupled from bentho-pelagic processes occurring at depths hundreds to thousands of metres deeper. A factor to distinguish between benthic and pelagic dives might have been more informative both biologically and in terms of predictive value.

3.3.5 Time-at-depth and foraging success

McIntyre et al. (2011) did not assess foraging success or body condition of the seals they studied, but suggest that the shorter time-at-depth during deeper dives points to less successful foraging. In the absence of *in situ* behavioural data, constructing a link between time-at-depth and foraging success is speculative. One could argue by the same token that foraging in warmer water is more efficient, or that the energetic costs of deeper diving are balanced by reduced heat loss in warmer water.

Furthermore, a comparison of time-at-depth between watermasses may be confounded by adaptive foraging behaviour for different prey species. Trawl data from our 2009 survey indicate distinct pelagic assemblages for decapod and lophogastrid crustaceans (Letessier et al., 2014), cephalopods (Laptikovsky et al., 2014) and fishes (K. Kemp, pers. comm.) across the Subantarctic Front. Prey-species specific diving behaviour is poorly understood in southern elephant seals but has been observed in other pinnipeds (e.g. Bowen et al., 2002). Recent research has indeed shown that despite lower catch rates in warmer waters,

no relationship was found between temperature-at-depth at the scale of individual foraging trips and daily or absolute mass gain, suggesting that elephant seals are compensating for lower catch rates by consuming larger/richer prey items in those waters (Guinet et al., 2014).

3.4 Conclusions

Climate change is likely to affect elephant seals in the southern Indian Ocean, for example through the intensification of eddy activity (Meredith and Hogg, 2006), which may change the locations and temporal availability of foraging opportunities. However, the correlation between ocean temperature and diving behaviour reported by McIntyre et al. (2011) is likely a demonstration of adaptive foraging behaviour in distinct pelagic biomes rather than a climatic effect. Furthermore, such adaptive behaviours are likely to vary at different scales reflecting scales of patchiness in food availability (Simmons et al., 2010).

Simplistic correlative analyses of environmental variables and behavioural responses are of limited usefulness for both studies of climate change and predator–prey interactions, particularly in dynamic pelagic systems. An investigation of climate change effects would require a different modelling framework, most importantly one where temperature data were stratified between watermasses, and seasonal effects were accounted for. Studies of predator–prey interactions should include prey distributions as well as potential indicators of foraging success and prey-specific foraging behaviour (e.g. Biuw et al., 2003; Dragon et al., 2012) rather than just environmental proxies.

Chapter 4

Scattering layers around atolls and a seamount in the Chagos archipelago

Abstract A survey of scattering layers in the Chagos Marine Protected Area found substantial increases of epi- and mesopelagic backscatter, a proxy for pelagic biomass, near abrupt topography. The findings provide insights into the connectivity between oceanic and neritic systems and may inform ecosystem-based management of large pelagic predators, such as tuna, in oceanic island environments by providing estimates of prey distributions.

4.1 Introduction

Sound scattering layers (SL) are ubiquitous in the oceanic environment. They are composed of marine animals belonging to a multitude of taxa, ranging in size from mesozooplankton ($\approx$ 1 mm) to large micronekton ($\approx$ 20 cm) and belonging to ecological guilds from grazers to piscivores (Farquhar, 1977). Scatterers form an important trophic link between surface production and top predators. In oligotrophic low-latitude habitats they represent a substantial part of the available prey biomass and are exploited by pelagic and demersal-dwelling predators ranging from coral reef-associated fishes (Hamner et al., 1988) to tuna (Potier et al., 2007) and marine mammals (Fiedler et al., 1998b).

A substantial proportion of SL biomass migrates daily between epipelagic and meso- and bathypelagic depths (200m to below 1000m). Shallow topography can block the descent of these animals when they are advected over it during their shallow phase, exposing them to predators and/or concentrating them on the summits and flanks of seamounts and island slopes (Genin, 2004). Lateral advection of pelagic animals further contributes to energy flux into demersal ecosystems both deep (>200 m; Genin, 2004) and shallow (<50 m; Hamner et al., 1988). Tidal fronts, the coupling between vertical migration and tidal flows and surf zone retention further act in concert to retain plankton in nearshore environments (Prairie et al., 2012). Topographic blockage mechanisms may provide sufficient concentrations of prey to attract and sustain substantial predator aggregations (Morato et al., 2008). The acoustic intensity of scattering layers is a proxy for the density of pelagic prey biomass (Farquhar, 1977), while their vertical structure (the depth horizon and thickness of individual layers and the spread or distribution of acoustic intensity within a layer) constrains the accessibility to foraging predators. Both are important factors in predicting top predator distribution and behaviour (Dagorn et al., 2000; Fiedler et al., 1998b), and are consequently informative for fisheries management and conservation (Bertrand et al., 2003). Since SLs link surface production to top predators of layer characteristics can be used as inputs into ecosystem models such as SEAPODYM, which has been used to explore conservation strategies for tropical tunas (Sibert et al., 2012).

In November and December 2012 we conducted a multi-disciplinary survey in the Chagos Marine Protected Area (MPA; British Indian Ocean Territory, central Indian Ocean). This included the use of active underwater acoustics to observe pelagic biota near abrupt topography in water depths from 5 m to 1 000 m. Our goal was to examine how acoustic backscatter intensity, a proxy for pelagic biomass, varied around topographic features.

One conservation aim of the Chagos MPA is the protection of wide-ranging oceanic predators such as tuna and sharks, but little is known about ecological processes of the reserve beyond its shallow reefs (Sheppard et al., 2012). Debate persists on whether mobile species are sufficiently resident within the reserve for their protection to be effective at the population level (Kaplan et al., 2013). Fundamental to resolving this so far data-poor debate is the collection of baseline information on pelagic species and their prey, with respect to their distribution and movements within the reserve.

4.2 Methods

We collected acoustic backscatter and hydrographic measurements during daylight hours (08:00-17:00 local time) from 22 November to 8 December 2012 in the Chagos Archipelago. The spatial extent of the acoustic surveys was from 5°2'S to 7°10'S and from 71°59'E to 72°24'E. The surveys targeted Sandes seamount (summit plateau at 70 m), the slopes of Speakers Bank (submerged atoll, reef crest at 6 m) and Petite Ile Coquillage, (island, Peros Banhos atoll), as well as deep water (>750 m) near Speakers Bank and Blenheim Reef (Fig. 4.1). Survey transects were between 1.5 km and 9 km long and oriented perpendicular to the slope gradient near topographic features ((Fig. 4.2). Over deep water the transects were oriented along the direction of the prevailing swell .

A calibrated split-beam echosounder (Simrad EK60, Kongsberg Maritime AS, Horten, Norway) was deployed from a rigid hulled inflatable boat (length = 6.5 m) using an overside mount (deployment depth = 1 m). The echosounder was operating at 38 kHz with a ping interval of 4 s, pulse duration of 1.024 ms and a beam width of 12°. Temperature, salinity, and fluorescence profiles were obtained to a maximum depth of 200 m using a Seabird SBE 19 CTD (Sea-Bird Electronics, Inc., Bellevue, WA, USA) deployed from FPV Pacific Marlin in the vicinity of acoustic transects. Additional temperature profiles were obtained from the ARGO float array (http://www.argo.ucsd.edu).

Acoustic data were processed in the same manner as in Chapter 2.2.2 using Echoview (v4.9, Myriax, Hobart, Tasmania, Australia) to remove background and intermittent noise (Anderson et al., 2005; De Robertis and Higginbottom, 2007). Sea-surface noise, seabed returns, false-bottoms and were also removed. Mean volume backscattering strength (MVBS; MacLennan et al., 2002) was integrated into 10 m vertical by 250 m horizontal bins. Acoustic single targets were detected with a minimum threshold of -60 dB re 1 m^2, and exported

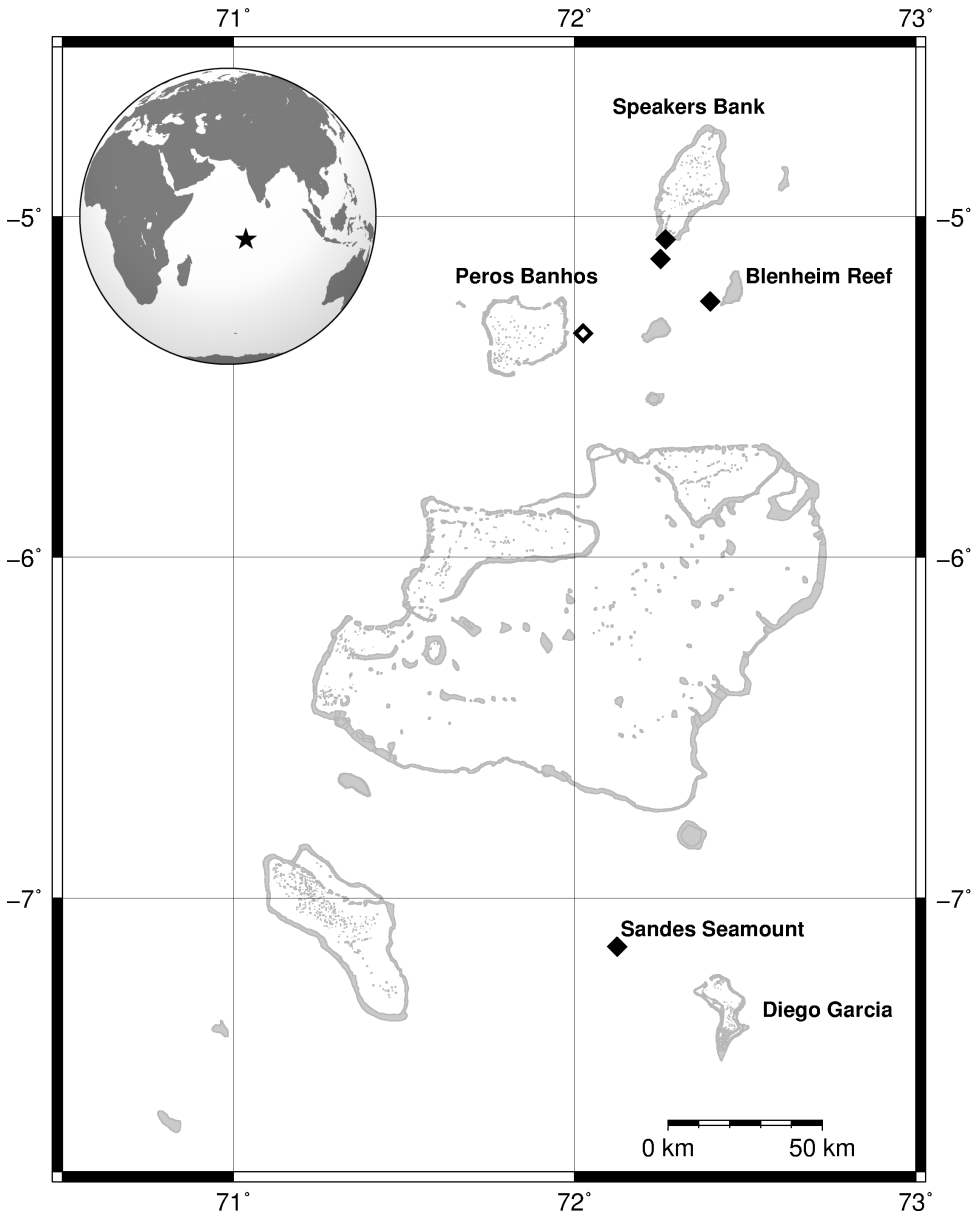

Figure 4.1: Map of the study area. The location of Chagos in the Indian Ocean is indicated by the star in the inset. Locations of acoustic surveys within the archipelago are indicated by diamond symbols. The open diamond marks the transect illustrated in Fig 4.3A. Grey shading indicates coral reef cover, most of which is permanently submerged.

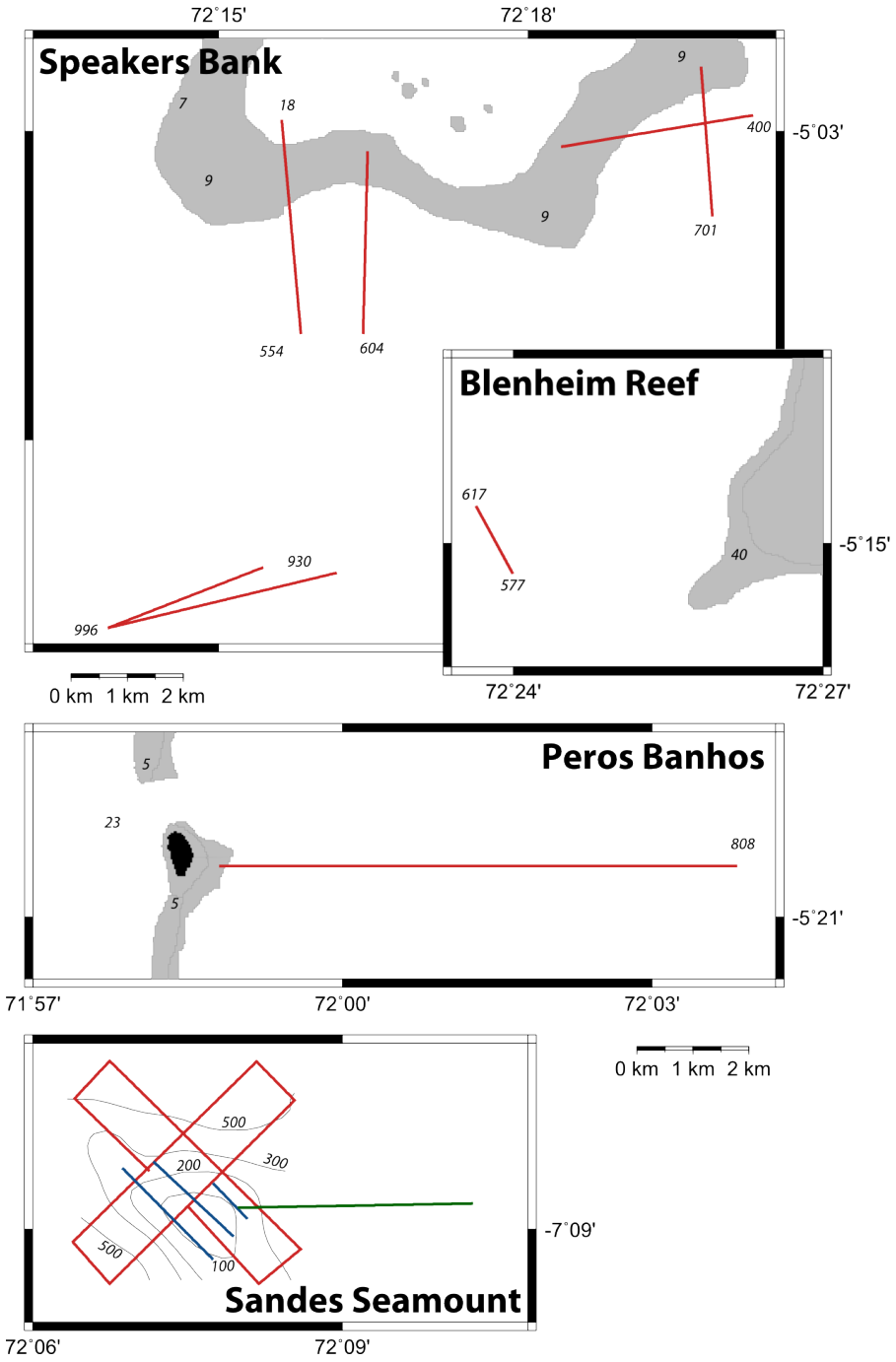

Figure 4.2: Maps of individual study sites. Coloured lines illustrate survey transects. Different colours in the bottom panel indicate transects that were surveyed on separate days. Grey shading indicates coral reef cover, most of which is permanently submerged. Black shading indicates ground above Mean High Water Springs. Italic numerals indicate depths in meters. All panels are to scale.

as individual observations of beam-geometry compensated target strength (TS; MacLennan et al., 2002). Species composition or biomass cannot typically be estimated from single frequency acoustic data alone but MVBS can be interpreted as a relative measure of scattering layer biomass and TS can be interpreted of a relative measure of animal size (Simmonds and MacLennan, 2005).

Distances from each acoustic sampling unit to the nearest topographic feature were calculated using GRASS (Version 7.svn Neteler et al., 2011) and the sp package for R (Bivand et al., 2008; R Development Core Team, 2010) as the minimum great circle distance to either Sandes Seamount or the shallow coral reefs as mapped by the Millennium Coral Reef Mapping Project (Andréfouët et al., 2006). CTD and Argo profiles were processed using the oce package for R (Kelley, 2012). Non-linear regression was used to investigate the relationship between MVBS of individual SL and distance to topographic features. This approach was based on a conceptual model where SL structure and backscattering strength are considered stable on spatial scales of 10s–100s km within watermasses and far from topographic features (Kloser et al., 2009). Topographic features were modelled as exerting an effect on SL that decreased with distance to a feature. The model took the form

$$\mathrm{S_v}(r) = (\mathrm{S_{v0}} - \mathrm{S_{v\infty}})e^{-\lambda r} + \mathrm{S_{v\infty}} \tag{4.1}$$

where r is the distance to a topographic feature, $\mathrm{S_{v0}}$ is the backscatter at $r = 0$, $\mathrm{S_{v\infty}}$ is the asymptote, i.e. the backscatter in the oceanic state and λ is the rate constant of the exponential process modelling the topographic effect. As residuals of ordinary least squares models showed significant spatial autocorrelation (Moran's I, $p < 0.001$), models were fitted using generalised least squares and a spherical spatial correlation structure, as implemented in the nlme package(Pinheiro et al., 2011). The sill range of the spherical variogram, i.e. the range of the spatial autocorrelation, was estimated to be between 1.4 and 1.6 km.

4.3 Results

Two SLs were discernible in the acoustic records (Fig. 4.3). A collection of shallow scattering layers (SSLs) ranging from the surface to approximately 180 m and a deep scattering layer (DSL) ranging from approximately 300 m to 600 m. The SSL collection was typified by two or more distinct sub-layers present at four out of five surveyed locations. The shallowest sub-layer in the SSL collection coincided with the subsurface fluorescence maximum F_{max} at approximately 65 m, while the lower boundary of the SSL collection coincided with

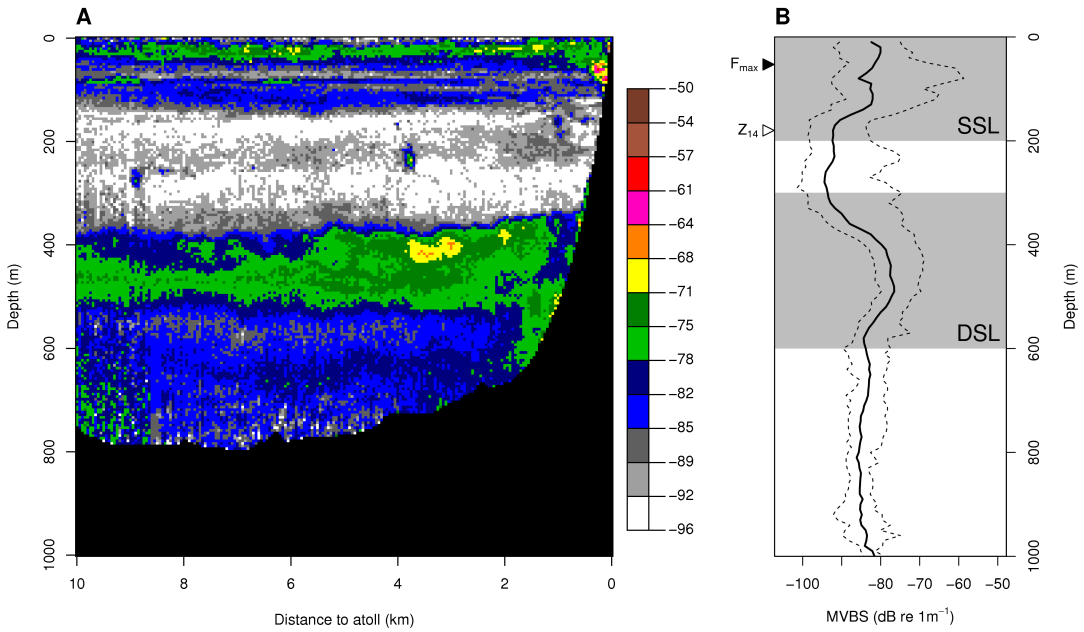

Figure 4.3: Vertical and horizontal patterns in scattering layer strength. (A) Example echogram of a transect running from offshore onto Peros Banhos atoll (cf. Fig. 4.1). Color scale is in dB re $1 m^{-1}$. (B) Vertical profile of MVBS (median and 0.95 percentiles) for the entire data set. Grey shaded depth intervals highlight the shallow (SSL) and deep scattering layer (DSL) analysed for horizontal backscatter gradients. The filled and open arrows indicate the mean depth of the fluorescence maximum F_{max} and the 14°C isotherm Z_{14}, respectively.

the lower end of the thermocline (defined by the 14°C isotherm Z_{14}; Meyers, 1979) at approximately 170 m (Fig. 4.3, 4.4). The depths of the mixed layer and the fluorescence maximum did not vary substantially between stations, although the intensity of the F_{max} was greater close to topography than at the deep water stations (Fig. 4.4B). The DSL was a single layer at all surveyed locations. It was located beyond the range of our CTD probe (300 m), but well below the thermocline in water temperatures between 8°C and 12°C, as recorded by ARGO floats.

Both SSL and DSL showed a marked increase in MVBS as the seabed shallowed around Sandes Seamount, submerged atolls and islands of the archipelago (Figure 4.5). MVBS in the SSL increased drastically towards topographic features. A decline in predicted SSL MVBS to within 1% of its asymptotic value ($S_{v\infty}$, Equation 4.1) occurred at 1.8 km and defined the boundary influence of a feature. MVBS in the immediate vicinity of a feature was over 100 times higher (+20.4 dB re $1 m^{-1}$, 95% CI [16.5, 24.4]) than MVBS beyond the 1.8 km feature boundary (Figure 4.5). The DSL exhibited a less pronounced change in

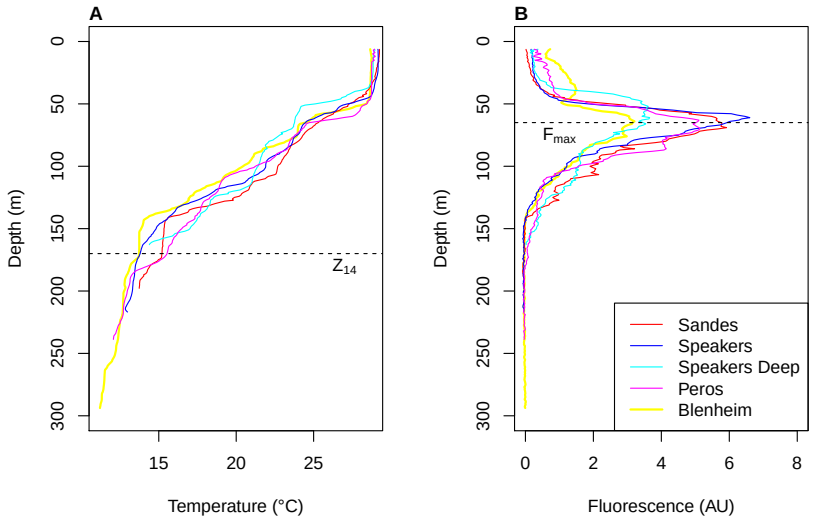

Figure 4.4: Representative CTD profiles of the near surface layers for each survey site. (A) Temperature. (B) Fluorescence. The dashed lines indicate the mean depth of the fluorescence maximum F_{max} and the 14°C isotherm Z_{14}, respectively.

backscatter intensity. DSL MVBS in the vicinity of deep slopes was about 4 times higher (+5.66 dB dB re 1 m^{-1}, 95% CI [3.38, 7.90]) than at the maximum distance surveyed (9 km).

4.4 Discussion

While we cannot determine species composition from the 38 kHz data alone, the vertical structure of SSL and DSL in the Chagos are similar to layers observed with a 30 kHz sonar between the Seychelles and Maldives, which contained over 150 species of fish and invertebrates (Bradbury et al., 1970). Mesopelagic micronekton forms an important part of the diet of yellowfin (*Thunnus albacares*) and bigeye tuna (*T. obesus*) in the western equatorial Indian Ocean (Potier et al., 2005, 2007), and both species were fished commercially in the Chagos by an international fleet of long-liners and purse-seiners before the no-take MPA was established (Sheppard et al., 2012). It is therefore likely that the layers observed form part of the tuna diet, particularly as the Chagos SSL and DSL overlap with diving depths of both species (Dagorn et al., 2000, 2006).

The increase in backscatter in the SSL near topographic features was caused by an intensification of the scattering layer itself near atolls (Speakers Bank and Peros Banhos) while on Sandes seamount it was largely attributable to individual aggregations of scat-

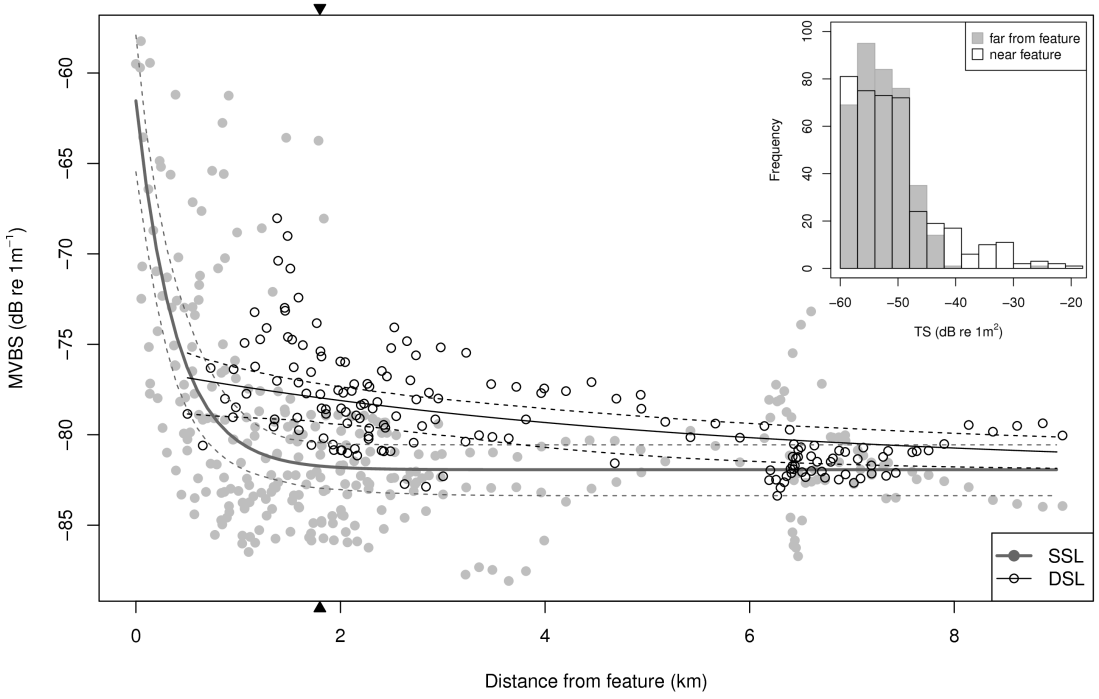

Figure 4.5: Observations (points) and non-linear regression models (lines, with 95% CI) of the shallow (SSL) and deep scattering layer (DSL). The filled triangles on the plot border indicate the estimated range of the topographic effect (1.80 km). The inset shows TS histograms for single targets in the SSL within and beyond the range of the topographic effect.

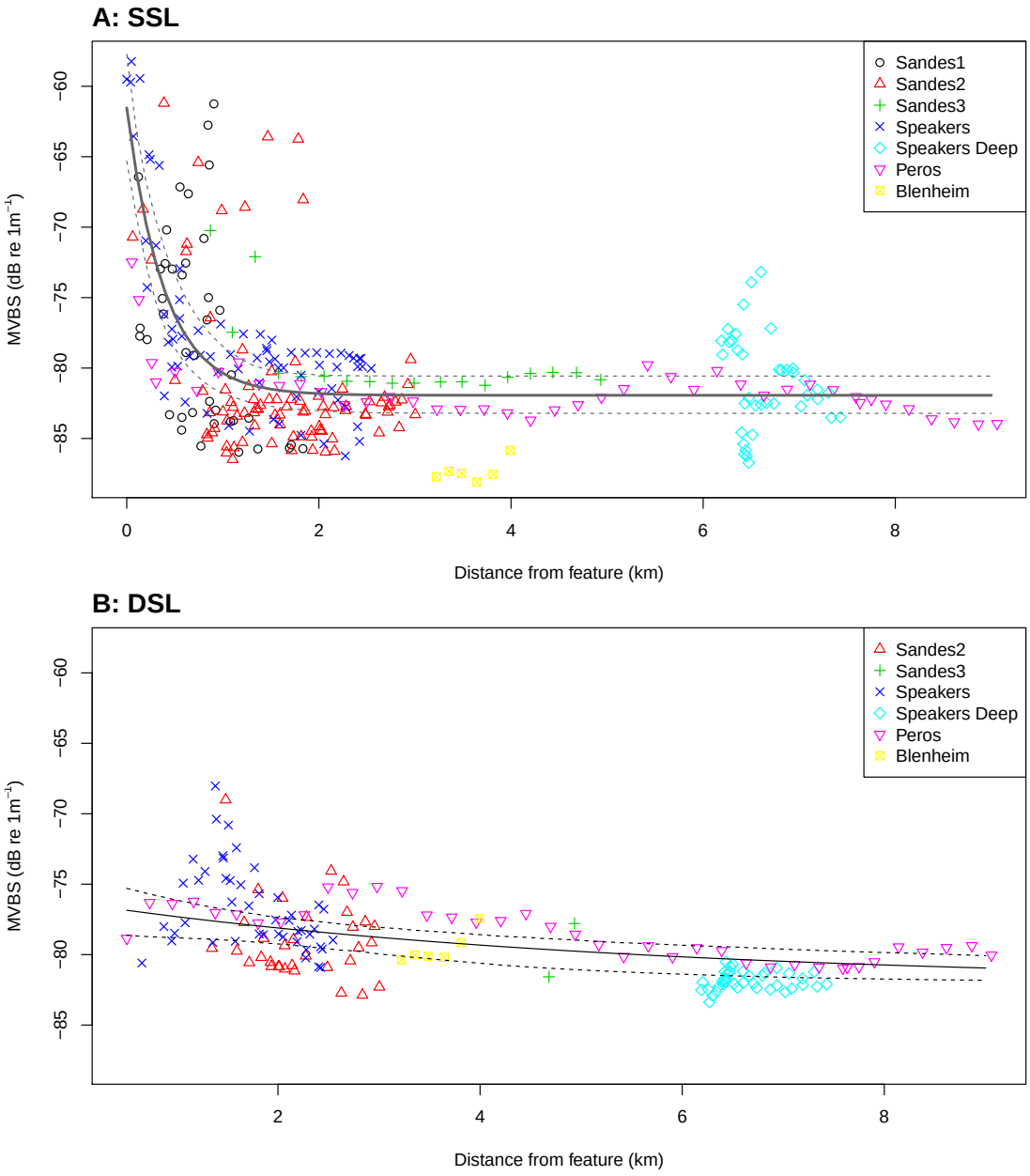

Figure 4.6: Observations (points) and non-linear regression models (lines, with 95% CI) of the shallow (SSL; panel A) and deep scattering layer (DSL; panel B) by survey site.

terers on the summit plateau and the upper slopes of the seamount. The general shape of the increase in MVBS, however, was similar between all three types of topographic features (Fig. 4.6A). Given the lack of replication at the island and reef sites, further research is required to establish whether topographic effects differ between seamounts, reefs and islands in this area of the Indian Ocean. Biologically, this increase probably results from higher densities of animals towards the features, and from a change in the species composition and size spectrum of the sampled biota. TS distributions of acoustically detected single targets within the SSL differed significantly (Two-sample Kolmogorov-Smirnov test, $D = 0.1417$, p-value < 0.001) between the zone of elevated MVBS and compensated TS observations beyond the 1.8 km boundary region. The difference was driven by the presence of strong acoustic targets (TS $\geq$ -40 dB re 1 m^2) near the topographic features, which were absent beyond the boundary region (unfilled bars, Fig. 4.5, inset). Our observations thus likely reflect a superposition of prey field and predators, such as the "wall of mouths" observed by Hamner et al. (1988). Reef associated species, which likely profit directly or indirectly from advected prey, used to be targeted in the Chagos MPA by a Mauritian inshore fishery (Sheppard et al., 2012) and form a prey resource for tunas and other pelagic predators (Fernandez and Allain, 2011).

The increase in backscatter in the DSL was caused by an intensification of the layer itself towards its interception with the slopes of topographic features (Figure 4.3). The highest density regions appeared to exist at a distance of about 1 km away from the feature at Sandes seamount and Speakers Bank, while the DSL at Peros Banhos did not show a comparable peak (Fig. 4.6B). Island associated scattering layers around Hawaii are formed by a distinct mesopelagic-boundary community (Reid et al., 1991). A similar community may be responsible for the observed increase in DSL backscatter, but no data from net sampling are available for the equatorial Indian Ocean.

Interpolated drifter data suggest that the area experienced a weak westward flow during the time of the surveys (Appendix D.1), however, during sampling strong and variable tidal currents were encountered. As topographic features were not sampled from all aspects, and as no *in-situ* data on ocean currents could be collected it is not possible to say if and how currents might have influenced the observed pattern.

Traditionally coral reef ecology has relied on SCUBA based observations, limited to depths shallower than c. 40 m, whereas ecological process in the open ocean have been studied from large ocean going research vessels and with trawls. Neither methodological approach are well suited for the transition zone between the reefs and the oceanic realm

and as a result the understanding of processes coupling demersal ecosystems with the open ocean is incomplete. This applies especially to ecological processes at mesophotic depths (40–150 m) downslope of shallow coral reefs (Kahng et al., 2010), where a substantial proportion of the pelagic backscatter in our study was observed.

Active hydroacoustics have not been widely applied to coral reef systems (Taylor and Ebert, 2012), although some pioneering studies have revealed detailed mechanistic insights into ecological processes (e.g. Genin et al., 2005). This study is the first to employ fisheries acoustic in the Chagos MPA. Our results demonstrate the suitability of fisheries acoustics from small vessels to span the gap between reefs and the open ocean, and provide evidence for interactions between these ecosystems, relevant for the conservation of coral reef fauna and large pelagic predators such as tuna. The spatial and temporal coverage of the acoustic surveys were limited and further, preferably non-extractive research, relevant in an MPA context, is needed to gain a better understanding of processes driving predator distributions within and outside the MPA, and thereby assess the efficacy of the conservation measures currently in place.

Chapter 5

Biophysical coupling and its impacts on seamount food-webs

> The literature gives a fairly clear picture of what mesopelagic fish eat, but it is less informative as to what eats mesopelagic fish.
>
> Gjøsæter and Kawaguchi (1980)

Abstract Seamounts can harbour large aggregations of fish, some of which are targeted by fisheries. These aggregations are thought to be sustained by localized trophic subsidies, provided by flow-topography interactions. Acoustic observations of mesopelagic micronekton and seamount-associated fishes from six seamounts in the SWIO were combined with stomach content analyses to investigated prey flux into seamount ecosystems. Acoustic observations revealed interactions between SLs, aggregations and topography on shallow (<200m) and intermediate (200-800m) seamounts at spatial scales ranging from 1 to 100 km. Furthermore the interception of a downward migrating SL by midwater aggregations at dawn was observed, providing insights into the mechanistic nature of predator-prey relationships in these habitats. Fish stomachs contained cephalopod beaks and fish otoliths from vertically migrating prey, supporting topographic blockage as an input mechanism of prey.

5.1 Introduction

The interaction of ocean currents with seamount topography provides the basis for diverse flow phenomena. This diversity originates in the great variability of seamount height, shape and latitude, as well as local oceanography, e.g. stratification, the amplitude and time dependence of passing currents. All these together determine the nature of the circulation, turbulence, and transport around a seamount (Lavelle and Mohn, 2010). Biophysical coupling, arising from flow-topography interactions, has long been thought to provide the trophic inputs for the rich benthic communities (e.g. Genin et al., 1986; Rowden et al., 2010c) and aggregations of large fishes (e.g. Hubbs, 1959; Koslow, 1996; O'Driscoll et al., 2012) often found on seamounts. However, the mechanistic understanding of processes that may retain or enhance primary and secondary production and/or import allochthonous material (Pitcher and Bulman, 2007) is incomplete. In addition to flow-topography interactions, animal behaviour plays a role in biophysical coupling: zooplankton and micronekton cannot be simply viewed as Lagrangian particles, and their behaviour adds further complexity to the processes governing prey supply to seamount ecosystems, most notably their diel vertical migration (Isaacs and Schwartzlose, 1965; Wilson and Boehlert, 2004).

This chapter aims to describe the biological consequences arising from the interactions of flow-topography effects and behavioural patterns, with a particular focus on the diets of seamount-associated fishes.

5.1.1 Biophysical coupling mechanisms

It used to be thought that local upwelling caused by seamount topography would enhance primary production in surface waters which would be retained through closed circulation cells known as Taylor columns, and energy would be transferred to higher trophic levels, thus sustaining resident fish populations largely from locally derived, or autochthonous production (Uda and Ishino, 1958; Hubbs, 1959). However, there is limited evidence for the occurrence of Taylor columns (Genin and Boehlert, 1985) and when they do appear, they rarely persist for periods of time that are long enough to transfer primary production to higher trophic levels (Genin and Dower, 2007; but see Meredith et al., 2003 for a notable exception). This suggests that energy supporting seamount fish populations has to arrive in the form of allochthonous trophic subsidies, including particulate matter, zooplankton and/or micronekton derived from primary production elsewhere (Tseytlin, 1985; Koslow, 1997; Morato et al., 2009).

The frequent occurrence of cold-water corals and other filter-feeding invertebrates on seamounts has often been ascribed to near-bottom acceleration of currents that enhances food supply (Genin et al., 1986; Davies et al., 2009), as well as clearing sediments from hard substrata, thereby creating habitat for sessile organisms. Stratified flow over isolated topography can also introduce disturbances such as turbulent wakes, internal waves or hydraulic jumps (Dewey et al., 2005). These waves can redistribute suspended particles in the benthic boundary layer and may also enhance surface productivity by increasing vertical nutrient fluxes, and are thereby involved in food supply to filter-feeding communities (Frederiksen et al., 1992; Davies et al., 2009).

Every day in the open ocean zooplankton and micronekton migrate between surface and deeper waters and this behaviour is so widespread that it likely represents the largest daily migration of animals on earth in terms of biomass (Hays, 2003). An abrupt topographic feature, such as a seamount, can trap diel migratory animals during their descent at dawn, leaving them exposed to predators. This mechanism was described as "topographic blockage" by Isaacs and Schwartzlose (1965) and is depicted in Figure 5.1. Studies have indicated that topographic blockage could explain the gut content of resident seamount fishes, with migrating zooplankton being found in the stomachs of alfonsino, *Beryx splendens*, (Horn et al., 2010), pelagic armorhead, *Pseudopentaceros* spp. (Seki and Somerton, 1994), rockfishes, *Sebastes* spp. (Genin et al., 1988) and in grenadiers (Macrouridae; Anderson, 2005). Topographic blockage can also explain the behaviour and distribution of the fish; a review by Uchida and Tagami (1984) found that highest fish catches by Soviet and Japanese deep-sea fisheries took place at intermediate depths, just below the photic layer, the depth where most of the migrating plankton are likely to be trapped. Also, some of the fish species themselves undergo a diel migration which is thought to follow that of their prey (Fock et al., 2002). Both Genin et al. (1988) and De Forest and Drazen (2009) discovered an absence of vertically migrating taxa over seamounts. The authors attributed this observation to displacement by advection and predation as well as active avoidance. However, despite considerable attention to the mechanism in the seamount literature, direct observations of topographic blockage are sparse. Trapping of vertically migrating animals has been observed using sonar technology in the Pacific (Isaacs and Schwartzlose, 1965; Genin, 2004). The original concept of topographic blockage (*sensu* Isaacs and Schwartzlose, 1965) was aimed at vertical imports, however, a recent study by Hirch and Christiansen (2010) has challenged the importance of vertical prey flux, and instead proposed that the lateral advection of smaller, non-migrating zooplankton is the main mechanism

providing prey to seamount-associated fish populations.

Behavioural mechanisms may help in retaining smaller micronektonic animals around seamounts, even when there is no physical retention because of closed circulation patterns. In a study by Wilson and Boehlert (2004), both micronektonic fish (*Maurolicus muelleri*) and mysid crustacean (*Gnathophausia longispina*) resisted advective loss from the seamount in the Northern Hawaiian Ridge, even when subjected to current-mediated influences. This behaviour by micronekton could form part of the trophic base for aggregations of commercially important fishes. There is also the possibility that it is not the promise of food that triggers aggregative behaviour, but reproductive behaviours: spawning aggregations are known for orange roughy (*Hoplostethus atlanticus*), pelagic armorhead (*Pseudopentaceros* spp.) and oreosomatids (Zeiformes) (Koslow et al., 2000).

5.1.2 Aims and relevance

This study employs a combination of fisheries acoustics and stomach content analysis, with the aim to unravel the trophic inputs to seamount ecosystems along the Southwest Indian Ridge (SWIR) and thus provide information that can be used in an ecosystem-based approach to fisheries management at seamounts (Thrush and Dayton, 2010). This is becoming increasingly more important as fisheries catches are increasing within the West Indian Ocean region (Ye, 2011), and it is also the region of the world where the highest proportions of exploited fish stocks are of unknown or uncertain status (Kimani et al., 2009), reflecting problems of fisheries management and ocean governance in the region. All three species of fish which have been investigated in this study are either commercially targeted or caught as by-catch and their current status (underexploited, fully exploited or overexploited/depleted) is unknown in the southwest Indian Ocean (SWIO).

5.2 Materials and Methods

5.2.1 Acoustic sampling

Sampling strategy

The acoustic data used in this chapter was collected during research cruise 2009-410 onboard *RV Dr. Fridtjof Nansen*, between Nov and Dec 2009. Acoustic backscatter was observed with a calibrated (Foote et al., 1987) split-beam echosounder Simrad EK60 (Kongs-

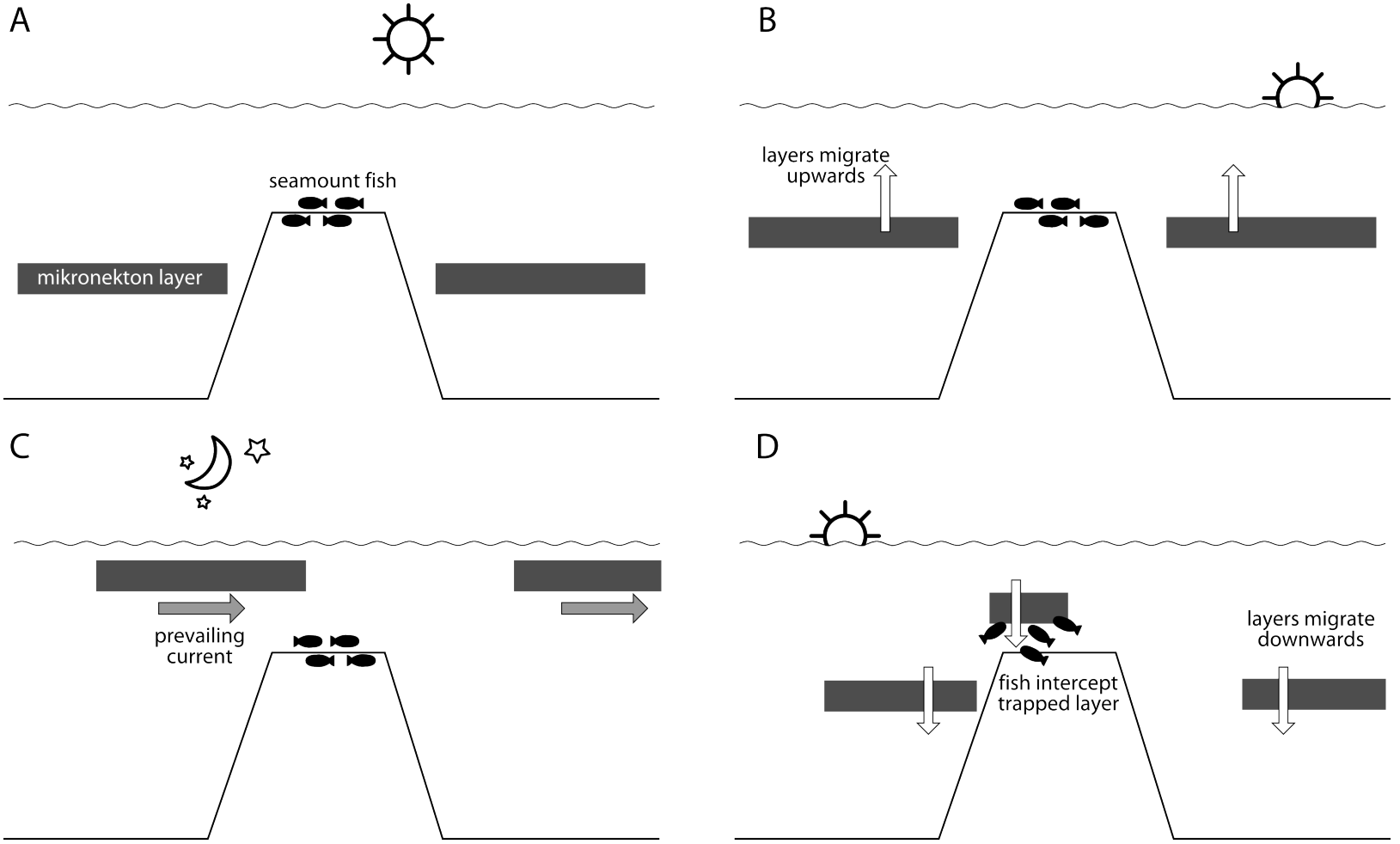

Figure 5.1: Schematic representation of the proposed topographic blockage mechanism. A: Daytime, micronekton layers are below the seamount summit. B: Dusk, layers migrate upwards. C: Night, layers drift over seamount summit. D: Dawn, layers migrate downward and are trapped on the seamount summit and intercepted by resident fishes. Adapted from Rogers (1994).

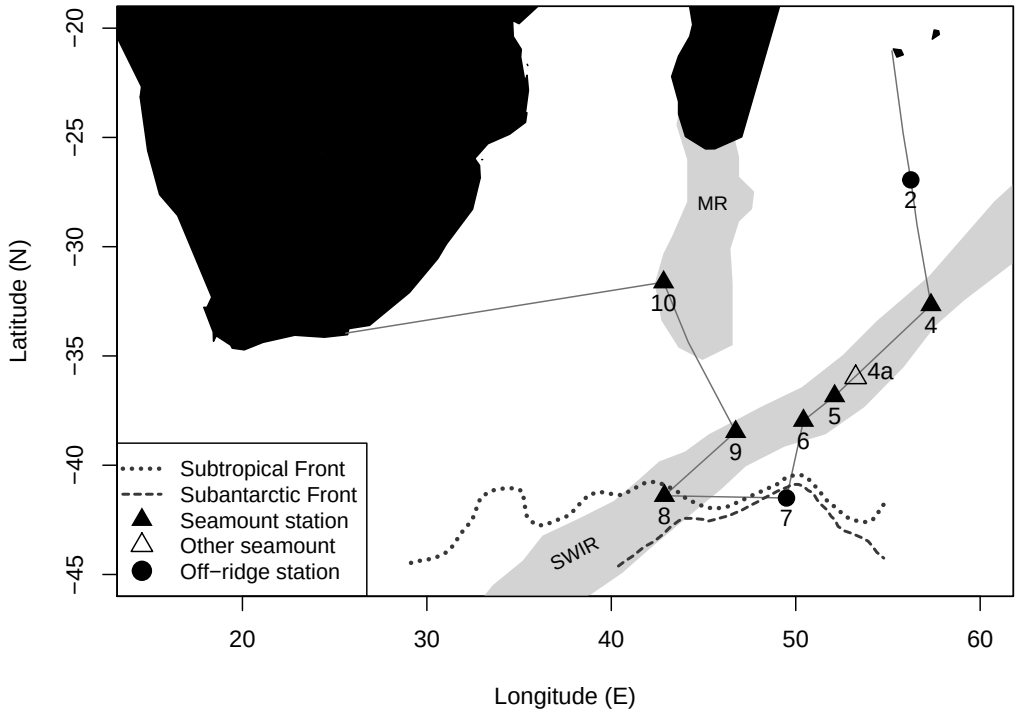

Figure 5.2: Map of the Southwest Indian Ocean and the trajectory of *Nansen* cruise 2009-410. Light shaded areas indicate submarine ridges. Dashed lines indicate approximate locations of hydrographic fronts during the survey (Read and Pollard, 2013a) Stations are: (2) Off-ridge North, (4) Atlantis Bank, (4a) Unnamed seamount near Sapmer, (5) Sapmer Bank, (6) Middle of What Seamount, (7) Off-ridge South, (8) Coral Seamount, (9) Melville Bank, (10) Unnamed seamount near Walter's Shoal. Solid symbols indicate full environmental stations. MR, Madagascar Ridge; SWIR, Southwest Indian Ridge.

berg Maritime AS, Horten, Norway) operating at 18 kHz and 38 kHz. The transducer array was mounted on a retractable keel at a deployed depth of 8.0 m. The EK60 was operated in synchronisation with a vessel mounted acoustic doppler current profiler (ADCP; 150 kHz RDI Ocean Surveyor, Teledyne RD Instruments, Poway, CA, USA) and a bottom-mapping multibeam echosounder (Simrad EM710 70–100 kHz, Kongsberg Maritime AS, Horten, Norway). The EK60's 38 kHz transducer set the master ping rate for the synchronisation unit. EK60 pings were transmitted with a pulse duration of 1.024 ms, transducer parameters are provided in Appendix B.1.

On full environmental stations (see Figure 5.2) acoustic data were collected on a survey grid comprised of a total of 10 parallel line transects with a length of 10 nautical miles (nmi) each. Transect orientation was chosen as a compromise between minimised weather impacts on vessel pitch and bubble entrainment on one hand and maximised seamount

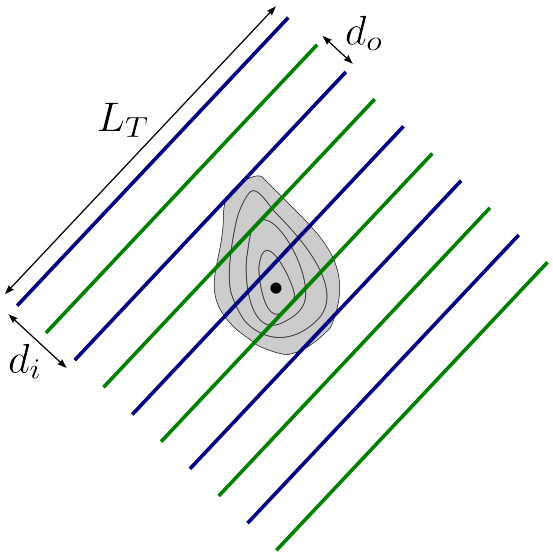

Figure 5.3: Schematic map of the acoustic grids surveyed on full environmental stations. Two interlaced regular grids of five transects were surveyed on consecutive days (indicated by different colours). Transect length L_T was usually 10 nautical miles (nmi), inter-transect spacing d_i = 2 nmi, offset between both grids d_o= 1 nmi.

coverage on the other. The centre points of the survey grids were chosen arbitrarily within the above constraints.

Acoustic grids were usually separated into two parallel, interlaced grids of 5 transects with a 2 nmi transect spacing, offset by 1 nmi (see Fig. 5.3. Both grids were usually surveyed within 48 hours of each other. Acoustic grids were surveyed during daytime only, usually from 1 hr after sunrise to mid-day. Apart from dedicated acoustic transect surveys, the EK60 was running and logging data throughout most of the cruise, including during fishing operations and 24-hour long CTD deployments, so-called CTD-Yoyos, when the vessel was virtually stationary.

Sampling and data processing

Echoview software (Version 4.90, Myriax Pty Ltd, Hobart, Tasmania, Australia) was used to visualise acoustic backscatter data in the form of calibrated echograms. Transducer parameters were adjusted during this step using calibration data and environmental parameters were calculated from CTD data using algorithms of Fofonoff and Millard (1983). Acoustic data were filtered to remove intermittent noise spikes (Anderson et al., 2005), attenuated

pings, persistent intermittent noise and finally background noise (De Robertis and Higginbottom, 2007). The processing workflow was identical to that in previous chapters and details are given in Appendix B.2. Integrated mean volume backscatter (S_v (dB re m^{-1}); MacLennan et al., 2002) was exported as georeferenced cells on a 250 m (horizontal) by 10 m (vertical) grid for the following analyses.

ADCP data were corrected during processing following the manufacturers procedures and corrected for the vessels heading, attitude and velocity. Processed ADCP data for the survey grids were provided by Jane F. Read (National Oceanography Centre, Southampton, UK) as averages on a grid of 12 minutes (c. 3.5 km; horizontal) by 100 m (vertical). Depth penetration of the ADCP rarely exceeded 200 m.

Backscatter maps

Maps of selected depth layers were created in R (Version 2.14; R Development Core Team, 2010) by averaging S_v for all n vertical integration cells in a horizontal sampling unit between two given depth horizons k and l in the linear domain

$$\langle S_v \rangle = 10 \log_{10} \left(\frac{1}{n} \sum_{i=k}^{l} 10^{S_{vi}/10} \right) \tag{5.1}$$

and mapping the results relative to the S_v for a given layer using the maptools (Lewin-Koh and Bivand, 2010) and lattice packages (Sarkar, 2010).

Directional analysis

Directional echograms were constructed to investigate possible links between current flow and backscatter distributions: Within each survey grid the bearing from North φ_N calculated for each acoustic sample relative to the centre point G of the corresponding seamount using functions from the Hijmans et al. (2012) package. Furthermore, the mean current vector $\vec{U}$ was calculated for each grid from ADCP data. The relative angle φ_U between each acoustic sample and the $\vec{U}$ was then calculated as the minimum angle between φ_N and $\vec{U}$ (see Fig. 5.4 for a diagram of the different quantities).

$$\varphi_U = \begin{cases} |\varphi_N - \vec{U}|, & \text{if } -180 < \varphi_N - \vec{U} < 180 \\ \varphi_N - \vec{U} + 360, & \text{otherwise} \end{cases} \tag{5.2}$$

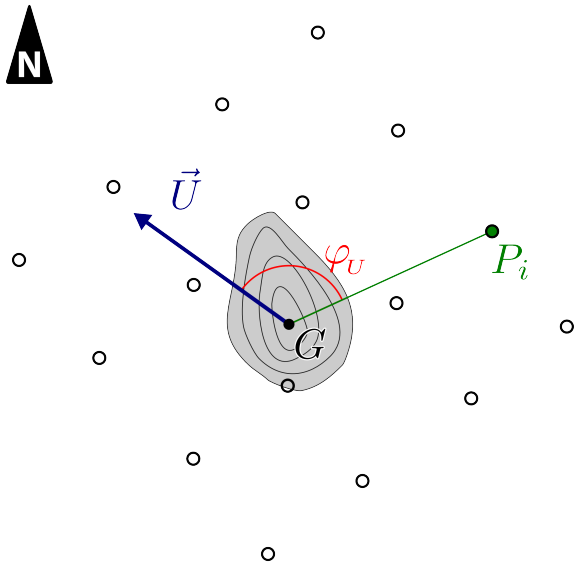

Figure 5.4: Schematic map of the quantities used in the analysis of flow-topography interactions. Grey contours represent a seamount with a central location G. Open circles are locations of sampling units. The relative current angle φ_U for an arbitrary sampling unit P_i is the angle between the mean current vector $\vec{U}$ and the line segment $\overline{GP_i}$. The black triangle indicates the direction to the north.

The resultant φ_U scales from 0° to 180°, where 0° corresponds to samples directly downstream of the seamount centre and 180° corresponds to samples directly upstream of the seamount centre. Acoustic samples were then allocated to 10° wide sectors relative to $\vec{U}$, and averaged (in the linear domain) for each sector and 10 m depth layer, yielding the data points for the directional echograms, that is plots of $\mathrm{S_v}(\varphi_U, z)$.

5.2.2 Biological samples

Scattering layers and seamount-associated aggregations were sampled using two medium sized pelagic Åkra trawls (Valdemarsen and Misund, 1995). The larger net (Flytetrål 152 MSK x 3200 mm) had a vertical net opening of 20 m, a door-spread of 110 m, and a 22 mm mesh cod-end with 4 mm mesh lining, and was used for the majority of trawls. The smaller net, with a 10 m vertical opening, was used for faster trawl attempts targeting what were believed to be aggregations of larger fish mainly at dawn. Both trawls were fitted to 24 mm wires (dual warp) and two combi trawl doors of 1750 kg each (Thyborøn Trawldoors, Thyborøn, Denmark). Trawling was largely undertaken between 300 m and 900 m at vessel

speeds between 2 and 3 knots. Trawl depth was monitored using a net sonde (Scanmar AS, Åsgårdstrand, Norway). Upon arrival on deck the cod end was immediately emptied and sorted into large trays of ice. A small amount of seawater was added to each tray to prevent the samples freezing to the ice. The catch was largely sorted into fish, cephalopod, crustacean, gelatinous zooplankton, and other abundant invertebrate groups. Large fish were identified, measured for total length and standard length, weighed and frozen individually. Additional head length and pre-anal fin length measurements were taken for grenadiers (Macrouridae).

Specimens were thawed in the laboratory, stomachs were sealed by ?xing cable ties around the oesophagus and the pyloric sphincter, then the oesophagus was cut in front of the oesophagus tie, and below the pyloric sphincter tie. Stomachs were perforated with a needle several times before fixing in 4% aqueous formaldehyde for 24 hrs and then transferred to 70% aqueous ethanol for storage. Stomachs and stomach contents were kept in 70% aqueous ethanol before, during and after processing. Before dissection, the full weight of each stomach was taken and recorded, and its 'fullness' was assigned a value on a five-point scale (0.0, 0.25, 0.5, 0.75, 1.0) with 0.0 being completely empty, and 1.0 being completely full. Stomachs were cut from the oesophageal sphincter to the pyloric sphincter and the contents washed out with 70% ethanol into a petri dish. The empty stomach lining was then re-weighed to calculate the mass of the contents. The digestive state of the stomach contents was also recorded on a five-point scale from 1-5, 1 being finely digested and 5 being completely undigested. Contents of the stomachs were sorted into the following categories: crustaceans, fish scales, fish bones, fish jaws, otoliths, eyes, cephalopod beaks and unidentified items, as well as any whole fish or contiguous pieces of tissue. These were also stored in 70% ethanol in individual labelled containers, and the containers were catalogued. Recognisable prey items were then identified under a stereoscopic microscope to the lowest taxon possible, using the identification guides detailed below. Each prey taxon was counted, and its wet mass recorded to the nearest 0.01 g. A fragmented prey count was based on the number of eyes, jaws, otoliths or other anatomical parts traceable to a single specimen. Prey items that were heavily digested and unrecognizable were classified as unidentifiable and were excluded from the analyses but retained for the diet description tables. Parasites were also excluded from the analysis.

Cephalopod identification

Each cephalopod beak extracted was identified as either an upper or a lower beak. For all beaks, both hood length (HL) and rostrum length (RL) were recorded using digital vernier calipers (see Figure 5.5 for an illustration of beak measures). Beaks were identified using Clarke (1986) for the lower beaks and Clarke (1962) for the upper beaks. Xavier and Cherel (2009) was used to clarify features and aid identification. Each beak was identified to the lowest taxonomic level possible. The body mass and mantle length of each squid was inferred from HL and RL of the beak using the species specific allometric equations from Clarke (1986); Lu and Ickeringill (2002); Xavier and Cherel (2009).

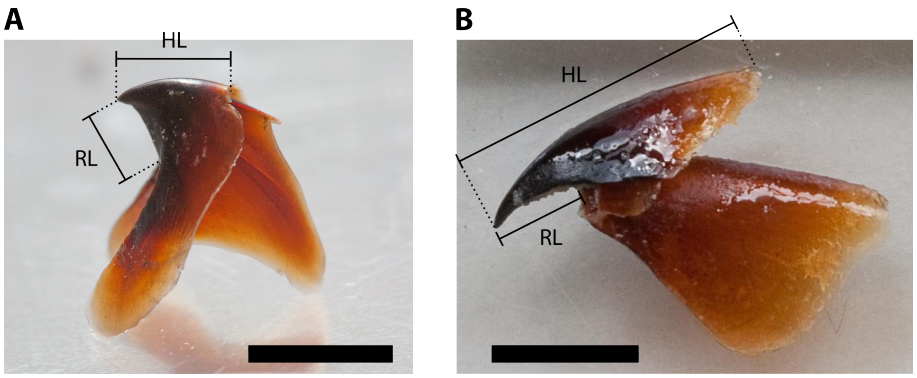

Figure 5.5: Lower (A) and upper (B) mandible of a cephalopod beak and measurements taken for allometric scaling calculations. Scale bar 5 mm. HL, hood length; RL, rostrum length. Photographs: Philipp Boersch-Supan.

Fish identification

Images were taken of all otoliths using a light microscope with a built-in camera (×16 magnification, Leica Microsystems, Milton Keynes, UK). Otolith diameter was measured using the microscope camera and a 0.2 mm scale. These images were then uploaded to the identification tool of the AFORO (Anàlisi de formes d'otòlits) database (Lombarte et al., 2006), which uses shape recognition techniques, to compare the otolith to a reference set of over 4000 otoliths from more than 1200 species. AFORO results were then used as a starting point to classical otolith identification based on keys and photographs in Smale et al. (1995).

Table 5.1: Summary of acoustic transect surveys. n_T: number of transects, L_T: transect length.

Station	Date	Start/End (GMT)		Orientation (deg.)	n_T	L_T (nmi)
02 Off-Ridge North	14/11	03:30	09:26	315	5	10
	15/11	01:59	07:53	315	5	10
04 Atlantis Bank	17/11	01:40	07:40	315	5	10
	19/11	02:45	08:40	315	5	10
05 Sapmer Bank	22/11	01:22	07:23	315	5	10.5
	24/11	03:25	09:30	315	5	10.5
06 Middle of What	25/11	06:56	12:54	315	5	10
	27/11	04:05	10:01	315	5	10
07 Off-Ridge South	30/11	01:00	11:38	350	10	10
08 Coral	2/12	02:08	08:04	340	5	10
	4/12	03:54	09:44	340	5	10
09 Melville Bank	7/12	03:47	16:15	345	9	10
	9/12	02:53	08:43	345	5	10
10 Walters NW	12/12	10:16	15:58	315	5	10
	13/12	02:45	08:23	315	5	10

5.3 Results

5.3.1 Acoustic observations

Time constraints and inclement weather conditions did not allow the scheme described above to be followed at all stations. As a result some transects were surveyed in the afternoon. At Melville Bank (Station 9) a part of the acoustic grid was resurveyed to account for poor data quality caused by gale-force winds and heavy seas during the first part of the acoustic survey. An overview of all acoustic grid surveys is given in Table 5.1.

Acoustic data collected during other sampling activities (e.g. CTDs, fishing) was often of poor quality because of noise and electrical interference from the vessels thrusters and winches.

Summit aggregations

A common feature on all ridge seamounts, even the deepest one (Middle of What, 970 m summit depth), were summit associated aggregations of scatterers, or plumes, examples of this are illustrated in Figure 5.6. These aggregations were usually large (tens to hundreds of metres in both vertical and horizontal extent) and substantially increased backscatter - up to one order of magnitude compared to the layer median (Fig. 5.7). Trawls targeting these aggregations indicate the presence of large predatory fishes, although micronekton

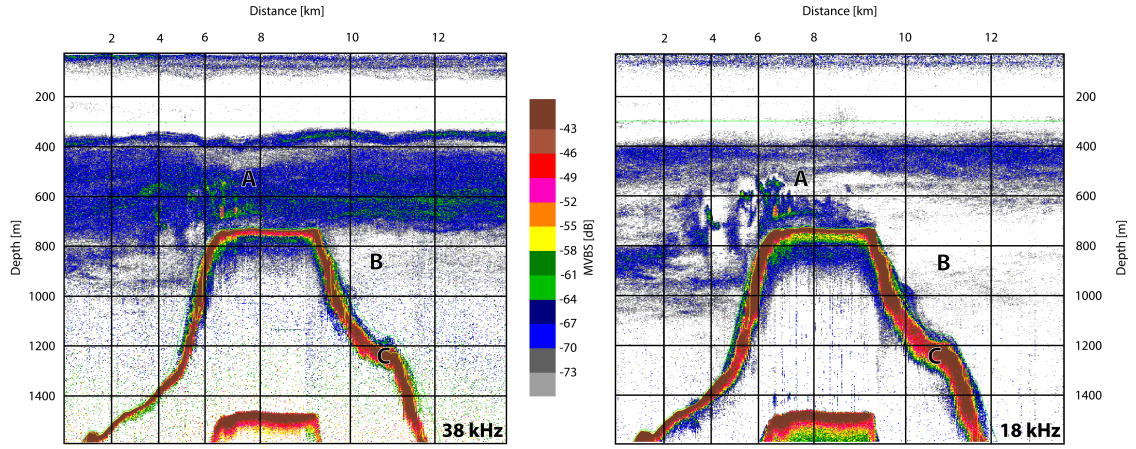

Figure 5.6: Acoustic transect across Atlantis Bank. The 38 kHz echogram (*left*) shows SSL (0-100 m) and DSL (350-800 m). Net current flow in the plane of the transect runs from left to right. A: Summit aggregations or "plumes" containing large swimbladdered fishes. B: Depleted scattering layer. C: Seabed echo. Color scale gives mean volume backscattering strength (dB re 1 m^{-1}).

Table 5.2: Summary of the observed effects on scattering layers around the surveyed seamounts.

Station	Depth	summit ∩ DSL	summit aggregations	DVM interception	dir. depletion	internal wave
4 Atlantis Bank	750 m	+	+	+	+	-
4a Unnamed	<475 m	+	+	N/A[a]	N/A[a]	+
5 Sapmer Bank	350 m	+	+	-	-	-
06 Middle of What	970 m	-	+	-	-	-
8 Coral	200 m	+	+	N/A[b]	-	-
9 Melville	100 m	+	+	N/A[b]	-	-
0 Walter's	1200 m	-	-	-	-	-

[a] no grid survey conducted

[b] too shallow to track DSL DVM

was numerically dominant in all trawls (K. Kemp, pers. comm.). Splendid alfonsino *Beryx splendens* were sampled at Atlantis bank and Sapmer seamount (Stations 4 and 5, Fig. 5.2), pelagic armorhead *Pseudopentaceros wheeleri* and spiky oreo, *Neocyttus rhomboidales* were sampled at Sapmer seamount, and bathypelagic grenadier *Mesobius antipodum* were sampled at Coral seamount (Station 8).

Directional depletion

Directional echograms did not show signs of a connection between mean current direction and backscatter at all but one station. Only on Atlantis Bank there was a marked decrease in backscatter at both frequencies in a 60°-100° wide sector downstream of the seamount (Figs. 5.6 and 5.8). For the 38 kHz data a 50% depletion of backscatter ($\Delta S_{v;38kHz} = -3$ dB) was noticeable only at depths deeper than the summit plateau (c. 750 m; Fig. 5.8C, D), whereas 18 kHz backscatter was depleted to just 6% of upstream values ($\Delta S_{v;18kHz} = -12$ dB) at below-summit depths as well as in a shallower depth stratum, corresponding to the part of the water column occupied by the summit-associated aggregations (500–750 m; Fig. 5.8A, B).

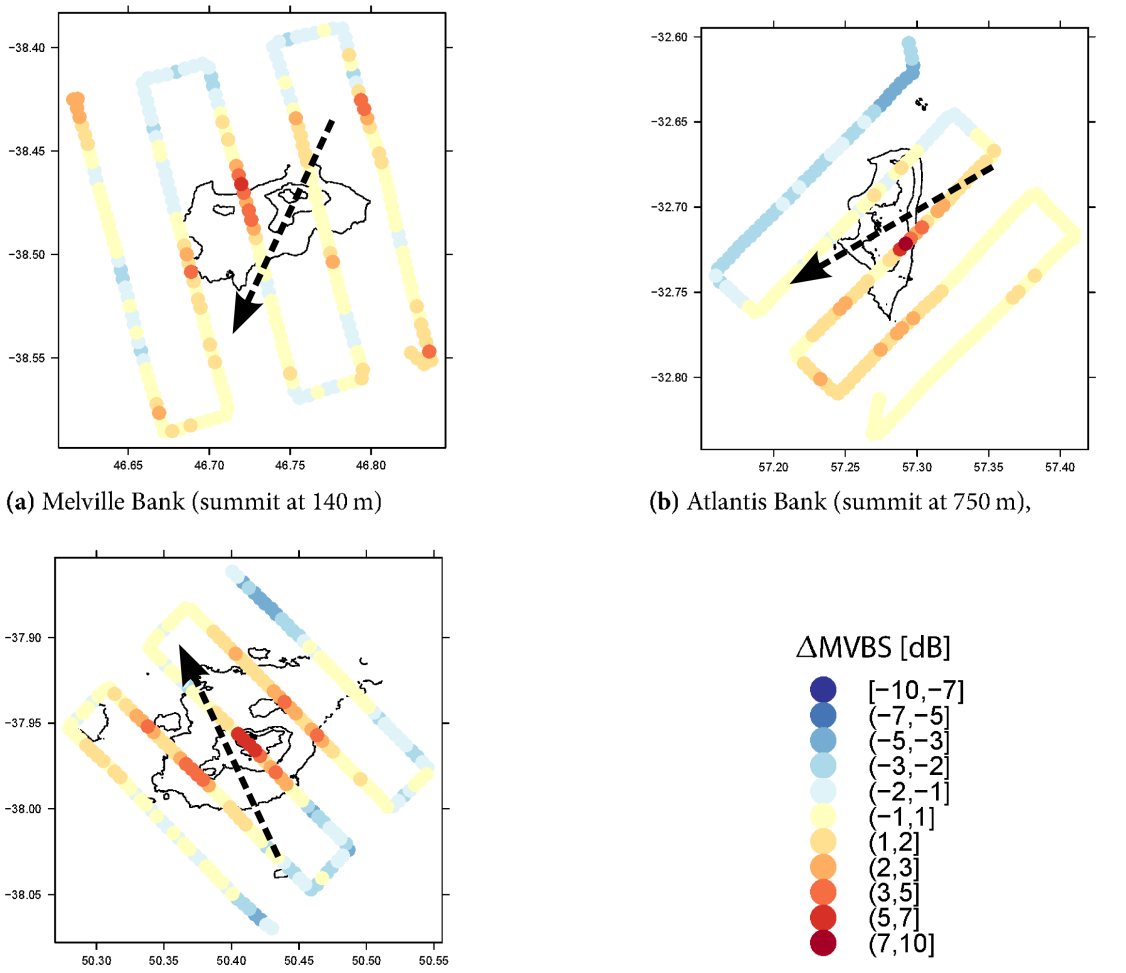

(a) Melville Bank (summit at 140 m)

(b) Atlantis Bank (summit at 750 m),

(c) Middle of What (summit at 970 m),

(d) Colour Legend: Difference to layer median (dB)

Figure 5.7: Seamount associated aggregations at a shallow (a), intermediate (b) and deep seamount (c). Relative backscatter is shown for a 200 m deep stratum overlying each summit. Dashed arrows indicate the direction of net current flow across the survey grid.

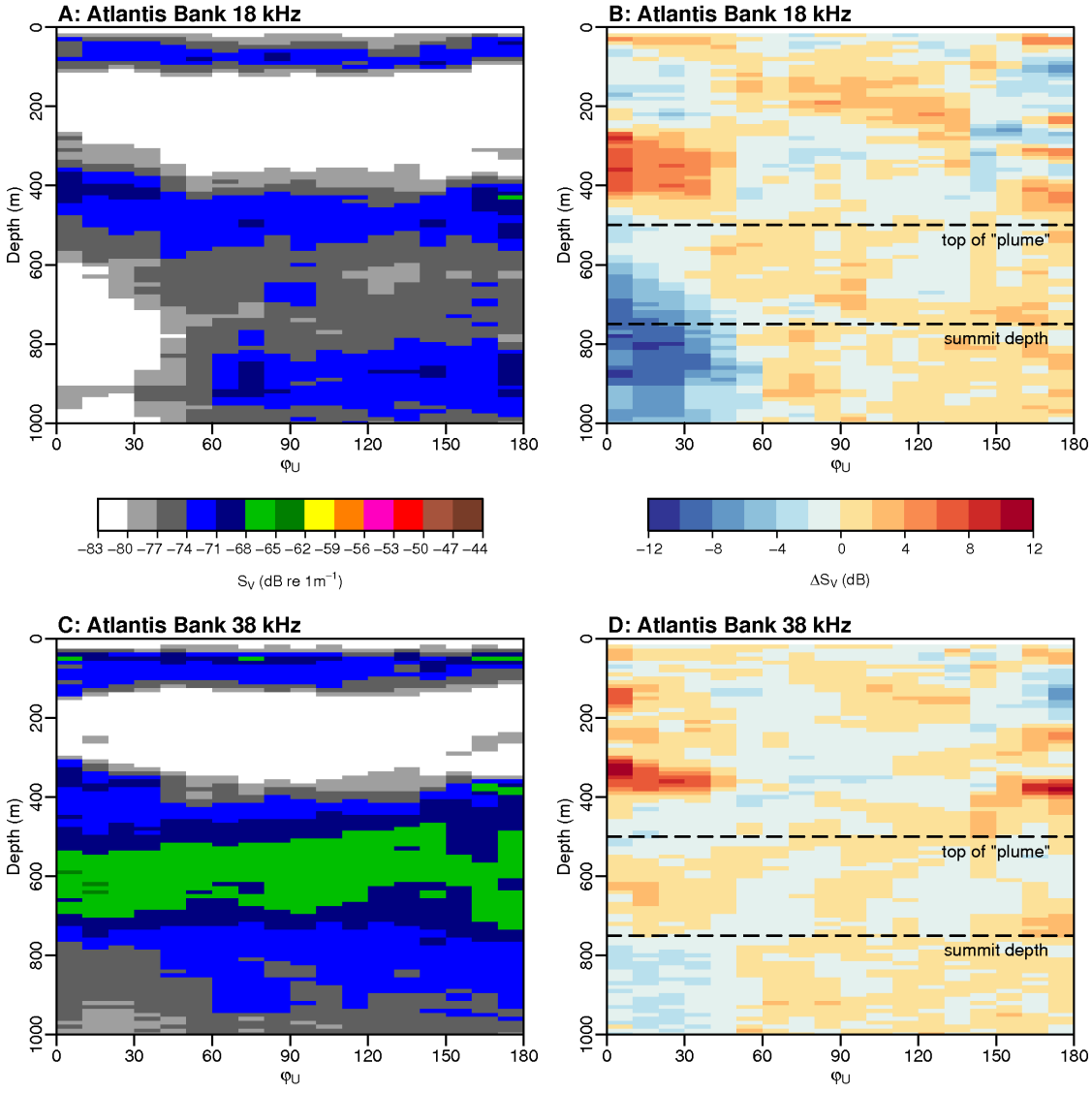

Figure 5.8: Directional echograms of the survey around Atlantis Bank; x-axis denotes the angle relative to the prevailing current φ_U. See Fig. 5.4 for a diagram of this angle. A, C: Echograms show mean volume backscatter (S_v). B, D: Echograms show backscatter relative to the median of each 10 m depth stratum (ΔS_v).

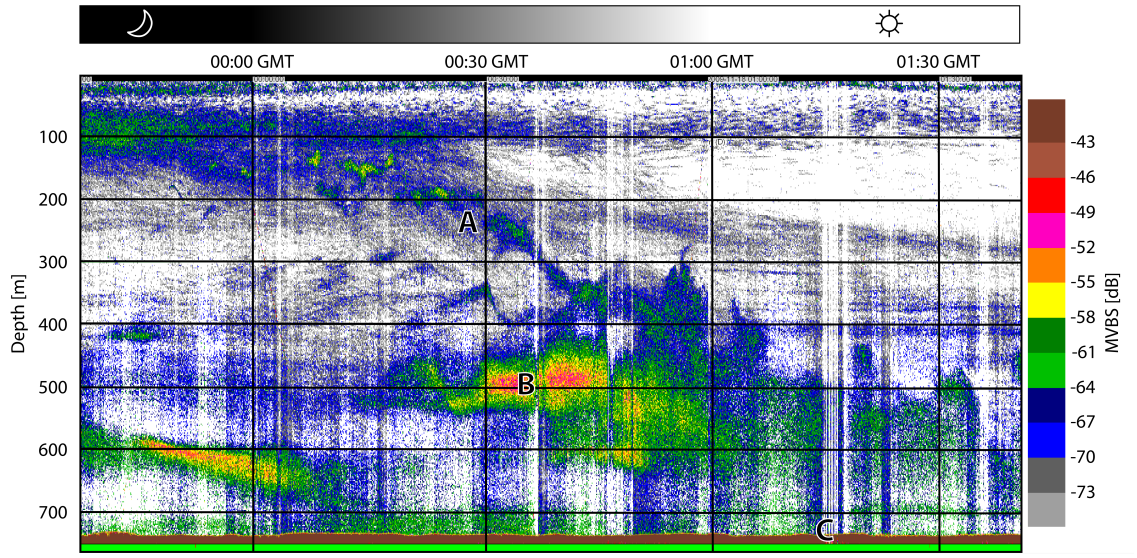

Figure 5.9: 38 kHz echogram of the summit of Atlantis Bank while the vessel was stationary (i.e. x-axis denotes time). As the sun rises - solar azimuth is indicated in the top panel - scatterers from the shallow scattering layer descend downwards (A), and are intercepted by an aggregation of stronger acoustic targets (B). C: Seabed echo.

"Topographic blockage"

Acoustic observations during the CTD-Yoyos appear to show the interception of scattering layers by fish aggregations on Atlantis Bank (see Fig. 5.9). During sunrise scatterers from the shallow scattering layer descend downwards, and are intercepted by an aggregation of stronger acoustic targets about 150 m above the seabed. The ultimate fate of the prey patch, in particular, whether it migrated further down the slope or was indeed blocked by the topography cannot be inferred from the data. This phenomenon was not observed elsewhere, although the locations of the CTD-Yoyos on Coral Seamount and Melville Bank were in too shallow water to track the vertical migration of the DSL.

Hydraulic jump

On 21/11/2009 around 15:00 hrs local time an unnamed seamount was traversed approx. 140 km northeast of Sapmer seamount at 35°59'S 53°15'E while the vessel was travelling at approx. 5 m/s on a heading of 228°. The shallowest point observed was 475 m deep. Concurrent ADCP measurements indicate a westward current (mean direction 275°) with a speed of approx. 0.5 m/s in the top 250 m of the water column, i.e. a net flow along the

direction of travel. Upstream of the seamount a well developed deep scattering layer (DSL) with a peak density at approx. 400 m was observed, downstream of the seamount the layer structure was perturbed at two different spatial scales (Fig. 5.10A). At a scale of 10^1 km the seamount created a wake that resulted in the upward displacement Δz_L of the upper boundary of the DSL by 95 m (Fig. 5.10C). The along-track wavelength λ_L of the perturbation was estimated to be on the order of 15 km. On a scale of 10^0 km the seamount created a perturbation with the appearance of a hydraulic jump (Fig. 5.10B; Dewey et al., 2005). The flow feature resulted in a downward displacement of the -62 dB isoline within the DSL onto the seabed ($\Delta z_{S3} = 95$ m; Fig. 5.10D), followed by a sharp upward displacement of the layer. The upper DSL boundary exhibited depth oscillations with an along-track wavelength λ_S of approx. 870 m and vertical displacements of up to 100 m relative to upstream of the seamount ($\Delta z_{S1} = 77$ m, $\Delta z_{S2} = 100$ m). Perturbations corresponding to the locations of peaks in the upper DSL boundary oscillation were also observed in the shallow scattering layer (<100 m; Fig. 5.10B). Internal wave effects were not observed on any of the survey grids, although the sampling design of parallel transects is not ideal to detect small-amplitude waves unless they propagate along the transects.

No inferences can be drawn about the presence or absence of a directional depletion effect at this particular seamount, as the seamount was traversed by a single transect only, which was oriented at an angle of 47° to the current flow (inset in Fig. 5.10A).

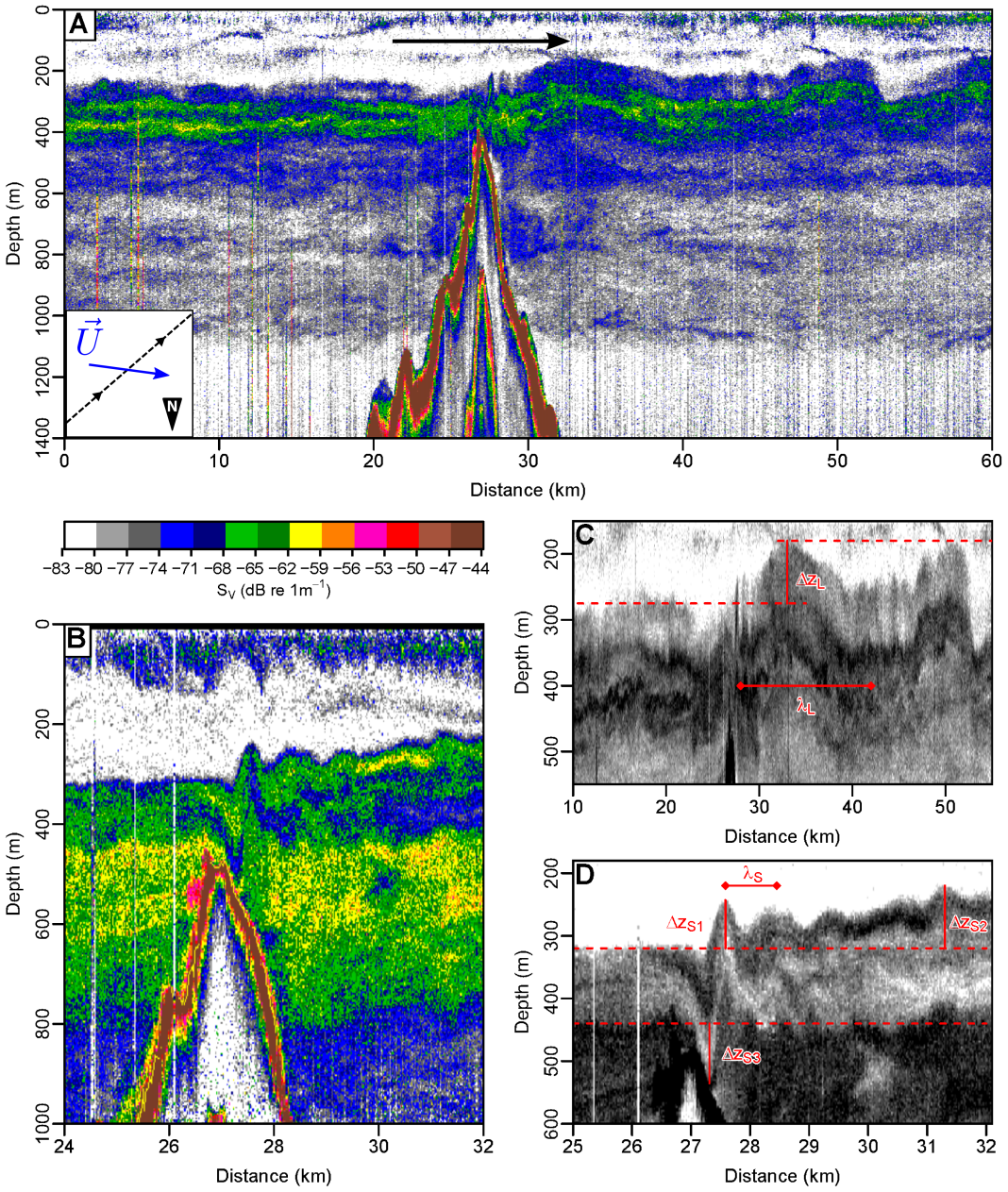

Figure 5.10: Internal wave effects on the deep scattering layer (DSL) observed on an unnamed seamount at 35°59'S 53°15'E. Net current flow across the top 250 m of the watercolumn in the plane of the echogram is indicated by the black arrow in panel A. A: 18 kHz echogram traversing the seamount from NE to SW, showing long wavelength perturbations of the main DSL (c. 250 m–450 m). The inset shows a schematic map of the survey track (dashed line) and the actual current flow $\vec{U}$ (blue arrow). The black tiangle indicates the direction to the North. B: 38 kHz echogram of the summit region, showing shorter wavelength perturbations within the surface (<200 m) and the deep scattering layer (>200m). C, D: Illustration of measurements taken from the echogram. Δz_i, vertical displacement; λ_i, wavelength estimate.

Table 5.3: Sample data for each of the three fish species (means ± std. dev.). n, sample size; F, fullness index [0;1]; m_C, mass of contents (g); D, digestive state index [1;5]

	B. splendens	*M. antipodum*	*P. richardsoni*
n	18	53	9
m_c	11.42 ± 18.7	0.6 ± 0.7	1.7 ± 1.3
F	0.5 ± 0.4	0.5 ± 0.3	0.5 ± 0.2
D	2.5 ± 1.3	2.9 ± 0.9	2.3 ± 0.7

Table 5.4: Frequency of occurrence (%) of prey categories among individuals of the three investigated species.

Prey category	*B. splendens*	*M. antipodum*	*P. richardsoni*
Fish	72.2	62.3	44.4
Scales	66.6	60.4	44.4
Jaws	50	11.3	22.2
Bones	27.8	45.3	22.2
Otoliths	38.9	1.9	0
Eyes	88.9	58.5	22.2
Beaks	61.1	20.8	0
Crustaceans	100	62.3	11.1
Other	50	22.6	100

5.3.2 Stomach contents

A total of 82 fish stomach samples were used for content analysis. Of the 19 stomach samples of splendid alfonsino, *Beryx splendens*, 1 stomach was empty and discarded from analyses. Of the 55 grenadier stomach samples, *Mesobius antipodum*, 2 stomachs were empty and discarded from analyses. Of the 9 stomach samples of pelagic armorhead, *Pseudopentaceros richardsoni*, none were empty, although 8 contained an unidentifiable amorphous substance and this was the most frequent item found. There were two stomach samples from the spiky oreo, *Neocyttus rhomboidalis*, however the stomach contents found were too digested to identify, apart from the jaw of a fish. Appendix E contains the raw prey item count data for all fish samples. Table 5.3 shows a summary of the sample data for each fish species, and Table 5.4 shows the frequency of occurrence F_o for each prey category:

$$F_o = \frac{\text{number of stomachs with each prey category}}{\text{total stomachs sampled for each species}} \times 100.$$

Evidence of piscivory incorporates the scales, eyes, bones, jaws and otolith catagories.

The two taxonomic groups investigated in this analysis were cephalopods, identified

Table 5.5: The frequency of occurrence F_o (%) and number N of cephalopod beaks found in stomach contents. Histioteuthidae and Onychoteuthidae are mesopelagic and there is considerable evidence that they both undertake diel vertical migrations.

Prey Species	*Beryx splendens*		*Mesobius antipodum*	
	N	*F*	*N*	*F*
Histioteuthidae	22	49	5	38
Onychoteuthidae	10	22	2	15
unidentifiable	11	24	6	46
Chranchiidae	1	2		
Sepiolodae	1	2		
Total	**45**	**100**	**13**	**100**

from beaks, and fish, identified from otoliths. However, it can be noted that crustaceans were an important prey item of *Beryx splendens* and *Mesobius antipodum*, being present in 100% and 62.3% of stomachs sampled, respectively.

Cephalopod beak data

A total of 58 cephalopod beaks were found in the stomachs of *B. splendens* and *M. antipodum*. As shown in Table 5.5, the majority of beaks were identified within the Histioteuthidae family, with 49% and 38.4% of beaks respectively, and Onychoteuthidae family, with 22.2% and 15.4% of beaks respectively. Just less than a quarter were too broken or too small to identify for *B. splendens* and just less than a half were unidentifiable for *M. antipodum*.

Where possible, rostrum length (RL) and hood length (HL) of beaks were measured, and from this, the mantle length of the prey item inferred. As seen from Figures 5.11 and 5.12, for both *B. splendens* and *M. antipodum*, the highest frequency RL was between 0-0.9 mm and the highest frequency HL was between 0-1.9 mm. For *B. splendens*, the RL range extends to 4.55 mm whereas the maximum RL recorded for *M. antipodum* was 2.6 mm. Similarly, for HL, the range was greater for *B. splendens*, 12.5 mm, than for *M. antipodum*, 4.3 mm. The range and frequency of inferred mantle lengths was smaller for *M. antipodum*, with a range from 7 mm to 47 mm and the highest frequency between 7-20 mm. For *B. splendens*, the inferred mantle lengths had a range three times greater, from 3.9 mm to 114.9 mm with the highest frequency between 21-40 mm. In all, although the frequency of RL and HL of prey beaks are similar for both species, the mean size and range of cephalopod prey does differ between species, with *B.splendens* consuming an average prey mantle length of 44.7 mm double that of *M. antipodum*, which had an average prey

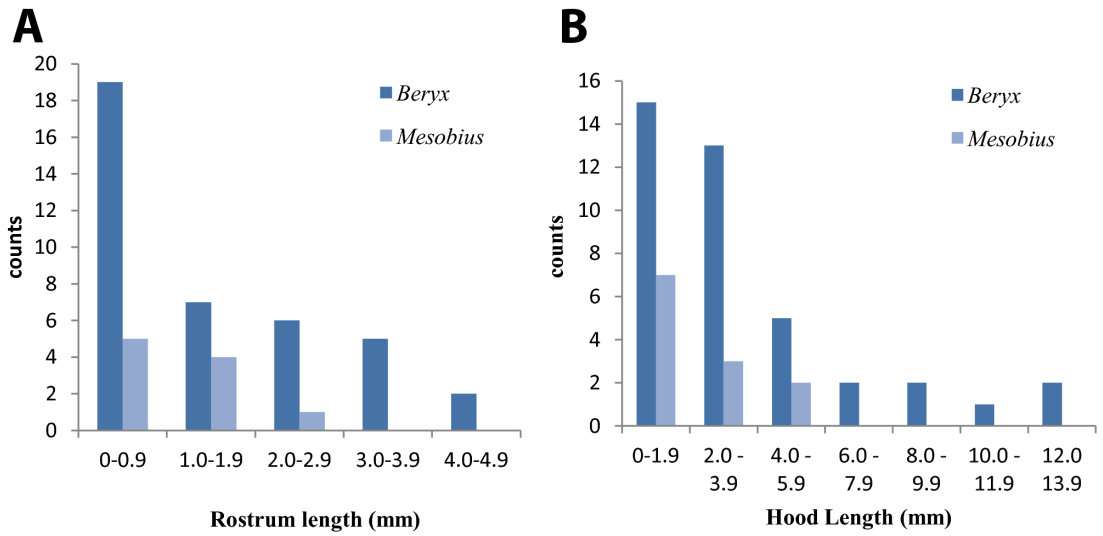

Figure 5.11: Histograms of rostrum and hood lengths of cephalopod beaks found in the stomachs of *Beryx splendens* and *Mesobius antipodum*. A: Rostrum lengths from all prey beaks, $n = 49$. B: Hood lengths from all prey beaks, $n = 52$.

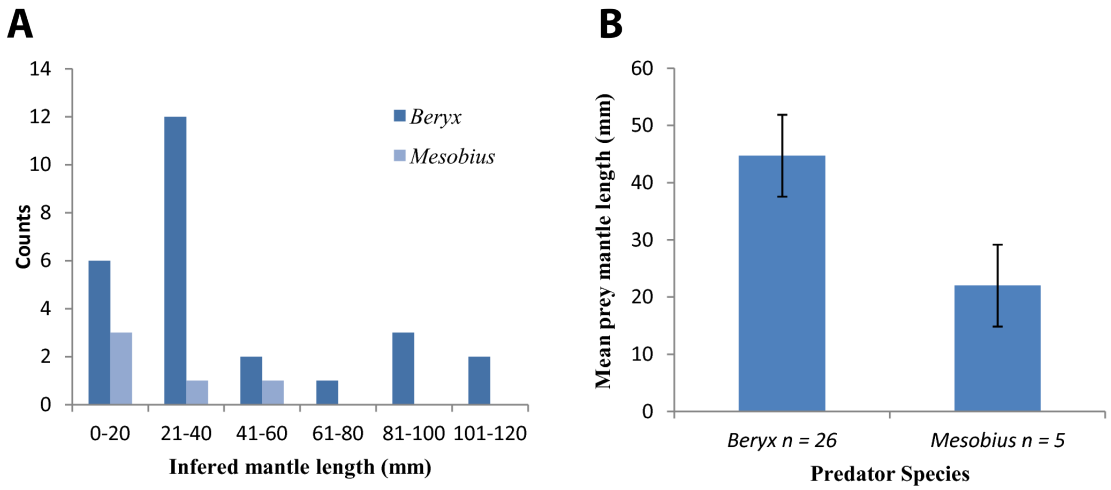

Figure 5.12: A: Frequency histogram of mantle lengths of squid prey, $n = 31$. B: Mean mantle length ($\pm$ std. err.) of squid prey.

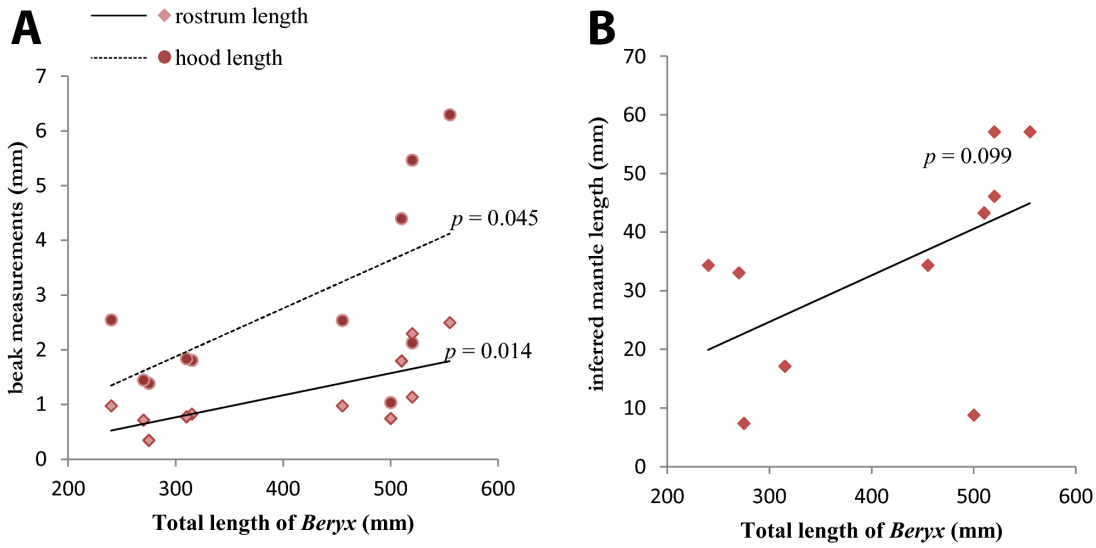

Figure 5.13: Relationship of *Beryx* total length with cephalopod prey measurements. The p-values of the slope coefficients are given. A: Length of *Beryx splendens* against averaged prey beak measurements, $n = 11$. B: Length of *Beryx splendens* against inferred mantle length from prey beaks, $n = 10$.

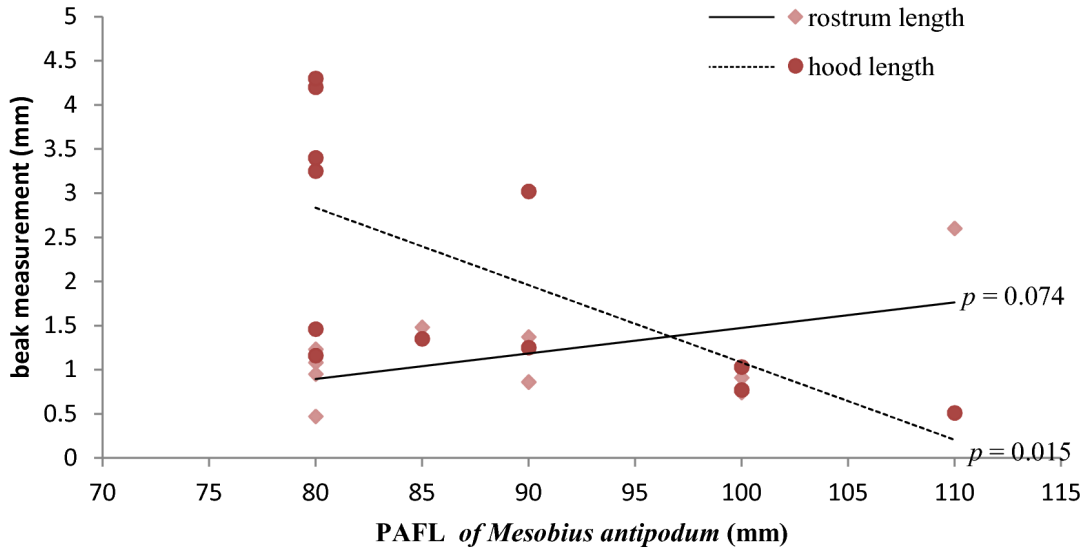

Figure 5.14: Relationship of pre-anal fin length (PAFL) of *M. antipodum* with cephalopod prey beak measurements, $n = 13$. The p-values of the slope coefficients are given.

mantle length of 22 mm (Fig. 5.12). However, the difference was not statistically significant (two sample t-test, p = 0.124). Linear regression reveals a significant positive relationship between the length of the *B. splendens* and the size of the prey item consumed (HL p=0.045; RL p=0.014), as shown in Figure 5.13. This trend is confirmed, although not significantly (p=0.099) by the mantle lengths of beaks which also increase with fish length. The trend is less clear for *M. antipodum*, seen in Figure 5.14, with RL increasing with fish length, although this is not significant (p=0.074) however HL significantly decreases with increasing fish length (p=0.015). Weight of fish did not show any relationship with beak measurements for either fish species.

Otolith data

A total of 13 otoliths were found, all but one coming from stomachs of *B. splendens*. Table 5.6 shows the otolith diameter and corresponding identifications. All otoliths had signs of digestion, with their prominent features and margins eroded as well as their surfaces becoming chalky. Figure 5.15 illustrates the effects of this erosion, and as such, identifications should be interpreted with caution. Five out of the 13 otoliths (38.5%) were identified to the family Myctophidae, the lanternfishes. Other deep-sea species identified include viper fish (*Chauliodus* sp.), grenadier (*Coryphaenoides* sp.), stout cardinal fish (*Rosenblattia robusta*) and ridgehead (*Melamphaes typhlops*). Three otoliths were so heavily digested that identification was not possible.

Although few otoliths were found in the stomachs of *M. antipodum* or *P. richardsoni*, some whole, largely undigested fish were found and identified as members of Myctophidae. In *M. antipodum*, the myctophid was 50 mm in total length and weighed 1.89 g. The two myctophids found in separate stomachs of *P. richardsoni* were 35 mm and 27 mm in total length and weighed 0.9 g and 0.75 g respectively.

Figure 5.15: : Images of otoliths (numbers 5, 6 and 13) showing different stages and effects of digestion. From left to right, least digested to most digested. Diameters are 4.8 mm, 3.4 mm and 4 mm respectively.

Table 5.6: Otolith identifications. ∅: Otolith diameter; Trawled: Congener or conspecific present in micronekton trawl samples (K. Kemp, pers. comm.).

	Otolith		Prey			
Predator	#	∅ (mm)	Taxon	Family	Depth range	Trawled
Beryx	1	3.0	*Symbolophorus* sp.	Myctophidae	nyctoepipelagic	✓
Beryx	2	6.5	*Melamphaes* sp.	Melamphidae	bathypelagic	✓
Beryx	3	7.1	*Notoscopelus* sp.	Myctophidae	nyctoepipelagic	✓
Beryx	4	4.0	unidentifiable			
Beryx	5	4.8	*Coryphaenoides* sp.	Macrouridae	bathypelagic	[a]
Beryx	6	3.4	*Chauliodus* sp.	Stomiidae	nyctoepipelagic	✓
Beryx	7	4.2	*Lampanyctus festivus*	Myctophidae	nyctoepipelagic	✓
Beryx	8	4.2	*Diaphus* sp.	Myctophidae	nyctoepipelagic	✓
Beryx	9	3.2	*Diaphus dumerilii*	Myctophidae	nyctoepipelagic	✓
Beryx	10	3.2	*Rosenblattia robusta*	Epigonidae	benthopelagic	✓
Mesobius	11	1.5	*Bathysolea* sp.	Soleidae	benthic	
Beryx	12	4.0	unidentifiable			
Beryx	13	4.0	unidentifiable			

[a] unidentified demersal macrourids were commonly observed in video surveys during JCO66/67

5.4 Discussion

5.4.1 Summit aggregations

The only consistent observation between the investigated seamounts was the presence of summit associated aggregations of scatterers. This is consistent with acoustic surveys of deep-water seamounts elsewhere showing fish aggregations up to 150 m high on the summit (e.g. Kloser et al., 2002; O'Driscoll et al., 2012). Species composition in these aggregations is often extremely uncertain. In the present study sampling of these plumes was attempted using pelagic trawls and yielded low numbers of large fish, including alfonsino (*Beryx* spp.), spiky oreos (*Neocyttus rhomboidales*), armorhead (*Pseudopentaceros richardsonii*), grenadiers (Macrouridae) and deep-water dogfish (*Etmopterus* spp.; K. Kemp, pers. comm.). Species composition, as well as low catchability with pelagic gear, are comparable to seamounts around Australia and New Zealand, where strong gear avoidance has been reported (Koslow et al., 1995; Kloser and Horne, 2003; O'Driscoll et al., 2012), and are also consistents with reports from the fishing industry (Shotton, 2006, G. Patchell, Sealord Group Ltd., pers. comm.). The uncertainty in species composition together with marked inter-specific differences in acoustic target strength (Kloser et al., 2002; McClatchie and Coombs, 2005) make the interpretation of backscatter in terms of biomass density impossible from vessel-borne echosounder data alone. Acoustic discrimination of species using combinations of towed multi-frequency acoustics and cameras shows some promise for some deep-water species (e.g. Kloser et al., 2013). Nonetheless, the biomass in these aggregations are sufficiently high to attract regular visits from deep-water trawlers in the region (Shotton, 2006, G. Patchell, Sealord Group Ltd., pers. comm.; pers. obs. during JCO66/67).

5.4.2 Hydraulic jump

Striking acoustic imagery of a strong lee wave, or hydraulic jump, was collected serendipitously during the transit across an unnamed seamount in the vicinity of Sapmer Bank. Internal waves have frequently been observed with echosounders (Kaneko et al., 1986; Farmer and Armi, 1999; Warren et al., 2003; Dewey et al., 2005, e.g.), but mostly in coastal environments with water depths <200 m and vertical amplitudes on the order of 10 m. Backscatter by internal waves is caused by a mixture of biological and physical sources, i.e. animals in the water column as well as variations in the temperature and salinity caused by turbulence (Warren et al., 2003). Turbulent wakes spanning hundreds of meters vertically

have been described in simulation studies (e.g. Legg and Huijts, 2006), but this may be the first echosounder observation of the phenomenon in the open ocean.

In the case at hand the internal wave appears to displace parts of the main DSL onto the seabed by some 100 m. Elsewhere similar hydrographic features have been linked to enhanced food availability for cold-water corals and other filter-feeders. Around the Faroe Islands, the highest abundances of a deep-water coral (*Lophelia pertusa*) were found in areas where the seabed slope is critical to the ray of an internal wave (Frederiksen et al., 1992). Internal waves have furthermore been found to transport fresh phytoplankton to deep-sea coral populations on carbonate mounds in the southeast Rockall Trough (NE Atlantic; Duineveld et al., 2007), and more recently the mechanistic details of tidal wave-mediated particle fluxes onto a cold-water coral reef of the Mingulay Reef complex (Outer Hebrides, Scotland) were unraveled by Davies et al. (2009). As deep-water coral reefs may provide essential habitat and nurseries for deep-water fishes (Husebø et al., 2002; Costello et al., 2005), seamount-associated fish stocks may profit directly or indirectly by internal wave mediated trophic inputs. The observation is also interesting from an oceanographic perspective, as recent research suggests that topography-induced internal waves may play a key role in deep-ocean mixing (Nikurashin and Ferrari, 2010, 2013).

5.4.3 Stomach contents

All three species investigated, *Beryx splendens*, *Mesobius antipodum* and *Pseudopentaceros richardsoni*, were found to be piscivorous, and fish, crustaceans and squid were the most abundant prey items. This supports previous stomach content analysis on these species (Seki and Somerton, 1994; Anderson, 2005; Horn et al., 2010) where mesopelagic fish were not only found, but were an important prey item in the diet of both *Beryx* and *Mesobius* species (Horn et al., 2010; Anderson, 2005). A previous study on pelagic armorhead diet around seamounts found the most important prey item to be pelagic tunicates (Seki and Somerton, 1994) which may account for the unidentifiable substance found in all of the armorhead stomachs analysed in this study.

As can be expected, larger fish were found to eat larger prey. This was significant within species but mean prey size was not significantly different between species, though a larger sample size is needed to give a more reliable estimate of the true variation of prey size, especially for *M. antipodum*, where only 5 mantle lengths were calculated, limiting the power of the $t-test$ used to compare mean prey size.

The difference in mean prey size between species could be an important factor of niche separation, allowing for large populations of both species to inhabit waters around these seamounts. However, *M. antipodum* were only caught around Coral Seamount and no *B. splendens* were caught at this seamount. These fish may therefore occupy different water masses and not compete because of geographic separation.

The ability to calculate cephalopod mantle lengths using allometric equations greatly increases the power with which to draw conclusions. For example, in *M. antipodum*, using hood length and rostrum length, measurements gave opposite trends when plotted against fish length. If the beaks found were not so fragmented as to prevent identification to species level, more mantle lengths could have been calculated in order to support the correct trend. For *B. splendens*, mantle lengths supported the positive trend that the raw beak measurements gave when plotted against fish length.

The AFORO database method was used for identifying otoliths in combination with keys and an otolith atlas and this combination proved helpful given the lack of information about the identity of the stomach contents. Nevertheless the database method has some limitations: there is a limited reference dataset, the scoring algorithm is not transparent and the reliability of identification is dependent on the quality of the otolith. In this study, otoliths which were heavily digested yielded implausible identifications such as the Panama grunt (*Pomadasys panamensis*), only found in the coastal waters of Panama, or a freshwater mosquito fish (*Gambusia holbrooki*). Nonetheless, the AFORO database is a quick and simple tool, giving greater access to non-specialists.

Cephalopods and fish are important prey groups to seamount fishes and the majority of prey identified in this study are mesopelagic and nyctoepipelagic (species that migrate to surface waters at night). For *B. splendens*, over 70% of the beaks belong to the squid genera *Histioteuthis* and *Onychoteuthis*, and for *M. antipodum*, these species make up over 50% of beaks found. Both Histioteuthidae and Onychoteuthidae are mesopelagic and there is considerable evidence that they both undertake diel vertical migrations (Voss et al., 1998).

Of the 10 otoliths identified, over one half were identified as nyctoepipelagic including all species of Myctophidae and Stomiidae. Future work should be directed at identifying the crustacean prey, as this group was numerically important and may provide further insights whether the prey consist mostly of migratory micronekton or not.

5.4.4 Topographic blockage

The results from stomach content analysis suggest the seamount fishes in the southwest Indian Ocean receive their trophic input, at least in part, by vertical topographic blockage. The stomach contents furthermore ground-truth the acoustic data that was recorded on Atlantis Bank (Fig. 5.9), showing an interaction between strong acoustic targets, presumably large, swim-bladdered fish, and the descending scattering layer.

Together, the acoustic data and stomach content analysis provide evidence of trophic connectivity between the vertically migrating animals of the pelagic environment and the larger fish species associated with Atlantis Bank. This is in contrast to the recent findings of Hirch and Christiansen (2010), who advocate horizontal advection of small zooplankton as the main energy input for seamount fishes. Their study focused on smaller fish species, such as *Macroramphosus* sp. (max. TL 14 cm), *Capros aper* (max. TL 11.6 cm) and *Anthias anthias* (max. TL 20 cm), likely associated with the seabed on seamounts rather than actively preying in the waters above seamounts. An analogous species observed on the same seamounts using remotely operated vehicles during *RRS James Cook Cruise JCO66/67* in November/December 2011 is the banded yellowfish, *Centriscops humerosus* (Rogers et al., unpublished data). This study therefore does not contradict the conclusions of Hirch and Christiansen (2010) because the investigated predators on SWIR seamounts are larger, less strongly associated with the seabed and thus likely to occupy a different niche. However, it does add evidence that vertical topographic blockage is a mechanism of relevance to commercially important fishes.

Acoustic data furthermore indicated a strong depletion of backscatter downstream of the seamount both below summit height and in the depth stratum occupied by summit aggregations, albeit the latter only applied to 18 kHz data. It appears therefore that both horizontal and vertical blockage occurs, and the different fluxes may be exploited by different guilds, although this is speculative given the sparse data available.

No conclusive evidence of directional depletion could be found at any other station, and this is likely to be a result of differences in the shapes and oceanographic settings of the investigated seamounts. Atlantis Bank differs from all other seamounts in this study by having an almost block-like shape with a flat summit plateau and very steep slopes. It was furthermore the seamount with the least turbulent flow environment, set in a steady southeastern current, whereas tidal currents and the influence of mesoscale eddies and the subtropical frontal system dominated the oceanography of the remaining SWIR seamounts

(Read and Pollard, 2013b,a). The implicit assumption of a unidirectional flow field made in constructing the directional echograms was therefore not fully met. Lastly, Atlantis Bank was the northernmost seamount, and experienced the largest vertical migration amplitude (cf. Chapter 2), which may have further increased blockage effects.

Lastly, it must be said, that the sampling design was a compromise aiming to maximise seamount coverage for the mapping of currents, bathymetry and pelagic backscatter, in a situation where there was little *a priori* information on either parameter. A star-shaped survey pattern, rather than parallel transects may have been more powerful to detect directional effects, but would have concentrated survey effort on the summit.

Chapter 6

Population genetics of the lovely hatchetfish *Argyropelecus aculeatus*

> The widespread occurrence and ease of capture of the Sternoptychidae make them ideally suited for studies involving population structure, speciation, and distribution in the midwater or mesopelagic environment.
>
> Baird (1971)

Abstract The hatchetfish *Argyropelecus aculeatus* is an abundant micronekton species found globally in the open ocean and around seamounts. A 508 bp fragment of mitochondrial cytochrome oxidase subunit 1 (COI) was used to assess the population structure and demography of 199 individuals from 6 stations along the SWIR, to investigate the retention potential of seamounts for pelagic species. Intra and inter-population analyses based on *F*-statistics revealed a high level of genetic diversity but a lack of genetic structure between stations, suggesting that seamount topographies do not isolate populations. These findings are suggestive of a single, well-connected population which can be attributed to the dynamic oceanography of the region. Results further indicate a recent population expansion around 0.14 million years ago.

6.1 Introduction

Population connectivity is the sum of dispersal, survival, and reproduction of migrants resulting in their contribution to a local gene pool (Hedgecock et al., 2007). Population connectivity is linked to demography, community composition, ecosystem resilience, and thus is a crucial factor for the design and implementation of management and conservation strategies (Shank, 2010). A mechanistic understanding of the processes involved in connecting or isolating populations is therefore crucial. Yet understanding these processes is not trivial as no single factor determines connectivity – many physical, biological and ecological factors interact together at different spatial and temporal scales, as will be discussed below. These factors control forces that can either homogenise populations, such as gene flow and migration, or differentiate populations, such as selection or genetic drift, by changing the frequency of alleles in the respective gene pools (Shank, 2010). The genetic make-up of populations represents the net result of these interactions and genetic markers can be used to assess and unravel them.

Investigating genetic connectivity around seamounts will address old and new paradigms such as endemism, retention, and seamounts acting as stepping stones to dispersal (Clark et al., 2010). Investigating genetic connectivity in the open ocean will increase our understanding of the factors influencing gene flow, evolution and diversity in the pelagic realm.

6.1.1 Genetic connectivity in the open ocean

Recent genetic analyses suggest that even though pelagic species may have similar morphology, they can vary genetically and physiologically (Pierrot-Bults and van der Spoel, 2003). This leads to the question whether cosmopolitan species are one highly variable species or a species complex with low morphological variation because of the constraints of the pelagic environment. Knowlton (1993) and Norris (2000) also conclude that traditional classification of morphospecies may greatly underestimate pelagic species richness. Genetic markers may provide a tool to reveal the true taxonomic diversity in the pelagos and to unravel the mechanisms causing this cryptic variation.

To date, evidence of genetic population differentiation and cryptic species in the pelagic environment is mixed. Genetic structure has been found in morphologically similar pelagic crustaceans, including the amphipod *Eurythenes gryllus*, using ribosomal RNA (France and Kocher, 1996) and various copepods and euphausiids (Bucklin et al., 1996; Goetze, 2011) using mitochondrial COI.

Few studies have looked at the phylogeography or connectivity of mesopelagic fishes. For mesopelagic fish, the gonostomatid *Cyclothone alba* was found to have 4 distinct populations within the Pacific Ocean with the intraspecific genetic differences in RNA genes similar to that expected of sister species (Miya and Nishida, 1996, 1997). Gordeeva (2011) investigated the genetic structure of myctophid populations in the southern Atlantic Ocean, finding evidence of genetic differentiation in some species but not others. Myctophid species have also been studied off South Africa (Florence et al., 2002) using isozyme loci, throughout the Southern Ocean, using microsatellites (Van de Putte et al., 2012), and between the east and west Pacific Ocean (Kojima et al., 2009), using mitochondrial cytochrome b, with none of the studies finding genetic structure between sampling locations.

The mechanisms controlling gene flow, population connectivity and, on an evolutionary time scale, speciation, in the open ocean are not fully known (Norris, 2000). Factors such as large population size, broad range, great dispersal potential and an apparent lack of physical barriers would suggest most pelagic populations have a homogeneous structure. Yet the rates of evolutionary turnover in open ocean species can be rapid (Norris, 2000) suggesting population ranges and connectivity could be more restricted than previously thought. Dispersal of zooplankton and micronekton, cannot simply be viewed as that of passive particles, as ecological and physical processes interact to influence connectivity (Cowen et al., 2007). Some of the key factors thought to influence genetic connectivity are discussed below.

Oceanography

Physical oceanographic factors include fronts, jets and tides which can act as hydrographic barriers (Cowen et al., 2007), even for deep-sea fish as Ward et al. (1998) found for the warty oreo, *Allocyttus verrucosus*, using allozymes and mitochondrial genes. Goetze (2011) studied the globally abundant pelagic copepod *Pleuromamma xiphias*, and found genetic breaks in mitochondrial COI sequences at oceanographic fronts in the Indian, Atlantic and Pacific oceans, resulting in structure at regional and basin scales. The Antarctic Polar Front is thought to be a major oceanographic barrier with limited gene flow to populations on either side (e.g. Shaw et al., 2004; Thornhill et al., 2008, and reviewed in Rogers, 2012). Darling et al. (2000), using ribosomal RNA, found the same species of foraminifera inhabiting both the North and South poles, suggesting that, for some species, these barriers are not absolute (McClain and Hardy, 2010). Topographies including mid-ocean ridges and

seamounts may segregate deep water masses causing geographic barriers within oceans, although they are most likely semi-permeable (McClain and Hardy, 2010). Some oceanographic factors such as currents, may act to increase gene flow, especially for species with a limited ability to actively swim a certain direction such as zooplankton (Bortolotto et al., 2011) and micronekton (Van de Putte et al., 2012).

6.1.2 Ecological and behavioural factors

Ecological influences on connectivity include aspects of life history strategies such as fecundity and dispersal ability. For example, Ball et al. (2003) found genetically distinct populations of red porgy, *Pagrus pagrus*, within the north Atlantic using microsatellite markers. In contrast, the wreckfish, *Polyprion americanus* was genetically indistinguishable, again using microsatellites, in the same basin (Ball et al., 2000) but showed differentiation between the north and south Atlantic (Sedberry et al., 1996). This difference was attributed to sedentary juveniles and non-pelagic larvae for red porgy, and a long, pelagic larval duration and migratory juveniles in wreckfish. Behaviour can alter a species' distribution and connectivity; plankton and micronekton can regulate their vertical position in the water column relative to tidal or non-tidal current flows in order to give movement in a certain direction (Hill, 1991). In addition, micronekton have been found to retain their position even against current flows (Wilson and Boehlert, 2004; Genin and Dower, 2007). Biological interactions, such as competition for shared resources between populations and interactions with natural predators can influence the distribution and genetic diversity of a species (Vamosi, 2003).

Historical factors

The choice of genetic marker depends on the temporal and spatial scale being investigated. In this study a mitochondrial marker will be used. Mitochondrial DNA has many advantages as a molecular marker; it is usually maternally inherited and normally does not undergo recombination. It is influenced by genetic drift more than nuclear DNA and therefore is more sensitive to differences between populations. Mitochondrial genes also generally have higher mutation rates than nuclear genes (Creasey and Rogers, 1999). Haplotype frequency and diversity can be used to infer a population's variability and demographic history.

One advantage of using mitochondrial genetic markers is that, by analysing the haplotypes present in populations, we can investigate their demographics and phylogeography; the historical processes that have shaped the evolution, present distribution, and connectivity of the populations. Historical oceanographic events such periods of glacial maxima can help explain the present distribution and diversity of seamount-associated and mesopelagic fish because changes in the environment and changes in oceanographic features over time can reduce or expand a species range, population size and diversity (Aboim et al., 2005; Kojima et al., 2009; Stefansson et al., 2009). The deep-sea environment is dependent on surface productivity (Gage and Tyler, 1991) and so even taxa in the deep are not exempt from major climatic events. The genetic characteristics found in present populations represent but a snapshot of their dynamic history (Norris and Hull, 2012) highlighting the need to include a temporal dimension to analyses.

Niche availability and adaptation

Availability of suitable habitat, even for pelagic species, can strongly alter the genetic connectivity of populations. On questioning pelagic processes, Norris (2000) conjectures that it is the availability of suitable habitat and the ability of species to maintain populations in certain habitats that influences genetic structure more than hydrographic barriers to gene flow, as zoogeographical evidence shows these to be semi-permeable. With dispersal not limited by external factors, the author suggests that genetic structure occurs in sympatry or parapatry, i.e. populations adapt to different niches with environmental gradients such as depth and temperature. These would affect the place or timing of reproduction, ultimately isolating populations. This differs from other hypotheses of isolation (allopatric and vicariance models) as these assume a limit to dispersal. Palumbi (1994) and Darling et al. (2000) both agree that pelagic species represent a challenge to allopatric models. Allopatric speciation has been hypothesised to contribute to high species diversity in the deep sea as a result of the presence of extreme oxygen minimum zones (Rogers, 2000), although this still involves adaptation to an environmental niche.

Gordeeva (2011) seems to support the idea of sympatry for deeper living taxa, where environmental variation in temperature, nutrients and salinity are reduced. She studied the structure of four closely related species of myctophid within the southern Atlantic Ocean. Two species out of four displayed significant genetic differentiation across three sampling regions. This indicated that even with identical abiotic environmental factors and similar

ecology and life cycles, species-specific patterns in structure are still seen. This could be the result of slightly differing adaptive strategies; the species that had spatial genetic structure also had greater feeding specialisation and showed differentiation with depth and around seamounts. These increased adaptations to prey and habitat location could be additional factors that increase genetic isolation of populations through time and space.

Altogether, these studies suggest some general patterns; population differentiation is possible even for highly dispersive, circumglobal species (Miya and Nishida, 1997; Goetze, 2011), and patterns of gene flow cannot be generalised, even for closely related species (Gordeeva, 2011). We now know that variable ecological, physical and adaptive barriers to connectivity exist in pelagic and deep-sea environments. It is still unclear whether physical factors completely prevent dispersal and migration or if they cause selection and adaptation to differing environmental gradients and habitats. Testing and determining these processes in the open ocean is difficult, but the importance of environmental factors infers that historical climatic changes may have affected the structure of marine populations too.

6.1.3 Genetic connectivity at seamounts

The occurrence of hydrographic features as well as the dispersal ability and behaviour of a species (Wilson and Boehlert, 2004) are factors that interact and determine connectivity around seamounts. Theoretically, these could all lead to reproductive and genetic barriers to gene flow at seamounts, resulting in speciation and endemism greater than that of comparable environments such as continental slopes (Rowden et al., 2010a). Hubbs (1959) put forward a stepping stone hypothesis where seamounts act as stepping stones for transoceanic dispersal of (demersal) species. Recent population genetic studies at seamounts suggest that seamounts do not generally support high rates of endemism, but that populations may have more complex patterns of connectivity than previously thought (Samadi et al., 2006; McClain et al., 2009). Previous studies investigating the effect of seamounts on gene flow have looked at benthic or demersal species; this project, investigates the population genetics of pelagic micronekton around seamounts, and aims to establish whether seamounts affect the connectivity of associated, pelagic fauna.

Factors limiting connectivity

The oceanographic setting of a seamount may cause its topography to be segregated from others by deep water, limiting benthic and demersal species connectivity to the rest of the

ocean, such as found using ribosomal RNA and microsatellites for the Patagonian toothfish *Dissostichus eleginoides* (Rogers et al., 2006). This segregation can cause a barrier to gene flow if the dispersal ability of a species is poor (Samadi et al., 2006; Castelin et al., 2010). While most commercially exploited fish species are genetically homogeneous between seamounts (e.g. Martin et al., 1992; Hoarau and Borsa, 2000; Levy-Hartmann et al., 2011), some species have shown population differentiation in mitochondrial markers between seamounts and at a regional scale, for example the blackbelly rosefish, *Helicolenus dactylopterus*, (Aboim et al., 2005). For others, such as the orange roughy, *Hoplostethus atlanticus*, evidence is conflicting between studies and markers (Smith and Benson, 1997; White et al., 2009; Carlsson et al., 2011).

For species not bound to seamount habitats, including pelagic species, a possible factor causing population differentiation is retention, through both hydrographic recirculation features (see section 1.4) and/or behaviour. If recirculating features are persistent enough, larval and/or adult dispersal may be limited. Even in the absence of recirculating flow over seamounts, micronekton have the ability to partially resist advective loss from seamounts (Wilson and Boehlert, 2004). Furthermore, oceanic islands as well as seamounts can harbour micronekton assemblages that are distinct from those in the open ocean (Reid et al., 1991; De Forest and Drazen, 2009). This may promote genetic differentiation of populations between isolated topographic features. Also, seamount habitats may allow selection and adaptation to a new environmental niche, resulting in increased genetic isolation between populations (Gordeeva, 2011).

Factors increasing connectivity

Seamounts may also increase the connectivity of populations at a regional scale with seamounts acting as stepping stones for dispersal. Then genetic similarity of populations between seamounts would be a negative function of geographic distance, as a result of dispersal occurring along 'steps' of suitable habitat (Rowden et al., 2010a). This has been observed for some benthic species, such as brittle stars (Cho and Shank, 2010) and algae (O'Hara et al., 2010), although the pattern does not seem to hold for the majority of investigated taxa (O'Hara et al., 2010).

Seamount chains could act as corridors for dispersal, thereby enhancing gene flow of pelagic species. For example, upwelling of cold water allows for polar species of foraminifera to disperse across tropical waters (Darling et al., 2000). Also, seamounts may provide nav-

igational waypoints during migration as well as enhanced foraging and mating opportunities for large pelagic animals, including tuna, sharks and marine mammals, thus increasing genetic connectivity of populations across ocean basins (e.g. Litvinov, 2007).

6.1.4 The lovely hatchetfish in the SW Indian Ocean: An ideal model to study genetic differentiation in the pelagos?

This study is based on the lovely hatchetfish, *Argyropelecus aculeatus* Valenciennes 1849. *Argyropelecus aculeatus* is an abundant mesopelagic (depth range 100-600 m) fish with a circumglobal distribution in temperate and tropical seas (Baird, 1971; Queró et al., 1990). It may be associated with seamounts (Froese and Sampang, 2004), although it is not restricted to seamount environments. It forms part of the vertically migrating community and thus may play an important role in seamount food-webs (see chapter 5).

The species' widespread occurrence and high catchability makes it well suited for studying the effect of oceanographic processes on population structure and distribution in the mesopelagic environment. Hatchetfish have traits which may counteract migration and connectivity including low larval expatriation (Baird, 1971) and, despite their small size (maximum observed size 75 mm SL, Queró et al. 1990), populations may be able to actively avoid advection off seamounts (Wilson and Boehlert, 2004).

Baird (1971) reported variation in morphological characters such as gill raker number and body depth between populations in the Atlantic and Pacific Ocean. He identifies six separate populations in the Caribbean, Gulf of Mexico, NW and NE Atlantic and the Central and SE Pacific. No data is presented for the Indian Ocean.

The Southwest Indian Ocean (SWIO) is structured by a system of oceanic fronts which may act as barriers to dispersal (see Section 1.5.2 and Fig. 1.8 in the introductory chapter). Alternatively the dynamic currents in the SWIO, most prominently the Agulhas current and its return flow, the Agulhas return current (ARC), may increase connectivity. This is analogous to the 'low structure–high gene flow' found as a result of dispersal by the Antarctic Circumpolar current (ACC) in the myctophid *Electrona antarctica* in the Southern Ocean (Van de Putte et al., 2012). The Agulhas current system is associated with many, highly dynamic mesoscale eddies, circulating masses of water pinched off from the ARC, which mix and distort water mass boundaries (Lutjeharms, 2006; Read and Pollard, 2013a), providing a further feature that may influence dispersal of *A. aculeatus* in the SWIO. On evolutionary timescales the frontal system has undergone profound changes,

Table 6.1: *Argyropelecus spp.* samples collected during EAF-Nansen cruise 2009-410. *n*, sample size.

Station No.	Station Name	Location	*n*
2	Off Ridge North (ORN)	26°56.6'S, 56°14.4'E	28
4	Atlantis Bank (ATL)	32°40.0'S, 57°20.0'E	13
5	Sapmer Bank (SAP)	36°50.0'S, 52°06.6'E	18
6	Middle of What Seamount (MOW)	37°57.6'S, 50°25.2'E	51
9	Melville Bank (MEL)	38°28.8'S, 46°46.2'E	54
10	Un-named Seamount (WAL)	31°37.5'S, 42°50.2'E	76

shifting northward at times and thereby separating temperate and warm water regions of the South Atlantic and Indian Ocean (Diekmann, 2007; Caley et al., 2012).

In summary there is limited evidence to suggest the possibility genetically differentiated populations of *A. aculeatus* on a basin scale. However, given the large population size and dynamic environment of the open ocean the level of genetic differentiation is expected to be very small, and may not be detectable using a single marker. At the same time, the dynamic history of the Southern Ocean frontal system may have changed the range and thus population size of this species on evolutionary time-scales, and this may have left a genetic signature in the population.

6.2 Materials and methods

6.2.1 Sample collection

Mesopelagic micronekton were collected with a medium sized mid-water trawl (Rogers et al., 2009), during EAF-Nansen cruise 2009-410 in November and December 2009. Hatchetfish (*Argyropelecus spp.*) specimens were obtained at four seamounts along the Southwest Indian Ocean Ridge (SWIOR), one seamount west of Walter's Shoal and one site ("Off-ridge North") over deep water, north of the SWIOR. *Argyropelecus aculeatus* was absent from two stations south of the subtropical front. Sampling locations and specimen numbers are detailed in Figure 6.1 and Table 6.1. A small sample of muscle tissue was excised behind the dorsal fin immediately following capture and preserved in 99% ethanol. Tissue samples were transported back to the Department of Zoology, University of Oxford, United Kingdom for genetic analysis.

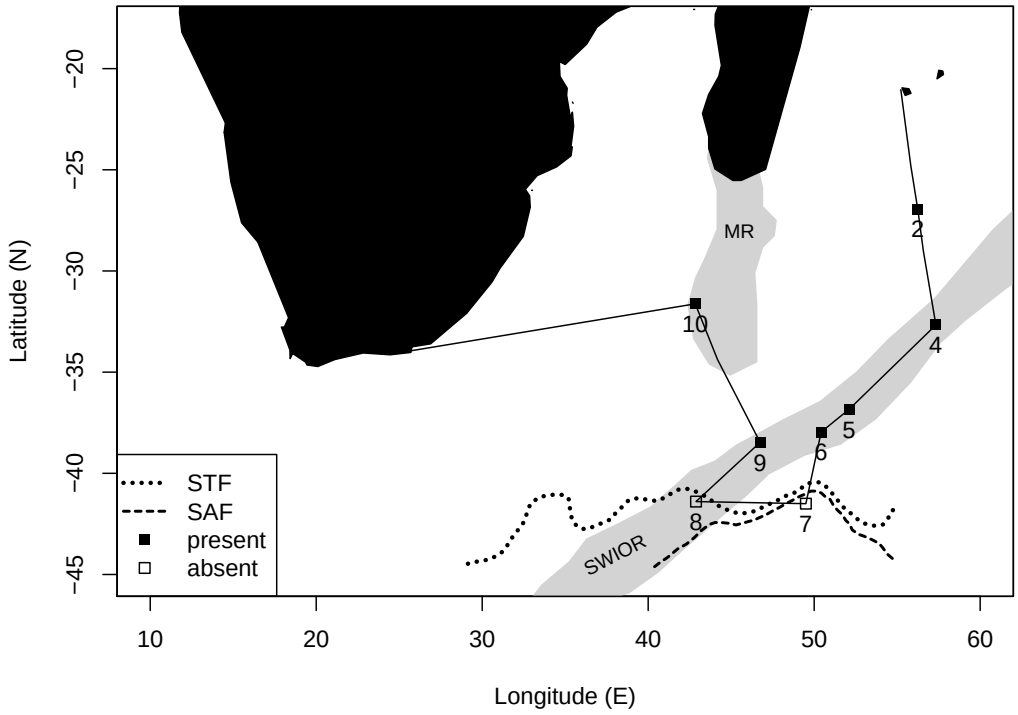

Figure 6.1: Map of the Southwest Indian Ocean and the trajectory of *Nansen* cruise 2009-410. Light shaded areas indicate submarine ridges. Dashed lines indicate approximate locations of hydrographic fronts during the survey (Read and Pollard, 2013a). Stations are: (2) Off-ridge North, (4) Atlantis Bank, (5) Sapmer Bank, (6) Middle of What Seamount, (7) Off-ridge South, (8) Coral Seamount, (9) Melville Bank, (10) Unnamed seamount near Walter's Shoal. Solid and open squares indicate trawl locations where *A. aculeatus* was present or absent, respectively. MR, Madagascar Ridge; SWIOR, Southwest Indian Ridge; STF, subtropical Front; SAF, subantarctic Front.

6.2.2 DNA Extraction

In the laboratory, excess ethanol was blotted from the tissue and total genomic DNA was extracted from 1–3 mg sections of tissue using the DNeasy Blood and Tissue kit (QIAGEN, Crawley, West Sussex, UK), following the manufacturer's instructions. The extracted DNA was re-suspended in elution buffer and stored at -20°C for further analysis.

6.2.3 Marker gene amplification and sequencing

Genetic variation was assessed using partial sequences of mitochondrial cytochrome c oxidase subunit I (COI). COI was chosen because of the availability of stomiiform specific primers and its utility as a dual purpose marker for species identification and population genetics (Hebert et al., 2003a; Bucklin et al., 2010b). This was necessary as most specimens were identified to genus level only at the time of tissue sampling. Reference sequences for

species identification were obtained from the Barcode of Life Database (Ratnasingham and Hebert, 2007).

Polymerase chain reaction (PCR) was performed to amplify a 655-870bp fragment of COI for 236 individuals. Stomiiform specific primers (Miya and Nishida, 1998) were used as well as a universal fish primer cocktail ("FishBOL primers"; Ivanova et al., 2007) on some individuals. Primer details and reaction conditions are provided in Table 6.2.

All amplification reactions had a total volume of 12µl, made up from 8µl HotStarTaq Master Mix (QIAGEN), 2µl sample DNA solution, 1.6µl primer mix (4µM) and 0.4µl water. All reactions were carried out on a thermal cycler (S1000/C1000, Bio-Rad Laboratories Ltd., Hemel Hempstead, UK).

Gel electrophoresis was used to visualise the PCR amplicons and to ascertain that they were of the correct fragment size. A 1% agarose gel was prepared using 100ml TAE buffer, 1g agarose and 3µl ethidium bromide solution. Gels were visualised using a UV cabinet and UVI proMW software (UVItech Ltd., Cambridge, UK). All amplified products were purified using QIAquick PCR purification kit (QIAGEN), following supplier's instructions.

Both strands of the PCR products were sequenced using BigDye Terminator v3.1 Cycle Sequencing Ready Reaction kit (Applied Biosystems, Paisley, UK) under the following reaction conditions: 10µl reactions (0.5µl BigDye, 2.5µl X5 buffer, 2.5µl purified PCR product, 2.5µl primer (forward or reverse, 0.8µM), 2µl water) at: 96°C 1 minute, 25 cycles of 96°C for 10 seconds, 50°C for 5 seconds, 60°C for 4 minutes, then a holding step of 4°C. All reactions were carried out on a thermal cycler (Bio Rad S1000/C1000). Samples were purified using an ethanol/EDTA precipitation method, with 30µl 100% ethanol and 2.5µl 125mM EDTA per reaction. Finally, the products were analysed using a 3100 DNA analyser (Applied Biosystems).

6.2.4 Analytical methods

COI sequence data was aligned using the programme Geneious 5.4 (Biomatters Ltd., Auckland, New Zealand, http://www.geneious.com). Sequence chromatograms were checked visually to resolve ambiguities where possible. Sequences were then trimmed from both ends to allow comparison of good sequence for the maximum number of individuals. A Basic Local Alignment Search Tool (BLAST; Altschul et al., 1997) search on GenBank (Benson et al., 2007) was used to confirm the species identification of the samples. Care was taken to use a final fragment length that did not include the FishBOL primer regions as

Table 6.2: Primers and reaction conditions used to amplify mitochondrial cytochrome oxidase I (mtCOI) of *Argyropelecus* samples. FL, Fragment length (base pairs).

Primer	Sequence 5' – 3'	FL	Reference	PCR conditions
CO1L5956	CACAAAGACATTGGCACCCT	≈870	Miya and Nishida (1998)	95°C – 15 min.
CO1H6864	AGWGTWGCKAGTCAGCTAAA			95°C – 45 sec.
				50°C – 60 sec.
				72°C – 60 sec.
				×35 cycles
				72°C – 10 min.
VF2_t1	TGTAAAACGACGGCCAGTCAACCAACCACAAAGACATTGGCAC	≈655	Ivanova et al. (2007)	95°C – 15 min.
FishF2_t1	TGTAAAACGACGGCCAGTCGACTAATCATAAAGATATCGGCAC			95°C – 30 sec.
FishR2_t1	CAGGAAACAGCTATGACACTTCAGGGTGACCGAAGAATCAGAA			52°C – 40 sec.
FR1d_t1	CAGGAAACAGCTATGACACCTCAGGGTGTCCGAARAAYCARAA			72°C – 60 sec.
M13F (-21)	TGTAAAACGACGGCCAGT			×35 cycles
M13R (-27)	CAGGAAACAGCTATGAC			72°C – 10 min.

this would have created a false polymorphism between samples amplified by the stomiiform primers and samples amplified by the FishBOL primers.

Ordinary least squares (OLS) regression was carried out using the R statistical environment (R Development Core Team, 2010) to investigate the relationship between sample size and the number of haplotypes per sample with the aim to assess whether sample sizes were sufficiently large to adequately reflect the haplotype diversity.

All population genetic analyses were computed using the software ARLEQUIN (Version 3.5.1.2; Excoffier and Lischer, 2010) and visualised using R. Intra-population diversity and diversity across all samples was analysed by estimating haplotype diversity h, the probability that two randomly chosen haplotypes are different (Nei, 1987), and nucleotide diversity π, the probability that randomly chosen homologous nucleotides are different (Tajima, 1983; Nei, 1987).

Molecular diversity indices were estimated for each sampling site using the population parameter

$$\theta = 2Mu, \tag{6.1}$$

where M is equal to the size of a haploid population, and u is the overall mutation rate at the haplotype level. θ_k was estimated using the expected number of alleles k, the sample size, and θ. θ_π was estimated using the number of pairwise differences π and θ.

Using ARLEQUIN, spatial genetic structure of populations was analysed using several methods including pairwise F_{ST} (Weir and Cockerham, 1984), the measure of extent of genetic differentiation among sub-populations (S) relative to the total variance (T). Analysis of Molecular Variance (AMOVA) was performed with partitioning of data in to hierarchical levels of spatial separation (Excoffier et al., 1992). For pairwise F_{ST} and AMOVA computations, both conventional F_{ST}'s (using haplotype frequencies only) and a pairwise nucleotide distance matrix were used as the choice of distance matrix. All pairwise F_{ST} and AMOVA were computed using 10,000 permutations.

Demographic history was also investigated using ARLEQUIN. By analysing the distribution of the number of pairwise differences between all haplotypes, we can discriminate whether a population has undergone a rapid population expansion (possibly after a bottleneck) or has remained stable over time. This was computed using 10,000 bootstrap replicates. The resulting mismatch distribution will appear unimodal (similar to a Poisson distribution) if accumulation of new mutations is greater than the loss of variation through genetic drift, and multimodal if the generation of new mutations is offset by random ge-

netic drift (Rogers and Harpending, 1992). Tajima's *D* test (Tajima, 1983) and Fu's F_S test of selective neutrality (Fu, 1997) were also performed using 10,000 simulations. Both of these tests are sensitive to population expansion, with Tajima's *D* showing a significant value and Fu's F_S showing a highly negative value if a population has undergone expansion. A minimum spanning tree among haplotypes was computed using ARLEQUIN and visualised using the pegas package in R (Paradis, 2010).

ARLEQUIN was used to perform a Mantel Test, comparing the linearized *F*-statistic

$$\frac{F_{ST}}{1 - F_{ST}}$$

with pairwise great-circle distances between the sampling stations, in order to test for isolation by distance (Smouse et al., 1986). Great-circle distances across a basin do not necessarily reflect the (predominantly meridional) environmental gradients, especially as the study spans similar zonal and meridional distances. Furthermore, mesoscale features such as eddies can disrupt basin scale environmental gradients. Isolation by distance was therefore also investigated based on temperature differences between sampling stations, using the mean water-column temperature of the upper 1000m, as this was deemed to be a more appropriate proxy of water mass and thus pelagic habitat type. Statistical significance of correlation coefficients was estimated using 10,000 permutations. Both conventional *F*-statistics (using haplotype frequencies only), and a nucleotide pairwise distance matrix were used as the choice of distance matrix.

6.3 Results

The nucleotide sequences of COI were determined for 199 samples of *Argyropelecus aculeatus*: 109 samples were sequenced using stomiiform-specific primers and 90 samples were successfully amplified using the FishBOL primers as they would not amplify using the stomiiform-specific primers. 12 samples did not give sufficient sequence data and 14 samples did not amplify using either primer combinations. A further 11 samples were identified as different species. 199 sequences of *Argyropelecus aculeatus* gave a 508 bp consensus sequence. All nucleotide sequences determined in this study will be deposited in Genbank.

6.3.1 Genetic diversity indices

Table 6.3 presents the basic diversity indices both within and between sampling stations. A large number of haplotypes was found, indicating a high genetic diversity at all stations. Sample size was a significant predictor of the number of haplotypes per sample (OLS regression, β=0.42, t_4=6.64, $p < 0.01$; cf. Figure 6.2). This pattern may begin to level off with the largest sample size, $n = 67$, although this data point still falls well into the confidence limits of the model.

Using θ_k as an indicator of molecular diversity, which takes in to account expected allele frequencies, highest within-station diversity was found at MOW seamount (station 6) and lowest within-station diversity was found at ORN (station 2), ATL (station 4) and SAP (station 5). Diversity is also high at WAL (station 10) but is lower for MEL (station 9). Using θ_π as an indicator of diversity, which takes in to account pairwise nucleotide differences, all populations had similarly small values. Both measures are illustrated in Figure 6.3.

AMOVA

No significant overall genetic differentiation could be found among populations regardless, whether haplotype frequency ($F_{ST} = 0.0035$, $p = 0.272$) or pairwise nucleotide distance ($F_{ST} = -0.00363$, $p = 0.579$) were used as a basis.

Pairwise F_{ST}

All pairwise F_{ST} estimates were non-significant using the pairwise distance matrix computation, as shown in Table 6.4. Using the haplotype frequency matrix, one significant pairwise estimate was found ($F_{ST} = 0.04798$, $p = 0.045$), between SAP and MEL, although this was not significant after Bonferroni correction ($p = 0.68$).

Mantel test

No significant correlation was seen between genetic distance and geographical distance both for haplotype frequency distance matrix ($p = 0.866$) and pairwise nucleotide distance matrix ($p = 0.779$). Replacing geographical distance values with temperature difference values showed a more pronounced structure using a haplotype frequency distance matrix ($p = 0.056$) but this is not significant using a pairwise nucleotide distance matrix ($p = 0.682$). Table 6.5 shows the geographic and temperature distance matrices used. A

Table 6.3: Summary of basic diversity indices from intra-population and inter-population analyses of *A. aculeatus*. *n*, sample size; N_h, number of haplotypes; *h*, haplotype diversity; π, nucleotide diversity

	2 ORN	4 ATL	5 SAP	6 MOW	9 MEL	10 WAL	mean	s.d.	all samples
n	27	6	15	46	38	67	33.167	22.085	199
N_h	11	4	7	26	19	27	15.667	9.791	69
h	0.8234	0.8000	0.7238	0.9043	0.8990	0.8747	0.838	0.069	0.8684
	(±0.0576)	(±0.1721)	(±0.1206)	(±0.0339)	(±0.0323)	(±0.0276)			
π	0.0047	0.0034	0.0038	0.0050	0.0054	0.0044	0.0045	0.001	0.0047
	(±0.0029)	(±0.0026)	(±0.0026)	(±0.0031)	(±0.0033)	(±0.0027)			

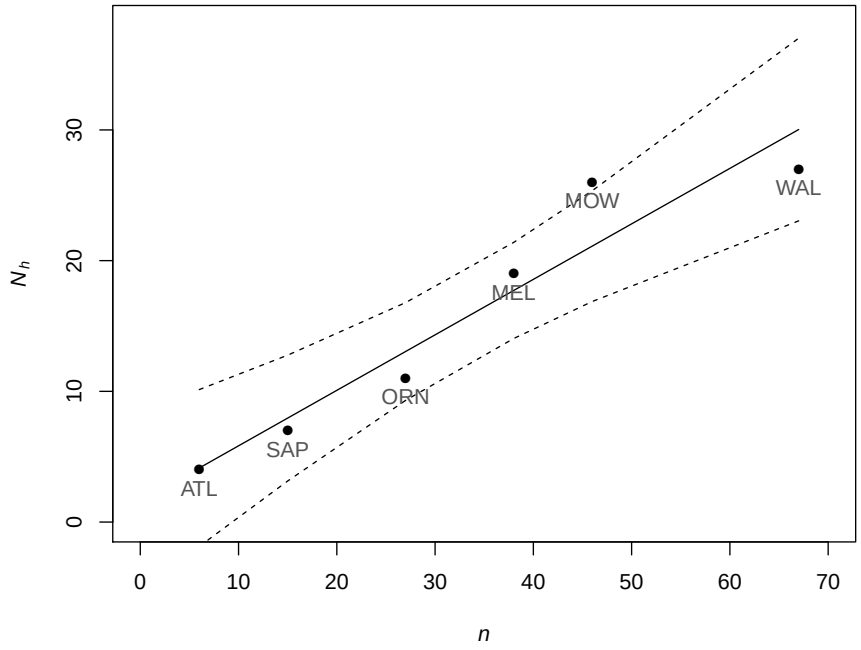

Figure 6.2: Relationship of sample size n and number of haplotypes N_h per station. Lines show ordinary least squares model fit and associated 95% confidence limits. The two variables are significantly related (β=0.42, t_4=6.64, $p < 0.01$)

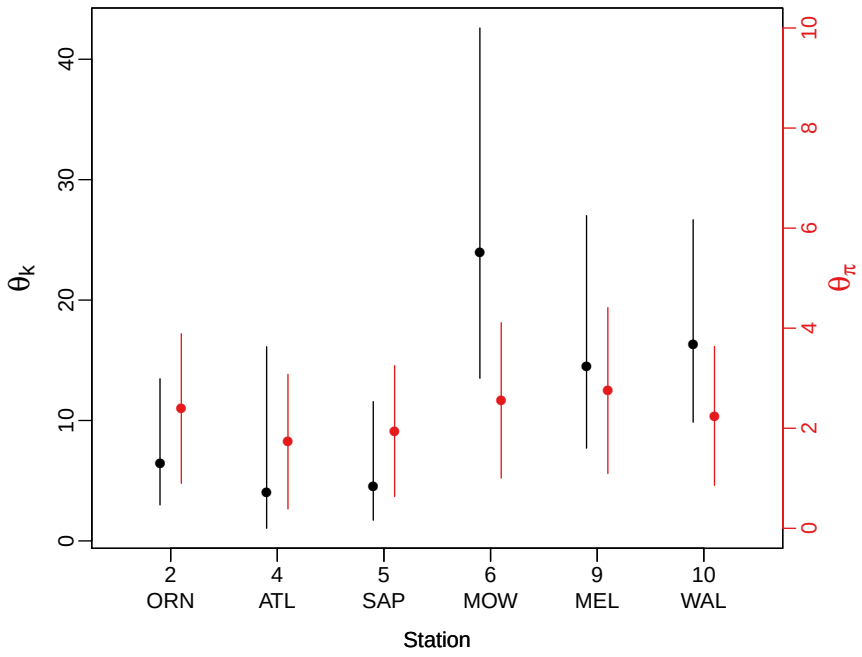

Figure 6.3: Intra-population molecular diversity. Stations are ordered from North (2) to South (9). θ_k, allele-based diversity index (black); θ_π, nucleotide-based diversity index (red).

Table 6.4: Observed F_{ST} and associated p-values (in parentheses) for pairwise comparison between sampling stations based on mtCOI sequence data, after Bonferroni corrections. Values using the nucleotide pairwise distance matrix are shown in the upper triangle, values using the conventional F_{ST} distance matrix are shown in the lower triangle.

	2 ORN	4 ATL	5 SAP	6 MOW	9 MEL	10 WAL
2 ORN	*	0.00001 (0.75)	0.00131 (0.35)	0.00259 (0.30)	0.00001 (0.77)	0.00001 (0.51)
4 ATL	0.05853 (0.14)	*	0.00001 (0.44)	0.00001 (0.75)	0.00001 (0.92)	0.00001 (0.90)
5 SAP	0.00339 (0.32)	0.09208 (0.11)	*	0.00001 (1.00)	0.02164 (0.17)	0.00001 (0.36)
6 MOW	0.00121 (0.34)	0.01466 (0.29)	0.00741 (0.25)	*	0.01755 (0.10)	0.00091 (0.31)
9 MEL	0 (0.38)	0.01792 (0.28)	0.04798 (0.68)	0.00307 (0.28)	*	0.00001 (0.37)
10 WAL	0.00001 (0.57)	0.0143 (0.29)	0.01816 (0.16)	0.00001 (0.68)	0.00001 (0.65)	*

Table 6.5: Pairwise geographic distances (great-circle distance, km) in lower triangle and pairwise temperature differences ΔT (difference of the mean temperature of the top 1000m, °C) in upper triangle.

	2 ORN	4 ATL	5 SAP	6 MOW	9 MEL	10 WAL
2 ORN	*	0.73	1.17	0.32	0.32	0.09
4 ATL	370	*	1.90	1.05	1.05	0.64
5 SAP	791	640	*	0.86	0.85	1.26
6 MOW	977	844	204	*	0.00	0.40
9 MEL	1321	1242	608	410	*	0.40
10 WAL	1527	1613	1102	971	694	*

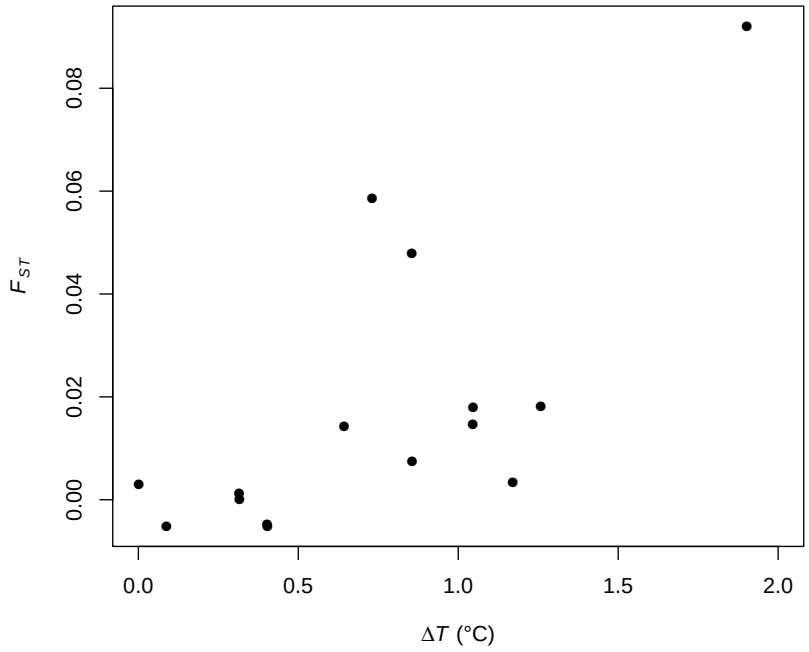

Figure 6.4: The scatterplot of pairwise F_{ST} (based on haplotype frequencies) and pairwise temperature differences ΔT (in °C) between stations.

tentatively positive relationship between F_{ST} and temperature difference can be seen in Figure 6.4.

Mismatch distribution and neutrality

As no significant structure was found between sampling stations, all individuals were pooled and treated as one single population. No significant difference was found between the observed mismatch distribution and a distribution expected under the sudden expansion model of Rogers and Harpending (1992, ; i.e. unimodal distribution) ($p > 0.05$) suggesting a recent population expansion or selective sweep. The estimated mismatch distribution with a mode $\tau = 2.875$ (95% CI [1.070, 4.684]) is illustrated in Figure 6.5. This expansion/sweep signature is also reflected in the results of Tajima's D test ($D = -2.245$, $p = 0.002$) and Fu's F_S statistic ($F_S = -26.781$, $p < 0.0001$).

The minimum spanning tree of haplotypes (Figure 6.6) is star shaped which is also consistent with a recent population expansion.

The time t since this expansion can be estimated from τ using the relationship

$$\tau = 2ut. \tag{6.2}$$

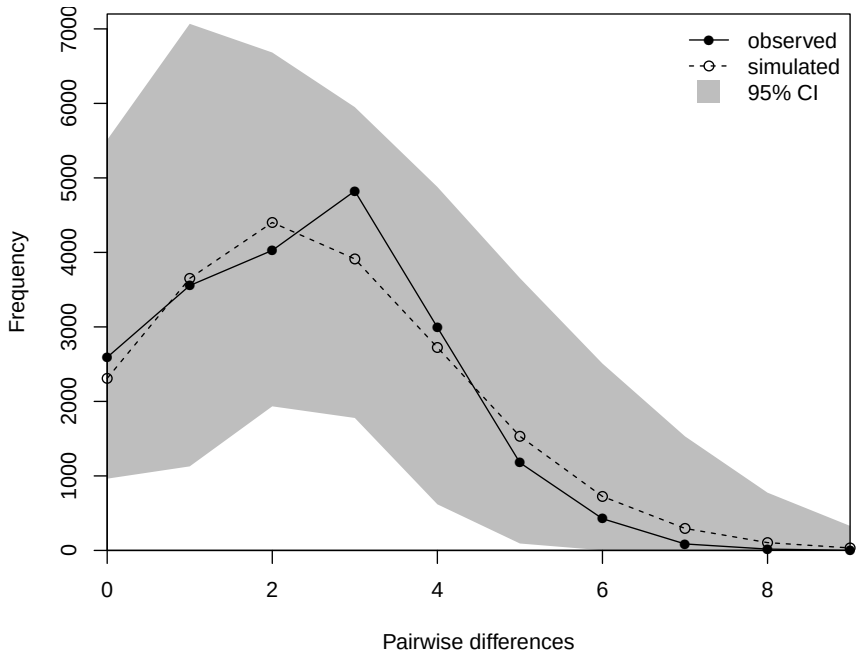

Figure 6.5: Observed and simulated mismatch distributions of pairwise differences of mtCOI sequences of *A. aculeatus* from the SWIO under the sudden expansion model of Rogers and Harpending (1992). The mode of the distribution $\tau = 2.875$ (95% CI [1.070, 4.684])

For a DNA sequence with m_T nucleotides and a mutation rate μ per nucleotide $u = m_T\mu$ (Rogers and Harpending, 1992). Using a mutation rate for mitochondrial genes of 2% per million years (Brown et al., 1979), the population expansion can be estimated to have happened 0.14 million years ago (mya; 95% CI [0.05,0.23]).

6.4 Discussion

This study is the first to investigate genetic structure in the genus *Argyropelecus* and the first population genetics study on a mesopelagic fish in the southwest Indian Ocean (SWIO). The results suggest a highly connected population of *Argyropelecus aculeatus* within the SWIO, with high gene flow, high genetic diversity and no significant spatial structure. This is consistent with previous studies on other mesopelagic fish off South Africa (Florence et al., 2002), in the Pacific Ocean (Kojima et al., 2009) and in the Southern Ocean (Van de Putte et al., 2012).

It can be noted that the original primer set used in this study, specific to the stomiiform order, did not work for a large proportion of samples, despite extensive troubleshooting

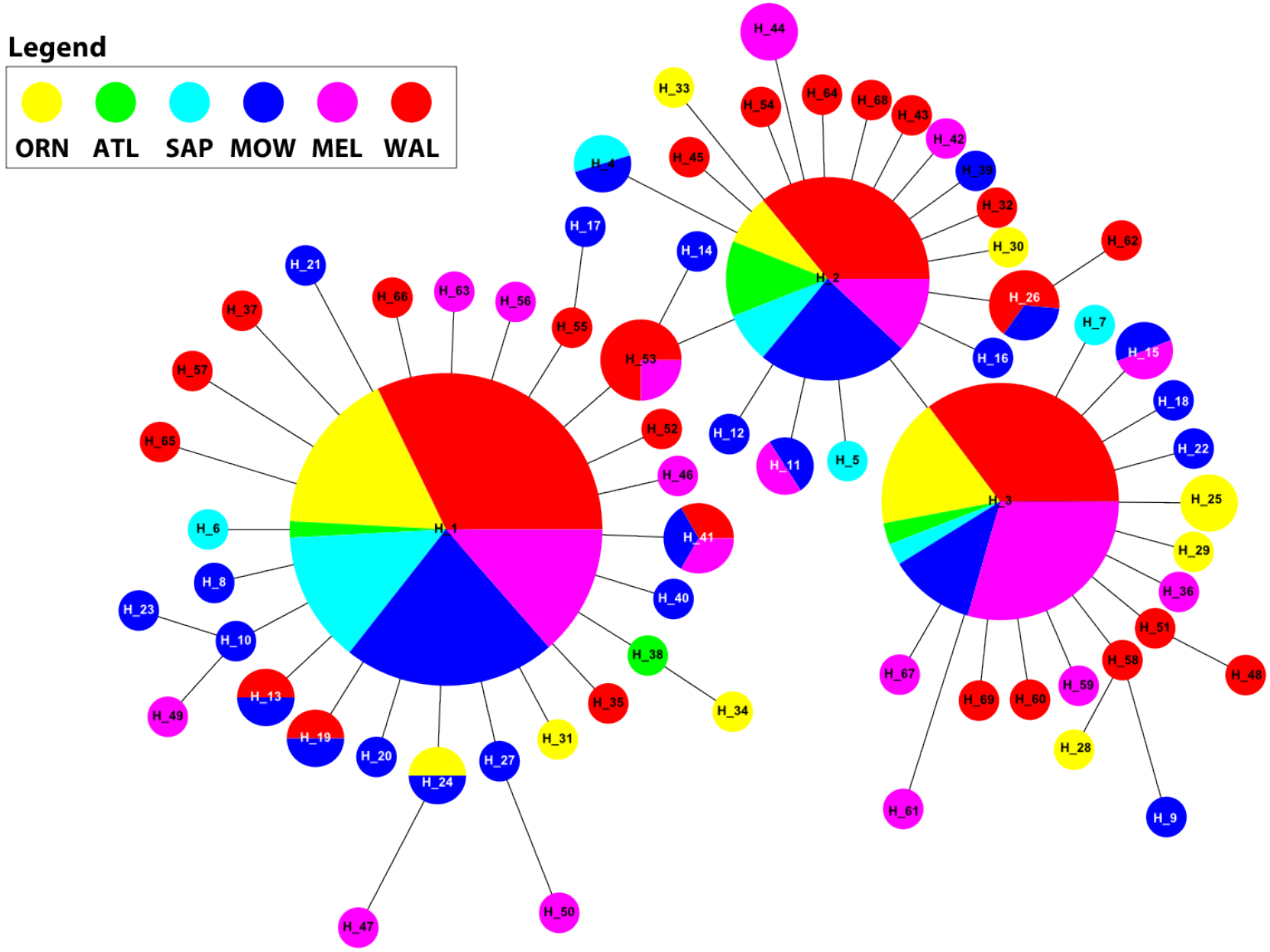

Figure 6.6: Minimum spanning tree of all haplotypes (identified by numbers in the circles), colour coded by station (see legend). The area of each haplotype circle is representative of the haplotype frequency among all sampling stations. The size of the coloured segments within each circle is representative of the haplotype frequency within a sampling station.

attempts and other primer sets working well on these samples. This could result from a mutation in the primer binding region of these individuals, although it was not possible to confirm the sequence of the binding site as all attempts to amplify the fragment in question were unsuccessful. I recommend future studies using the COI marker for stomiiform species to use the FishBOL primer set for more consistent results.

The southwest Indian Ocean has a dynamic system of oceanographic fronts and currents (Read et al., 2000; Read and Pollard, 2013a) and these, particularly the surface currents and associated eddies have influenced the distribution and diversity of the hatchetfish. Firstly, no hatchetfish were sampled at station 8 and 9 which are situated on the Subantarctic Front (SAF), suggesting this front marks the edge of their range limit. The SAF has been demonstrated to be a biogeographic boundary in this region, both by previous studies (Vierros et al., 2009; Pakhomov et al., 1994), and the results of biogeographic analyses across multiple trophic levels from bacteria (Djurhuus and Rogers, 2013) to crustaceans (Letessier et al., 2014), cephalopods (Laptikovsky et al., 2014) and fishes (K. Kemp, personal communication) collected at the same time as the hatchetfish employed in the present study. Also, it appears that the distribution of *A. aculeatus* is largely determined by ocean currents, explaining their low spatial structure; all seamounts are influenced by the Agulhas Return Current (ARC) and some even by dynamic mesoscale eddies that have broken off of the ARC (Schott et al., 2009; Read and Pollard, 2013a). These surface currents are most likely acting to connect populations throughout the SWIO, similar to the findings of Van de Putte et al. (2012) where the Antarctic Circumpolar Current acts to connect populations of mesopelagic myctophid fish.

One interesting result is the pattern of increasing genetic differentiation (larger *F*-statistic values) with increasing temperature difference between stations (Figure 6.4). The largest temperature difference was not found between most northern and southern stations as would be expected from the warm, northern sub-tropical zone and cold, southern sub-Antarctic zone, but between Sapmer Bank and Atlantis Bank, stations 5 and 4 respectively. This is because of the thermocline depth differences at each station at the time of sampling; strongest stratification was detected at Atlantis Bank, giving it the lowest mean water column temperature of 12°C, with similar observations at station 10 on the Madagascar Ridge. Weakest stratification was detected at Sapmer Bank, giving it the highest mean temperature of 14°C, with similar observations at stations 6 and 9 (Read and Pollard, 2013a,b). These temperature differences are a result of stations 5, 6 and 9 being influenced by a deep-extending anticyclonic eddy of warmer water from the ARC, with station 5 situated in the

middle of the eddy (Read and Pollard, 2013a).

It is clear that eddies are frequent and an important oceanographic feature in the SWIO, creating eddy-mediated mixing of water masses (Read et al., 2000; Read and Pollard, 2013a). This limits the conclusions that can be drawn about the frontal systems acting as barriers to gene flow, because their boundaries are distorted and mesoscale eddies can act to relocate micronekton and other biota along the SWIOR (Ansorge et al., 2010). Furthermore, as haplotype frequencies correlate with temperature differences caused by these eddies, it can be hypothesised that the hatchetfish found around the northern subtropical zone (i.e. station 2), are connected to southerly located hatchetfish around stations 5, 6 and 9 because warmer water is transported via the ARC and frequently intercepts these stations in the form of mesoscale, anticyclonic eddies. Stations 4 and 10, situated at latitudes between station 2 and station 5, are not in the pathway of most eddies and their ocean chemistry differs in that water is colder, less dense and exhibits stronger stratification (Read and Pollard, 2013a) which could explain the haplotype frequency differences between warmer and colder stations.

This leads to the conclusion that external physical and environmental factors as well as the biology of *A. aculeatus* (their small size and inability to overcome oceanic currents) are underlying processes affecting their dispersal and thus connectivity. Nevertheless more information must be considered before conclusions can be drawn, including the persistence of mesoscale eddies, temporal consistency of these patterns and our sample size. Despite a positive correlation between F_{ST} and temperature difference, the tests for isolation by distance are non-significant, indicating gene flow between all stations is sufficient to prevent population differentiation. Baird (1971) demonstrated within-basin population differentiation in morphological characters, but these differences may be occurring on the phenotypic level, or mtCOI may lack the resolution to detect genetic differentiation at this scale and/or for these characters. Further studies are needed to target other micronekton species and larger spatial scales, such as between ocean basins, although it is likely that patterns of connectivity, fundamentally built upon numerous and variable factors, will be equally variable.

Seamounts on the SWIR, do not harbour isolated populations of *A.aculeatus* as no significant structure was found between seamounts. If *A. aculeatus* are able to resist advection and maintain their position around seamounts, this behaviour is not strong enough to cause any significant genetic structure; in addition, larvae and juveniles are less likely to be able to resist advection, thus potentially overriding retentive behaviour of adult hatchetfish.

There is also no evidence that the seamounts along the ridge enhance the connectivity of *A. aculeatus* by acting as stepping stones for dispersal as no isolation by geographical distance was detected. This is most likely a result of the fact that these are pelagic fish with no dependence on seamounts as a habitat. Genetic diversity around seamounts was no higher than at off-seamount stations 2 and 10. In fact, diversity was least over Sapmer Bank, possibly a result of a sample size artefact or because it was in the middle of a mesoscale eddy, which are known to reduce abundance of micronekton relative to surrounding waters (Ansorge et al., 2010).

Altogether these mesopelagic micronekton do not seem to conform to the seamount paradigms of retention or endemism and their connectivity is largely independent of the submarine topography. However, each seamount is influenced differently by mesoscale eddies which, as discussed, may affect population diversity and differentiation between the seamounts. As this is the first population genetic study on seamount-associated micronekton, our results have no similar comparisons, although results of well-connected populations match the majority of seamount fish studies (e.g. Martin et al., 1992; Hoarau and Borsa, 2000; White et al., 2009). Studies that have found genetic structure between seamounts are of species that are directly associated with the seamount topography or have poor dispersal capacity (Castelin et al., 2010), neither of which is applicable to *A. aculeatus*.

A high genetic diversity and low nucleotide diversity was found at all stations. High genetic diversity conforms to previous studies on abundant pelagic fish species (McCusker and Bentzen, 2010) and low nucleotide diversity could be because this statistic is more sensitive to past historical events, indicating a recent population expansion (Grant and Bowen, 1998; McCusker and Bentzen, 2010). Molecular diversity based on allele frequencies θ_k was found to be highest at stations 6, Middle of What Seamount, and station 10, Walter's Shoal, and lowest at northern stations 2, Off Ridge North, 4, Atlantis Bank, and 5, Sapmer Bank, along with the most southern station, 9 Melville Bank. As this was the first study on this species, there was no *a priori* information on the sampling size necessary and so this pattern could be a sample size artefact as stations with a larger sample size have higher molecular diversity. Figure 6.2 gives an indication that haplotype numbers may begin to reach an asymptote with large sample size ($n > 45$), suggesting that the large sample sizes give an accurate representation of haplotype diversity. However, the large sample sizes are still well within the confidence bands of the regression model, thus sample size may still limit our inferences.

An alternative conclusion is that diversity is highest in the convergence zone – where

the Subtropical Front and Subantarctic Front interact and productivity is higher than surrounding waters - and diversity decreases towards peripheral stations – where northern stations are close to the less productive subtropical Indian Ocean gyre and southern stations are close to the species range limit. The fact that sample size was higher at central stations further suggests that the convergence zone is the central, most populous region, although there is some uncertainty whether the employed trawl samples micronekton quantitatively (Heino et al., 2011). This pattern matches that of the central-marginal hypothesis which states that when a species colonises a gradient of environmental conditions, it should be most abundant at the centre of the range where survival and population growth is highest, and increasingly less abundant towards range limits as conditions depart from this optimum (Brown, 1984). Lower genetic diversity was observed at peripheral stations, but no significant differentiation was found which would have been expected if there was a smaller effective population size at peripheral stations (Eckert et al., 2008). However, the largest nucleotide pairwise difference was found between central station 5, Sapmer Bank and the southernmost sampling location of *A.aculeatus* at station 9, Melville Bank, potentially indicating a lack of power in the employed analysis due to small sample sizes.

Processes that determine the genetic characteristic of populations are also influenced by demography, both past and present. The mismatch distribution, haplotype network and neutrality tests all indicate that populations of *A. aculeatus* in the SWIO have undergone a recent expansion or selective sweep which can be dated, albeit approximately, to around 0.14 mya. Assuming an expansion, this would indicate a population bottleneck in the late Pleistocene. In fact, the expansion time estimate t corresponds well with major glacial terminations at 0.13 mya and 0.24 mya (Peeters et al., 2004). Sediment data indicate that Quaternary glaciations had a profound effect on the large scale circulation of the southern Indian and Atlantic ocean (cf. Figure 1.8). The entire frontal system of the ACC, including the STF, shifted northwards during glaciations (Bard and Rickaby, 2009; Diekmann, 2007), resulting in a cessation of Agulhas leakage, i.e. the transport of Indian Ocean surface waters into the South Atlantic (Caley et al., 2012). A major pertubation to the Agulhas current system, as well as the northward movement of the STF, which currently appears to bound the distribution of *A. aculeatus*, is likely to have impacted both habitat availability and dispersal pathways of the species. The expansion signature is near the lower bound of other deep-sea fish expansion estimates (Aboim et al., 2005; Kojima et al., 2009) from the Atlantic and Pacific Oceans, ranging from 1.24 – 0.11 mya, adding further evidence that even highly abundant, mesopelagic species are vulnerable to major climatic changes.

Chapter 7

Evaluating the use of DNA barcodes to identify cryptic larvae of potential seamount spawners

> The most profound transformation at a single moult known among Decapoda is that of the *Phyllosoma* to the post-larval stage [...]
>
> Gurney (1942)

Abstract Dispersal and recruitment are key ecological processes structuring the communities inhabiting seamounts. They are of direct relevance for the management of exploited fish and invertebrate populations, such as spiny lobsters, which are harvested by an unregulated fishery in the SWIO. The identification of dispersal stages is often difficult as larvae can lack characteristic features. Genetic barcoding can elucidate the identity of cryptic larval specimens. Mitochondrial cytochrome oxidase I and 16S ribosomal RNA were employed to identify larval stages of eels (leptocephali) and spiny lobsters (phyllosomata). Identification success was limited due to poor PCR success and a lack of reference sequences for species identification. Nonetheless results indicated the presence of 3 to 4 phyllosoma clades and 5 to 6 leptocephalus clades along the SWIR.

7.1 Introduction

Dispersal and recruitment are key ecological processes structuring the communities inhabiting seamounts. They pertain to some of the core paradigms of seamount ecology, such as Hubbs' (1959) stepping stone hypothesis and are of direct relevance for the management of exploited fish and invertebrate populations on seamounts. The larvae of meroplanktonic organisms are crucial in dispersal and recruitment of seamount inhabitants, but studies of dispersal and recruitment are dependent on the correct identification of each ontogenic stage of these species. This is often particularly difficult for larvae because of their lack of resemblance to conspecific adults and their high degree of similarity with congenerics at the same stage of development.

Traditional methods of investigating larval forms rely on rearing larvae obtained in the field or from spawning adults and the resulting descriptions have proved useful in systematic, evolutionary and ecological studies (Williamson, 1982; Miller, 2009). However, these methods are time consuming and often carry a high degree of uncertainty when the species diversity of the sampling area is high. Early ontogenetic stages are often only differentiated between species by minute and/or fragile morphological structures, some of which are easily damaged during collection.

Molecular markers are powerful tools for the identification of species in many zoological groups (Hebert et al., 2003a) and can thus be a good alternative for the identification of cryptic larval stages, especially when many closely related species are collected simultaneously.

This chapter aims to evaluate the utility of genetic barcodes and morphology as means to identify phyllosoma and leptocephalus larvae, as a prerequisite for ecological investigations into the dispersal of seamount-associated species.

7.1.1 Leptocephali and phyllosomata: cryptic larvae of seamount spawners?

The phyllosoma larvae of the spiny and slipper lobsters (Crustacea, Decapoda, Achelata) and the leptocephalus larvae of the eels (Elopomorpha, Anguilliformes) provide a clear illustration of the difficulties encountered in morphological identification of larvae. Their transparent nature and fragile morphology makes intact specimens difficult to capture, and any damage can significantly hinder morphological identification. Both zoological groups

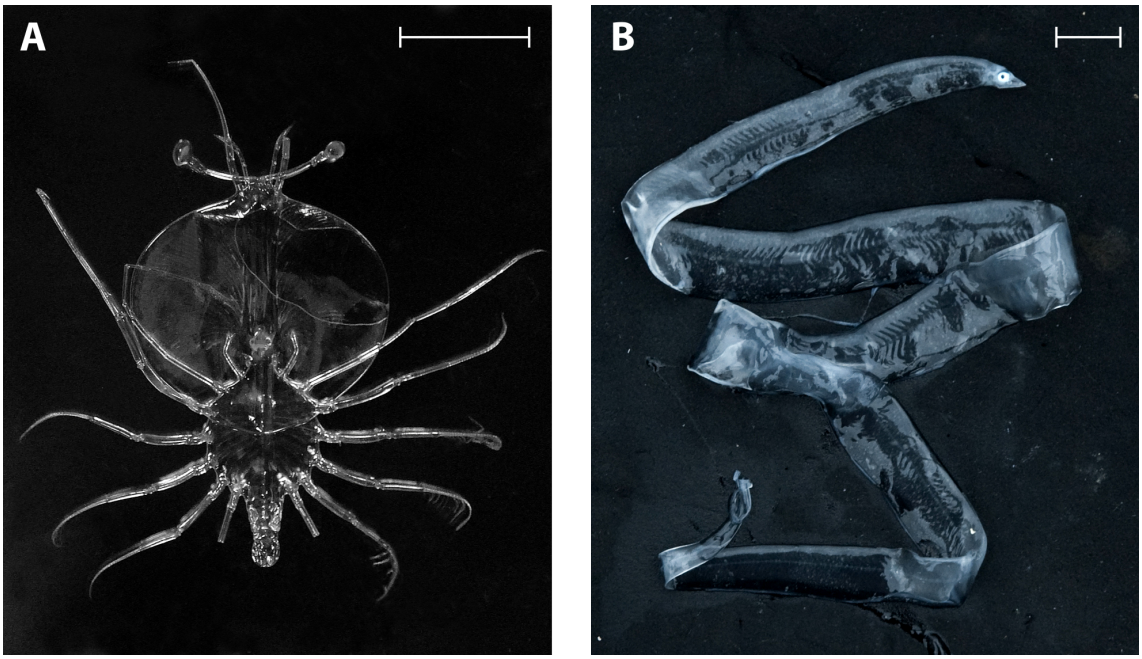

Figure 7.1: Pelagic larvae obtained during cruise 2009-410. A: Late stage phyllosoma exhibiting a typical leaf-like appearance and elongated antennae, diagnostic of the family Palinuridae. B: Unidentified leptocephalus. Scalebar 1 cm. Photos: Oddgeir Alvheim.

were chosen for this study as the life cycles of some commercially important species in both groups are closely linked to seamount habitats.

Spiny lobsters (Family Palinuridae) are a target species for coastal and high-seas fisheries along the African continental shelf and the Madagascar ridge (Holthuis, 1991) as well as the Southwest Indian Ridge (SWIR; Groeneveld et al., 2012, see also this study, Figure 7.8). There is a growing body of literature on the genetic structure of spiny lobster populations in the region (Gopal et al., 2006; Groeneveld et al., 2007, 2006, 2012) but very little is known about the ecology of their larvae.

Seamounts have recently been suggested to be important spawning grounds for freshwater eels in the Pacific Ocean (Tsukamoto, 2006), however, the current knowledge of leptocephalus ecology in the Southwest Indian Ocean, and elsewhere, is limited (Miller, 2009). A better understanding of dispersal ranges and pathways should deliver important baseline information for fisheries management in the southwest Indian Ocean.

The life histories of Achelata

The systematic position of Decapod larval forms was a matter of strong controversy in early crustacean taxonomy and it was not until the 1840s that metamorphosis was principally accepted as the process of larval development, leaving the difficult task of relating the larval genera to the adults (Gurney, 1942). Phyllosoma larvae had been placed into a genus of their own, *Phyllosoma* Leach 1817, and it was only in the late 19th century that they were demonstrated to be the larval forms of the Achelata (Dohrn, 1870), an infra-order containing the claw-less spiny and slipper lobsters.

Upon hatching, phyllosomata measure 1-2 mm long, and grow through a series of moults to reach several cm in length (Fig. 7.1A; Phillips et al., 2006). The planktonic phyllosoma stage can last a year or more in most palinurids (Booth and Phillips, 1994), and typically a few months in scyllarids (Robertson, 1979). Final-stage larvae metamorphose into the puerulus, a free swimming post-larval stage closely resembling the adult form. The puerulus settles in suitable adult habitats where it goes through a final metamorphosis to a juvenile, benthic form (Phillips et al., 2006). Phyllosomata are poor swimmers, suggesting a passive drifting stage that plays a role in their dispersal, although recent evidence suggests they are able to navigate currents to some extent through vertical movements in the water-column (Ziegler et al., 2010).

The life histories of Anguilliformes

All eels spawn in the ocean, and produce planktonic leptocephalus larvae, which like phyllosomata were originally placed in a separate genus, *Leptocephalus* Scopoli (ex Gronow), 1777, based on their unique morphology (Miller, 2009). Freshwater eels (anguillids) spawn offshore in deep water, with offshore distances of under 100 km in tropical species, to thousands of km in temperate anguillids (Aoyama et al., 2003; Tsukamoto, 2006). Marine eels on the other hand, tend to spawn locally (Miller, 2009). Upon hatching, a poorly developed preleptocephalus of 3-7 mm is released (Tsukamoto et al., 1992; Kuroki et al., 2006). The leptocephalus stage begins when the eyes and teeth are fully formed and can last between 100 and 250 days (Miller, 2009). During this time the larvae grow to a final length of 50 mm to 300 mm, depending on the species (Fig. 7.1B). Leptocephali then metamorph into "glass eels", an unpigmented intermediary stage and finally into muscular and fully pigmented juvenile eels.

7.1.2 DNA barcoding and molecular identification

DNA barcoding relies on sequencing a short genetic marker and comparing it to a reference sequence that has been obtained from an unambiguously identified specimen. If the barcode is not more different from the reference sequence than a pre-specified divergence threshold, an identification can be assigned. The threshold itself relies on the presence of the so-called "barcoding gap". The barcoding gap is a conceptual model, based on the assumption that genetic variation is partitioned hierarchically within and between species, and with minimal overlap between these partitions (Hebert et al., 2003a; Meyer and Paulay, 2005).

Ribosomal and mitochondrial markers are commonly used as barcoding markers, as they have a high copy number, are easy to amplify and have a relatively high level of variation in many species (Hebert et al., 2003a; Bucklin et al., 2010b). In recent years, the mitochondrial cytochrome c oxidase I (COI) gene has been promoted as a universal barcoding gene for metazoans (Hebert et al., 2003a,b) and is now employed in large-scale DNA identification projects on various metazoan groups, including fishes (Ward et al., 2009) and marine invertebrates (Bucklin et al., 2010a). COI has some advantages over other genes. Insertions and deletions are rare, third codon position nucleotides show a high incidence of base substitutions (Hebert et al., 2003a), and robust universal primers that facilitate large-scale sequencing initiatives are available (Folmer et al., 1994; Ivanova et al., 2007). 16S ribosomal RNA was chosen as an alternative marker. Again this was because of the availability of robust universal primers, and because this gene is commonly employed in phylogenetic studies (e.g. Palero et al., 2009) and as a result there is a relatively large number of reference sequences available.

It is important to note, however, that there are conceptual as well as practical limitations to DNA barcoding (e.g. Smith, 2005; Wheeler, 2005; Srivathsan and Meier, 2012), and that barcoding should ideally be seen as a complement to traditional morphological taxonomy rather than a replacement (DeSalle et al., 2005).

In the absence of reference sequences, DNA barcodes of unidentified specimens may still be clustered by sequence similarity. Clusters differing by a pre-defined divergence threshold then form so called molecular operational taxonomic units (MOTUs; Floyd et al., 2002), and are commonly used as units of diversity in ecological studies. It is not always clear whether MOTU richness corresponds to species or ecological diversity, and the equivalence between MOTUs and species-level groups identified in traditional taxonomy has to

be validated independently for every investigated taxon (Vogler and Monaghan, 2007).

7.2 Materials and methods

7.2.1 Specimen collection

Phyllosoma and leptocephalus larvae were collected with a medium sized mid-water trawl (4 mm mesh in the codend), during EAF-Nansen cruise 2009-410 in November and December 2009 (Rogers et al., 2009). Larvae were obtained at four seamounts along the Southwest Indian Ocean Ridge (SWIOR), one seamount west of Walter's Shoal and two sites over deep water, north and south of the ridge (see Figure 1.7). Neither larval type was encountered at the southernmost seamount trawl station (Coral Seamount). Sampling locations and specimen numbers are detailed in Tables 7.3 and 7.4.

All larvae were fixed and stored in 95% ethanol immediately after capture and freighted to the University of Oxford post cruise. Leptocephalus samples were subsequently sent to South Africa in 2010 for morphological identification, and re-packed in ethanol-soaked muslin. Because of a series of logistical issues, samples were not returned immediately but left at ambient temperature for over 2 months, which led to a visible degradation of the tissue.

7.2.2 Morphological identifications

Phyllosomata were analysed under a dissecting microscope. Morphological keys and species descriptions (Gurney, 1936; Baisre, 1994) were used to assign the samples to the spiny lobster family Palinuridae or to the slipper lobster family Scyllaridae. Leptocephali were identified to family level by Peter Konstantinidis (Natural History Museum, London, United Kingdom) at a workshop in the Institute for Aquatic Biodiversity, Grahamstown, South Africa.

7.2.3 DNA Extraction

Phyllosoma tissue samples (2 mm diameter) were taken from the cephalic shield using a disposable biopsy punch (Fig. 7.2A; Chow et al., 2006). Leptocephalus tissue samples were obtained by excising a 4 mm^2 section from the dorsal side. Tissue samples were incubated

Table 7.1: Primers used to amplify 16S rRNA and mtCOI from phyllosoma samples.

Primer	Locus	Sequence 5'–3'	Reference
16SarL	16S	CGCCTGTTTATCAAAAACAT	Palumbi (1996)
16SbrH	16S	CCGGTCTGAACTCAGATCACGT	
LC01490	COI	CCGGTCTGAACTCAGATCACGT	Folmer et al. (1994)
HCO2198	COI	GGTCAACAAATCATAAAGATATTGG	
CrustDF1	COI	GGTCWACAAAYCATAAAGAYATTGG	Radulovici et al. (2009)
CrustDR1	COI	TAAACYTCAGGRTGACCRAARAAYCA	

Table 7.2: Primers used to amplify mtCOI of leptocephalus samples.

Primer	Sequence 5'–3'	Reference
VF2_t1	TGTAAAACGACGGCCAGTCAACCAACCACAAAGACATTGGCAC	Ivanova et al. (2007)
FishF2_t1	TGTAAAACGACGGCCAGTCGACTAATCATAAAGATATCGGCAC	
FishR2_t1	CAGGAAACAGCTATGACACTTCAGGGTGACCGAAGAATCAGAA	
FR1d_t1	CAGGAAACAGCTATGACACCTCAGGGTGTCCGAARAAYCARAA	
M13F (-21)	TGTAAAACGACGGCCAGT	
M13R (-27)	CAGGAAACAGCTATGAC	

at 55°C for 2 min or blotted on paper to remove excess ethanol. DNA was extracted using the DNeasy Blood & Tissue Kit (QIAGEN, Crawley, United Kingdom) with an extended lysis period of 36 h in a shaking incubator and final elution volumes of 75 µl. DNA concentration and sample purity were assessed using a NanoDrop 2000 spectrometer (Thermo Scientific, Wilmington, United States). Extracts were stored at -20°C.

7.2.4 Marker gene amplification and sequencing

Two genes were amplified in this study: 16S ribosomal RNA and mitochondrial COI. Primers used on phyllosoma samples were universal 16S (Palumbi, 1996) and COI primers (Folmer et al., 1994) and crustacean specific COI primers (Radulovici et al., 2009). For leptocephali and adult fish, a universal fish COI primer cocktail was used that contained M13 tails to facilitate DNA sequencing (Ivanova et al., 2007). Primer sequences are shown in Table 7.1.

Polymerase chain reactions (PCRs) were carried out in volumes of 14 µl in a C1000 Thermal Cycler (Bio-Rad Laboratories, Hemel Hempstead, United Kingdom), using 2 µl template DNA, 1.6 µl primers (10 µM) in equal ratios, 8 µl HotStarTaq Master Mix (QIAGEN, United Kingdom), 2 µl CoralLoad buffer (QIAGEN, Crawley, United Kingdom) and 0.4 µl PCR-grade water. For troubleshooting purposes, the addition of 2 µl of QMix (QIAGEN, Crawley, United Kingdom) and a Taq PCR Core Kit (QIAGEN, Crawley, United King-

dom) were also used. For 16S primers, invertebrate COI primers, and fish COI primers, PCR cycling conditions were: initial denaturation at 95°C for 5 min (HotStart), followed by 35 cycles at 96°C for 10 sec, 50°C for 5 sec, 60°C for 4 min (Ivanova et al., 2007). For crustacean COI primers, PCR cycling conditions were: initial denaturation at 95°C for 5 min (HotStart), followed by 5 cycles at 94°C for 40 sec, 45°C for 40 sec, 72°C for 1 min, and 35 cycles at 94°C for 40 sec, 51°C for 40 sec, and 72°C for 1 min (Radulovici et al., 2009). Following PCR, the presence of products was checked using agarose gel electrophoresis and visualised using ethidium bromide staining.

All PCR products were purified using a QIAquick PCR Purification Kit (QIAGEN, Crawley, United Kingdom). Sequencing reactions were carried out for both forward and reverse primers in volumes of 10.75 µl, using 2.5 µl DNA product, 2.5 µl primer (10 µM), 2.5 µl X5 Buffer (Applied Biosystems, Warrington, United Kingdom), 0.5 µl BigDye Terminator v3.1 Ready Reaction Mix (Applied Biosystems, Warrington, United Kingdom) and 2.75 µl water. PCR cycling conditions were: initial denaturation at 96°C for 1 min, followed by 25 cycles at 96°C for 10 sec, 50°C for 5 sec, 60°C for 4 min.

Samples were purified using an ethanol/EDTA precipitation method, with 30µl 100% ethanol and 2.5µl 125mM EDTA per reaction. Finally, the products were analysed using a 3100 DNA analyser (Applied Biosystems).

7.2.5 Database searches

Sequence chromatograms were visually evaluated for quality, and ambiguities were resolved where possible alongside an alignment of forward and reverse sequence pairs using Geneious 5.3 (Biomatters Ltd., Auckland, New Zealand, http://www.geneious.com). Nucleotide sequences were queried in the GenBank database using the BLAST algorithm (Altschul et al., 1997), and COI sequences were queried in the Barcode of Life Database (BOLD; Ratnasingham and Hebert, 2007). BLAST returns the closest near matches found in GenBank. Searches in the BOLD species level identification database return a high confidence match at species level (and sometimes only at genus level if a barcode has not been identified beyond genus level) when the appropriate reference sequence is available, but does not list more distant species. Searches among all BOLD barcode records, return the nearest match found, but with no measure of confidence of placement in that particular taxon.

7.2.6 Phylogenetic reconstruction

Phyllosoma 16S rRNA sequences were aligned alongside 35 reference sequences from the infraorder Achelata and two outgroups (Palero et al., 2009, see Appendix F for corresponding GenBank accession numbers). Two species of Nephropoidea (Infraorder: Astacidea), *Homarus americanus* and *Nephrops norvegicus*, were selected as outgroups, as Achelata and Astacidea are sister taxa (Tsang et al., 2008). The resulting alignment was trimmed to 486 bp. Gaps and hyper-variable regions were removed prior to phylogenetic analysis using GBlocks (v0.91b Castresana, 2000).

Leptocephalus COI sequences were aligned alongside 54 reference sequences from the order Anguilliformes (Inoue et al., 2010, see Appendix F for corresponding GenBank accession numbers). Two species from the Notacanthidae family (*Notacanthus chemnitzi*) and the Elopidae family (*Elops hawaiensis*) were included as outgroups as they both display an Anguilliform-like leptocephalus stage (Inoue et al., 2010). The final alignment was trimmed to a length of 450 bp.

Alignments were produced in Geneious 5.3 using MUSCLE (Edgar, 2004) on default settings, and checked visually for ambiguities. Maximum likelihood consensus trees were constructed using 1000 bootstrap replicates in MEGA 5.0 (Tamura et al. 2011). Nucleotide substitution models were selected under the Akaike information criterion by jModelTest 0.1.1 (Posada, 2008). The GTR+G+I model was selected for 16S, and the GTR+I model for COI. The Achelata tree was rooted to *Polycheles typhlops* (Family: Polychelidae). The Anguilliform tree was rooted to *Elops hawaiensis*.

7.2.7 MOTU analysis

MOTU richness was determined within the phyllosoma 16S rRNA sequences and the leptocephali COI sequences respectively using MOTU Define 2.04 (Blaxter et al., 2005). The software uses BLAST-based similarity matching to determine MOTUs from DNA barcode data using arbitrarily specified sequence divergence cut-offs. Cut-off values ranged from 1 to 100 bp and 100 replicates using random resampling orders were performed for each cut-off value (Ács et al., 2010). Results were processed and visualised in R (R Development Core Team, 2010).

7.3 Results

7.3.1 Morphological identification

Phyllosomata

A total of 25 phyllosomata were collected and morphologically analysed. All specimens had been damaged during the collection process and key morphological character were missing (e.g. broken pereiopods, dactyls and/or maxillae; see Fig. 7.2A), severely complicating identification. Family level identification was, however, possible for all samples based on the shape of the first and second antennae (Fig. 7.2A, B). Family assignments are listed in Table 7.3.

Leptocephali

Of 46 leptocephali, 14 (30%) could be identified to family level, although none with high degrees of confidence. Results are summarised in Table 7.4.

7.3.2 PCR and sequencing success

PCR success rates were low despite comprehensive troubleshooting. Of 25 phyllosoma specimens, 11 16S sequences (44%) and 2 COI sequences (8%) were obtained. Only two high quality phyllosomata COI sequences were obtained, and hence were not selected for further analysis.

7.3.3 Molecular identifications and phylogenetic analyses

All 11 phyllosoma 16S sequences resulted in genus level identification, including 9 to species level (Table 7.5). Ten larvae were identified as palinurids, with 8 matched to *Jasus lalandii*, one to the genus *Jasus* and one to the genus *Panulirus*. One sequence was identified as a scyllarid, but could not be identified further.

Out of 46 leptocephali specimens, 18 COI sequences (39%) were obtained. Sequences were produced after up to 4 amplification attempts. For leptocephali, 3 out of 17 COI sequences were assigned to genus level, including one sequence to species level (Table 7.6). Two larvae were identified as *Gorgasia* sp. (Congridae family), and one as *Serrivomer beanii*

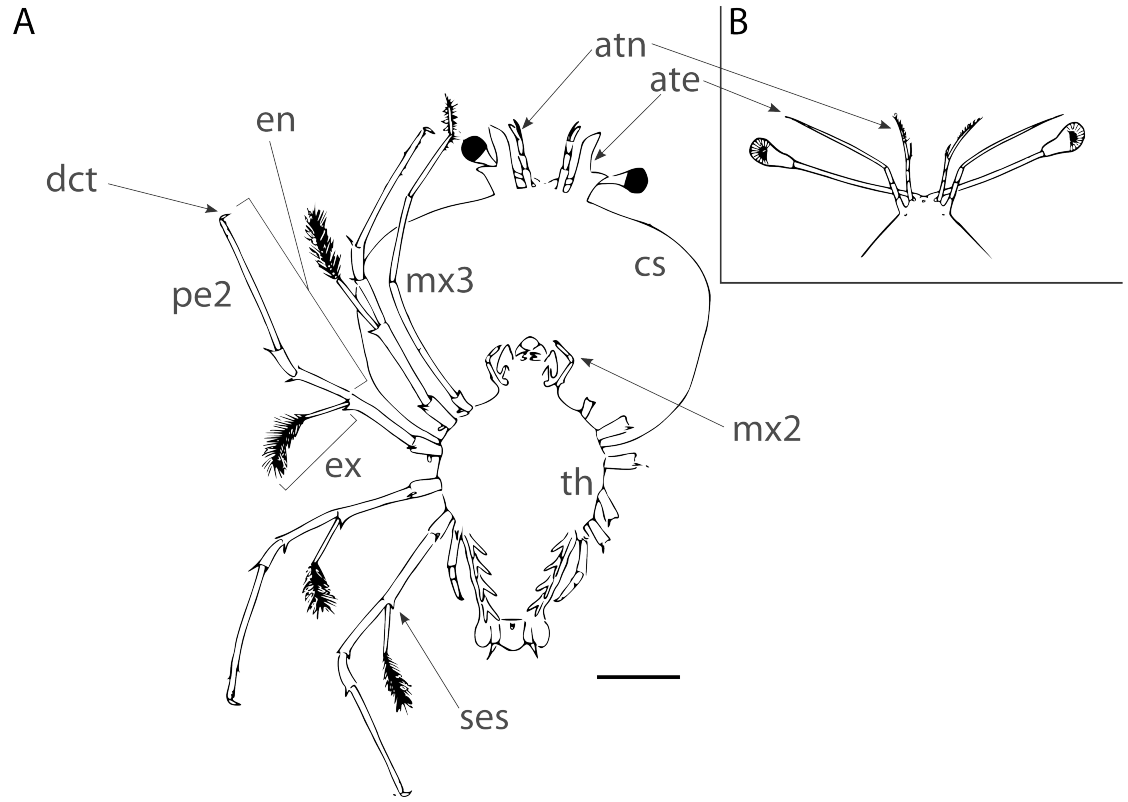

Figure 7.2: A: Final stage phyllosoma larva of *Scyllarus pygmaeus* (Bate, 1888) adapted from Palero et al. (2008), showing morphological features (ventral view, most left-side appendages omitted for clarity). Scale bar 5 mm. B: Detail of stage IX phyllosoma of *Panulirus ornatus* (Fabricius) adapted from Johnson (1971). Not to scale. ate, antenna; atn, antennule; cs, cephalic shield; dct, dactylus; en, endopod; ex, exopod; mx2, 2nd maxilla; mx3, 3rd maxilla; pe2, 2nd pereiopod; ses, subexopodal spine; th, thorax.

Table 7.3: Overview of sampling locations, morphological identification and PCR success for the phyllosoma larvae used in this study.

Station		Latitude	Longitude	Sample	Morphological ID	PCR Success
2	Off-Ridge North	26°56.60'S	56°14.40'E	Phyllosoma 14		
5	Sapmer Bank	36°50.00'S	52°06.60'E	Phyllosoma 3	Palinuridae	Yes
				Phyllosoma 4	Palinuridae	
				Phyllosoma 5	Palinuridae	Yes
				Phyllosoma 9	Palinuridae	
				Phyllosoma 10	Palinuridae	Yes
				Phyllosoma 15	Palinuridae	
6	Middle of What	37°57.60'S	50°25.20'E	Phyllosoma 6	Palinuridae	
				Phyllosoma 12	Palinuridae	Yes
				Phyllosoma 13	Palinuridae	
				Phyllosoma 23	Palinuridae	Yes
				Phyllosoma 24	Palinuridae	
				Phyllosoma 25	Palinuridae	Yes
9	Melville Bank	38°44.95'S	46°22.97'E	Phyllosoma 1	Palinuridae	
				Phyllosoma 8	Palinuridae	
10	Walter's Shoal	31°37.48'S	42°50.22'E	Phyllosoma 2	Scyllaridae	
				Phyllosoma 7	Scyllaridae	Yes
				Phyllosoma 11	Scyllaridae	
				Phyllosoma 16	Palinuridae	Yes
				Phyllosoma 17	Palinuridae	
				Phyllosoma 18	Palinuridae	
				Phyllosoma 19	Palinuridae	Yes
				Phyllosoma 20	Scyllaridae	Yes
				Phyllosoma 21	Palinuridae	
				Phyllosoma 22	Scyllaridae	

Table 7.4: Overview of leptocephalus samples analysed in this study.

Station		Latitude	Longitude	Sample ID	Morphology	PCR Success
4	Atlantis Bank	32°40.00'S	57°20.00'E	Leptocephalus 14		
				Leptocephalus 23		Yes
				Leptocephalus 25	Congridae	
				Leptocephalus 29		
				Leptocephalus 37	Congridae	Yes
				Leptocephalus 42		
				Leptocephalus 43		
				Leptocephalus 44		
5	Sapmer Bank	36°50.00'S	52°06.60'E	Leptocephalus 16		
				Leptocephalus 20		
				Leptocephalus 21		Yes
				Leptocephalus 24	Congridae	
				Leptocephalus 31		
				Leptocephalus 33	Nemichthydae	
				Leptocephalus 39		
				Leptocephalus 40		
6	Middle of What	37°57.60'S	50°25.20'E	Leptocephalus 13		
				Leptocephalus 17	Congridae	Yes
				Leptocephalus 18	Nemichthydae	Yes
				Leptocephalus 28		Yes
				Leptocephalus 34		
				Leptocephalus 36	Nemichthydae	
				Leptocephalus 41		
7	Off-Ridge South	41°30.00'S	49°30.00'E	Leptocephalus 46		
9	Melville Bank	38°44.95'S	46°22.97'E	Leptocephalus 1		
				Leptocephalus 2		
				Leptocephalus 3		
				Leptocephalus 4		Yes
				Leptocephalus 5		Yes
				Leptocephalus 6		
				Leptocephalus 7		
				Leptocephalus 8	Congridae	Yes
				Leptocephalus 9		
				Leptocephalus 10	Nemichthydae	
				Leptocephalus 15	Congridae	
				Leptocephalus 26		
				Leptocephalus 27		Yes
				Leptocephalus 35		
10	Walter's Shoal	31°37.48'S	42°50.22'E	Leptocephalus 11		
				Leptocephalus 12	Congridae	
				Leptocephalus 19	Congridae	Yes
				Leptocephalus 22	Congridae	Yes
				Leptocephalus 30		
				Leptocephalus 32		Yes
				Leptocephalus 38	Congridae	
				Leptocephalus 45		

Table 7.5: Phyllosomata BOLD and Phylogenetic Analysis Results. GenBank matches are given in sequence similarity %. Consensus: The likely identity of the specimen.

Specimen ID	Stn.	Morphology	GenBank Closest Match			16S Phylogeny Closest Match		Consensus	
		Family	Family	Species	%	Family	Species	Family	Species
Phyllosoma 3	5	Palinuridae	Palinuridae	*Jasus lalandii*	99	Palinuridae	*Jasus sp.*	Palinuridae	*Jasus lalandii*
Phyllosoma 5	5	Palinuridae	Palinuridae	*Jasus lalandii*	99	Palinuridae	*Jasus sp.*	Palinuridae	*Jasus lalandii*
Phyllosoma 9	5	Palinuridae	Palinuridae	*Jasus lalandii*	99	Palinuridae	*Jasus sp.*	Palinuridae	*Jasus lalandii*
Phyllosoma 10	5	Palinuridae	Palinuridae	*Jasus lalandii*	99	Palinuridae	*Jasus sp.*	Palinuridae	*Jasus lalandii*
Phyllosoma 15	5	Palinuridae	Palinuridae	*Jasus lalandii*	99	Palinuridae	*Jasus sp.*	Palinuridae	*Jasus lalandii*
Phyllosoma 23	6	Palinuridae	Palinuridae	*Panulirus homarus*	97	Palinuridae	*Panulirus sp.*	Palinuridae	*Panulirus sp.*
Phyllosoma 25	6	Palinuridae	Palinuridae	*Jasus lalandii*	99	Palinuridae	*Jasus sp.*	Palinuridae	*Jasus lalandii*
Phyllosoma 1	9	Palinuridae	Palinuridae	*Jasus lalandii*	99	Palinuridae	*Jasus sp.*	Palinuridae	*Jasus lalandii*
Phyllosoma 16	10	Palinuridae	Palinuridae	*Jasus lalandii*	99	Palinuridae	*Jasus sp.*	Palinuridae	*Jasus lalandii*
Phyllosoma 19	10	Palinuridae	Palinuridae	*Jasus lalandii*	99	Palinuridae	*Jasus sp.*	Palinuridae	*Jasus lalandii*
Phyllosoma 20	10	Scyllaridae	Scyllaridae	*Scyllarus pigmaeus*	91	Scyllaridae	*Scyllarus*	Scyllaridae	-

Table 7.6: Leptocephalus BOLD and Phylogenetic Analysis Results. GenBank matches are given in sequence similarity %. Consensus: The likely identity of the specimen. *S. beanii* was the only species with a barcode found in both databases.

ID	Stn.	Morphology	BOLD Closest Match			COI Phylogeny Closest Match		Consensus	
		Family	Family	Species	%	Family	Species	Family	Species
L23	4		Congridae	*Poeciloconger kapala*	89.93	Congridae	*A. shiroanago*	Congridae	-
L25	4		Serrivomeridae	*Serrivomer beanii*	99.28	Serrivomeridae	*S. beanii*	Serrivomeridae	*Serrivomer beanii*
L22	5	-	Congridae	*Gnathophis grahami*	96.70				-
L17	6	Congridae	Congridae	*Gorgasia sp.*	100.00	Congridae	*A. shiroanago*	Congridae	*Gorgasia sp.*
L18	6	Nemichthyidae	Congridae	*Gorgasia sp.*	99.44	Congridae	*A. shiroanago*	Congridae	*Gorgasia sp.*
L28	6	-	Congridae	*Gorgasia sp.*	100.00	Congridae	*A. shiroanago*	Congridae	*Gorgasia sp.*
L2	9		Congridae	*Gnathophis grahami*	95.79		-	-	
L4	9		Congridae	*Gnathophis grahami*	96.74		-		
L5	9	-	Congridae	*Ariosoma howensis*	89.93	Congridae	*A. shiroanago*		
L7	9	-	Congridae	*Gnathophis grahami*	97.07				
L8	9		Congridae	*Poeciloconger kapala*	89.71	Congridae	*A. shiroanago*		
L27	9		Congridae	*Ariosoma howensis*	89.61	Congridae	*A. shiroanago*		
L37	9	-	Congridae	*Poeciloconger kapala*	90.36	Congridae	*A. shiroanago*		
L12	10	Congridae	Congridae	*Gnathophis grahami*	97.19				
L19	10	Congridae	Congridae	*Poeciloconger kapala*	90.36				
L22	10	Congridae	Congridae	*Gnathophis grahami*	96.12				
L30	10	-	Congridae	*Ariosoma howensis*	90.41	Congridae	*A. shiroanago*		
L32	10		Congridae	*Poeciloconger kapala*	89.70	Congridae	*A. shiroanago*		

(Serrivomeridae family). The matches with *Gorgasia* are actually exact matches to the reference sequence, and it is the reference sequence itself that has only been identified to genus level.

Achelata 16S phylogeny

The 16S tree for Achelata is relatively well-resolved and supported at species level (Figure 7.3), however, 16S seems to be poor at resolving the base of the tree. Within *Jasus*, eight phyllosomata (1, 3, 5, 10, 15, 16, 19, 25) form a strongly supported clade with *J. lalandii* and *J. edwardsii*. The relationships between species in this clade are not well resolved. Phyllosoma 16 is placed in a strongly supported sister branch and is in a polytomy with *J.tristanii*. These results suggest that there may be two *Jasus* species among these phyllosomata. Within *Panulirus*, phyllosoma 23 is placed on a well supported sister branch to *P. homarus homarus*. Phyllosoma 20 is in a polytomy with *Scyllarides arctus* and sister to a poorly supported *Scyllarus* clade, and hence no conclusions can be made with regards to its' identity beyond family level. Overall, the 16S phylogeny suggests the presence of 3 to 4 species among the sampled phyllosomata.

Anguilliformes COI phylogeny

The COI phylogeny for Anguilliformes is relatively well resolved at species level (Figure 7.4) but not at higher taxonomic levels. For example, one of the outgroup taxa, *Notacanthus chemnitzi* did not fall to the base of the tree. Leptocephalus 25 is placed within *Serrivomer* and is on a sister branch to *S. beanii*, although this is weakly supported. Clade A, containing Leptocephali 12 and 22, and clade B (Leptocephali 4, 7, 19, 21) are in strongly supported sister clades that do not cluster with any of the species on the tree, and hence their identity cannot be inferred. In clade A, leptocephali 12 and 22 are placed on short but well-supported sister branches, and may represent two separate species. These results suggest the presence of one and perhaps two species in clade A, and another species in clade B. Three leptocephali (17, 18, 28) form clade C, and seven leptocephali (5, 8, 24, 27, 30, 32, 37) form clade D which are well supported sister clades that cluster with *Ariosoma shiroanago*. Overall, the phylogeny points to 5 or 6 species among the sampled leptocephali.

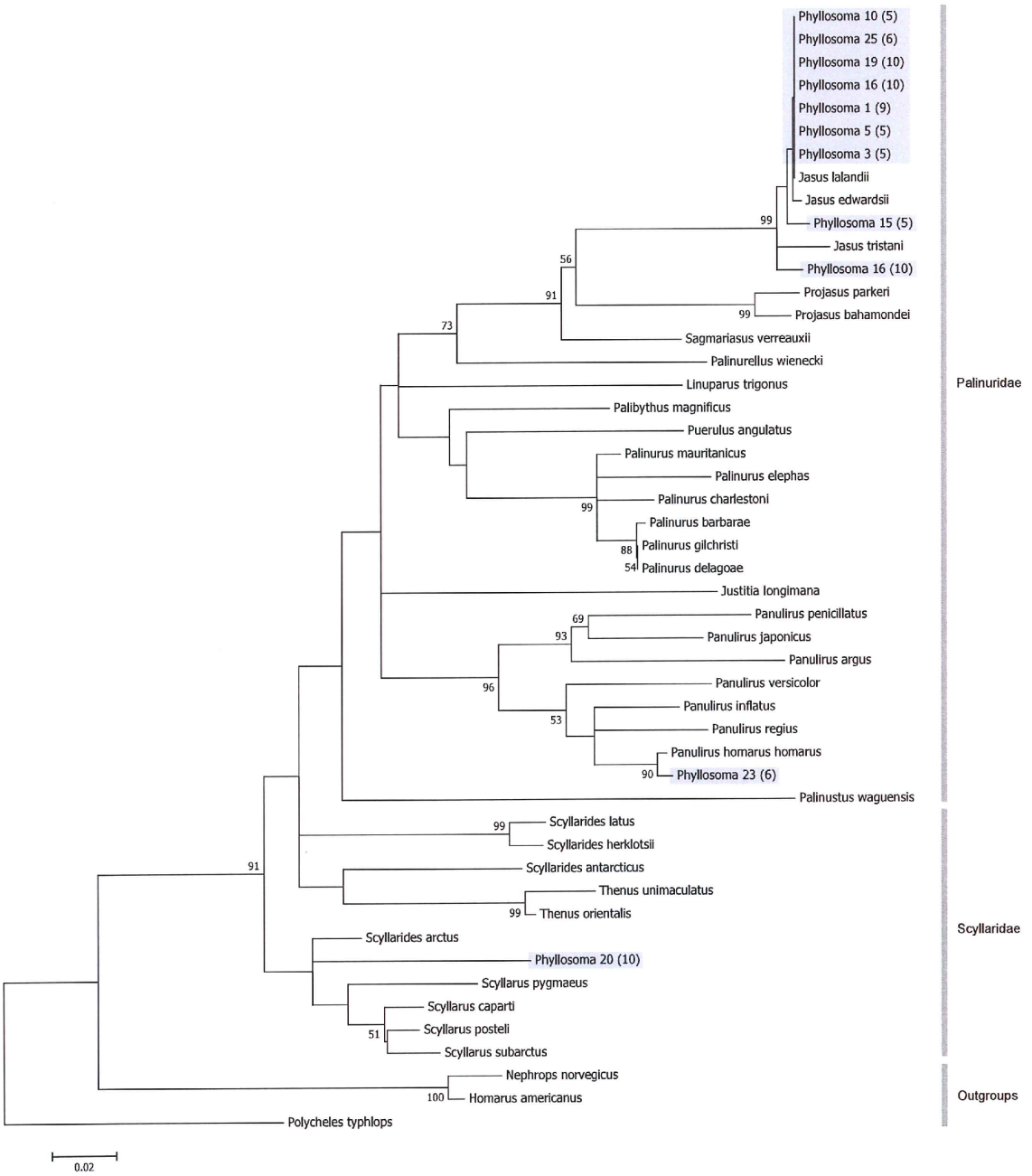

Figure 7.3: Maximum likelihood phylogeny of achelate lobsters using 16S rRNA. Station numbers are in brackets.

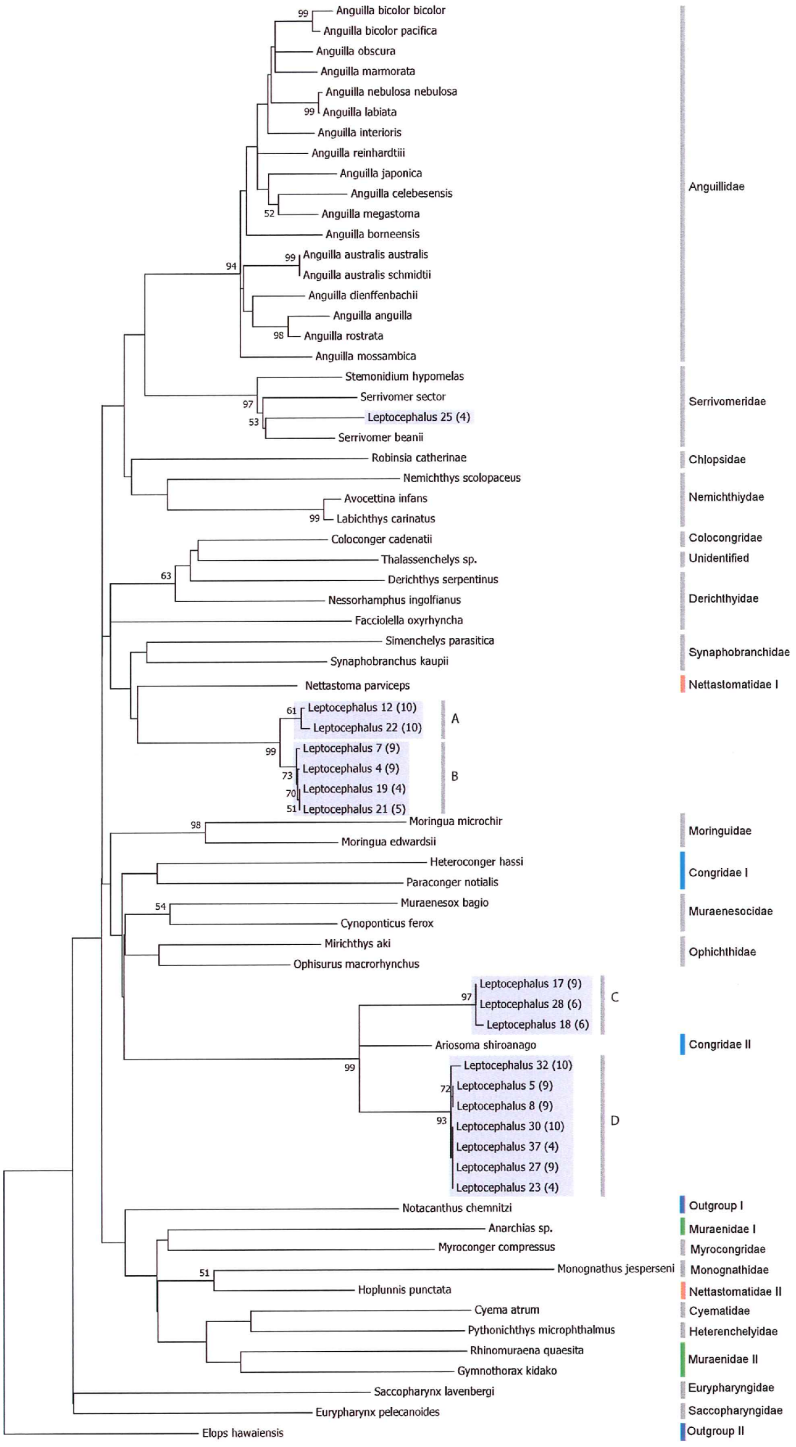

Figure 7.4: Maximum likelihood phylogeny of Anguilliformes using mtCOI. Station numbers are in brackets. Letters A-D denote clades that are discussed in the text.

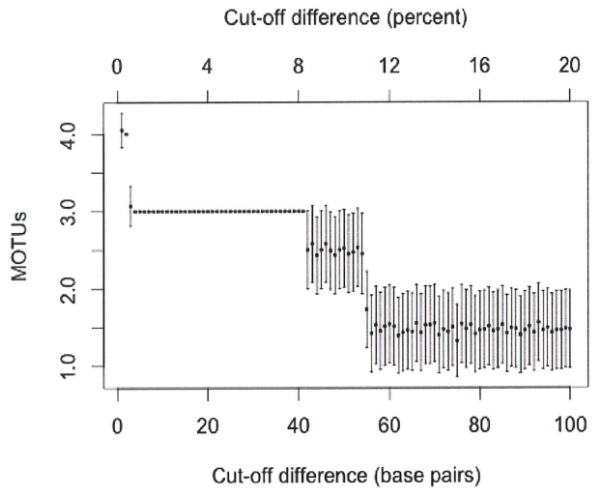

Figure 7.5: 16S MOTU results. A stable region is obtained for 3 MOTUs, corresponding to 1-9% sequence divergence.

7.3.4 MOTU Analysis

The relationship between numbers of MOTUs and the sequence divergence cut-off used to define them is shown for both investigated taxa in Figures 7.5 and 7.6. Both markers show a stable MOTU count over a large range of cut-off values suggesting the presence of a barcoding gap. The phyllosoma sequences were assigned to 3 MOTUs (1-9% divergence cut-off). Leptocephalus sequences were assigned to 5 MOTUs (1-2% divergence cut-off).

7.3.5 Community Composition

An original aim of this study was to assess the composition of larval assemblages across the survey area. This was not possible due to the limited number of identifiable specimens.

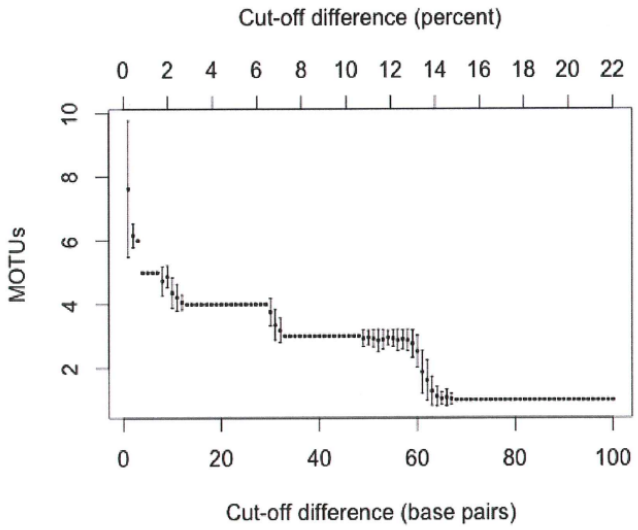

Figure 7.6: COI MOTU results. A stable region is obtained for 5 MOTUs, corresponding to 1-2% sequence divergence.

7.4 Discussion

7.4.1 Improving PCR success

The study highlights the difficulties of DNA barcoding for larval specimens. In particular, PCR amplification success was low despite comprehensive troubleshooting. Primers were selected according to their high specificity to target species, and PCR protocols proved to be very effective when tested on adult muscle tissue. However, unlike adult tissue, phyllosoma and leptocephalus tissue is weakly developed, transparent and thin, resulting in low DNA yields. So low, in fact that the DNA concentration in many samples was near the detection limit of the NanoDrop spectrometer. More starting material, longer lysis times and lower elution volumes were chosen in an attempt to concentrate DNA during extraction, but without success. Concentrating DNA extracts furthermore has the drawback of concentrating PCR inhibitors, such as mucopolysaccharides which make up a large proportion of leptocephalus tissue (Pfeiler, 1991).

The long storage of the leptocephali under semi-dry conditions and the resulting tissue degradation may have had impacts on DNA quality, although extracted concentrations of DNA were too low to assess fragment length distributions or similar parameters.

Low PCR success rates for marine larvae are not confined to this study. In an effort to identify over 2000 marine invertebrate larvae using COI, 16S or 18S rRNA markers, Heimeier et al. (2010) reported amplification rates of ca. 30% and similar DNA contamination issues.

7.4.2 Specimen identification

Phyllosomata

Morphological analysis successfully distinguished Palinurids from Scyllarids for 24 out of 25 samples. Molecular analysis proved to be useful at identifying phyllosomata further, as out of 11 sequences, 10 led to a genus level identification.

The 9 phyllosomata most closely matched to *J. lalandii* in GenBank (99% sequence similarity) could not be identified beyond *Jasus* from the 16S phylogeny. It is possible to speculate on their identity however. A total of 8 phyllosomata clustered with *J. lalandii* and *J. edwardsii*. There are 7 known *Jasus* species found globally (Holthuis, 1991). *Jasus lalandii* is found in Indian Ocean, and is typically located off the coast of Southern Africa

(Groeneveld et al., 2007). *Jasus edwardsii* is found throughout coastal waters of southern Australia and New Zealand (Booth and Ovenden, 2000). It is therefore likely that these 8 phyllosomata are *J. lalandii*, which have been swept off the shelf region by the Agulhas return current. The remaining *Jasus* phyllosoma is placed on a well-supported sister branch alongside *J. tristanii*, even though the closest GenBank match is *J. lalandii*. *Jasus tristanii* was thought to be endemic to the islands of the Tristan da Cunha group in the southern Atlantic, but a recent molecular analysis suggests that it is in fact conspecific to *J. paulensis*, a species found around the St. Paul and Amsterdam islands in the Southern Indian Ocean and on seamounts to the northeast of these islands (Groeneveld et al., 2012). The identity of this larva is therefore likely to be *J. paulensis*.

The phyllosoma identified as *Panulirus* is perhaps a *P. homarus* subspecies. GenBank lists a 97% match and the phylogeny clearly places it in a well-supported sister branch to *P. h. homarus*, which suggests that it is different from *P. h. homarus*, based on . There are 3 described *P. homarus* subspecies, of which 2 are found in the Indian Ocean (Holthuis, 1991), however 16S sequences are only available for *P. h. homarus*. A comparison with *P. h. rubellus*, which is found off the coasts of Madagascar and Southern Africa (Holthuis, 1991), may provide more clues as to the identity of this phyllosoma.

Little can be said about the phyllosoma identified as a scyllarid. The closest GenBank match came at only 91% sequence similarity as *Scyllarus pygmaeus*, a species found in the Mediterranean and South Atlantic (Holthuis, 1991). There are far fewer published 16S sequences for this family than for palinurids, which is likely explained by the fact that many more palinurid species support large fisheries worldwide, and hence have been more intensely studied (Spanier and Lavalli, 2006).

The 16S gene was originally chosen because of the availability of Achelata 16S sequences in GenBank, and because 16S was much more readily amplified than COI. It is clear, however, that 16S does not adequately resolve the relationships between *Jasus* species.

Leptocephali

Few leptocephali could be morphologically identified to family level. Molecular analyses proved to be of limited use, as out of 17 COI sequences, just 2 were identified as matching to *Gorgasia* (Congridae), and one assigned to species level as *Serrivomer beanii* (Serrivomeridae). The 3 leptocephali assigned to a genus or species in BOLD were identified using the species level identification database and hence are likely to be correctly identified, bear-

ing in mind the limitations of barcoding discussed previously. *Gorgasia*, or garden eels, is a family of reef-associated eels which counts 19 known species (Michael, 1998; Fricke, 1999), of which several are found in the Indian Ocean, although their distribution across the oceans is poorly studied. *S. beanii* is a deep-sea species found in the Southwest Indian Ocean, with locations around Cape and Natal off the coast of South Africa, and near Reunion (Smith and Castle, 1986; Fricke, 1999)

Near matches of ca. 89% to 97% sequence similarity were obtained in the all barcode records database for the remaining 14 sequences, and they all listed species belonging to the Congridae family. These results have to be interpreted with caution. One might conclude that although a species level match cannot be made, the sequences displaying higher similarity may belong to the Congridae family. Only 27% of the 800+ known anguilliform species have a COI barcode (www.fishbol.org ; accessed August 2013), with a majority of BOLD barcodes covering species from the Congridae family. Therefore, a specimen with a near match to a species from the Congridae family may actually belong to an entirely different family that is not yet represented in the database.

With the exception of *S. beanii*, which has a COI barcode available in both GenBank and BOLD, phylogenetic analyses were constrained by the fact that none of the barcodes for species found to be near matches in BOLD are in the public domain, and hence could not be included in the analysis. Attempts were made to find species from the same genus or family, but once again this was not always possible. Sister clades A and B point to the presence of two unidentified anguilliform species among the collected larvae. Morphological analysis suggests that some species within both clade A and B may be Congridae, but these identifications were not assigned with a high degree of confidence.

Sister clades C and D cluster with *A. shiroanago*, a species from the Northwest Pacific (Masuda and Muzik, 1984) and the only *Ariosoma* species with a COI barcode in GenBank (but not in BOLD). However, all members of clade C were identified in BOLD as *Gorgasia sp.*, for which there was no publicly available COI sequence. There are 26 *Ariosoma* species, with at least 3 found in the western Indian Ocean, but little is known about their biogeography and dispersal pathways across the study area (Castle, 1968). These results suggest that clades C and D belong to the Congridae family, with clade C representing a *Gorgasia* species and clade D a closely related second species, possibly an *Ariosoma* species. Moreover, this tree and other molecular phylogenies (Inoue et al., 2010) recover the Congridae family as polyphyletic, which does not lend a high degree of confidence in the identification of clade D (Meyer and Paulay, 2005).

Overall, the COI gene seems reasonably adequate for delimiting species within the tree, as illustrated by the Anguillidae. Currently, however, far more sequences would be needed for species level matches. A thoroughly sampled taxon is particularly important when families are recovered as polyphyletic, as species are likely to be misidentified (Meyer and Paulay, 2005). In addition, the current morphological categorisation of Anguilliforms is disputed and in need of a review (Inoue et al., 2010; López et al., 2007).

7.4.3 MOTU concordance

Table 7.7: MOTU concordance

Taxon	Identification Results	MOTU Results
Phyllosomata	3 — 4 clades	3 MOTUs
Leptocephali	5 — 6 clades	5 MOTUs

The number of MOTUs recovered were three and five for phyllosomata and leptocephali, respectively. This corresponds well to the results of the phylogenetic analyses. The three crustacean MOTU's correspond to the *Jasus* complex, the *Palinurus* sp. specimen and the scyllarid specimen. For the eels the five MOTUs correspond to clades A-D in the phylogeny and the *S. beanii* specimen.

7.4.4 Larval distributions across the survey area

Phyllosoma larvae

Jasus species are commercially important shallow water lobsters found in coastal waters and around seamounts (Booth and Ovenden, 2000; Booth and Phillips, 1994) Holthuis 1991). *Jasus lalandii* are known mainly in depths of <200 m in southern temperature waters (Holthuis, 1991), and are typically found from Cape Cross, Namibia, in the Atlantic Ocean to Algoa Bay, South Africa, straddling the Cape of Good Hope (Holthuis, 1991). They support a large fishery along the East and Western Cape of South Africa where they occur in high densities (Branch and Clark, 2006). Several phyllosomata in this study were thought to be *J. lalandii*, and were caught across the SWIR at seamount stations (Fig. 7.7). *Jasus lalandii* phyllosomata occur in the vicinity (no more than several 100 km) of parental grounds (Gurney, 1936; Booth and Ovenden, 2000) and local eddies, gyres and counter

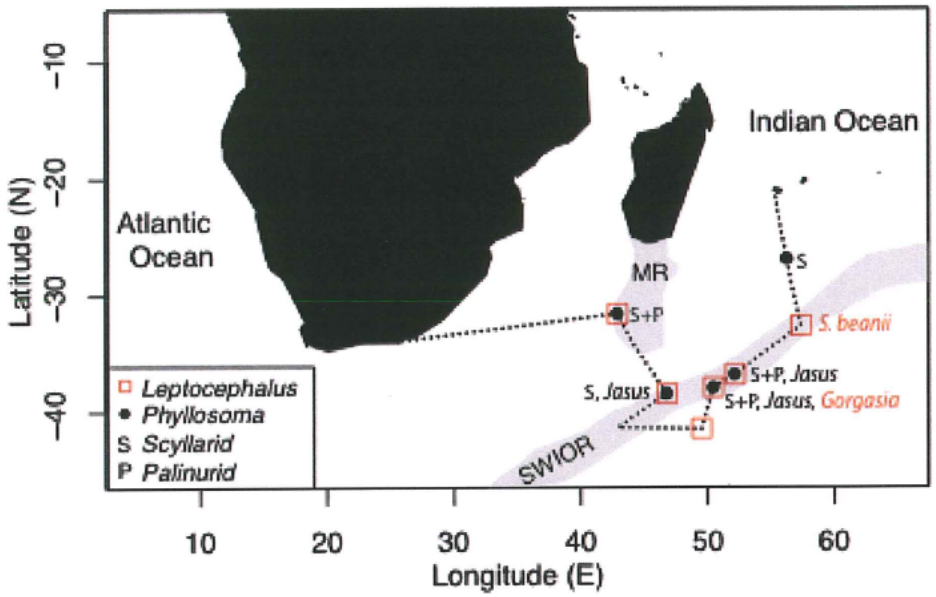

Figure 7.7: Location of specimens collected in this study, with identifications where available.

currents have showed to play a role in preventing their wide dispersal (Booth and Phillips, 1994; Phillips et al., 2006). However, in the SWIO, *J. lalandii* phyllosomata have been found over larger distances eastwards and are thought to be transported by the Agulhas Return Current (see Figure 1.8; Booth and Ovenden, 2000). The *J. lalandii* phyllosomata caught in this study may have been transported in the same manner across the SWIR and there were no samples found beyond the tropical front or in cold waters, although it is also possible that there may be undiscovered adult *J. lalandii* populations living across seamounts on the SWIR.

Populations of *J. paulensis* on the SWIR (Groeneveld et al., 2012) as well as observations of adult *Jasus* specimens that were morphologically intermediate between *J. paulensis* and *J. tristani* during a subsequent cruise to the SWIR (Figure 7.8; Rogers and Taylor, 2012), may pinpoint the source of the putative *J. paulensis* phyllosoma.

A phyllosoma specimen caught at a seamount station was identified as a *Panulirus* species, and perhaps a *P. homarus* subpsecies. *Panulirus homarus* is widely distributed along the Indian Ocean and is subjected to intense fisheries (Holthuis, 1991). In the SWIO, *P. homarus* is subjected to artisanal fisheries activity off the east coast of Africa and south-east of Madagascar, and is considered overexploited (Phillips and Melville-Smith, 2006; Steyn et al., 2008). The distribution of *P. homarus* and other *Panulirus* species found in

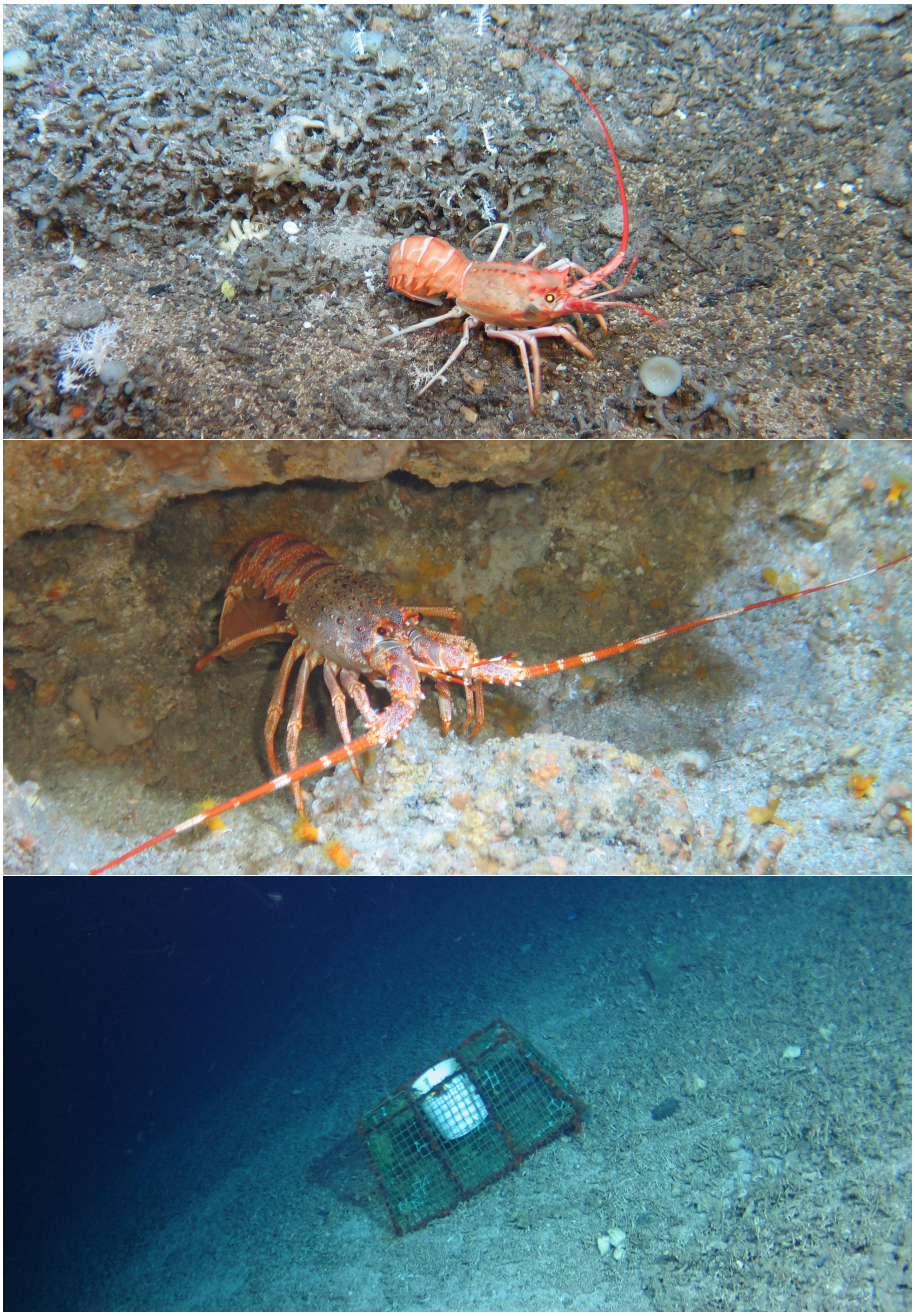

Figure 7.8: Adult spiny lobsters and fishing activities observed on Melville Bank during research cruise JCO66. Top: *Projasus parkeri*; middle: ?*Jasus paulensis*; bottom: Lost creels.

the SWIO is poorly studied. *Panulirus homarus* are considered coastal species (Holthuis, 1991; Phillips and Melville-Smith, 2006), and perhaps the *Panulirus* phyllosoma from this study has been transported across the ridge by the Northeast and Southeast Madagascar Currents.

Several specimens in this study were identified as scyllarids. Scyllarids are typically found off the continental shelf found at depths of up to 500 m (Spanier and Lavalli, 2006), and have been reported on seamounts (Santana et al., 2007). Some species are known to the SWIO, such as *Parribacus antarcticus*, *Thenus unimaculatus*, *T. orientalis* and *Scyllarides elisabethae*. Scyllarid phyllosomata have been found during research cruises across the Indian Ocean in lower numbers than palinurids (Booth and Ovenden, 2000; Gurney, 1936). Scyllarids are very poorly studied, and in contrast to palinurids, little is known about their larval distribution (Spanier and Lavalli, 2006). Studies, however, have found that unlike in most palinurids, some species of scyllarid phyllosomata do not appear to disperse far beyond coastal waters (Booth et al., 2005).

Leptocephalus larvae

Seamounts have recently been suggested to be important spawning grounds for freshwater eels in the Pacific Ocean (Tsukamoto, 2006), however, no leptocephalus were identified as belonging to the Anguillidae family.

Leptocephali, thought to be garden eel of the genus *Gorgasia*, were recovered from a seamount in the Subtropical Front. *Gorgasia* are reef-associated fossorial species that are found predominantly in tropical to subtropical shallow waters, where they burrow in sea floor sediments (Castle, 1997). Garden eels and other marine eels have been shown to spawn locally in the Pacific (Moyer and Zeiser, 1982; Miller, 2009), but little is known about *Gorgasia* in the SWIO. *Gorgasia* spp. have been reported off the island of Reunion (Quero and Saldanha, 1995) and other Mascarene Islands, and from the Mozambique Channel (Castle, 1997), but not on Walter's shoal, where there is hardly any sediment cover in shallow water (Collette and Parin, 1991).

The leptocephali identified as *Gorgasia* in this study may have originated from spawning grounds located in the Mascarene Islands and transported to the ridge by the Northeast and Southeast Madagascar Currents (see Figure 1.8 in Chapter 1). One specimen was identified as *S. beanii*, a deep-sea species found in the SWIO, with locations recorded near Cape and Natal off the coast of South Africa, and near Reunion (Smith and Castle, 1986; Quero and

Saldanha, 1995; Fricke, 1999). Although little is known of *Serrivomer* species in the SWIO, their larvae have been found elsewhere in the open ocean near parental grounds as a result of local spawning (Miller and McCleave, 1994; Miller, 2009). Several adult *S. beanii* were caught along the ridge during the same cruise (K. Kemp, pers. comm.). This could suggest that *S. beanii* adult populations also spawn locally in the SWIO.

7.5 Conclusions

This study highlights the difficulties encountered when attempting to identify cryptic marine larvae even when using a combination of morphological and molecular methods. While a large proportion of specimens could not be identified, the combination of morphological and molecular methods still proved to be more informative than either approach on its own. Indeed, while morphological identifications were often limited to family-level or simply not possible beyond order, DNA barcodes could not be obtained for the majority of specimens. Poor PCR amplification rates among many species of marine larvae have been reported elsewhere (e.g. Sawada et al., 2008; Heimeier et al., 2010), and unless protocols are developed to improve PCR success, larger sample sizes will be required for meaningful ecological studies.

Molecular analyses were constrained by poor PCR success, leading to single locus analyses instead of the intended two-marker approach. For phyllosomata, 16S did not resolve species-level relationships in *Jasus*, while for leptocephali, COI proved to be a poor choice for resolving family-level taxonomy. In these cases identification beyond an MOTU requires comprehensive taxon sampling of the reference dataset. While DNA barcoding does not aim at providing phylogenetic information at this level, family-level identifications are desirable in the absence of species specific or congeneric reference sequences. The use of a single and partial COI sequence to build reference databases for species identification may prove to be short-sighted. A multi-locus approach using both mitochondrial and nuclear genes should prove more powerful for identification purposes of sparsely sampled taxa, assuming sufficient quantities of amplifiable DNA can be obtained from the samples that are to be identified.

Chapter 8

Final remarks

> To some extent, generalizations about seamounts are challenging, as seamounts should not be expected to function alike given varying bathymetry, substrate, currents and topography.
>
> McClain (2007)

> At seamounts there is plenty of motion, commotion, and biophysical connection left to be measured, modelled, and understood.
>
> Lavelle and Mohn (2010)

This thesis set out to investigate the effects of abrupt topography on the ecology of pelagic zooplankton and nekton along the Southwest Indian Ridge (SWIR). The work developed beyond this geographic focus to include observations from the central Indian Ocean, namely the Chagos archipelago, and observations from ships of opportunity extending as far east as the Broken Plateau (Fig. 1.7). Research presented here had an emphasis on the use of acoustic observations to infer ecological relationships, but also employed stomach content analysis, population genetics and DNA barcoding to investigate the distribution, dispersal and trophic interactions of pelagic biota.

8.1 Results and implications

Topographic and oceanographic effects on scattering layers: Are seamounts special?

The basin-scale analysis of sound scattering layers in Chapter 2 showed a heterogeneous distribution of pelagic backscatter across the southwest Indian Ocean. The strongest predictors of backscattering strength were sea surface temperature, with increased backscatter at both the Subtropical Front (STF) and Subantarctic Front (SAF), and time of day, reflecting the diel vertical migration cycle of mesopelagic biota. The vertical structure of the scattering layers also varied across the basin. Daytime deep scattering layer (DSL) depth shallowed from tropical waters towards the subtropical convergence zone (SCZ) and a step change in layer structure occurred at the SAF. This step change is thought to reflect a biogeographical boundary at the front that was observed in biological samples obtained from trawls (e.g. Letessier et al., 2014; Laptikovsky et al., 2014), i.e. scattering layers north and south of the SAF are made up of distinct biological assemblages, and thus have distinct scattering properties, as was exemplified by a suspected upward shift of the resonance depth as a result of changes in the swimmbladder size between different assemblages.

The differing vertical organisation of backscatter may also explain distinct foraging behaviours of elephant seals (*Mirounga leonina*) in the frontal zone (Chapter 3), and indeed recent research has added further evidence, that these animals target distinct prey items across this front (Guinet et al., 2014). No strong evidence of a ridge effect on backscattering strength or scattering layer structure was found in the basin-scale analysis (100s-1000s km). This is in agreement with backscatter observations from a mid-latitude segment of the Mid-Atlantic Ridge (Opdal et al., 2008; Cox et al., 2013), but contrasts with observations from the Reykjanes Ridge, which showed substantially increased DSL backscatter on the scale

of 100s km either side of the ridge crest (Priede et al., 2013).

On the scale of 10-100 km, internal wave effects were observed impacting scattering layers downstream of an unnamed seamount on the SWIR (Chapter 5). This finding highlights the role seamounts play in ocean mixing (Garrett, 2003; Nikurashin and Ferrari, 2013). Internal waves can increase the flux of particulate matter to the seabed, a process that is exploited by benthic filter feeders such as cold-water corals who can form dense colonies in areas of slopes that are prone to experience this hydrographic phenomenon (Duineveld et al., 2007; Davies et al., 2009). No information is available about benthic communities on this particular seamount, but rich assemblages of cold-water corals and sponges were observed in current-exposed locations on Atlantis Bank and Sapmer Seamount, to the north and south of the unnamed seamount, respectively, and also on the other seamounts surveyed during cruises JCO66/67 (pers. obs.).

On the scale of 1-10 km, a strong effect on scattering layer strength was observed on the slopes of atolls and shallow banks (<100 m summit depth) in the Chagos archipelago, where backscattering strength increased exponentially towards topographic features (Chapter 4). A less clear picture emerged from seamounts along the SWIR (Chapter 5). While aggregations of backscatterers were associated with all surveyed seamount summits, the scattering layers around these features were largely homogeneous. A notable exception was Atlantis Bank where a downstream depletion of the scattering layer was observed both below the summit and in a depth stratum above the summit that was occupied by micronekton predators.

In summary, this study established that flow-topography interactions around abrupt topography along the SWIR and in the Chagos archipelago impact pelagic biota on a range of scales from 1–100 km around individual features. Effects, however, variable, and included local enrichmant of scattering layers, the displacement of scattering layers by internal waves, and the depletion of scattering layers downstream of a seamount. In several cases no effects were observed on scattering layers. This diversity of effects likely results from the variation in summit depth, slope morphology and the oceanographic settings. On the basin-scale no topographic effect was observed, and the mesoscale oceanography dominated the observed pattern of scattering layer distribution and structure. No distinction could be found between the effect exerted on scattering layers by seamounts, islands and shallow banks in the Chagos archipelago, and indeed, the aggregations found over SWIO seamounts may be the result of similar processes causing scattering layer intensification over mid-ocean ridge crests, as observed along the Mid-Atlantic Ridge (Priede et al.,

2013), the slopes of the Hawaiian islands (Reid et al., 1991; Benoit-Bird and Au, 2004), and along the continental slopes (Genin, 2004). It is therefore difficult to ascribe seamounts a unique role in their interactions with pelagic biota.

Are seamounts sinks of oceanic production?

Trophic modelling suggests that the standing stock of seamount-associated fishes can only be sustained by a net import of allochthonous production (Tseytlin, 1985; Morato et al., 2009; Koslow, 1997), raising the question whether seamounts function as sinks of oceanic production. The observations made on Atlantis Bank (Chapter 5) could indicate a removal of deep pelagic biomass by seamount-associated biota, however, in the absence of target strength estimates for the depleted scatterers it is difficult to interpret the ecological significance of this process. However, even if seamounts and seamount-associated biota were responsible for a net removal of pelagic biomass, this flux may not terminate at seamounts. Energy and matter are likely to be re-exported to the open ocean to some extent, for example through the resuspension of sediments, the export of eggs and planktonic larvae from the seamount inhabitants, the predation on seamount biota by non-resident predators such as seabirds, tuna and marine mammals (Morato et al., 2008; Maxwell et al., 2012; Litvinov, 2007) as well as harvesting by man (Watson et al., 2007; Pitcher et al., 2010).

Genetic approaches to seamount and micronekton ecology

The investigation of the population genetics of the hatchetfish *Argyropelecus aculeatus* (Chapter 6) demonstrated a highly connected population within the SWIO, with high gene flow, high genetic diversity and no significant spatial structure. This result was consistent with genetic studies of other mesopelagic fishes (Florence et al., 2002; Kojima et al., 2009; Van de Putte et al., 2012) and likely a result of the dynamic oceanography of the study region paired with the fact that *A. aculeatus* is not an obligate seamount species. Genetic analyses further indicated a recent population expansion or selective sweep in the late Pleistocene. This event may have been linked to glaciation events in the Quarternary and provides evidence, that even large and widespread pelagic populations are impacted by global climate cycles.

The study of larval spiny lobsters and eels (Chapter 7) highlighted the difficulties encountered in the identification of cryptic marine larvae. Only a small part of the original samples could be unequivocally identified. Nonetheless, the combination of morphologi-

cal and molecular methods yielded some insights into the diversity of pelagic larvae in the SWIO. Of particular relevance in a seamount context were the spiny lobster larvae, as adult palinurids were abundant during video surveys of SWIR seamounts (pers. obs.). The identification of leptocephalus larvae was hindered by a lack of reference sequences, a problem that time might solve, as several large-scale DNA barcoding initiatives are building up ever larger reference data sets (e.g. the ongoing Fish Barcoding of Life programme; Ward et al., 2009).

8.2 Future directions

The application of shipborne echosounders to biological problems provides an opportunity to create datasets that cover pelagic processes across spatial scales ranging from sub-meter to hundreds of meters vertically and from 10s of meters to 1000s of kilometers horizontally. However, acoustic data also has limitations, the most significant being that acoustic data provide little if any taxonomic information on the observed scatterers. Acoustic data needs to be 'ground-truthed' with other methods, such as nets or optical systems to determine, the identity and biomass of the scatterers. Progress has been made using multi-frequency acoustic methods and combined optical and acoustic sensors that allow species discrimination and *in situ* measurements of size, orientation and/or target strength (Kloser et al., 2002, 2009; Benoit-Bird, 2009; Letessier et al., 2013). Strategic efforts to ground-truth acoustic observations from large surveying efforts, such as the IMOS Bio-Acoustics Subfacility (Ryan, 2011), would add great value to this already very rich data set.

With time and improvements in sampling technology the amount of data collected in acoustic surveys will continue to increase. This creates the need to develop new computational and statistical tools to extract relevant ecological information from vast acoustic datasets. Some tools for the automation of backscatter data processing have been developed in recent years (e.g. noise filters; Anderson et al., 2005; De Robertis and Higginbottom, 2007), but there is still a need to develop better statistical tools for efficient analysis of these complex and highly autocorrelated datasets.

Priede et al. (2013) proposed that the effect of mid-ocean ridges on total biomass in an ocean basin is neutral, as the increased benthic biomass on the ridge surface is balanced by the displacement of pelagic biomass by the topography itself. At present, this hypothesis cannot be tested for the SWIR as the acoustic data lack ground-truthing that would enable

biomass estimation, and no standing stock estimates of benthic biota are currently available for the region. However, a wealth of data on benthic and demersal biota was collected during the overarching multidisciplinary research project that this PhD was a part of, and as this data is being analysed, a test of Priede et al.'s hypothesis might become possible.

Despite large research efforts in the past decade (Schlacher et al., 2010; Stocks et al., 2012), our understanding of seamount ecology is still incomplete. As this thesis demonstrates, a research vessel-based approach to seamount exploration, i.e. surveys over several days or a few weeks, can only provide snapshots of these ecosystems. A comprehensive mechanistic understanding, however, is often obscured by the complex interplay of physical and biological processes operating across multiple temporal and spatial scales such as tides and mesoscale circulation, diel and seasonal vertical migration. Observation platforms, such as moorings (e.g. Urmy et al., 2012), autonomous underwater vehicles (e.g. Brierley et al., 2002) or gliders (Ohman et al., 2013) may provide a more cost effective way of surveying individual seamounts over months or years and provide data that can help unravel the complex interactions occurring on and around seamounts.

While there are a number of ecological explanations for the lack of genetic structure in the hatchetfish (*Argyropelecus aculeatus*) investigated in this study, part of the null result might also have been caused a lack of resolution in the employed genetic marker. Microsatellite markers are currently under development for this species (J. Freer, pers. comm.) and should enable a more in-depth look at population differentiation within the basin. Given the poor understanding of gene flow and speciation in pelagic animals, additional samples of *A. aculeatus* should be obtained from other ocean basins to look at the population structure of this cosmopolitan species at a global scale.

Further research is also required to achieve a better understanding of larval dispersal of seamount biota. This is particularly relevant for spiny lobsters, as they are being exploited at unknown levels and in an unregulated fashion along the SWIR (Groeneveld et al., 2012, pers. obs.). Recent research has shed some light on population connectivity in some of the exploited lobster species (Gopal et al., 2006; Von der Heyden et al., 2007; Groeneveld et al., 2012) but recruitment is poorly understood (Booth and Ovenden, 2000).

Questions about the role of mid-trophic level biota are becoming increasingly urgent given that the productivity, geographic range and composition of marine ecosystems are likely to shift as a result of global climate change (Brierley and Kingsford, 2009; Doney et al., 2012). Ascertaining the response of migrating zooplankton, micronekton and fish populations to such large-scale environmental perturbations will require systematic monitoring

of the mesopelagic zone, along with targeted studies aimed at resolving the distribution, diversity and biogeochemical function of organisms present in the twilight zone (Robison, 2004; Robinson et al., 2010).

Bibliography

Aboim, M. A., G. M. Menezes, T. Schlitt, and A. D. Rogers, 2005. Genetic structure and history of populations of the deep-sea fish *Helicolenus dactylopterus* (Delaroche, 1809) inferred from mtDNA sequence analysis. *Molecular Ecology* **14**:1343–1354.

Ács, Z., R. J. Challis, P. Bihari, M. Blaxter, A. Hayward, G. Melika, G. Csóka, Z. Pénzes, J. Pujade-Villar, J.-L. Nieves-Aldrey, et al., 2010. Phylogeny and DNA barcoding of inquiline oak gallwasps (Hymenoptera: Cynipidae) of the western palaearctic. *Molecular Phylogenetics and Evolution* **55**:210–225.

Agassiz, A., 1892. Reports on the dredging operations off the west coast of Central America to the Galapagos, to the west coast of Mexico, and in the Gulf of California, in charge of Alexander Agassiz, carried on by the U. S. Fish Commission Steamer *"Albatross"*, Lieut. Commander Z. L. Tanner, U. S. N, Commanding. II. General sketch of the expedition of the *"Albatross"* from February to May, 1891. *Bulletin of the Museum of Comparative Zoology* **23**:1–89.

Akaike, H., 1973. Information theory and an extension of the maximum likelihood principle. *In* B. Petran and F. Csaaki (eds.) Second international symposium on information theory, pp. 267–281. Akademinai Kiado, Budapest, Hungary.

Al-Mutairi, H. and M. R. Landry, 2001. Active export of carbon and nitrogen at Station ALOHA by diel migrant zooplankton. *Deep Sea Research Part II: Topical Studies in Oceanography* **48**:2083–2103.

Altschul, S. F., T. L. Madden, A. A. Schäffer, J. Zhang, Z. Zhang, W. Miller, and D. J. Lipman, 1997. Gapped blast and psi-blast: a new generation of protein database search programs. *Nucleic Acids Research* **25**:3389–3402.

Anderson, C., A. Brierley, and F. Armstrong, 2005. Spatio-temporal variability in the distribution of epi- and meso-pelagic acoustic backscatter in the Irminger Sea, North Atlantic, with implications for predation on *Calanus finmarchicus*. *Marine Biology* **146**:1177–1188.

Anderson, M., 2005. Food habits of some deep-sea fish off South Africa's west coast and Agulhas Bank. 1. The grenadiers (Teleostei: Macrouridae). *African Journal of Marine Science* **27**:409–426.

Andréfouët, S., F. Muller-Karger, J. Robinson, C. Kranenburg, D. Torres-Pulliza, S. Spraggins, and B. Murch, 2006. Global assessment of modern coral reef extent and diversity for regional science and management applications: a view from space. *In* Proceedings of the 10th International Coral Reef Symposium, pp. 1732–1745. Japanese Coral Reef Society.

Angel, M., 1985. Vertical migrations in the oceanic realm: Possible causes and probable effects. *Contributions in Marine Science.* **27**:45–70.

Anon., 2010. ESA DUE GlobColour – Global Ocean Colour for Carbon Cycle Research, Product User Guide. ACRI-ST/LOV, UoP, NIVA, BC, DLR, ICESS consortium. Reference: GC-UM-ACR-PUG-01, Version 1.4.

Ansorge, I. J., E. A. Pakhomov, S. Kaehler, J. R. E. Lutjeharms, and J. V. Durgadoo, 2010. Physical and biological coupling in eddies in the lee of the south-west indian ridge. *Polar Biology* **33**:747–759.

Aoyama, J., S. Wouthuyzen, M. J. Miller, T. Inagaki, and K. Tsukamoto, 2003. Short-distance spawning migration of tropical freshwater eels. *The Biological Bulletin* **204**:104–108.

Arranz, P., N. de Soto, P. Madsen, A. Brito, F. Bordes, and M. Johnson, 2011. Following a foraging fish-finder: Diel habitat use of Blainville's beaked whales revealed by echolocation. *PLoS ONE* **6**:e28353.

Backus, R. and J. Craddock, 1977. Pelagic faunal provinces and sound-scattering levels in the Atlantic Ocean. *In* N. Andersen and B. Zahuranec (eds.) Oceanic sound scattering prediction, *Marine Science*, vol. 5, pp. 529–547. Plenum Press, New York.

Bailleul, F., J. Charrassin, P. Monestiez, F. Roquet, M. Biuw, and C. Guinet, 2007. Successful foraging zones of southern elephant seals from the Kerguelen Islands in relation to oceanographic conditions. *Philosophical Transactions of the Royal Society B: Biological Sciences* **362**:2169–2181.

Bailleul, F., C. Cotté, C. Guinet, et al., 2010. Mesoscale eddies as foraging area of a deep-diving predator, the southern elephant seal. *Marine Ecology Progress Series* **408**:251–264.

Baird, R. C., 1971. The systematics, distribution, and zoogeography of the marine hatchetfishes (family sternoptychidae). *Bulletin of the Museum of Comparative Zoology at Harvard University* **142**:1–128.

Baisre, J. A., 1994. Phyllosoma larvae and the phylogeny of Palinuroidea (Crustacea: Decapoda): a review. *Marine & Freshwater Research* **45**:925–944.

Ball, A. O., G. R. Sedberry, J. H. Wessel, and R. W. Chapman, 2003. Large-scale genetic differentiation of *Pagrus pagrus* in the atlantic. *Journal of Fish Biology* **62**:1232–1237.

Ball, A. O., G. R. Sedberry, M. S. Zatcoff, R. W. Chapman, and J. L. Carlin, 2000. Population structure of the wreckfish *Polyprion americanus* determined with microsatellite genetic markers. *Marine Biology* **137**:1077–1090.

Banse, K., 1994. Overview of research efforts and results in the Arabian Sea, 1960-1990. *In* Biogeochemical processes in the Arabian Sea: US-CIS Arabian Sea Workshop Sevastopol, Crimea, Ukraine September 20-25, 1993, p. 7. MHI UNAS.

Barange, M., E. Pakhomov, R. Perissinotto, P. Froneman, H. Verheye, J. Taunton-Clark, and M. Lucas, 1998. Pelagic community structure of the subtropical convergence region south of Africa and in the mid-Atlantic Ocean. *Deep-Sea Research Part I* **45**:1663–1687.

Bard, E. and R. E. Rickaby, 2009. Migration of the subtropical front as a modulator of glacial climate. *Nature* **460**:380–383.

Barham, E. G., 1957. Biology of sonic scattering layers in the Monterey Bay area. MSc dissertation, Stanford University, Pacific Grove, CA.

———, 1966. Deep scattering layer migration and composition: observations from a diving saucer. *Science* **151**:1399–1403.

———, 1970. Deep-sea fishes lethargy and vertical orientation. *In* G. Farquhar (ed.) Proceedings of an International Symposium on Biological Sound Scattering in the Ocean, pp. 100–118. Maury Center for Ocean Science, Washington, D.C.

Beckmann, A. and C. Mohn, 2002. The upper ocean circulation at Great Meteor Seamount. *Ocean Dynamics* **52**:194–204.

Behrenfeld, M. J. and P. G. Falkowski, 1997. Photosynthetic rates derived from satellite-based chlorophyll concentration. *Limnology and Oceanography* **42**:1–20.

Belkin, I. and A. Gordon, 1996. Southern Ocean fronts from the Greenwich meridian to Tasmania. *Journal of Geophysical Research* **101**:3675–3696.

Benfield, M. C., A. C. Lavery, P. H. Wiebe, C. H. Greene, T. K. Stanton, and N. J. Copley, 2003. Distributions of physonect siphonulae in the Gulf of Maine and their potential as important sources of acoustic scattering. *Canadian Journal of Fisheries and Aquatic Sciences* **60**:759–772.

Benoit-Bird, K., 2009. The effects of scattering-layer composition, animal size, and numerical density on the frequency response of volume backscatter. *ICES Journal of Marine Science* **66**:582.

Benoit-Bird, K. and W. Au, 2001. Target strength measurements of Hawaiian mesopelagic boundary community animals. *The Journal of the Acoustical Society of America* **110**:812–819.

———, 2002. Energy: Converting from acoustic to biological resource units. *The Journal of the Acoustical Society of America* **111**:2070–2075.

Benoit-Bird, K. J. and W. W. Au, 2004. Diel migration dynamics of an island-associated sound-scattering layer. *Deep Sea Research Part I: Oceanographic Research Papers* **51**:707–719.

Benson, D. A., I. Karsch-Mizrachi, D. J. Lipman, J. Ostell, and D. L. Wheeler, 2007. Genbank. *Nucleic Acids Research* **35**:D21–D25.

Bertrand, A., E. Josse, P. Bach, and L. Dagorn, 2003. Acoustics for ecosystem research: lessons and perspectives from a scientific programme focusing on tuna-environment relationships. *Aquatic Living Resources* **16**:197–203.

Bianchi, D., E. D. Galbraith, D. A. Carozza, K. Mislan, and C. A. Stock, 2013a. Intensification of open-ocean oxygen depletion by vertically migrating animals. *Nature Geoscience* .

Bianchi, D., C. Stock, E. D. Galbraith, and J. L. Sarmiento, 2013b. Diel vertical migration: Ecological controls and impacts on the biological pump in a one-dimensional ocean model. *Global Biogeochemical Cycles* .

Biuw, M., L. Boehme, C. Guinet, M. Hindell, D. Costa, J.-B. Charrassin, F. Roquet, F. Bailleul, M. Meredith, S. Thorpe, Y. Tremblay, B. McDonald, Y.-H. Park, S. R. Rintoul, N. Bindoff, M. Goebel, D. Crocker, P. Lovell, J. Nicholson, F. Monks, and M. A. Fedak, 2007. Variations in behavior and condition of a Southern Ocean top predator in relation to in situ oceanographic conditions. *Proceedings of the National Academy of Sciences* **104**:13705–13710.

Biuw, M., B. McConnell, C. Bradshaw, H. Burton, and M. Fedak, 2003. Blubber and buoyancy: monitoring the body condition of free-ranging seals using simple dive characteristics. *Journal of Experimental Biology* **206**:3405–3423.

Biuw, M., O. Nøst, A. Stien, Q. Zhou, C. Lydersen, and K. Kovacs, 2010. Effects of hydrographic variability on the spatial, seasonal and diel diving patterns of southern elephant seals in the eastern Weddell Sea. *PLoS ONE* **5**:e13816.

Bivand, R. S., E. J. Pebesma, and V. Gómez-Rubio, 2008. Applied spatial data analysis with R. Springer, New York London.

Blaxter, M., J. Mann, T. Chapman, F. Thomas, C. Whitton, R. Floyd, and E. Abebe, 2005. Defining operational taxonomic units using DNA barcode data. *Philosophical Transactions of the Royal Society B: Biological Sciences* **360**:1935.

Boehlert, G. and M. Seki, 1984. Enhanced micronekton abundance over mid-Pacific seamounts. *EOS, Transactions of the American Geophysical Union* **65**:928.

Boehme, L., M. Meredith, S. Thorpe, M. Biuw, and M. Fedak, 2008. Antarctic circumpolar current frontal system in the south Atlantic: Monitoring using merged Argo and animal-borne sensor data. *Journal of Geophysical Research* **113**:C09012.

Boersch-Supan, P., L. Boehme, J. Read, A. Rogers, and A. Brierley, 2012. Elephant seal foraging dives track prey distributions, not temperature: Comment on McIntyre et al. (2011). *Marine Ecology Progress Series* **461**:293–298.

Booth, J. and J. Ovenden, 2000. Distribution of *Jasus spp.* (Decapoda: Palinuridae) phyllosomas in southern waters: implications for larval recruitment. *Marine Ecology Progress Series* **200**:241–255.

Booth, J. D. and B. F. Phillips, 1994. Early life history of spiny lobster. *Crustaceana* **66**:271–294.

Booth, J. D., W. R. Webber, H. Sekiguchi, and E. Coutures, 2005. Review: Diverse larval recruitment strategies within the Scyllaridae. *New Zealand Journal of Marine and Freshwater Research* **39**:581–592.

Bortolotto, E., A. Bucklin, M. Mezzavilla, L. Zane, and T. Patarnello, 2011. Gone with the currents: lack of genetic differentiation at the circum-continental scale in the antarctic krill euphausia superba. *BMC Genetics* **12**:32.

Bowen, W., D. Tully, D. Boness, B. Bulheier, and G. Marshall, 2002. Prey-dependent foraging tactics and prey profitability in a marine mammal. *Marine Ecology Progress Series* **244**:235–245.

Bradbury, M., D. Abbot, R. Bovbjerg, R. Mariscal, W. Fielding, R. Barber, V. Pearse, S. Proctor, J. Ogden, J. Wourms, L. Taylor Jr., J. Christofferson, J. Christofferson, R. McPhearson, M. Wynne, and P. Stromberg Jr., 1970. Studies on the fauna associated with the deep scattering layers in the equatorial Indian Ocean, conducted on R/V TE VEGA during October and November 1964. *In* G. Farquhar (ed.) Proceedings of an International Symposium on Biological Sound Scattering in the Ocean, pp. 409–452. Maury Center for Ocean Science, Washington, D.C.

Branch, G. M. and B. M. Clark, 2006. Fish stocks and their management: the changing face of fisheries in South Africa. *Marine Policy* **30**:3–17.

Brierley, A., M. Brandon, and J. Watkins, 1998a. An assessment of the utility of an acoustic Doppler current profiler for biomass estimation. *Deep-Sea Research Part I* **45**:1555–1573.

Brierley, A., P. Ward, J. Watkins, and C. Goss, 1998b. Acoustic discrimination of Southern Ocean zooplankton. *Deep-Sea Research Part II* **45**:1155–1173.

Brierley, A. S., P. G. Fernandes, M. A. Brandon, F. Armstrong, N. W. Millard, S. D. McPhail, P. Stevenson, M. Pebody, J. Perrett, M. Squires, et al., 2002. Antarctic krill under sea ice: elevated abundance in a narrow band just south of ice edge. *Science* **295**:1890–1892.

Brierley, A. S. and M. J. Kingsford, 2009. Impacts of climate change on marine organisms and ecosystems. *Current Biology* **19**:R602–R614.

Brodeur, R., 2001. Habitat-specific distribution of Pacific ocean perch (*Sebastes alutus*) in Pribilof Canyon, Bering Sea. *Continental Shelf Research* **21**:207–224.

Brown, J. H., 1984. On the relationship between abundance and distribution of species. *American Naturalist* pp. 255–279.

Brown, W. M., M. George, and A. C. Wilson, 1979. Rapid evolution of animal mitochondrial DNA. *Proceedings of the National Academy of Sciences* **76**:1967–1971.

Bucklin, A., T. LaJeunesse, E. Curry, J. Wallinga, and K. Garrison, 1996. Molecular diversity of the copepod, *Nannocalanus minor*: genetic evidence of species and population structure in the North Atlantic Ocean. *Journal of Marine Research* **54**:285–310.

Bucklin, A., B. D. Ortman, R. M. Jennings, L. M. Nigro, C. J. Sweetman, N. J. Copley, T. Sutton, and P. H. Wiebe, 2010a. A 'Rosetta Stone' for metazoan zooplankton: DNA barcode analysis of species diversity of the Sargasso Sea (Northwest Atlantic Ocean). *Deep Sea Research II* **57**:2234–2247.

Bucklin, A., D. Steinke, and L. Blanco-Bercial, 2010b. DNA barcoding of marine metazoa. *Annual Review of Marine Science* **3**.

Buesseler, K. O. and P. W. Boyd, 2009. Shedding light on processes that control particle export and flux attenuation in the twilight zone of the open ocean. *Limnology and Oceanography* **54**:1210.

Burgos, J. and J. Horne, 2008. Characterization and classification of acoustically detected fish spatial distributions. *ICES Journal of Marine Science* **65**:1235.

Caley, T., J. Giraudeau, B. Malaizé, L. Rossignol, and C. Pierre, 2012. Agulhas leakage as a key process in the modes of quaternary climate changes. *Proceedings of the National Academy of Sciences* **109**:6835–6839.

Campagna, C., A. Piola, M. Rosa Marin, M. Lewis, and T. Fernández, 2006. Southern elephant seal trajectories, fronts and eddies in the Brazil/Malvinas confluence. *Deep-Sea Research Part I: Oceanographic Research Papers* **53**:1907–1924.

Carlsson, J., S. Shephard, J. Coughlan, C. N Trueman, E. Rogan, and T. F. Cross, 2011. Fine-scale population structure in a deep-sea teleost (orange roughy, *Hoplostethus atlanticus*). *Deep Sea Research Part I: Oceanographic Research Papers* **58**:627–636.

Castelin, M., J. Lambourdiere, M. Boisselier, P. Lozouet, A. Couloux, C. Cruaud, and S. Samadi, 2010. Hidden diversity and endemism on seamounts: focus on poorly dispersive neogastropods. *Biological Journal of the Linnean Society* **100**:420–438.

Castle, P., 1997. Garden eel leptocephali: characters, generic identification, distribution, and relationships. *Bulletin of Marine Science* **60**:6–22.

Castle, P. H. J., 1968. The congrid eels of the western indian ocean and the red sea. *Ichthyological Bulletin* **33**:685–726.

Castresana, J., 2000. Selection of conserved blocks from multiple alignments for their use in phylogenetic analysis. *Molecular Biology and Evolution* **17**:540–552.

Charrassin, J., M. Hindell, S. Rintoul, F. Roquet, S. Sokolov, M. Biuw, D. Costa, L. Boehme, P. Lovell, R. Coleman, et al., 2008. Southern Ocean frontal structure and sea-ice formation rates revealed by elephant seals. *Proceedings of the National Academy of Sciences* **105**:11634.

Cho, W. and T. M. Shank, 2010. Incongruent patterns of genetic connectivity among four ophiuroid species with differing coral host specificity on north atlantic seamounts. *Marine Ecology* **31**:121–143.

Chow, S., N. Suzuki, H. Imai, and T. Yoshimura, 2006. Molecular species identification of spiny lobster phyllosoma larvae of the genus *Panulirus* from the northwestern Pacific. *Marine Biotechnology* **8**:260–267.

Christensen, R., G. Duvall, and J. MW Johnson RL Ely, 1946. Stratification of sound scatterers in the sea. Tech. Rep. M397, University of California War Research Division, U.S. Navy Electronics Laboratory, San Diego, CA.

Chun, C., 1887. Die pelagische Thierwelt in grösserem Meerestiefen und ihre Beziehungen zu der Oberflächenfauna. *Bibliotheca Zoologica* **1**:1–66.

———, 1899. Die Deutsche Tiefsee Expedition. A. Berichte des Leiters der Expedition Professor Dr. Chun an das Reichs-Amt des Innern. *Zeitschrift der Gesellschaft für Erdkunde zu Berlin* **34**:75–134.

Ciannelli, L., P. Fauchald, K.-S. Chan, V. N. Agostini, and G. E. Dingsør, 2008. Spatial fisheries ecology: recent progress and future prospects. *Journal of Marine Systems* **71**:223–236.

Cisewski, B., V. Strass, M. Rhein, and S. Krägefsky, 2010. Seasonal variation of diel vertical migration of zooplankton from ADCP backscatter time series data in the Lazarev Sea, Antarctica. *Deep Sea Research Part I: Oceanographic Research Papers* **57**:78–94.

Clark, M. R., A. A. Rowden, T. Schlacher, A. Williams, M. Consalvey, K. I. Stocks, A. D. Rogers, T. D. O'Hara, M. White, T. M. Shank, and J. M. Hall-Spencer, 2010. The ecology of seamounts: Structure, function, and human impacts. *Annual Review of Marine Science* pp. 253–278.

Clarke, M. R., 1962. The identification of cephalopod "beaks" and the relationship between beak size and total body weight. *Bulletin of the British Museum (Natural History), Zoology* **8**:419–480.

———, 1986. A handbook for the identification of cephalopod beaks. Clarendon Press, Oxford.

Coffin, M., L. Gahagan, and L. Lawver, 1998. Present-day plate boundary digital data compilation. Tech. Rep. 174, University of Texas Institute for Geophysics.

Cole, H., G. Bryan, and A. Gordon, 1970. The deep scattering layer: patterns across the Gulf Stream and the Sargasso Sea. *In* G. Farquhar (ed.) Proceedings of an International Symposium on Biological Sound Scattering in the Ocean, pp. 281–293. Maury Center for Ocean Science, Washington, D.C.

Collette, B. B. and N. Parin, 1991. Shallow-water fishes of Walters shoals, Madagascar ridge. *Bulletin of Marine Science* **48**:1–22.

Conte, M., J. Bishop, and R. Backus, 1986. Nonmigratory, 12-kHz, deep scattering layers of Sargasso Sea origin in warm-core rings. *Deep-Sea Research Part A: Oceanographic Research Papers* **33**:1869–1884.

Corripio, J. G., 2013. insol: Solar Radiation. URL http://CRAN.R-project.org/package=insol. R package version 1.1.

Costa, D., L. Huckstadt, D. Crocker, B. McDonald, M. Goebel, and M. Fedak, 2010. Approaches to studying climatic change and its role on the habitat selection of Antarctic pinnipeds. *Integrative and Comparative Biology* **50**:1018–1030.

Costa, D. P., 1993. The relationship between reproductive and foraging energetics and the evolution of the Pinnipedia. *Symposia of the Zoological Society of London* **66**:293–314.

Costello, M. J., M. McCrea, A. Freiwald, T. Lundälv, L. Jonsson, B. J. Bett, T. C. van Weering, H. de Haas, J. M. Roberts, and D. Allen, 2005. Role of cold-water *Lophelia pertusa* coral reefs as fish habitat in the NE Atlantic. *In* Cold-water corals and ecosystems, pp. 771–805. Springer.

Cowen, R., G. Gawarkiewicz, J. Pineda, S. Thorrold, and F. Werner, 2007. Population connectivity in marine systems: An overview. *Oceanography* **20**:14–21.

Cox, M. J., T. B. Letessier, and A. S. Brierley, 2013. Zooplankton and micronekton biovolume at the Mid-Atlantic Ridge and Charlie-Gibbs Fracture Zone estimated by multi-frequency acoustic survey. *Deep Sea Research II* In press; http://dx.doi.org/10.1016/j.dsr2.2013.07.020.

Creasey, S. S. and A. Rogers, 1999. Population genetics of bathyal and abyssal organisms. *Advances in Marine Biology* **35**:1–151.

Dagorn, L., P. Bach, and E. Josse, 2000. Movement patterns of large bigeye tuna (*Thunnus obesus*) in the open ocean, determined using ultrasonic telemetry. *Marine Biology* **136**:361–371.

Dagorn, L., K. N. Holland, J. Hallier, M. Taquet, G. Moreno, G. Sancho, D. G. Itano, R. Aumeeruddy, C. Girard, J. Million, et al., 2006. Deep diving behavior observed in yellowfin tuna (*Thunnus albacares*). *Aquatic Living Resources* **19**:85–88.

Darling, K. F., C. M. Wade, I. A. Stewart, D. Kroon, R. Dingle, and A. J. L. Brown, 2000. Molecular evidence for genetic mixing of Arctic and Antarctic subpolar populations of planktonic foraminifers. *Nature* **405**:43–47.

Davies, A. J., G. C. Duineveld, M. S. Lavaleye, M. J. Bergman, H. van Haren, and J. M. Roberts, 2009. Downwelling and deep-water bottom currents as food supply mechanisms to the cold-water coral *Lophelia pertusa* (Scleractinia) at the Mingulay Reef complex. *Limnology and Oceanography* **54**:620–629.

Davison, P., 2011a. The export of carbon mediated by mesopelagic fishes in the Northeast Pacific Ocean. Ph.D. thesis, University of California, San Diego, USA.

———, 2011b. The specific gravity of mesopelagic fish from the northeastern pacific ocean and its implications for acoustic backscatter. *ICES Journal of Marine Science* **68**:2064–2074.

De Forest, L. and J. Drazen, 2009. The influence of a Hawaiian seamount on mesopelagic micronekton. *Deep Sea Research I* **56**:232–250.

De Robertis, A. and I. Higginbottom, 2007. A post-processing technique to estimate the signal-to-noise ratio and remove echosounder background noise. *ICES Journal of Marine Science* **64**:1282.

Demer, D., 2004. An estimate of error for the CCAMLR 2000 survey estimate of krill biomass. *Deep Sea Research II* **51**:1237–1251.

DeSalle, R., M. G. Egan, and M. Siddall, 2005. The unholy trinity: taxonomy, species delimitation and DNA barcoding. *Philosophical Transactions of the Royal Society B: Biological Sciences* **360**:1905–1916.

Dewey, R., D. Richmond, and C. Garrett, 2005. Stratified tidal flow over a bump. *Journal of Physical Oceanography* **35**:1911–1927.

Dick, H., J. Lin, and H. Schouten, 2003. An ultraslow-spreading class of ocean ridge. *Nature* **426**:405–412.

Diekmann, B., 2007. Sedimentary patterns in the late Quaternary Southern Ocean. *Deep Sea Research Part II: Topical Studies in Oceanography* **54**:2350–2366.

Djurhuus, A. and A. Rogers, 2013. Marine microbial populations of the southwest Indian Ocean Ridge system. Presentation PS-8.07; EMBO Conference on Aquatic Microbial Ecology: SAME13; Stresa, Italy.

Dohrn, A., 1870. Untersuchungen über Bau und Entwicklung der Arthropoden. VI. Zur Entwicklungsgeschichte der Panzerkrebse (Decapoda Loricata.). *Zeitschrift für wissenschaftliche Zoologie* **20**:249–271.

Doney, S. C., M. Ruckelshaus, J. E. Duffy, J. P. Barry, F. Chan, C. A. English, H. M. Galindo, J. M. Grebmeier, A. B. Hollowed, N. Knowlton, et al., 2012. Climate change impacts on marine ecosystems. *Marine Science* **4**.

Donlon, C. J., M. Martin, J. Stark, J. Roberts-Jones, E. Fiedler, and W. Wimmer, 2012. The operational sea surface temperature and sea ice analysis (OSTIA) system. *Remote Sensing of Environment* **116**:140–158.

Dragon, A., A. Bar-Hen, P. Monestiez, and C. Guinet, 2012. Horizontal and vertical movements as predictors of foraging success in a marine predator. *Marine Ecology Progress Series* **447**:243–257.

Dragon, A., P. Monestiez, A. Bar-Hen, and C. Guinet, 2010. Linking foraging behaviour to physical oceanographic structures: Southern elephant seals and mesoscale eddies east of Kerguelen Islands. *Progress in Oceanography* **87**:61–71.

Duineveld, G. C., M. S. Lavaleye, M. J. Bergman, H. De Stigter, and F. Mienis, 2007. Trophic structure of a cold-water coral mound community (Rockall Bank, NE Atlantic) in relation to the near-bottom particle supply and current regime. *Bulletin of Marine Science* **81**:449–467.

Eckert, C. G., K. E. Samis, and S. C. Lougheed, 2008. Genetic variation across species' geographical ranges: the central-marginal hypothesis and beyond. *Molecular Ecology* **17**:1170–1188.

Edgar, R. C., 2004. Muscle: multiple sequence alignment with high accuracy and high throughput. *Nucleic Acids Research* **32**:1792–1797.

Escobar-Flores, P., R. L. O'Driscoll, and J. C. Montgomery, 2013. Acoustic characterization of pelagic fish distribution across the south pacific ocean. *Marine ecology. Progress series* **490**:169–183.

Excoffier, L. and H. E. L. Lischer, 2010. Arlequin suite ver 3.5: a new series of programs to perform population genetics analyses under linux and windows. *Molecular Ecology Resources* **10**:47–50.

Excoffier, L., P. E. Smouse, and J. M. Quattro, 1992. Analysis of molecular variance inferred from metric distances among DNA haplotypes - application to human mitochondrial-DNA restriction data. *Genetics* **131**:479–491.

Eyring, C., R. Christensen, R. Raitt, C. Parker, T. Shafer, J. Frautschy, and M. Sheehy, 1942. Reverberation studies at 24 kc. Tech. Rep. U7, University of California War Research Division, U.S. Navy Radio and Sound Laboratory, San Diego, CA.

Falkowski, P. and Z. Kolber, 1995. Variations in chlorophyll fluorescence yields in phytoplankton in the world oceans. *Australian Journal of Plant Physiology* **22**:341–355.

Farmer, D. and L. Armi, 1999. The generation and trapping of solitary waves over topography. *Science* **283**:188–190.

Farquhar, G., 1977. Biological sound scattering in the oceans: a review. *In* N. Andersen and B. Zahuranec (eds.) Oceanic sound scattering prediction, *Marine Science*, vol. 5, pp. 493–527. Plenum Press, New York.

Farquhar, G. B. (ed.), 1970. Proceedings of an International Symposium on Biological Sound Scattering in the Ocean. U.S. Naval Oceanographic Office, Department of the Navy, Washington, D.C.

Fernandes, P., R. Korneliussen, A. Lebourges-Dhaussy, J. Masse, M. Iglesias, N. Diner, E. Ona, T. Knutsen, J. Gajate, and R. Ponce, 2006. The SIMFAMI project: species identification methods from acoustic multifrequency information. Final Report to the EC No Q5RS-2001-02054.

Fernandes, P. G., F. Gerlotto, D. V. Holliday, O. Nakken, and E. J. Simmonds, 2002. Acoustic applications in fisheries science: the ICES contribution. *ICES Marine Science Symposia* **215**:483–492.

Fernandez, E. and V. Allain, 2011. Importance of reef prey in the diet of tunas and other large pelagic species in the western and central Pacific Ocean. *SPC Fisheries Newsletter* **133**:35–39.

Fiedler, P., S. Reilly, R. Hewitt, D. Demer, V. Philbrick, S. Smith, W. Armstrong, D. Croll, B. Tershy, and B. Mate, 1998a. Blue whale habitat and prey in the California Channel Islands. *Deep-Sea Research Part II: Topical Studies in Oceanography* **45**:1781–1801.

Fiedler, P. C., J. Barlow, and T. Gerrodette, 1998b. Dolphin prey abundance determined from acoustic backscatter data in eastern Pacific surveys. *Fishery Bulletin* **96**:237–247.

Fisher, R. and A. Goodwillie, 1997. The physiography of the Southwest Indian Ridge. *Marine Geophysical Researches* **19**:451–455.

Florence, W., P. Hulley, B. Stewart, and M. Gibbons, 2002. Genetic and morphological variation of the lanternfish *Lampanyctodes hectoris* (Myctophiformes: Myctophidae) off southern Africa. *South African Journal of Marine Science* **24**:193–203.

Floyd, R., E. Abebe, A. Papert, and M. Blaxter, 2002. Molecular barcodes for soil nematode identification. *Molecular Ecology* **11**:839–850.

Fock, H., B. Matthiessen, H. Zidowitz, and H. Westernhagen, 2002. Diel and habitat-dependent resource utilisation by deep-sea fishes at the Great Meteor seamount: niche overlap and support for the sound scattering layer interception hypothesis. *Marine Ecology Progress Series* **244**:219–233.

Fofonoff, N. and R. Millard, 1983. Algorithms for computation of fundamental properties of seawater. *Unesco Technical Papers in Marine Science* **44**:46–50.

Folmer, O., M. Black, W. Hoeh, R. Lutz, and R. Vrijenhoek, 1994. DNA primers for amplification of mitochondrial cytochrome c oxidase subunit I from diverse metazoan invertebrates. *Molecular Marine Biology and Biotechnology* **3**:294–299.

Foote, K., H. Knudsen, G. Vestnes, D. MacLennan, and E. Simmonds, 1987. Calibration of acoustic instruments for fish density estimation: a practical guide. *ICES Cooperative Research Reports* **144**:69.

Forbes, E., 1844. On the light thrown on geology by submarine researches; being the substance of a communication made to the Royal Institution of Great Britain. Friday Evening, the 23d February 1844. *Edinburgh New Philosophical Journal* **36**:319–327.

Forcada, J., P. Trathan, and E. Murphy, 2008. Life history buffering in Antarctic mammals and birds against changing patterns of climate and environmental variation. *Global Change Biology* **14**:2473–2488.

de Forges, B., J. Koslow, and G. Poore, 2000. Diversity and endemism of the benthic seamount fauna in the southwest Pacific. *Nature* **405**:944–947.

France, S. C. and T. Kocher, 1996. Geographic and bathymetric patterns of mitochondrial 16S rRNA sequence divergence among deep-sea amphipods, *Eurythenes gryllus*. *Marine Biology* **126**:633–643.

Francois, R. and G. Garrison, 1982. Sound absorption based on ocean measurements. part ii: Boric acid contribution and equation for total absorption. *The Journal of the Acoustical Society of America* **72**:1879–1890.

Frederiksen, R., A. Jensen, and H. Westerberg, 1992. The distribution of the scleractinian coral *Lophelia pertusa* around the Faroe Islands and the relation to internal tidal mixing. *Sarsia* **77**:157–171.

Fricke, R., 1999. Fishes of the Mascarene Islands (Réunion, Mauritius, Rodriguez): an annotated checklist, with descriptions of new species. Koeltz Scientific Books, Koenigstein, Germany.

Froese, R. and A. Sampang, 2004. Taxonomy and biology of seamount fishes. *University of British Columbia Fisheries Centre Research Reports* **12**:25–31.

Fu, Y. X., 1997. Statistical tests of neutrality of mutations against population growth, hitchhiking and background selection. *Genetics* **147**:915–925.

Fuchs, T., 1882. Ueber die pelagische Flora und Fauna. *Verhandlungen der k. k. geologischen Reichsanstalt* **1882**:49–55.

Gage, J. D. and P. A. Tyler, 1991. Deep-sea biology: a natural history of organisms at the deep-sea floor. Cambridge University Press, Cambridge.

Garrett, C., 2003. Internal tides and ocean mixing. *Science* **301**:1858–1859.

GEBCO, 2010. General Bathymetric Chart of the Oceans – The GEBCO 08 Grid. Version 20100927, http://www.gebco.net.

Genin, A., 1987. Effects of seamount topography and currents on biological processes. Ph.D. thesis, University of California, San Diego, USA.

———, 2004. Bio-physical coupling in the formation of zooplankton and fish aggregations over abrupt topographies. *Journal of Marine Systems* **50**:3–20.

Genin, A. and G. W. Boehlert, 1985. Dynamics of temperature and chlorophyll structures above a seamount: an oceanic experiment. *Journal of Marine Research* **43**:907–924.

Genin, A., P. Dayton, P. Lonsdale, and F. Spiess, 1986. Corals on seamount peaks provide evidence of current acceleration over deep-sea topography. *Nature* **322**:59–61.

Genin, A. and J. Dower, 2007. Seamount plankton dynamics. *In* T. J. Pitcher, T. Morato, P. J. B. Hart, M. R. Clark, N. Haggan, and R. S. Santos (eds.) Seamounts: Ecology, Fisheries and Conservation, *Fish and Aquatic Resources Series*, vol. 12, chap. 5, pp. 85–100. Blackwell Scientific, Oxford, UK.

Genin, A., C. Greene, L. Haury, P. Wiebe, G. Gal, S. Kaartvedt, E. Meir, C. Fey, and J. Dawson, 1994. Zooplankton patch dynamics: daily gap formation over abrupt topography. *Deep Sea Research Part I: Oceanographic Research Papers* **41**:941–951.

Genin, A., L. Haury, and P. Greenblatt, 1988. Interactions of migrating zooplankton with shallow topography: predation by rockfishes and intensification of patchiness. *Deep Sea Research Part A. Oceanographic Research Papers* **35**:151–175.

Genin, A., J. S. Jaffe, R. Reef, C. Richter, and P. J. Franks, 2005. Swimming against the flow: a mechanism of zooplankton aggregation. *Science* **308**:860–862.

Genin, A., M. Noble, and P. Lonsdale, 1989. Tidal currents and anticyclonic motions on two North Pacific seamounts. *Deep Sea Research Part A. Oceanographic research papers* **36**:1803–1815.

Gille, S., 2002. Warming of the Southern Ocean since the 1950s. *Science* **295**:1275.

Gjøsæter, J. and K. Kawaguchi, 1980. A review of the world resources of mesopelagic fish. *FAO Fisheries Technical Paper* **193**.

Godø, O., R. Patel, and G. Pedersen, 2009. Diel migration and swimbladder resonance of small fish: some implications for analyses of multifrequency echo data. *ICES Journal of Marine Science* **66**:1143.

Godø, O. R., A. Samuelsen, G. J. Macaulay, R. Patel, S. S. Hjøllo, J. Horne, S. Kaartvedt, and J. A. Johannessen, 2012. Mesoscale eddies are oases for higher trophic marine life. *PLoS ONE* **7**:e30161.

Goetze, E., 2011. Population differentiation in the open sea: Insights from the pelagic copepod *Pleuromamma xiphias*. *Integrative and Comparative Biology* **51**:580–597.

Gopal, K., K. Tolley, J. Groeneveld, and C. Matthee, 2006. Mitochondrial DNA variation in spiny lobster *Palinurus delagoae* suggests genetically structured populations in the southwestern Indian Ocean. *Marine Ecology Progress Series* **319**:191–198.

Gordeeva, N. V., 2011. On structure of species in pelagic fishes: results of population-genetic analysis of four species of lanternfishes (Myctophidae) of the Southern Atlantic. *Journal of Ichthyology* **51**:152–165.

Gower, J. C., 1971. A general coefficient of similarity and some of its properties. *Biometrics* **27**:857–871.

Grant, W. S. and B. W. Bowen, 1998. Shallow population histories in deep evolutionary lineages of marine fishes: Insights from sardines and anchovies and lessons for conservation. *Journal of Heredity* **89**:415–426.

Groeneveld, J., K. Gopal, R. George, and C. Matthee, 2007. Molecular phylogeny of the spiny lobster genus *Palinurus* (Decapoda: Palinuridae) with hypotheses on speciation in the NE Atlantic/Mediterranean and SW Indian Ocean. *Molecular Phylogenetics and Evolution* **45**:102–110.

Groeneveld, J., C. Griffiths, and A. Van Dalsen, 2006. A new species of spiny lobster, *Palinurus barbarae* (Decapoda, Palinuridae) from Walters Shoals on the Madagascar Ridge. *Crustaceana* **79**:821–833.

Groeneveld, J. C., S. von der Heyden, and C. A. Matthee, 2012. High connectivity and lack of mtDNA differentiation among two previously recognized spiny lobster species in the southern Atlantic and Indian Oceans. *Marine Biology Research* **8**:764–770.

Guinet, C., J. Vacquié-Garcia, B. Picard, G. Bessigneul, Y. Lebras, A. C. Dragon, M. Viviant, J. P. Arnould, and F. Bailleul, 2014. Southern elephant seal foraging success in relation to temperature and light conditions: insight into prey distribution. *Marine Ecology Progress Series* **499**:285–301.

Gurney, R., 1936. Larvae of decapod crustacea. *Discovery Reports* **XII**:377–440.

———, 1942. Larvae of Decapod Crustacea, vol. 129. The Ray Society, London.

Hamner, W., M. Jones, J. Carleton, I. Hauri, and D. M. Williams, 1988. Zooplankton, planktivorous fish, and water currents on a windward reef face: Great Barrier Reef, Australia. *Bulletin of Marine Science* **42**:459–479.

Haury, L., C. Fey, C. Newland, and A. Genin, 2000. Zooplankton distribution around four eastern North Pacific seamounts. *Progress in Oceanography* **45**:69–105.

Haury, L., J. McGowan, and P. Wiebe, 1978. Patterns and processes in the time-space scales of plankton distributions. *In* J. Steele (ed.) Spatial pattern in plankton communities, *NATO Conference Series in Marine Sciences*, vol. 3, pp. 277–327. Plenum Press, New York, NY.

Hays, G. C., 2003. A review of the adaptive significance and ecosystem consequences of zooplankton diel vertical migrations. *Hydrobiologia* **503**:163–170.

Hazen, E. and D. Johnston, 2010. Meridional patterns in the deep scattering layers and top predator distribution in the central equatorial Pacific. *Fisheries Oceanography* **19**:427–433.

Hebert, P., A. Cywinska, S. Ball, and J. Dewaard, 2003a. Biological identifications through DNA barcodes. *Proceedings of the Royal Society of London. Series B: Biological Sciences* **270**:313–321.

Hebert, P. D., S. Ratnasingham, and J. R. de Waard, 2003b. Barcoding animal life: cytochrome c oxidase subunit 1 divergences among closely related species. *Proceedings of the Royal Society of London. Series B: Biological Sciences* **270**:S96–S99.

Hedgecock, D., P. Barber, and S. Edmands, 2007. Genetic approaches to measuring connectivity. *Oceanography* **20**:70–79.

Heimeier, D., S. Lavery, and M. A. Sewell, 2010. Using DNA barcoding and phylogenetics to identify antarctic invertebrate larvae: Lessons from a large scale study. *Marine Genomics* **3**:165–177.

Heino, M., F. Porteiro, T. Sutton, T. Falkenhaug, O. Godø, and U. Piatkowski, 2011. Catchability of pelagic trawls for sampling deep-living nekton in the mid-North Atlantic. *ICES Journal of Marine Science* **68**:377.

Hidaka, K., K. Kawaguchi, M. Murakami, and M. Takahashi, 2001. Downward transport of organic carbon by diel migratory micronekton in the western equatorial Pacific: its quantitative and qualitative importance. *Deep Sea Research I* **48**:1923–1939.

Hijmans, R. J. and J. van Etten, 2012. raster: Geographic data analysis and modeling. URL http://CRAN.R-project.org/package=raster. R package version 2.0-41.

Hijmans, R. J., E. Williams, and C. Vennes, 2012. geosphere: Spherical Trigonometry. URL http://CRAN.R-project.org/package=geosphere. R package version 1.2-28.

Hill, A., 1991. Vertical migration in tidal currents. *Marine Ecology Progress Series* **75**:39–54.

Hindell, M., C. Bost, J. Charrassin, N. Gales, S. Goldsworthy, M. Lea, M. O'Toole, and C. Guinet, 2011. Foraging habitats of top predators, and areas of ecological significance on the Kerguelen Plateau. *In* G. Duhamel and D. Welsford (eds.) The Kerguelen Plateau: marine ecosystem and fisheries, pp. 203–215. Société Française d'Ichtyologie, Paris.

Hirch, S. and B. Christiansen, 2010. The trophic blockage hypothesis is not supported by the diets of fishes on Seine Seamount. *Marine Ecology* **31**:107–120.

Hoarau, G. and P. Borsa, 2000. Extensive gene flow within sibling species in the deep-sea fish *Beryx splendens*. *Comptes Rendus de l'Académie des Sciences - Series III* **323**:315–325.

Holliday, D., 1972. Resonance structure in echoes from schooled pelagic fish. *The Journal of the Acoustical Society of America* **51**:1322–1332.

Holthuis, L., 1991. Marine lobsters of the world, *FAO species catalogue*, vol. 13. FAO.

Horn, P., J. Forman, and M. Dunn, 2010. Feeding habits of alfonsino *Beryx splendens*. *Journal of Fish Biology* **76**:2382–2400.

Horne, p. J., I. c. Kaplan, K. n. Marshall, p. s. levin, c. J. Harvey, a. J. Hermann, and E. a. Fulton., 2010. Design and parameterization of a spatially explicit ecosystem model of the central California Current. *NOAA Technical Memorandum* **104**:1–140.

Howey-Jordan, L. A., E. J. Brooks, D. L. Abercrombie, L. K. Jordan, A. Brooks, S. Williams, E. Gospodarczyk, and D. D. Chapman, 2013. Complex movements, philopatry and expanded depth range of a severely threatened pelagic shark, the oceanic whitetip (*Carcharhinus longimanus*) in the western North Atlantic. *PLoS ONE* **8**:e56588.

Hubbs, C., 1959. Initial discoveries of fish faunas on seamounts and offshore banks in the Eastern Pacific. *Pacific Science* **13**:311–316.

Husebø, Å., L. Nøttestad, J. Fosså, D. Furevik, and S. Jørgensen, 2002. Distribution and abundance of fish in deep-sea coral habitats. *Hydrobiologia* **471**:91–99.

Ingole, B. and J. Koslow, 2005. Deep-sea ecosystems of the Indian Ocean. *Indian Journal of Marine Sciences* **34**:27–34.

Inoue, J. G., M. Miya, M. J. Miller, T. Sado, R. Hanel, K. Hatooka, J. Aoyama, Y. Minegishi, M. Nishida, and K. Tsukamoto, 2010. Deep-ocean origin of the freshwater eels. *Biology Letters* **6**:363–366.

Irigoien, X., T. Klevjer, A. Røstad, U. Martinez, G. Boyra, J. Acuña, A. Bode, F. Echevarria, J. Gonzalez-Gordillo, S. Hernandez-Leon, S. Agusti, D. Aksnes, C. Duarte, and S. Kaartvedt, 2014. Large mesopelagic fishes biomass and trophic efficiency in the open ocean. *Nature communications* **5**.

Isaacs, J. and R. Schwartzlose, 1965. Migrant sound scatterers: interaction with the sea floor. *Science* **150**:1810–1813.

Ivanova, N., T. Zemlak, R. Hanner, and P. Hebert, 2007. Universal primer cocktails for fish DNA barcoding. *Molecular Ecology Notes* **7**:544–548.

Johnson, M. W., 1971. On palinurid and scyllarid lobster larvae and their distribution in the South China Sea (Decapoda, Palinuridea). *Crustaceana* **21**:247–282.

Kaartvedt, S., A. Staby, and D. Aksnes, 2012. Efficient trawl avoidance by mesopelagic fishes causes large underestimation of their biomass. *Marine Ecology Progress Series* **456**:1–6.

Kaartvedt, S., J. Titelman, A. Røstad, and T. A. Klevjer, 2011. Beyond the average: Diverse individual migration patterns in a population of mesopelagic jellyfish. *Limnology and Oceanography* **56**:2189–2199.

Kahng, S., J. Garcia-Sais, H. Spalding, E. Brokovich, D. Wagner, E. Weil, L. Hinderstein, and R. Toonen, 2010. Community ecology of mesophotic coral reef ecosystems. *Coral Reefs* **29**:255–275.

Kaneko, A., H. Honji, K. Kawatate, S. Mizuno, A. Masuda, and T. Miita, 1986. A note on internal wavetrains and the associated undulation of the sea surface observed upstream of seamounts. *Journal of the Oceanographical Society of Japan* **42**:75–82.

Kaplan, D. M., P. Bach, S. Bonhommeau, E. Chassot, P. Chavance, L. Dagorn, T. Davies, S. Dueri, R. Fletcher, A. Fonteneau, et al., 2013. The true challenge of giant marine reserves. *Science* **340**:810–811.

Kaufman, L. and P. J. Rousseeuw, 1990. Finding groups in data: an introduction to cluster analysis. Wiley, New York.

Kelley, D., 2012. oce: Analysis of Oceanographic data. URL http://CRAN.R-project.org/package=oce. R package version 0.8-6.

Kim, S.-S. and P. Wessel, 2011. New global seamount census from altimetry-derived gravity data. *Geophysical Journal International* **186**:615–631.

Kimani, E. N., G. M. Okemwa, and J. M. Kazungu, 2009. Fisheries in the Southwest Indian Ocean: Trends and governance challenges. *In* The Indian Ocean; Resource and Governance Challenges, pp. 3–90. The Henry L. Stimson Centre, Washington, D.C., USA.

Klevjer, T. A., D. J. Torres, and S. Kaartvedt, 2012. Distribution and diel vertical movements of mesopelagic scattering layers in the red sea. *Marine Biology* **159**:1833–1841.

Kloser, R. and J. Horne, 2003. Characterizing uncertainty in target-strength measurements of a deepwater fish: orange roughy (*Hoplostethus atlanticus*). *ICES Journal of Marine Science: Journal du Conseil* **60**:516–523.

Kloser, R., T. Ryan, P. Sakov, A. Williams, and J. Koslow, 2002. Species identification in deep water using multiple acoustic frequencies. *Canadian Journal of Fisheries and Aquatic Sciences* **59**:1065–1077.

Kloser, R., T. Ryan, J. Young, and M. Lewis, 2009. Acoustic observations of micronekton fish on the scale of an ocean basin: potential and challenges. *ICES Journal of Marine Science* **66**:998.

Kloser, R. J., G. J. Macaulay, T. E. Ryan, and M. Lewis, 2013. Identification and target strength of orange roughy (*Hoplostethus atlanticus*) measured in situ. *The Journal of the Acoustical Society of America* **134**:97.

Knowlton, N., 1993. Sibling species in the sea. *Annual Review of Ecology and Systematics* **24**:189–216.

Kojima, S., M. Moku, and K. Kawaguchi, 2009. Genetic diversity and population structure of three dominant myctophid fishes (*Diaphus theta*, *Stenobrachius leucopsarus*, and *S. nannochir*) in the North Pacific Ocean. *Journal of Oceanography* **65**:187–193.

Korneliussen, R. and E. Ona, 2003. Synthetic echograms generated from the relative frequency response. *ICES Journal of Marine Science* **60**:636–640.

Koslow, J., 1996. Energetic and life-history patterns of deep-sea benthic, benthopelagic and seamount-associated fish. *Journal of Fish Biology* **49**:54–74.

———, 1997. Seamounts and the ecology of deep-sea fisheries. *American Scientist* **85**:168–176.

Koslow, J., R. Kloser, and A. Williams, 1997. Pelagic biomass and community structure over the mid-continental slope off southeastern australia based upon acoustic and midwater trawl sampling. *Marine Ecology Progress Series* **146**:21–35.

Koslow, J. A., G. W. Boehlert, J. D. M. Gordon, R. L. Haedrich, P. Lorance, and N. Parin, 2000. Continental slope and deep-sea fisheries: implications for a fragile ecosystem. *ICES Journal of Marine Science* **57**:548–557.

Koslow, J. A., P. Davison, A. Lara-Lopez, and M. D. Ohman, 2013. Epipelagic and mesopelagic fishes in the southern California Current System: Ecological interactions and oceanographic influences on their abundance. *Journal of Marine Systems* URL http://www.sciencedirect.com/science/article/pii/S0924796313002017. Http://dx.doi.org/10.1016/j.jmarsys.2013.09.007.

Koslow, J. A., R. Goericke, A. Lara-Lopez, and W. Watson, 2011. Impact of declining intermediate-water oxygen on deepwater fishes in the California Current. *Marine Ecology Progress Series* **436**:207–218.

Koslow, J. A., R. Kloser, and C. Stanley, 1995. Avoidance of a camera system by a deepwater fish, the orange roughy (*Hoplostethus atlanticus*). *Deep Sea Research Part I: Oceanographic Research Papers* **42**:233–244.

Kuroki, M., J. Aoyama, M. J. Miller, S. Wouthuyzen, T. Arai, and K. Tsukamoto, 2006. Contrasting patterns of growth and migration of tropical anguillid leptocephali in the western Pacific and Indonesian Seas. *Marine Ecology Progress Series* **309**:233–246.

Laptikovsky, V., P. Boersch-Supan, K. Kemp, T. Letessier, and A. Rogers, 2014. Cephalopods of the Southwest Indian Ocean Ridge: a hotspot of extreme biological diversity and absence of endemism. Unpublished manuscript.

Lara-Lopez, A., P. Davison, and J. Koslow, 2012. Abundance and community composition of micronekton across a front off Southern California. *Journal of Plankton Research* **34**:828–848.

Lavelle, J. and C. Mohn, 2010. Motion, commotion, and biophysical connections at deep ocean seamounts. *Oceanography* **23**:90–103.

Legendre, P., 1993. Spatial autocorrelation: trouble or new paradigm? *Ecology* **74**:1659–1673.

Legg, S. and K. M. Huijts, 2006. Preliminary simulations of internal waves and mixing generated by finite amplitude tidal flow over isolated topography. *Deep Sea Research Part II: Topical Studies in Oceanography* **53**:140–156.

Lehodey, P., R. Murtugudde, and I. Senina, 2010. Bridging the gap from ocean models to population dynamics of large marine predators: a model of mid-trophic functional groups. *Progress in Oceanography* **84**:69–84.

Lehodey, P., I. Senina, and R. Murtugudde, 2008. A spatial ecosystem and populations dynamics model (seapodym)–modeling of tuna and tuna-like populations. *Progress in Oceanography* **78**:304–318.

Letessier, T., S. De Grave, P. Boersch-Supan, K. Kemp, A. Brierley, and A. Rogers, 2014. The biogeography of pelagic shrimps (Decapoda) and Gnathophausiids (Lophogastridea) on seamounts of the South-West Indian Ocean Ridge. Unpublished manuscript.

Letessier, T. B., S. Kawaguchi, R. King, J. J. Meeuwig, R. Harcourt, and M. J. Cox, 2013. A robust and economical underwater stereo video system to observe antarctic krill (euphausia superba). *Open Journal of Marine Science* **3**:148–153.

Levy-Hartmann, L., V. Roussel, Y. Letourneur, and D. Y. Sellos, 2011. Global and New Caledonian patterns of population genetic variation in the deep-sea splendid alfonsino, *Beryx splendens*, inferred from mtDNA. *Genetica* **139**:1349–1365.

Lewin-Koh, N. J. and R. Bivand, 2010. maptools: Tools for reading and handling spatial objects. URL http://CRAN.R-project.org/package=maptools. R package version 0.7-34.

Ling, J. and M. Bryden, 1992. *Mirounga leonina*. *Mammalian Species* **391**:1–8.

Litvinov, F., 2007. Fish visitors to seamounts: Aggregations of large pelagic sharks above seamounts. *In* T. Pitcher, T. Morato, P. J. B. Hart, M. R. Clark, N. Haggan, and R. S. Santos (eds.) Seamounts: Ecology, Fisheries and Conservation, pp. 282–295. Blackwell Scientific, Oxford, UK.

Lombarte, A., O. Chic, V. Parisi-Baradad, R. Olivella, J. Piera, and E. Garcia-Ladona, 2006. A web-based environment for shape analysis of fish otoliths - the AFORO database. *Scientia Marina* **70**:147–152.

Longhurst, A., 1998. Ecological Geography of the Sea. Academic Press, San Diego CA, USA.

Longhurst, A., S. Sathyendranath, T. Platt, and C. Caverhill, 1995. An estimate of global primary production in the ocean from satellite radiometer data. *Journal of Plankton Research* **17**:1245–1271.

López, J. A., M. W. Westneat, and R. Hanel, 2007. The phylogenetic affinities of the mysterious anguilliform genera *Coloconger* and *Thalassenchelys* as supported by mtDNA sequences. *Copeia* **2007**:959–966.

Lorance, P., F. Uiblein, and D. Latrouite, 2002. Habitat, behaviour and colour patterns of orange roughy *Hoplostethus atlanticus* (Pisces: Trachichthyidae) in the Bay of Biscay. *Journal of the Marine Biological Association of the UK* **82**:321–331.

Lu, C. and R. Ickeringill, 2002. Cephalopod beak identification and biomass estimation techniques: tools for dietary studies of southern Australian finfishes. No. 6 in Museum Victoria Science Reports. Museum Victoria.

Lutjeharms, J. R. E., 2006. The Agulhas current. Springer, Berlin New York.

Lyman, J., 1947. The sea's phantom bottom. *The Scientific Monthly* **66**:87–88.

MacArthur, R. and E. Wilson, 1967. The theory of island biogeography Princeton University Press. *Princeton, NJ, USA* .

MacLennan, D. N., P. G. Fernandes, and J. Dalen, 2002. A consistent approach to definitions and symbols in fisheries acoustics. *ICES Journal of Marine Science* **59**:365–369.

Madureira, L., I. Everson, and E. Murphy, 1993. Interpretation of acoustic data at two frequencies to discriminate between Antarctic krill (*Euphausia superba* Dana) and other scatterers. *Journal of Plankton Research* **15**:787–802.

Maechler, M., P. Rousseeuw, A. Struyf, M. Hubert, and K. Hornik, 2012. cluster: Cluster Analysis Basics and Extensions. R package version 1.14.3.

Mair, A., P. Fernandes, A. Lebourges-Dhaussy, and A. Brierley, 2005. An investigation into the zooplankton composition of a prominent 38-kHz scattering layer in the North Sea. *Journal of Plankton Research* **27**:623–633.

Mapstone, G. M., 2014. Global diversity and review of siphonophorae (cnidaria: Hydrozoa). *PloS one* **9**:e87737.

Marshall, N. B., 1951. Bathypelagic fishes as sound scatterers in the ocean. *Journal of Marine Research* **10**:1–17.

———, 1960. Swimbladder structure of deep-sea fishes in relation to their systematics and biology. *Discovery Reports* **31**:1–122.

Martin, A. P., R. Humphreys, and S. R. Palumbi, 1992. Population genetic-structure of the armourhead, *Pseudopentaceros wheeleri* in the North Pacific ocean – application of the polymerase chain reaction to fisheries problems. *Canadian Journal of Fisheries and Aquatic Sciences* **49**:2386–2391.

Martin, B. and B. Christiansen, 2009. Distribution of zooplankton biomass at three seamounts in the NE Atlantic. *Deep Sea Research II* **56**:2671–2682.

Masuda, H. and K. M. Muzik, 1984. The fishes of the Japanese Archipelago, vol. 2. Tokai University Press Tokyo.

Maxwell, S., J. Frank, G. Breed, P. Robinson, S. Simmons, D. Crocker, J. Gallo-Reynoso, and D. Costa, 2012. Benthic foraging on seamounts: A specialized foraging behavior in a deep-diving pinniped. *Marine Mammal Science* **28**:E333–E344. doi: 10.1111/j.1748-7692.2011.00527.x.

McClain, C., 2007. Seamounts: identity crisis or split personality? *Journal of Biogeography* **34**:2001–2008.

McClain, C. and S. Hardy, 2010. The dynamics of biogeographic ranges in the deep sea. *Proceedings of the Royal Society B: Biological Sciences* **277**:3533–3546. URL http://dx.doi.org/10.1098/rspb.2010.1057.

McClain, C., L. Lundsten, M. Ream, J. Barry, and A. DeVogelaere, 2009. Endemicity, biogeography, composition, and community structure on a Northeast Pacific Seamount. *PLoS ONE* **4**:e4141.

McClatchie, S. and R. Coombs, 2005. Low target strength fish in mixed species assemblages: the case of orange roughy. *Fisheries Research* **72**:185–192.

McClatchie, S., G. Macaulay, and R. Coombs, 2004. Acoustic backscatter and copepod secondary production across the Subtropical Front to the east of New Zealand. *Journal of Geophysical Research* **109**:C03013.

McConnell, B. J. and M. A. Fedak, 1996. Movements of southern elephant seals. *Canadian Journal of Zoology* **74**:1485–1496.

McCusker, M. R. and P. Bentzen, 2010. Positive relationships between genetic diversity and abundance in fishes. *Molecular Ecology* **19**:4852–4862.

McIntyre, T., I. Ansorge, H. Bornemann, J. Plötz, C. Tosh, and M. Bester, 2011. Elephant seal dive behaviour is influenced by ocean temperature: implications for climate change impacts on an ocean predator. *Marine Ecology Progress Series* **441**:257–272.

Meeus, J., 1998. Astronomical algorithms. Willmann-Bell, Richmond, Va.

Mélice, J., J. Lutjeharms, M. Rouault, and I. Ansorge, 2003. Sea-surface temperatures at the sub-Antarctic islands Marion and Gough during the past 50 years. *South African Journal of Science* **99**:363–366.

Menard, H. W., 1964. Marine geology of the Pacific. McGraw-Hill, New York.

Meredith, M. and A. Hogg, 2006. Circumpolar response of Southern Ocean eddy activity to a change in the southern annular mode. *Geophysical Research Letters* **33**:16608.

Meredith, M. P., J. L. Watkins, E. J. Murphy, N. J. Cunningham, A. G. Wood, R. Korb, M. J. Whitehouse, S. E. Thorpe, and F. Vivier, 2003. An anticyclonic circulation above the Northwest Georgia Rise, Southern Ocean. *Geophysical research letters* **30**:2061.

Meyer, C. and G. Paulay, 2005. DNA barcoding: error rates based on comprehensive sampling. *PLoS Biology* **3**:2229.

Meyers, G., 1979. Annual variation in the slope of the 14° C isotherm along the equator in the Pacific Ocean. *Journal of Physical Oceanography* **9**:885–891.

Michael, S. W., 1998. Reef fishes: a guide to their identification, behavior, and captive care. Microcosm.

Miller, M. J., 2009. Ecology of anguilliform leptocephali: remarkable transparent fish larvae of the ocean surface layer. *Aqua-BioScience Monographs* **2**:1–94.

Miller, M. J. and J. D. McCleave, 1994. Species assemblages of leptocephali in the subtropical convergence zone of the Sargasso Sea. *Journal of Marine Research* **52**:743–772.

Mitson, R., Y. Simard, and C. Goss, 1996. Use of a two-frequency algorithm to determine size and abundance of plankton in three widely spaced locations. *ICES Journal of Marine Science* **53**:209.

Miya, M. and M. Nishida, 1996. Molecular phylogenetic perspective on the evolution of the deep-sea fish genus *Cyclothone* (Stomiiformes: Gonostomatidae). *Ichthyological Research* **43**:375–398.

———, 1997. Speciation in the open ocean. *Nature* **389**:803–804.

———, 1998. Molecular phylogeny and evolution of the deep-sea fish genus *Sternoptyx*. *Molecular Phylogenetics and Evolution* **10**:11–22.

Mohn, C. and A. Beckmann, 2002a. Numerical studies on flow amplification at an isolated shelf-break bank, with application to Porcupine Bank. *Continental Shelf Research* **22**:1325–1338.

———, 2002b. The upper ocean circulation at Great Meteor Seamount. *Ocean Dynamics* **52**:179–193.

Mohn, C., M. White, I. Bashmachnikov, F. Jose, and J. L. Pelegri, 2009. Dynamics at an elongated, intermediate depth seamount in the North Atlantic (Sedlo Seamount, 40°20'N, 26°40'W). *Deep Sea Research Part II: Topical Studies in Oceanography* **56**:2582–2592.

Morato, T., C. Bulman, and T. Pitcher, 2009. Modelled effects of primary and secondary production enhancement by seamounts on local fish stocks. *Deep Sea Research II* **56**:2713–2719.

Morato, T., D. Varkey, C. Damaso, M. Machete, M. Santos, R. Prieto, R. Santos, and T. Pitcher, 2008. Evidence of a seamount effect on aggregating visitors. *Marine Ecology Progress Series* **357**:23–32.

Moseley, H., 1880. Deep-sea dredging and life in the deep sea. *Nature* **21**:543–547.

Moser, H. and W. Watson, 2006. Ichthyoplankton. *In* L. Allen, D. Pondella, and M. Horn (eds.) Ecology of California marine fishes, pp. 269–319. University of California Press, Berkeley, CA.

Moyer, J. and M. Zeiser, 1982. Reproductive behavior of moray eels *Gymnothorax kidako* at Miyake-jima, Japan. *Japanese Journal of Ichthyology* **28**.

Murase, H., T. Kitakado, T. Hakamada, K. Matsuoka, S. Nishiwaki, and M. Naganobu, 2013. Spatial distribution of Antarctic minke whales (*Balaenoptera bonaerensis*) in relation to spatial distributions of krill in the Ross Sea, Antarctica. *Fisheries Oceanography* **22**:154–173.

Nagpaul, P., 1999. Guide to advanced data analysis using IDAMS software. UNESCO, Paris.

Naito, Y., D. P. Costa, T. Adachi, P. W. Robinson, M. Fowler, and A. Takahashi, 2013. Unravelling the mysteries of a mesopelagic diet: a large apex predator specializes on small prey. *Functional Ecology* **27**:710–717.

Nei, M., 1987. Molecular Evolutionary Genetics. Columbia University Press, New York.

Neighbors, M. and B. Nafpaktitis, 1982. Lipid compositions, water contents, swimbladder morphologies and buoyancies of nineteen species of midwater fishes (18 myctophids and 1 neoscopelid). *Marine Biology* **66**:207–215.

Neteler, M., M. Bowman, M. Landa, and M. Metz, 2011. GRASS GIS: a multi-purpose open source GIS. *Environmental Modelling & Software* **31**:124–130.

Nikurashin, M. and R. Ferrari, 2010. Radiation and dissipation of internal waves generated by geostrophic motions impinging on small-scale topography: Application to the Southern Ocean. *Journal of Physical Oceanography* **40**:2025–2042.

———, 2013. Overturning circulation driven by breaking internal waves in the deep ocean. *Geophysical Research Letters* **40**:3133–3137.

Norris, R., 2000. Pelagic species diversity, biogeography, and evolution. *Paleobiology* **26**:236–258.

Norris, R. D. and P. M. Hull, 2012. The temporal dimension of marine speciation. *Evolutionary Ecology* **26**:393–415.

O'Driscoll, R., S. Gauthier, and J. Devine, 2009. Acoustic estimates of mesopelagic fish: as clear as day and night? *ICES Journal of Marine Science* **66**:1310–1317.

O'Driscoll, R. L., P. de Joux, R. Nelson, G. J. Macaulay, A. J. Dunford, P. M. Marriott, C. Stewart, and B. S. Miller, 2012. Species identification in seamount fish aggregations using moored underwater video. *ICES Journal of Marine Science* **69**:648–659.

O'Hara, T. D., M. Consalvey, H. P. Lavrado, and K. I. Stocks, 2010. Environmental predictors and turnover of biota along a seamount chain. *Marine Ecology* **31**:84–94.

Ohman, M., D. Rudnick, A. Chekalyuk, R. Davis, R. Feely, M. Kahru, H.-J. Kim, M. Landry, T. Martz, C. Sabine, and U. Send, 2013. Autonomous ocean measurements in the california current ecosystem. *Oceanography* **26**:18–25.

Opdal, A., O. Godø, O. Bergstad, and Ø. Fiksen, 2008. Distribution, identity, and possible processes sustaining meso-and bathypelagic scattering layers on the northern Mid-Atlantic Ridge. *Deep-Sea Research Part II* **55**:45–58.

Pakhomov, E., R. Perissinotto, and C. McQuaid, 1994. Comparative structure of the macrozooplankton / micronekton communities of the Subtropical and Antarctic Polar Fronts. *Marine Ecology Progress Series* **111**:155–169.

Pakhomov, E. A. and P. W. Froneman, 2000. Composition and spatial variability of macroplankton and micronekton within the antarctic polar frontal zone of the indian ocean during austral autumn 1997. *Polar Biology* **23**:410–419.

Palero, F., K. A. Crandall, P. Abelló, E. Macpherson, and M. Pascual, 2009. Phylogenetic relationships between spiny, slipper and coral lobsters (Crustacea, Decapoda, Achelata). *Molecular Phylogenetics and Evolution* **50**:152–162.

Palero, F., G. Guerao, and P. Abelló, 2008. Morphology of the final stage phyllosoma larva of *Scyllarus pygmaeus* (crustacea: Decapoda: Scyllaridae), identified by DNA analysis. *Journal of Plankton Research* **30**:483–488.

Palumbi, S., 1996. Nucleic acids II: the polymerase chain reaction. *Molecular Systematics* **2**:205–247.

Palumbi, S. R., 1994. Genetic divergence, reproductive isolation, and marine speciation. *Annual Review of Ecology and Systematics* **25**:547–572.

Paradis, E., 2010. pegas: an r package for population genetics with an integrated-modular approach. *Bioinformatics* **26**:419–420.

Parin, N. and V. Prut'ko, 1985. The thalassial mesobenthopelagic ichthyocoene above the Equator Seamount in the western tropical Indian Ocean. *Oceanology* **25**:781–783.

Pearre, S., 2003. Eat and run? The hunger/satiation hypothesis in vertical migration: history, evidence and consequences. *Biological Reviews* **78**:1–79.

Peeters, F. J., R. Acheson, G.-J. A. Brummer, W. P. De Ruijter, R. R. Schneider, G. M. Ganssen, E. Ufkes, and D. Kroon, 2004. Vigorous exchange between the Indian and Atlantic oceans at the end of the past five glacial periods. *Nature* **430**:661–665.

Petitgas, P., 2001. Geostatistics in fisheries survey design and stock assessment: models, variances and applications. *Fish and Fisheries* **2**:231–249.

Pfeiler, E., 1991. Glycosaminoglycan composition of anguilliform and elopiform leptocephali. *Journal of Fish Biology* **38**:533–540.

Phillips, B., J. D. Booth, J. S. Cobb, A. Jeffs, and P. McWilliam, 2006. Larval and postlarval ecology. *In* B. Phillips (ed.) Lobsters: biology, management, aquaculture and fisheries, chap. 7, pp. 1–44. Wiley-Blackwell.

Phillips, B. F. and R. Melville-Smith, 2006. Panulirus species. *In* B. Phillips (ed.) Lobsters: biology, management, aquaculture and fisheries, chap. 11, pp. 359–384. Wiley-Blackwell.

Pierrot-Bults, A. and S. van der Spoel, 2003. Macrozooplankton diversity: how much do we really know? *Zoologische Verhandelingen* **345**:297–312.

Pinheiro, J. and D. Bates, 2000. Mixed-effects models in S and S-PLUS. Springer, New York, NY u.a.

Pinheiro, J., D. Bates, S. DebRoy, D. Sarkar, and R Development Core Team, 2011. nlme: Linear and Nonlinear Mixed Effects Models. R package version 3.1-102.

Pitcher, T. and C. Bulman, 2007. Raiding the larder: a quantitative evaluation framework and trophic signature for seamount food webs. *In* T. J. Pitcher, T. Morato, P. J. B. Hart, M. R. Clark, N. Haggan, and R. S. Santos (eds.) Seamounts: Ecology, Fisheries and Conservation, *Fish and Aquatic Resources Series*, vol. 12, chap. 14, pp. 282–295. Blackwell Scientific, Oxford, UK.

Pitcher, T., M. Clark, T. Morato, and R. Watson, 2010. Seamount fisheries: Do they have a future. *Oceanography* **23**:134–144.

Pitcher, T., T. Morato, P. Hart, M. Clark, N. Haggan, and R. Santos (eds.) 2007. Seamounts: Ecology, Fisheries & Conservation. Blackwell Scientific, Oxford, UK.

Posada, D., 2008. jmodeltest: phylogenetic model averaging. *Molecular Biology and Evolution* **25**:1253–1256.

Potier, M., F. Marsac, Y. Cherel, V. Lucas, R. Sabatié, O. Maury, and F. Ménard, 2007. Forage fauna in the diet of three large pelagic fishes (lancetfish, swordfish and yellowfin tuna) in the western equatorial Indian Ocean. *Fisheries Research* **83**:60–72.

Potier, M., F. Marsac, V. Lucas, R. Sabatié, J. Hallier, and F. Ménard, 2005. Feeding partitioning among tuna taken in surface and mid-water layers: The case of yellowfin (*Thunnus albacares*) and bigeye (*T. obesus*) in the western tropical Indian Ocean. *Western Indian Ocean Journal of Marine Science* **3**:51–62.

Prairie, J. C., K. R. Sutherland, K. J. Nickols, and A. M. Kaltenberg, 2012. Biophysical interactions in the plankton: A cross-scale review. *Limnology & Oceanography: Fluids & Environments* **2**:121–145.

Priede, I. G., O. A. Bergstad, P. I. Miller, M. Vecchione, A. Gebruk, T. Falkenhaug, D. S. M. Billett, J. Craig, A. C. Dale, M. A. Shields, G. H. Tilstone, T. T. Sutton, A. J. Gooday, M. E. Inall, D. O. B. Jones, V. Martinez-Vicente, G. M. Menezes, T. Niedzielski, o. Sigurðsson, N. Rothe, A. Rogacheva, C. H. S. Alt, T. Brand, R. Abell, A. S. Brierley, N. J. Cousins, D. Crockard, A. R. Hoelzel, Å. Høines, T. B. Letessier, J. F. Read, T. Shimmield, M. J. Cox, J. K. Galbraith, J. D. M. Gordon, T. Horton, F. Neat, and P. Lorance, 2013. Does presence of a mid-ocean ridge enhance biomass and biodiversity? *PLoS ONE* **8**:e61550.

Van de Putte, A., J. Van Houdt, G. Maes, B. Hellemans, M. Collins, and F. Volckaert, 2012. High genetic diversity and connectivity in a common mesopelagic fish of the Southern Ocean: The myctophid *Electrona antarctica*. *Deep Sea Research Part II: Topical Studies in Oceanography* **59-60**:199–207.

Queró, J., J. Njock, and M. De la Hoz, 1990. Sternoptychidae. *In* Quéro, JC and Hureau, JC and Karrer, C and Post, A and Saldanha, L (ed.) Checklist of the Fishes of the Eastern Tropical Atlantic (CLOFETA), vol. 1, pp. 278–279. UNESCO, Paris.

Quero, J.-C. and L. Saldanha, 1995. Poissons anguilliformes de l'île de la Réunion (Océan Indien): description d'une nouvelle espèce. *Cybium* **19**:61–88.

R Development Core Team, 2010. R: A Language and Environment for Statistical Computing. R Foundation for Statistical Computing, Vienna, Austria. URL http://www.R-project.org.

Radulovici, A., B. Sainte-Marie, and F. Dufresne, 2009. DNA barcoding of marine crustaceans from the estuary and Gulf of St Lawrence: a regional-scale approach. *Molecular Ecology Resources* **9**:181–187.

Ratnasingham, S. and P. D. N. Hebert, 2007. BOLD : The Barcode of Life Data System (www.barcodinglife.org). *Molecular Ecology Notes* **7**:355–364.

Read, J. F., M. I. Lucas, S. E. Holley, and R. T. Pollard, 2000. Phytoplankton, nutrients and hydrography in the frontal zone between the Southwest Indian Subtropical gyre and the Southern Ocean. *Deep Sea Research Part I: Oceanographic Research Papers* **47**:2341–2367.

Read, J. F. and R. T. Pollard, 2013a. Circulation stratification and seamounts in the Southwest Indian Ocean. Unpublished manuscript.

———, 2013b. An introduction to the physical oceanography of six seamounts in the Southwest Indian Ocean. Unpublished manuscript.

Reid, S., J. Hirota, R. Young, and L. Hallacher, 1991. Mesopelagic-boundary community in Hawaii: micronekton at the interface between neritic and oceanic ecosystems. *Marine Biology* **109**:427–440.

Richardson, P., 1980. Anticyclonic eddies generated near the Corner Rise seamounts. *Journal of Marine Research* **38**:673–686.

Rivoirard, J., J. Simmonds, K. Foote, P. Fernandes, and N. Bez, 2000. Geostatistics for estimating fish abundance. Wiley-Blackwell, Oxford, UK.

Robertson, P. B., 1979. Biological results of the University of Miami deep-sea expeditions. 131. Larval development of the scyllarid lobster *Scyllarus planorbis* Holthuis reared in the laboratory. *Bulletin of Marine Science* **29**:320–328.

Robinson, C., D. K. Steinberg, T. R. Anderson, J. Arístegui, C. A. Carlson, J. R. Frost, J.-F. Ghiglione, S. Hernández-León, G. A. Jackson, R. Koppelmann, et al., 2010. Mesopelagic zone ecology and biogeochemistry–a synthesis. *Deep Sea Research Part II: Topical Studies in Oceanography* **57**:1504–1518.

Robison, B. H., 2004. Deep pelagic biology. *Journal of Experimental Marine Biology and Ecology* **300**:253–272.

Roden, G., 1987. Effect of seamounts and seamount chains on ocean circulation and thermohaline structure. *In* B. Keating, P. B. R. Fryer, and G. Boehlert (eds.) Seamounts, Islands and Atolls, *Geophysical Monograph*, vol. 43, pp. 335–354. American Geophysical Union, Washington, USA.

Rogers, A., 1994. The biology of seamounts. *Advances in Marine Biology* **30**:305–350.

Rogers, A., O. Alvheim, E. Bemanaja, D. Benivary, P. Boersch-Supan, T. Bornman, R. Cedras, N. D. Plessis, S. Gotheil, Å. Høines, K. Kemp, J. Kristiansen, T. Letessier, V. Mangar, N. Mazungula, T. Mørk, P. Pinet, J. Read, and T. Sonnekus, 2009. Preliminary Cruise Report "Dr. Fridtjof Nansen" Southern Indian Ocean Seamounts (IUCN/UNDP/ASCLME/NERC/EAF Nansen Project 2009 Cruise 410) 12th November–19th December. International Union for Conservation of Nature, Gland, CH.

Rogers, A., S. Morley, E. Fitzcharles, K. Jarvis, and M. Belchier, 2006. Genetic structure of patagonian toothfish (*Dissostichus eleginoides*) populations on the Patagonian Shelf and Atlantic and western Indian Ocean sectors of the Southern Ocean. *Marine Biology* **149**:915–924.

Rogers, A. and M. Taylor (eds.) 2012. Benthic biodiversity of seamounts in the southwest Indian Ocean Cruise report – R/V James Cook 066 – Southwest Indian Ocean Seamounts expedition – November 7th – December 21st, 2011. University of Oxford / NERC.

Rogers, A. D., 2000. The role of the oceanic oxygen minima in generating biodiversity in the deep sea. *Deep Sea Research II* **47**:119–148.

———, 2012. Evolution and biodiversity of Antarctic organisms. *In* A. Rogers, N. Johnston, E. Murphy, and A. Clarke (eds.) Antarctic Ecosystems: An Extreme Environment in a Changing World, pp. 417–467. Wiley Publishers, Oxford, UK.

Rogers, A. R. and H. Harpending, 1992. Population-growth makes waves in the distribution of pairwise genetic-differences. *Molecular Biology and Evolution* **9**:552–569.

Romanov, E., 2003. Summary and review of Soviet and Ukrainian scientific and commercial fishing operations on the deepwater ridges of the southern Indian Ocean. *FAO Fisheries Circular* **991**.

Rousseeuw, P. J., 1987. Silhouettes: a graphical aid to the interpretation and validation of cluster analysis. *Journal of Computational and Applied Mathematics* **20**:53–65.

Rowden, A., J. Dower, T. Schlacher, M. Consalvey, and M. Clark, 2010a. Paradigms in seamount ecology: fact, fiction and future. *Marine Ecology* **31**:226–241.

Rowden, A. A., T. A. Schlacher, A. Williams, M. R. Clark, R. Stewart, F. Althaus, D. A. Bowden, M. Consalvey, W. Robinson, and J. Dowdney, 2010b. A test of the seamount oasis hypothesis: seamounts support higher epibenthic megafaunal biomass than adjacent slopes. *Marine Ecology* **31**:95–106.

———, 2010c. A test of the seamount oasis hypothesis: seamounts support higher epibenthic megafaunal biomass than adjacent slopes. *Marine Ecology* **31**:95–106.

Ryan, T., 2011. Overview of data collection, management and processing procedures of underway acoustic data - IMOS BASOOP sub-facility. CSIRO, Division of Marine and Atmospheric Research - Hobart, Australia. Version 1.0.

Ryan, T. and R. Kloser, 2004. Improving the precision of ES60 and EK60 echosounder applications. Tech. Rep. CM 2004/B:06, ICES Working Group on Fisheries Acoustic Science and Technology.

Samadi, S., L. Bottan, E. Macpherson, B. De Forges, and M. Boisselier, 2006. Seamount endemism questioned by the geographic distribution and population genetic structure of marine invertebrates. *Marine Biology* **149**:1463–1475.

Santana, W., A. P. Pinheiro, and J. E. L. Oliveira, 2007. Additional records of three *Scyllarides* species (Palinura: Scyllaridae) from Brazil, with the description of the fourth larval stage of *Scyllarides aequinoctialis*. *Nauplius* **15**:1–6.

Sarkar, D., 2010. lattice: Lattice Graphics. URL http://CRAN.R-project.org/package=lattice. R package version 0.18-3.

Sawada, H., H. Saito, M. Hosoi, and H. Toyohara, 2008. Evaluation of PCR methods for fixed bivalve larvae. *Journal of the Marine Biological Association of the UK* **88**:1441–1449.

Schlacher, T. A., A. A. Rowden, J. F. Dower, and M. Consalvey, 2010. Seamount science scales undersea mountains: new research and outlook. *Marine Ecology* **31**:1–13.

Schott, F. A., S.-P. Xie, and J. P. McCreary, 2009. Indian Ocean circulation and climate variability. *Reviews of Geophysics* **47**:RG1002.

Sclater, J., N. Grindlay, J. Madsen, and C. Rommevaux-Jestin, 2005. Tectonic interpretation of the Andrew Bain transform fault: Southwest Indian Ocean. *Geochemistry, Geophysics, Geosystems* **6**:1–21.

Sedberry, G. R., J. L. Carlin, R. W. Chapman, and B. Eleby, 1996. Population structure in the pan-oceanic wreckfish *Polyprion americanus* (Teleostei: Polyprionidae), as indicated by mtDNA variation. *Journal of Fish Biology* **49**:318–329.

Seki, M. P. and D. A. Somerton, 1994. Feeding ecology and daily ration of the pelagic armorhead, *Pseudopentaceros wheeleri*, at Southeast Hancock Seamount. *Environmental Biology of Fishes* **39**:73–84.

Shank, T., 2010. Seamounts: deep-ocean laboratories of faunal connectivity, evolution, and endemism. *Oceanography* **23**:109–122.

Shaw, P., A. Arkhipkin, and H. Al-Khairulla, 2004. Genetic structuring of Patagonian toothfish populations in the Southwest Atlantic Ocean: the effect of the Antarctic Polar Front and deep-water troughs as barriers to genetic exchange. *Molecular Ecology* **13**:3293–3303.

Sheppard, C., M. Ateweberhan, B. Bowen, P. Carr, C. Chen, C. Clubbe, M. Craig, R. Ebinghaus, J. Eble, N. Fitzsimmons, et al., 2012. Reefs and islands of the Chagos Archipelago, Indian Ocean: why it is the world's largest no-take marine protected area. *Aquatic Conservation: Marine and Freshwater Ecosystems* **22**:232–261. DOI: 10.1002/aqc.1248.

Shotton, R., 2006. Management of demersal fisheries resources of the Southern Indian Ocean. *FAO Fisheries Circular* **1020**.

Sibert, J., I. Senina, P. Lehodey, and J. Hampton, 2012. Shifting from marine reserves to maritime zoning for conservation of Pacific bigeye tuna (*Thunnus obesus*). *Proceedings of the National Academy of Sciences* **109**:18221–18225.

Simmonds, E. and D. MacLennan, 2005. Fisheries acoustics: theory and practice. 2nd ed. Blackwell Scientific, Oxford, UK.

Simmons, S., D. Crocker, J. Hassrick, C. Kuhn, P. Robinson, Y. Tremblay, and D. Costa, 2010. Climate-scale hydrographic features related to foraging success in a capital breeder, the northern elephant seal *Mirounga angustirostris*. *Endangered Species Research* **10**:233–243.

Sloss, P. W., 2005. ETOPO5 Global Surface Relief. NOAA National Geophysical Data Center. URL http://www.ngdc.noaa.gov/mgg/global/relief/ETOPO5/.

Smale, M. J., G. Watson, and T. Hecht, 1995. Otolith atlas of southern African marine fishes. No. 1 in Ichthyological Monographs. JLB Smith Institute of Ichthyology, Grahamstown, South Africa.

Smith, M. and P. Castle, 1986. Serrivomeridae. *In* Smith's Sea Fishes. Springer, Berlin.

Smith, P. and P. Benson, 1997. Genetic diversity in orange roughy from the east of New Zealand. *Fisheries Research* **31**:197–213.

Smith, V. S., 2005. DNA barcoding: Perspectives from a "partnerships for enhancing expertise in taxonomy" (PEET) debate. *Systematic Biology* **54**:841–844.

Smouse, P. E., J. C. Long, and R. R. Sokal, 1986. Multiple regression and correlation extensions of the mantel test of matrix correspondence. *Systematic zoology* **35**:627–632.

Spanier, E. and K. L. Lavalli, 2006. Scyllarides species. *In* Lobsters: biology, management, aquaculture and fisheries, pp. 462–496. Blackwell Publishing, Oxford.

Srivathsan, A. and R. Meier, 2012. On the inappropriate use of Kimura-2-parameter (K2P) divergences in the DNA-barcoding literature. *Cladistics* **28**:190–194.

Staby, A., A. Røstad, and S. Kaartvedt, 2011. Long-term acoustical observations of the mesopelagic fish *Maurolicus muelleri* reveal novel and varied vertical migration patterns. *Marine Ecology Progress Series* **441**:241–255.

Stanton, T., 2009. Broadband acoustic sensing of the ocean. *Journal of the Marine Acoustics Society of Japan* **36**:95–107.

Stanton, T. K., D. Chu, and P. H. Wiebe, 1996. Acoustic scattering characteristics of several zooplankton groups. *ICES Journal of Marine Science* **53**:289–295.

Staudigel, H., A. A. Koppers, J. W. Lavelle, T. J. Pitcher, and T. M. Shank, 2010. Defining the word "seamount". *Oceanography* **23**:20–21.

Steele, J., 1978. Some Comments on Plankton Patches. *In* J. Steele (ed.) Spatial pattern in plankton communities, *NATO Conference Series in Marine Sciences*, vol. 3, pp. 1–20. Plenum Press, New York, NY.

Stefansson, M. O., T. Sigurdsson, C. Pampoulie, A. K. Danielsdottir, B. Thorgilsson, A. Ragnarsdottir, D. Gislason, J. Coughlan, T. F. Cross, and L. Bernatchez, 2009. Pleistocene genetic legacy suggests incipient species of *Sebastes mentella* in the Irminger Sea. *Heredity* **102**:514–524.

Steinberg, D. K., B. A. V. Mooy, K. O. Buesseler, P. W. Boyd, T. Kobari, and D. M. Karl, 2008. Bacterial vs. zooplankton control of sinking particle flux in the ocean's twilight zone. *Limnology and Oceanography* **53**:1327.

Steyn, E., P. Fielding, and M. Schleyer, 2008. The artisanal fishery for East Coast rock lobsters *Panulirus homarus* along the Wild Coast, South Africa. *African Journal of Marine Science* **30**:497–506.

Stocks, K. I., M. R. Clark, A. A. Rowden, M. Consalvey, and T. A. Schlacher, 2012. CenSeam, an international program on seamounts within the Census of Marine Life: Achievements and lessons learned. *PloS ONE* **7**:e32031.

Tajima, F., 1983. Evolutionary relationship of DNA sequences infinite populations. *Genetics* **105**.

Talley, L. D., G. L. Pickard, W. J. Emery, and J. H. Swift, 2011. Descriptive physical oceanography: an introduction. 6th ed. Academic Press, Amsterdam.

Taylor, J. and E. Ebert, 2012. Mapping coral reef fish schools and aggregations with high-frequency multibeam and split-beam sonars. *In* Proceedings of Meetings on Acoustics, vol. 17, p. 070041. Acoustical Society of America.

Thornhill, D., A. Mahon, J. Norenberg, and K. Halanych, 2008. Open-ocean barriers to dispersal: a test case with the Antarctic Polar Front and the ribbon worm *Parborlasia corrugatus* (Nemertea: Lineidae). *Molecular Ecology* **17**:5104–5117.

Thrush, S. F. and P. K. Dayton, 2010. What can ecology contribute to ecosystem-based management? *Annual Review of Marine Science* **2**:419–441.

Tomczak, M. and J. Godfrey, 1994. Regional Oceanography: an Introduction. Pergamon, New York.

Tont, S., 1976. Deep scattering layers: patterns in the Pacific. *CalCOFI Reports* **18**:112–117.

Tsang, L., K. Ma, S. Ahyong, T.-Y. Chan, and K. Chu, 2008. Phylogeny of Decapoda using two nuclear protein-coding genes: origin and evolution of the Reptantia. *Molecular Phylogenetics and Evolution* **48**:359–368.

Tseytlin, V., 1985. The energetics of fish populations inhabiting seamounts. *Oceanology* **25**:237–239.

Tsukamoto, K., 2006. Spawning of eels near a seamount. *Nature* **439**:929.

Tsukamoto, K., A. Umezawa, and T. Ozawa, 1992. Age and growth of *Anguilla japonica* leptocephali collected in western North Pacific in July 1990. *Bulletin of the Japanese Society of Scientific Fisheries* **58**.

Tucker, G., 1951. Relation of fishes and other organisms to the scattering of underwater sound. *Journal of Marine Research* **10**:215–238.

Uchida, R. N. and D. T. Tagami, 1984. Groundfish fisheries and research in the vicinity of seamounts in the North Pacific Ocean. *U.S. National Marine Fisheries Service Marine Fisheries Review* **46**:1–17.

Uda, M. and M. Ishino, 1958. Enrichment pattern resulting from eddy systems in relation to fishing grounds. *Journal of the Tokyo University of Fisheries* **1-2**:105–119.

Urmy, S., J. Horne, and D. Barbee, 2012. Measuring the vertical distributional variability of pelagic fauna in Monterey Bay. *ICES Journal of Marine Science* **69**:184–196.

Valdemarsen, J. and O. Misund, 1995. Trawl design and techniques used by norwegian research vessels to sample fish in the pelagic zone. *In* A. Hylen (ed.) Precision and relevance of pre-recruit studies for fishery management related to fish stocks in the Barents Sea and adjacent waters. Proceedings of the sixth IMR-PINRO symposium, Bergen, pp. 14–17. Institute of Marine Research, Bergen, Norway.

Valle-Levinson, A., A. Trasviña Castro, G. Gutiérrez de Velasco, and R. González Armas, 2004. Diurnal vertical motions over a seamount of the southern Gulf of California. *Journal of Marine Systems* **50**:61–77.

Vamosi, S. M., 2003. The presence of other fish species affects speciation in three spine sticklebacks. *Evolutionary Ecology Research* **5**:717–730.

Vastano, A. and B. Warren, 1976. Perturbations to the Gulf Stream by Atlantis II Seamount. *Deep-Sea Research* **23**:681–694.

Vereshchaka, A. L., 1995. Macroplankton in the near-bottom layer of continental slopes and seamounts. *Deep Sea Research Part I: Oceanographic Research Papers* **42**:1639–1668.

Vierros, M., I. Cresswell, E. E. Briones, J. Rice, and J. Ardron (eds.) 2009. Global Open Oceans and Deep Seabed (GOODS) - Biogeographic Classification, *IOC Technical Series*, vol. 84. UNESCO-IOC, Paris, France.

Vogler, A. and M. Monaghan, 2007. Recent advances in DNA taxonomy. *Journal of Zoological Systematics and Evolutionary Research* **45**:1–10.

Von der Heyden, S., J. Groeneveld, and C. Matthee, 2007. Long current to nowhere? Genetic connectivity of Jasus tristani populations in the southern Atlantic Ocean. *African Journal of Marine Science* **29**:491–497.

Voss, N. A., K. N. Nesis, and P. G. Rodhouse, 1998. The cephalopod family Histioteuthidae (Oegopsida): systematics, biology, and biogeography. *Smithsonian Contributions to Zoology* **586**:193–372.

Ward, R. D., N. G. Elliott, P. M. Grewe, P. R. Last, P. S. Lowry, B. H. Innes, and G. K. Yearsley, 1998. Allozyme and mitochondrial DNA variation in three species of oreos (Teleostei : Oreosomatidae) from Australasian waters. *New Zealand Journal of Marine and Freshwater Research* **32**:233–245.

Ward, R. D., R. Hanner, and P. D. N. Hebert, 2009. The campaign to DNA barcode all fishes, FISH-BOL. *Journal of Fish Biology* **74**:329–356.

Warren, J. D., T. K. Stanton, P. H. Wiebe, and H. E. Seim, 2003. Inference of biological and physical parameters in an internal wave using multiple-frequency, acoustic-scattering data. *ICES Journal of Marine Science: Journal du Conseil* **60**:1033–1046.

Watson, R., A. Kitchingman, and W. Cheung, 2007. Catches from world seamount fisheries. *In* T. J. Pitcher, T. Morato, P. J. B. Hart, M. R. Clark, N. Haggan, and R. S.Santos (eds.) Seamounts: Ecology, Fisheries and Conservation, vol. 12, pp. 400–412. Blackwell Scientific.

Weir, B. S. and C. C. Cockerham, 1984. Estimating f-statistics for the analysis of population-structure. *Evolution* **38**:1358–1370.

Wheeler, Q., 2005. Losing the plot: DNA "barcodes" and taxonomy. *Cladistics* **21**:405–407.

White, M., I. A. J. Bashmachnikov, and A. Martins, 2007. Physical processes and seamount productivity. *In* T. J. Pitcher, T. Morato, P. J. B. Hart, M. R. Clark, N. Haggan, and R. S.Santos (eds.) Seamounts: Ecology, Fisheries and Conservation, *Fish and Aquatic Resources Series*, vol. 12, chap. 4, pp. 65–84. Blackwell Scientific, Oxford, UK.

White, T. A., S. Stefanni, J. Stamford, and A. R. Hoelzel, 2009. Unexpected panmixia in a long-lived, deep-sea fish with well-defined spawning habitat and relatively low fecundity. *Molecular Ecology* **18**:2563–2573.

Williamson, D., 1982. Larval morphology and diversity. *In* L. Abele (ed.) The biology of Crustacea, pp. 43–110. Academic Press, New York.

Wilson, C., 1992. Interactions of ocean currents and diel migrators at a seamount in the central north Pacific Ocean. Ph.D. thesis, University of Hawaii, USA.

Wilson, C. and G. Boehlert, 2004. Interaction of ocean currents and resident micronekton at a seamount in the central North Pacific. *Journal of Marine Systems* **50**:39–60.

Wood, S., 2006. Generalized Additive Models: An Introduction with R. Chapman & Hall, London, UK.

Xavier, J. C. and Y. Cherel, 2009. Cephalopod Beak Guide For The Southern Ocean. British Antarctic Survey, Cambridge, UK. 129pp.

Yasuma, H., K. Sawada, T. Ohshima, K. Miyashita, and I. Aoki, 2003. Target strength of mesopelagic lanternfishes (family Myctophidae) based on swimbladder morphology. *ICES Journal of Marine Science* **60**:584–591.

Yasuma, H., K. Sawada, Y. Takao, K. Miyashita, and I. Aoki, 2010. Swimbladder condition and target strength of myctophid fish in the temperate zone of the Northwest Pacific. *ICES Journal of Marine Science* **67**:135–144.

Ye, Y., 2011. Western Indian Ocean. *In* FAO (ed.) Review of the state of world marine fishery resources, no. 569 in FAO Fisheries and Aquaculture Technical Paper, pp. 121–132. Food and Agriculture Organization of the United Nations, Rome.

Yesson, C., M. R. Clark, M. L. Taylor, and A. D. Rogers, 2011. The global distribution of seamounts based on 30-second bathymetry data. *Deep Sea Research I* **58**:442–453.

Zavala Sanson, L. and A. Provenzale, 2009. The effects of abrupt topography on plankton dynamics. *Theoretical Population Biology* **76**:258–267.

Zeitschel, B. (ed.) 1973. The biology of the Indian Ocean. Springer-Verlag, Berlin, Germany.

Zender, C. S., 2008. Analysis of self-describing gridded geoscience data with netCDF Operators (NCO). *Environmental Modelling & Software* **23**:1338–1342.

Ziegler, T. A., J. H. Cohen, and R. B. Forward, 2010. Proximate control of diel vertical migration in phyllosoma larvae of the Caribbean spiny lobster *Panulirus argus*. *The Biological Bulletin* **219**:207–219.

Zwolinski, J., P. G. Fernandes, V. Marques, and Y. Stratoudakis, 2009. Estimating fish abundance from acoustic surveys: calculating variance due to acoustic backscatter and length distribution error. *Canadian Journal of Fisheries and Aquatic Sciences* **66**:2081–2095.

Appendix A

Disclaimer of collaborative contributions

Some elements of this thesis arose from collaborative efforts with scientists from various institutions as well as students under my supervision at the University of Oxford. The disclaimers of contributions are given below:

Chapter 2 The study was conceived by Andrew Brierley, Alex Rogers and me. Acoustic data were either collected and processed by me, or obtained as processed grids from the IMOS repository. *In situ* oceanographic data were collected as part of cruises *Nansen* 2009-410 and JC066/67 by shipboard technicians and processed by me. All analyses were conducted by me. The manuscript was written by me with inputs from A. Brierley and A. Rogers.

Chapter 3 The work presented in this chapter has been published as:

Boersch-Supan, P., L. Boehme, J. Read, A. Rogers, and A. Brierley, 2012. Elephant seal foraging dives track prey distributions, not temperature: Comment on McIntyre et al. (2011). *Marine Ecology Progress Series* **461**:293–298.

The comment was initiated by Andrew Brierley and Lars Boehme (Sea Mammal Research Unit, University of St Andrews). Acoustic data were collected and processed by me, oceanographic data were collected and processed by Jane Read (National Oceanography Centre, Southampton). Figures were created by me. The manuscript was written by me with inputs from all authors.

Chapter 4 The work presented in this chapter is currently being prepared for publication as

Boersch-Supan, P., M.J. Cox, A.S. Brierley, and T.B. Letessier. Scattering layers around atolls and a seamount in the Chagos archipelago.

The study was conceived by me with inputs from Martin Cox (Australian Antarctic Division), Tom Letessier (University of Western Australia) and Andrew Brierley. Data were collected by me and M. Cox. M. Cox processed echosounder calibrations and developed code for the prediction interval estimation of the non-linear models. Acoustic data were processed and analysed by me. Figures were prepared by me. The manuscript was written by me with inputs from all authors.

Chapter 5 The research presented in this chapter was undertaken in collaboration with Jennifer Freer, who was a master's student under my day-to-day supervision. The study was conceived by Andrew Brierley, Alex Rogers and me. All acoustic data were collected, processed and analysed by me. Specimens were collected and sampled by me with the assistance of the *Nansen* 2009-410 scientific party. Stomachs were sampled by me and sorted and analysed by J. Freer, me and undergraduate students. Prey data analyses were carried out by J. Freer and myself. Processed ADCP data were provided by Jane Read. The manuscript was written by me with inputs from J. Freer, A. Rogers and A. Brierley.

Chapter 6 The research presented in this chapter was undertaken in collaboration with Jennifer Freer, who was a master's student under my day-to-day supervision. The study was conceived by Alex Rogers. Specimens were collected and sampled by me with the assistance of the *Nansen* 2009-410 scientific party. Lab work was carried out largely by J. Freer under my supervision. Data analyses were carried out by J. Freer and me. The manuscript was written by me and J. Freer with inputs from A. Rogers.

Chapter 7 The research presented in this chapter was undertaken in collaboration with Celia Bell, who was a master's student under my day-to-day supervision. The study was conceived by Alex D. Rogers and me. Specimens were collected and sampled by me with the assistance of the *Nansen* 2009-410 scientific party. Lab work was carried out by C. Bell and me. Data analyses were carried out by C. Bell and me. The manuscript was written by me and C. Bell with inputs from A. Rogers.

Appendix B

Echosounder calibration parameters

B.1 Calibration parameters

Table B.1: Transducer parameters and specifications for the EK60 echosounders employed in this thesis. All calibrations were conducted following the recommendations of Foote et al. (1987).

	RV Dr. F. Nansen		*RRS James Cook*		*FPV Pacific Marlin*[†]
	18kHz	38kHz	18kHz	38kHz	38kHz
Transducer model	ES18-11	ES38-B	ES18-11	ES38-B	ES38-12
Serial number	593	489	2067	30637	
Absorption coefficient (dB/km)	2.2	8.5	2.2	8.5	5.6
Transmitted power (W)	1000	2000	2000	2000	2000
Two-way beam angle (dB re 1 sr)	-17	-20.6	-17.3	-21.0	-15.8
Transducer gain (dB)	20.76	25.82	23.22	23.87	20.96
S_A correction (dB)	-0.62	-0.53	-1.19	-0.6	-0.27
Transmitted pulse length (μs)	1024	1024	1024	1024	1024
Alongship angle (degrees)	0.08	0.11	-0.07	-0.3	0.05
Athwartship angle (degrees)	0.02	0.05	0.06	-0.6	0.12
Minor-axis 3dB beam angle (degrees)	11.06	7.05	11.21	7.06	14.71
Major-axis 3dB beam angle (degrees)	10.98	7.06	11.26	7.22	14.17
Calibration date	14/06/2009		07/11/2011		21/11/2012
Location	Baia dos Elefantes 13°13'S 12°44'E		Cape Town 33°54'S 18°15'E		Sandes Seamount 7°09'S 72°08'E

[†] Echosounder was deployed from a fast rescue craft, not the patrol vessel itself.

B.2 Acoustic data processing workflow

Processing of acoustic data followed the IMOS processing framework (Ryan, 2011) which consisted of four sequential filters: i) simple intermittent spike, ii) attenuated signal, iii) persistent intermittent noise and iv) background noise. Ryan (2011) defines two types of noise: *Background noise* is considered to be at a consistent value for many pings. *Intermittent noise* consists of signal from unwanted sources that is only present for a portion of a ping. Intermittent noise may only exist for a moment (i.e. at a certain range) within one ping, but may persist across multiple pings at a similar range.

B.2.1 Simple intermittent noise spike filter

A typical intermittent noise 'spike' is interference from another echosounder, adding unwanted signal momentarily at a range and persisting only for a single ping. The filter is based on a method described by Anderson et al. (2005) it operates as follows:

1. Data are resampled into cells of 20 m height and 1 ping width by taking the median of the original data to reduce within ping vertical variability.
2. The resampled data are time shifted by ± 1 pings.
3. The original data are compared pixel by pixel with the time-shifted echograms and original pixels (are rejected if the original pixel is greater than the preceeding and subsequent pixels by 10 dB and is greater than -80 dB. The -80 dB minimum threshold is set to avoid rejecting samples from low signal regions which often are very variable.

B.2.2 Attenuated signal filter

This filter is used to identify and eliminate pings whose signal has been attenuated by an amount exceeding a user defined threshold. In bad weather vessel-wave interactions can cause bubble entrainment on the transducer face which may severly attenuate the acoustic signal. In such situations the acoustic signal will be attenuated by the same amount throughout the duration of a ping. Attenuation can persist for several pings until the water beneath the vessel becomes bubble-free.

The filter assumes that there are reasonable levels of localised homogeneity in the deep scattering layer (DSL). Pings whose signal is less than the median localised value of the DSL by a user define amount are identified as being attenuated. It operates as follows:

1. Data within the DSL region are resampled in two ways:
    a) Each ping, the data in the defined DSL region are resampled at a width of 1 ping and a single value of the 25th percentile of the DSL data for each ping.
    b) The DSL is resampled to give a single median value within a resampling window of 30-300 pings. Window size is adjusted following inspection the echograms and reviewing the effectiveness of the attenuation filter.
2. A comparison is made between the per-ping lower 25th percentile value within the DSL region and the median value over the resampled window. If the per-ping value is less than the localised median value by 8 dB, then the data is considered to be attenuated and the entire ping is excluded.

B.2.3 Persistent intermittent noise

This filter eliminates elevated signal that persists over multiple pings and is therefore not captured by the simple intermittent noise spike filter. This filter works in a similar, but not identical, way to the attenuated signal filter:

1. Input data are converted using a $40 \log r$ range compensation. This has the effect of overemphasising the signal as a function of range, thereby highlighting the spike noise at deeper depths where they tend to be more problematic.
2. Range compensated data are resampled to give the lower percentile (nominal value 15th percentile) for cells of 50 pings wide and height of 10 metres over the entire echogram range. These samples will give a measure that can be used as a benchmark to compare ping-by-ping deviations from the localised resampled values.
3. The lower percentile resampled values are subtracted from the range compensated data. Intermittent noise data will deviate from the lower percentile resampled values by a greater amount than clean data.
4. Original data samples that deviate from the lower percentile resampled data by more than 15 dB are excluded, unless they are from low signal regions (<-70 dB)

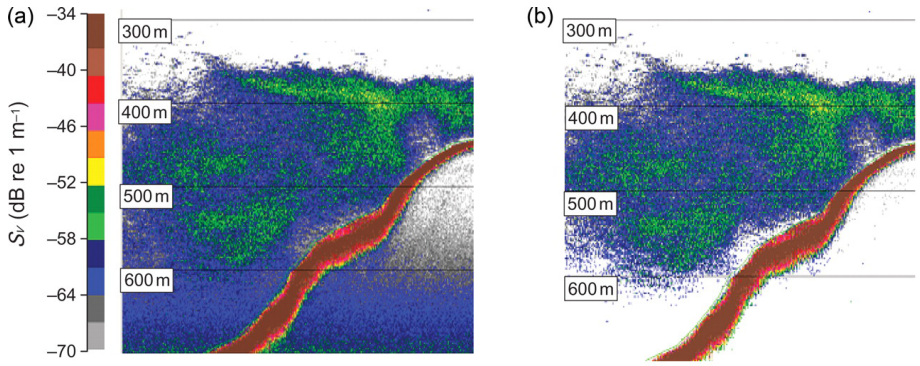

Figure B.1: An example of noise reduction and signal-to-noise thresholding applied to a 2 nautical mile 120 kHz echogram. An fish aggregation is evident between depths of 350 and 650 m. (a) Original echogram. (b) Noise-reduced echogram. Adapted from De Robertis and Higginbottom (2007).

The filter is only applied to data below 300 m to avoid the rejection of small high signal regions such as fish schools which are typically observed in the upper water column, and where noise spikes are generally less of a problem.

B.2.4 Background noise

The final stage in the workflow is the removal of background noise using the method of De Robertis and Higginbottom (2007). This method assumes the presence of a noise-dominated region in the data. In practice this assumption is met at the ranges between 1500 m and 2000 m of the echogram, where spreading losses have reduced the return signal to insignificant levels compared to the constant background noise. The method estimates noise at these long ranges and subtracts it from the data, thereby yielding noise-corrected data as well as an estimate of the signal-to-noise ratio (SNR). Pixels with a SNR below 6 dB are then excluded to yield the final echogram.

Appendix C

Backscatter GAMM models

The diagnostics plots for the selected models indicate that none of the model assumptions have been violated. The response variable is linear on the predictor scale. There is no apparent relationship between fitted values and residuals. The model fit residuals are normally distributed and model predictions show an adequate relationship between response and fitted values.

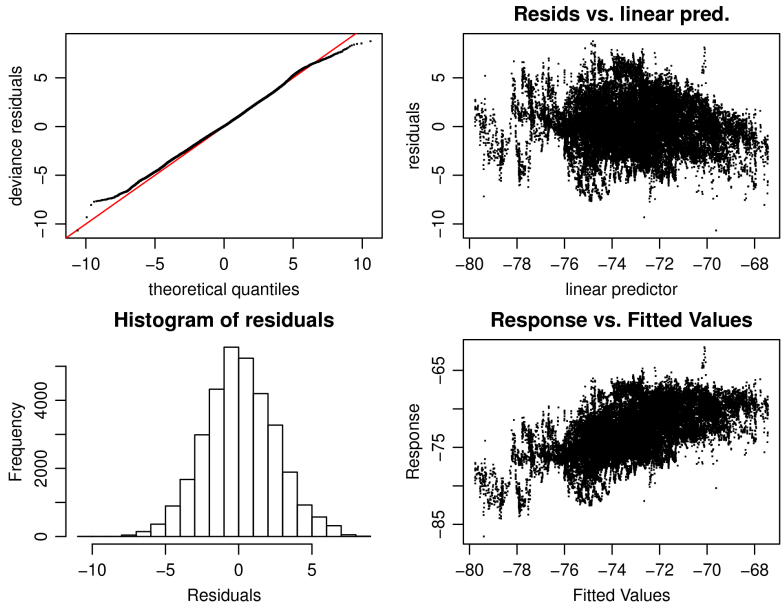

Figure C.1: Diagnostic plots for the $S_V^{\mathbf{DSL}38}$ generalized additive mixed model.

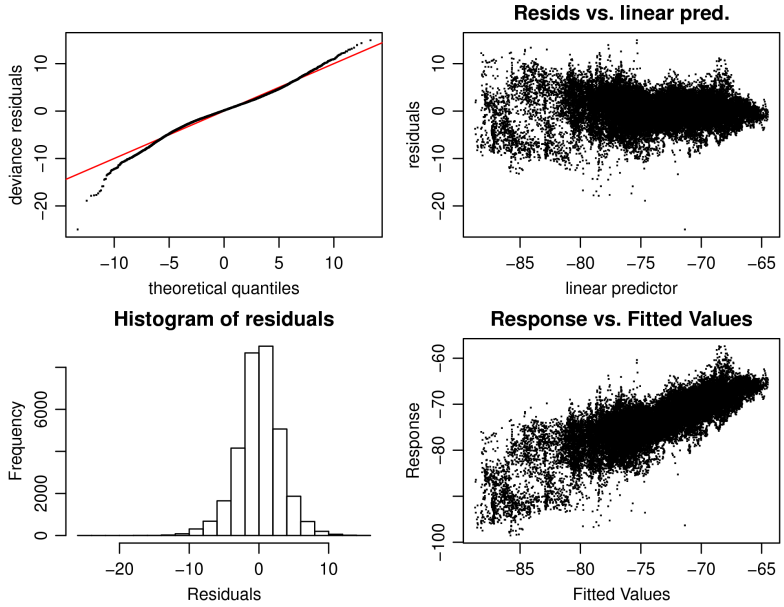

Figure C.2: Diagnostic plots for the $S_V^{\mathbf{SSL}38}$ generalized additive mixed model.

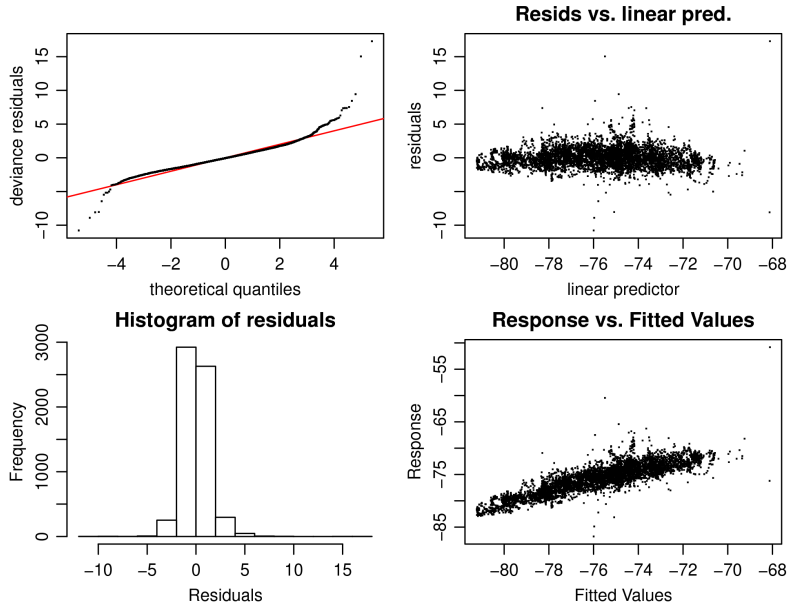

Figure C.3: Diagnostic plots for the $S_V^{\mathbf{DSL}18}$ generalized additive mixed model.

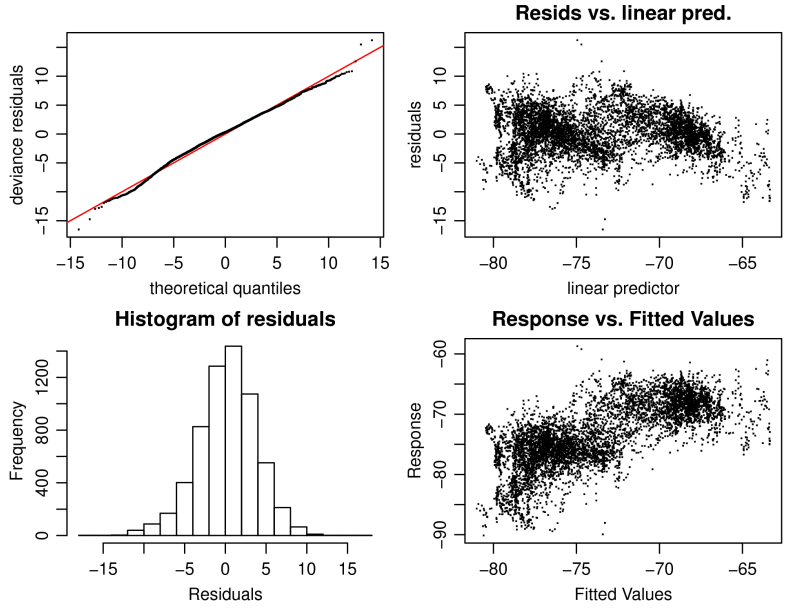

Figure C.4: Diagnostic plots for the $S_V^{\mathbf{SSL}18}$ generalized additive mixed model.

Appendix D

BIOT surface currents

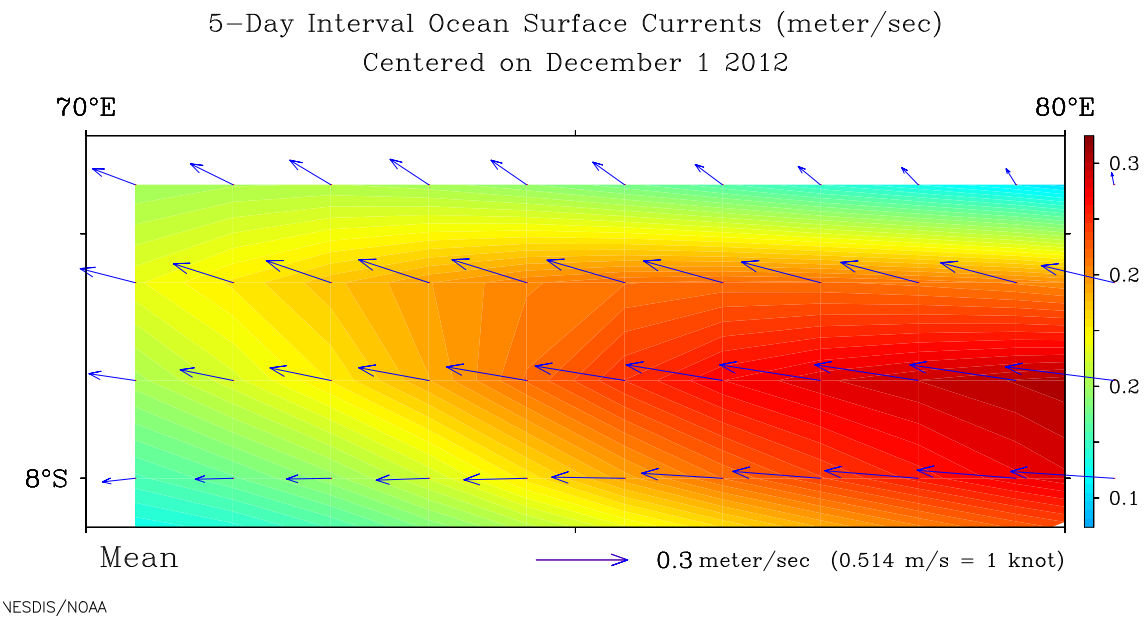

Figure D.1: Surface currents in the study area during the Chagos expedition. Source: http://www.oscar.noaa.gov/.

Appendix E

Raw prey count data

Table E.1: Stomach content data. m_F, mass of full stomach; F, fullness index [0;1]; m_C, mass of contents; D, digestive state index [1;5]; P_{Sc}, presence/absence of fish scales; P_{Ot}, presence/absence of otoliths; P_{CB}, presence/absence of cephalopod beaks; P_{Cr}, presence/absence of crustacean remains; P_{Ey}, presence/absence of eyes; P_{Jw}, presence/absence of fish jaws; P_{Fb}, presence/absence of fish bones; P_O, presence/absence of other prey items.

Species	ID	m_F (g)	F	m_C (g)	D	P_{Sc}	P_{Ot}	P_{CB}	P_{Cr}	P_{Ey}	P_{Jw}	P_{Fb}	P_O
B. splendens	1435	63.01	0.75	40.61	4	P	1	9	P	17	P	P	P
B. splendens	1471	79.87	1.00	58.16	4	P	2	4	P	17	P	P	P
B. splendens	1487	68.37	1.00	48.75	2	P	3?	8	P	13	P	P	P
B. splendens	1491	13.76	0.25	3.35	3	P	1	1	P	13	A	A	P
B. splendens	1463	29.19	0.50	12.28	4	P	0	7	P	25	P	P	P
B. splendens	4725	2.97	0.25	0.54	3	A	0	1	P	46	P	A	P
B. splendens	4780	3.14	0.50	0.64	1	P	0	2	P	18	A	A	P
B. splendens	1969	2.97	0.75	0.17	1	A	0	4	P	11	A	A	A
B. splendens	1330	26.67	0.75	5.56	2	P	2?	2	P	11	P	A	P
B. splendens	2146	3.45	0.00	0.15	4	A	0	1	P	0	A	A	A
B. splendens	1911	3.54	0.25	0.24	2	P	0	3	P	10	A	A	A
B. splendens	4337	2.46	0.00	0.07	0	P	0	0	P	0	P	A	A
B. splendens	4831	3.22	1.00	0.28	2	A	0	0	P	44	A	A	A
B. splendens	1591	17.14	1.00	3.27	1	P	5	0	P	2	P	A	A
B. splendens	1431	29.73	0.75	5.35	1	P	0	0	P	11	P	A	P
B. splendens	1358	41.91	1.00	25.13	3	P	3	0	P	34	A	P	P
B. splendens	4866	3.96	0.25	1	4	A	0	0	P	108	A	A	A
B. splendens	1997	–	–	–	–	–	–	–	–	–	–	–	–
B. splendens	4309	4.40	0.00	0.06	3	A	0	0	P	5	A	A	A
M. antipodum	2092	1.05	0.75	0.28	4	P	0	2	P	6	A	P	A
M. antipodum	G-8	1.81	0.50	0.04	3	P	0	0	A	0	A	P	A
M. antipodum	4905	2.00	1.00	1.01	4	A	0	0	P	0	A	A	A
M. antipodum	1984	0.50	0.25	0.06	3	A	0	0	P	1	A	A	P
M. antipodum	5728	2.43	0.00	0.03	2	A	0	0	P	0	A	A	A

continued on next page…

Table E.1: continued

Species	ID	m_F (g)	F	m_C (g)	D	P_{Sc}	P_{Ot}	P_{CB}	P_{Cr}	P_{Ey}	P_{Jw}	P_{Fb}	P_O
M. antipodum	4082	0.55	0.25	0.02	3	A	0	1	P	3	A	A	A
M. antipodum	5612	1.22	0.75	0.45	2	A	0	0	P	0	A	A	A
M. antipodum	4994	0.86	0.25	0.12	2	A	0	0	P	0	A	A	A
M. antipodum	4424	1.39	0.75	0.88	3	P	0	0	P	2	A	A	P
M. antipodum	5475	2.81	0.75	0.44	3	A	0	0	A	0	A	A	A
M. antipodum	4223	0.91	0.50	0.05	2	A	0	0	P	2	A	A	A
M. antipodum	1993	1.96	1.00	0.65	4	p	0	1	P	4	A	P	A
M. antipodum	4742	2.06	0.75	0.42	4	P	0	0	P	3	A	P	A
M. antipodum	4110	1.38	0.25	0.18	3	A	0	0	P	0	A	A	P
M. antipodum	5307	0.92	0.25	0.15	3	A	0	0	P	2	A	A	A
M. antipodum	G-11	1.51	0.75	0.58	2	P	0	0	P	4	A	P	A
M. antipodum	G-9	2.35	0.50	0.38	3	P	0	1	P	1	A	P	A
M. antipodum	4329	1.14	0.25	0.17	3	A	0	0	P	1	A	A	A
M. antipodum	4111	3.04	0.50	0.40	3	P	0	0	P	3	A	P	A
M. antipodum	5464	2.61	0.25	0.32	4	A	0	0	P	0	A	A	A
M. antipodum	G-7	2.12	0.50	0.13	3	P	0	1	A	0	A	A	A
M. antipodum	1986	2.95	1.00	1.43	4	P	0	0	P	0	A	P	A
M. antipodum	2044	1.49	0.75	0.16	2	A	0	2	P	0	A	A	A
M. antipodum	4712	2.22	0.25	0.56	2	A	1	0	P	2	A	A	A
M. antipodum	5472	4.13	0.75	0.41	3	P	0	0	A	1	P	P	A
M. antipodum	2091	1.23	0.25	0.06	4	P	0	0	P	0	A	A	A
M. antipodum	1930	3.09	1.00	0.69	4	P	0	0	P	2	P	P	A
M. antipodum	1999	4.04	0.25	0.58	3	A	0	0	P	0	A	A	A
M. antipodum	G-3	4.98	0.50	1.02	4	P	0	0	P	0	P	P	A
M. antipodum	5735	–	0.00	–	–	–	–	–	–	–	–	–	–
M. antipodum	G-5	3.92	0.25	0.10	2	P	0	0	A	1	A	P	A
M. antipodum	4413	5.51	1.00	1.71	4	P	0	2	P	4	A	P	A
M. antipodum	2123	1.32	0.00	0.02	3	A	0	0	P	0	A	A	A
M. antipodum	2021	4.05	0.75	0.05	2	P	0	2	A	0	A	A	P
M. antipodum	G-6	2.44	0.00	0.04	3	P	0	0	A	0	A	A	P
M. antipodum	5784	2.87	0.50	1.54	3	P	0	0	A	2	0	P	A
M. antipodum	G-15	3.46	0.25	0.48	4	P	0	0	P	0	A	P	A
M. antipodum	5462	11.23	0.75	2.91	3	P	0	0	A	7	P	P	P
M. antipodum	4998	4.96	1.00	1.50	4	A	0	1	P	8	A	A	A
M. antipodum	G-12	2.98	0.25	0.20	3	A	0	0	P	0	A	A	A
M. antipodum	5613	7.03	0.25	1.83	2	P	0	0	A	1	A	A	A
M. antipodum	1995	7.81	0.25	2.35	1	P	0	0	A	1	A	P	P
M. antipodum	G-13	–	0	–	–	–	–	–	–	–	–	–	–
M. antipodum	4974	4.96	0.50	0.36	1	A	0	2	A	4	A	A	P
M. antipodum	5585	3.66	0.25	0.03	2	P	0	0	A	1	A	P	A
M. antipodum	4869	6.22	0.25	0.45	2	P	0	0	A	1	A	A	P
M. antipodum	5639	5.84	0.25	1.23	2	A	0	0	P	0	A	A	A
M. antipodum	2149	5.19	0.75	1.14	3	P	0	0	P	2	P	P	P
M. antipodum	4953	7.63	1.00	2.62	4	P	0	0	P	4	A	P	P
M. antipodum	2014	7.65	0.00	0.19	3	P	0	0	A	1	A	P	A
M. antipodum	1958	2.46	1.00	1.77	5	P	0	0	P	1	P	P	A

continued on next page…

Table E.1: continued

Species	ID	m_F (g)	F	m_C (g)	D	P_{Sc}	P_{Ot}	P_{CB}	P_{Cr}	P_{Ey}	P_{Jw}	P_{Fb}	P_O
M. antipodum	1937	3.04	0.25	0.09	3	P	0	0	A	1	A	A	P
M. antipodum	G-14	9.01	0.25	0.69	2	P	0	0	A	0	A	P	A
M. antipodum	4652	–	–	–	3	P	0	2	A	10	A	P	P
P. richardsoni	1475	14.72	0.75	1.43	2	A	0	0	P	0	A	A	P
P. richardsoni	1571	30.56	0.50	0.72	2	A	0	0	A	0	A	A	P
P. richardsoni	1324	21.86	0.25	0.25	2	A	0	0	A	0	A	A	P
P. richardsoni	1459	52.94	0.75	2.29	2	P	0	0	A	0	A	A	P
P. richardsoni	1561	40.69	0.25	1.32	4	P	0	0	A	2	P	P	P
P. richardsoni	1503	14.31	0.50	0.81	2	A	0	0	A	0	A	A	P
P. richardsoni	1533	30.35	0.25	4.62	2	A	0	0	A	0	A	A	P
P. richardsoni	1543	15.83	0.50	0.90	3	P	0	0	A	2	P	P	P
P. richardsoni	1589	76.76	0.50	2.56	2	P	0	0	A	0	A	A	P
N. rhomboidalis	2119	2.49	0.25	0.08	2	A	0	0	A	0	A	A	P
N. rhomboidalis	2065	5.95	0.25	0.13	3	A	0	0	A	0	P	A	P
L. caudatus	2023	12.86	0.00	0.14	2	A	0	0	A	0	A	A	P

Appendix F

Sequences obtained from GenBank

Table F.1: Overview of Anguilliformes COI sequences used in the phylogenetics analysis. Selection based on Inoue et al. (2010).

Family	Species	GenBank Accession
Anguillidae	*Anguilla japonica*	AB038556
	A. reinhardtii	AP007248
	A. megastoma	AP007243
	A. celebesensis	AP007239
	A. marmorata	AP007242
	A. nebulosa nebulosa	AP007246
	A. nebulosa labiata	AP007245
	A. interioris	AP007241
	A. obscura	AP007247
	A. bicolor bicolor	AP007236
	A. bicolor pacifica	AP007237
	A. mossambica	AP007244
	A. borneensis	AP007238
	A. dieffenbachii	AP007240
	A. australis australis	AP007234
	A. australis schmidtii	AP007235
	A. rostrata	AP007249
	A. anguilla	AP007233
Heterenchelyidae	*Pythonichthys microphthalmus*	AP010842
Moringuidae	*Moringua edwardsi*	AP010840
	M. microchir	AP010841
Chlopsidae	*Kaupichthys hyoproroides*	AP010845
	Robinsia catherinae	AP010846
Myrocongridae	*Myroconger compressus*	AP010847
Muraenidae	*Anarchias sp.*	AP010843
	Gymnothorax kidako	AP002976
	Rhinomuraena quaesita	AP010844
Synaphobranchidae	*Ilyophis brunneus*	AP010848

continued on next page

Table F.1: continued

Family	Species	GenBank Accession
	Synaphobranchus kaupii	AP002977
	Simenchelys parasitica	AP010849
Ophichthidae	*Ophisurus macrorhynchus*	AP002978
	Myrichthys aki	AP010862
Colocongridae	*Coloconger cadenati*	AP010863
Derichthyidae	*Nessorhamphus ingolfianus*	AP010850
	Derichthys serpentinus	AP010851
Muraenesocidae	*Muraenesox bagio*	AP010852
	Cynoponticus ferox	AP010853
Nemichthyidae	*Nemichthys scolopaceus*	AP010854
	Avocettina infans	AP010855
	Labichthys carinatus	AP010856
Congridae	*Heteroconger hassi*	AP010859
	Paraconger notialis	AP010860
	Ariosoma shiroanago	AP010861
	Conger myriaster	AB03838
Nettastomatidae	*Nettastoma parviceps*	AP010864
	Hoplunnis punctata	AP010865
	Facciolella oxyrhyncha	AP010866
Serrivomeridae	*Serrivomer sector*	AP007250
	Serrivomer beanii	AP010857
	Stemonidium hypomelas	AP010858
Cyematidae	*Cyema atrum*	AP010870
Eurypharyngidae	*Eurypharynx pelecanoides*	AB046473
Monognathidae	*Monognathus jesperseni*	AP010869
Elopidae	*Elops hawaiensis*	AB051070
Notacanthidae	*Notacanthus chemnitzi*	AP002975

Table F.2: GenBank Sequences employed in the Achelata 16S phylogenetics analysis. Selection based on Palero et al. (2009).

Family	Species	GenBank Accession
Palinuridae	*Palinurus barbarae*	FJ174903
	Palinurus charlestoni	FJ174902
	Palinurus detagoae	FJ174904
	Palinurus elephas	FJ174900
	Palinurus gilchristi	FJ174905
	Palinurus mauritanicus	FJ174901
	Panulirus argus	AF502947
	Panulirus homarus	AF337962
	Panulirus inflatus	AF337960
	Panulirus japonicus	AF337968
	Panulirus penicillatus	AF337974
	Panulirus regius	FJ174899
	Panulirus versicolor	AF337978
	Linuparus trigonus	AF502946
	Palinustus waguensis	AF502952
	Puerulus angulatus	AF502951
	Justitia longimana	AF502953
	Jasus edwardsii	FJ174894
	Jasus lalandii	FJ174895
	Jasus tristani	FJ174893
	Sagmariasus verreauxii	FJ174896
	Projasus parkeri	FJ174898
	Projasus bahamondei	FJ174897
	Palinurellus wienecki	AF502954
	Palibythus magnificus	AF502950
Scyllaridae	*Scyllarus arctus*	FJ174911
	Scyllarus caparti	FJ174909
	Scyllarus posteli	FJ174910
	Scyllarus pygmaeus	FJ174908
	Scyllarus subarctus	FJ174912
	Thenus unimaculatus	FJ174915
	Thenus orientatis	FJ174914
	Scyllarides herklotsii	FJ174906
	Scyllarides latus	FJ174907
Nephropidae	*Homarus americanus*	FJ174888
	Nephrops norvegicus	FJ174889
Polychelidae	*Polycheles typhlops*	FJ174890